CFD investigation of industrial cyclone preheaters

Mirzaei, Mohamadali

Publication date:
2023

Document Version
Publisher's PDF, also known as Version of record

CFD investigation of industrial cyclone preheaters

PhD Thesis
by
Mohamadali Mirzaei

Supervisors:

Weigang Lin (DTU Chemical Engineering)
Peter Arendt Jensen (DTU Chemical Engineering)
Haosheng Zhou (ROCKWOOL A/S)
Mohammadhadi Nakhaei (FLSmidth A/S)

DTU Chemical Engineering
Department of Chemical and Biochemical Engineering

CHEC Research Centre
January 2023

Technical University of Denmark
Department of Chemical and Biochemical Engineering
Søltofts Plads 229, building 229,
2800 Kgs. Lyngby, Denmark
Phone: +45 4525 2800
Email: kt@kt.dtu.dk

To my Parents, Esmaeil and Parvin, to whom I owe everything.
And to my sister, Elham, light of my life.

Preface

This thesis is the result of three years of research, from 2020 to 2023, in the Combustion and Harmful Emissions Control (CHEC) Research Center of the Department of Chemical and Biochemical Engineering at the Technical University of Denmark (DTU). The project is being conducted in collaboration with FLSmidth A/S and ROCKWOOL A/S as part of the ProBu project: Process Technology for Sustainable Building Materials Production. The project was funded by Innovation Fund Denmark (grant number: 8055-00014B), as well as FLSmidth A/S, Rockwool A/S and the Technical University of Denmark.

The main supervisor professor Weigang Lin (DTU), the co-supervisor senior researcher Peter Arendt Jensen (DTU), and the industrial co-supervisors, chief R&D engineer Haosheng Zhou (ROCKWOOL), R&D Engineer Mohammadhadi Nakhaei (FLSmidth), and former fluid dynamics specialist Sam Zakrzewski (FLSmidth) deserve great thanks for their generous support throughout the project. Professor Hao Wu (DTU) and R&D specialist Kasper Jønck (ROCKWOOL) have also been part of the supervision team. I would like to thank all members of the supervision team for sharing their great knowledge, productive discussions in meetings, and critical feedback and contributions.

Furthermore, I am grateful to Senior Scientist Sønnik Clausen (DTU) for conducting industrial experiments to provide validation data for the present study. I would also like to thank all people involved in the ProBu project especially Lars Skaarup Jensen (FLSmidth) for their support, contributions and suggestions, members of the FLSmidth CFD team for the valuable discussions we had during meetings, and the Ansys technical support team especially Katya Menter and Amine Ben Hadj Ali for providing technical support and helping to resolve bugs in the software. I would like to thank FLSmidth and Rockwool for providing their plant data to be used as validation data in the present study. I am also grateful to the people at the Rockwool Doense plant for providing the opportunity for inspection and conducting measurements.

I would like to thank all my supportive colleagues at CHEC and KT, especially, Giovanni, Emil, Jie, Gcinisizwe, and Hamed who made my working atmosphere an enjoyable place.

More than anything else, I would like to deeply thank my beloved parents, Esmaeil and Parvin, and my caring sister, Elham, for their sacrificial and unconditional support and love throughout my years of study

and through these three years. I would also like to extend my deepest gratitude to my dear friends Shayan, Erfan, Ali, Hamid, Reza, Milad, Mohammadreza, Saman, Yasaman, Hossein, Mahtab, Bahaman, Mina, and Aref. These three years would not have passed nearly as memorable had it not been for the presence and support of my family and friends.

January 2023

Mohamadali Mirzaei

Abstract

Cyclone preheaters are important components in cement and stone wool production plants. They are used to preheat the raw material by recovering the thermal energy of the high-temperature flue gas produced in a kiln or a melting reactor. Despite their deceptive simplicity, the complicated multiphase flow field within cyclone preheaters makes their design and optimization challenging. Conventionally, the design of cyclones is based on empirical approaches developed for simplified, generic, and small-scale cyclones which are not reliable for industrial-scale cases. Therefore, Computational Fluid Dynamics (CFD) has become, in recent years, an essential tool in the analysis, design, and evaluation of cyclones by providing a detailed picture and understanding of the flow field inside these devices.

The present study aimed to develop a well-validated and comprehensive CFD model for simulation of highly loaded large-scale cyclone preheaters. The model should be capable of predicting important performance parameters such as pressure drop, separation efficiency, heat transfer rate, as well as flow pattern and erosion pattern. For this purpose, an Eulerian–Lagrangian multiphase model, i.e., Dense Discrete Phase Model (DDPM) coupled with a robust turbulence model was developed.

The developed model was first validated against experimental measurements of pressure drop in an isothermal highly loaded lab-scale cyclone (diameter of 0.2 m) operating with coarse particles (diameter of 2 mm). The results indicated that the model is promising for the simulation of this complex case. The model was further implemented to simulate an iso-thermal, highly loaded pilot-scale (1.6 m in diameter) cement cyclone operating with relatively fine particles, i.e., Sauter mean diameter of 5 μm. However, preliminary simulations showed that the model highly underpredicted separation efficiency and overpredicted pressure drop. It turned out that this was because the agglomeration phenomenon, which plays a vital role in the case of fine particles, was missing. Therefore, an agglomeration model based on a stochastic Lagrangian inter-particle collision model was then implemented into the CFD model. The new model significantly improved predictions in terms of both pressure drop and separation efficiency.

The performance of the developed model may be influenced by sub-models (e.g., turbulence models, drag models, etc.), model parameters (e.g., particle-particle restitution coefficient and particle-wall rebound coefficient), and numerical parameters (e.g., parcel/grain size, time step size and order of discretization), to

different extents. An extensive investigation was performed to suggest a set of sub-models, model parameters, and numerical parameters providing the best prediction of the hydrodynamics of large-scale highly loaded cyclones. The investigation showed that the turbulence model and particle-particle restitution coefficient have the strongest influence on the performance of the developed model.

In the next step, heat transfer modeling was added to the developed model, and an industrial-scale (1.6 m in diameter), non-isothermal, highly loaded cyclone preheater with relatively coarse particles, i.e., Sauter mean diameter of 375 µm, was studied. The studied cyclone operates at Integrate Melting Furnace (IMF) system of a stone wool production plant. Plant operating parameters, i.e., pressure drop and global heat transfer rate and the data from a measurement campaign, i.e., local measurements of gas velocity profiles, using LDA, and gas temperature profiles, using thermocouple and FTIR were used for further validation of the CFD model.

In all these cases, reasonable agreements between the measurements and simulation predictions were obtained. In addition, the developed model was accurate enough to capture the major observed trends caused by the changes in the operating parameters; for example, the improvement in separation efficiency of cyclones due to an increase in particle load is well captured by the developed model.

Lastly, to conduct erosion investigation in highly loaded cyclones, the well-known erosion model of Oka et al. was implemented into the developed CFD model. After successfully testing the model on a lab-scale cyclone, in which erosion was measured experimentally, the model was used to investigate erosion in the industrial cyclone preheater. The predicted erosion pattern and locations with severe erosion were qualitatively matched with observations.

Furthermore, throughout this study, parametric studies on operating conditions including gas and solid flow rates, particle size distribution, and gas inlet temperature were performed and the impacts on pressure drop, separation efficiency, heat transfer rate, and erosion, considered as key performance parameters of cyclone preheaters, were evaluated.

In essence, a CFD model has been developed that is computationally affordable and provides validated predictions of key performance parameters of cyclone preheaters, such as pressure drop, separation efficiency, and heat transfer rate. Additionally, by properly representing critical present physical phenomena, including turbulence, gas-particle interactions, particle-particle interactions, agglomeration, etc., the developed model provides valid predictions of flow patterns, temperature profiles and erosion patterns. Therefore, the developed model can probably also be used for other industrial applications to troubleshoot, redesign, and optimize industrial cyclone preheaters.

Dansk Resumé

Cyklonforvarmere er vigtige komponenter i cement og stenuld produktionsanlæg. De anvendes til forvarmningen af råmateriale, for at genvinde den termiske energi fra røggas produceret i en roterovn eller en smelteovn. Det komplicerede flerfasede strømningsfelt i cyklonforvarmere gør at design og optimering er udfordrende. Konventionelt, er cyklonernes design baseret på empirisk baserede formler og måledata fra forsimplede småskala cykloner, som ikke er repræsentative for installationer i industriel-skala. Derfor er Computational Fluid Dynamics (CFD) de seneste år, blevet et væsentligt værktøj i analyse, design, og evalueringen af cykloner, via at modellerne giver et detaljeret billede og en forståelse af strømningsfeltet i disse enheder.

Formålet for nærværende studie, var at udvikle en velvalideret og omfattende CFD-model, til simulering af storskala cyklonforvarmere under høj partikel belastning. Modellen bør være i stand til at forudsige vigtige procesparametre, så som trykfald, separationseffektivitet, varmeoverførselshastighed, samt strømningsmønster og erosionsmønster. Til dette formål, er en Eulerian–Lagrangian flerfase-model, dvs. Dense Discrete Phase Model (DDPM) koblet med en robust turbulensmodel, blevet udviklet.

Den udviklede model blev først valideret op imod eksperimentelle målinger af trykfald i en isoterm højbelastet laboratorieskala cyklon (diameter på 0.2 m) opereret med store partikler (diameter på 2 mm). Valideringen konkluderede, at modellen er lovende til simulering af dette system. Derefter blev CFD modelen anvendt for en isoterm, højbelastet, storskala (1.6 m i diameter) cyklon, der opererer med relativt små partikler (en Sauter-middeldiameter på 5 μm). Imidlertid blev det ved de indledende simuleringer observeret, at modellen i dette tilfælde kraftigt underestimerede separationseffektiviteten og overestimerede trykfald. Dette skyldtes, at agglomerationsfænomener spiller en afgørende rolle for fine partikler, og dette fænomen var ikke inkluderet i modellen. Derfor blev en agglomerationsmodel implementeret baseret på en stokastisk Lagrangian inter-partikel kollisions model, og dette forbedrede væsentligt forudsigelserne af både trykfald og separationseffektivitet.

Præcisionen af den udviklede model blev i varierende udstrækning påvirket af undermodeller (f.eks. turbulensmodeller, gasmodstandsmodeller, osv.), modelparametre (f.eks. partikel-partikel restitutionskoefficient, og partikel-væg rebound-koefficient), og numeriske parametre (f.eks.

gruppe/kornstørrelse, tidstrinstørrelse, og diskretiseringens rækkefølge). En omfattende parameter undersøgelse blev udført, for at kunne udvælge et set af undermodeller, modelparametre, og numeriske parametre, der gav den bedste forudsigelse af hydrodynamikken for højtbelastede storskala cykloner. Studiet viste at turbulens modellen og partikel til partikel restitutionskoefficienten har den største indflydelse på modellens resultater.

Derefter blev modelleringen af varmeoverførsel tilføjet til den udviklede model, og en storskala (1.6 m i diameter), ikke-isoterm, højbelastet cyklonforvarmer med relativt grove partikler (en Sauter middeldiameter på 375 μm) undersøgt. De undersøgte cykloner anvendes som en del af et Integreret smelteovns (IMF) system, som bruges til produktion af stenuld. Anlæggets drifts parameter (som trykfald, varmeoverføringsrate osv.) og måledata fra målekampagnen (som lokale hastigheder og temperaturer) blev anvendt til en validering af CFD modellen.

I alle de undersøgte tilfælde blev der opnået en rimelig overensstemmelse mellem de eksperimentelle målinger og simuleringsforudsigelserne. Derudover var modellen nøjagtig nok til at fange de vigtigste observerede tendenser, forårsaget af ændringer i driftsparametre; for eksempel forudsiges forbedringen i cykloners separationseffektivitet, på grund af en stigning i partikelbelastning, godt af modellen.

Til sidst blev en velkendt erosions model (Oka erosionsmodel) implementeret i CFD-modellen for at udføre erosionsundersøgelse i højbelastede cykloner. Efter vellykkede test af modellen med laboratorieskala cyklon erosions måledata, blev modellen brugt til at undersøge erosion i en industriel cyklonforvarmer; og det modellerede erosionsmønster stemte kvalitativt overens med observationer i den industrielle cyklon .

Ydermere blev der gennem hele dette studie udført parameterundersøgelser af indflydelsen af driftsforhold, inklusive strømningshastigheder for gas og faststof, partiklers størrelsesfordeling, og gasens indløbstemperatur; og desuden blev indvirkningen på nøgleparametre som trykfald, separationseffektivitet, varmeoverførselshastighed, og erosion evalueret.

I dette projekt blev en CFD-modell udviklet, som er beregningsmæssigt overkommelig, og giver validerede forudsigelser af cyklonforvarmeres nøgleparametre, såsom trykfald, separationseffektivitet og varmeoverførselshastighed. Desuden giver den udviklede model en korrekt repræsentation af kritiske fysiske fænomener som turbulens, gas-partikel interaktioner, partikel-partikel interaktioner, agglomeration, og så videre. Modellen giver herudover gyldige forudsigelser af strømningsmønstre, temperaturprofiler, og erosionsmønstre. Derfor kan også andre industri sektorer formentlig bruge denne udviklede model til at fejlsøge, re-designe, og optimere industrielle cyklonforvarmere.

Nomenclature

A_{face} = The area of the computation face on the wall surface, $1/\mathrm{m}^2$

A_p = Projected particle surface area, m^2

a = Constants for the collision efficiency correlation

Bi = Biot number

b = Constants for the collision efficiency correlation

C_D = Drag coefficient

C_p = Heat capacity, $\mathrm{J/kg.K}$

C_{RL} = Rotational lift coefficient

C_ω = Rotational drag coefficient

$C_{1\varepsilon}$ = Constant in turbulence modeling

$C_{2\varepsilon}$ = Constant in turbulence modeling

D = Cyclone Diameter, m

$D_{L,ij}$ = Molecular diffusion tensor, $\mathrm{kg/m.s}^3$

$D_{T,ij}$ = Turbulent diffusion tensor, $\mathrm{kg/m.s}^3$

D_{32} = Sauter mean diameter, m

d' = Reference diameter, m

d_{ij} = Deformation tensor

d_p = Particle diameter, m

E = Erosion rate, $\mathrm{kg/s}$

E^R = Erosion flux, $\mathrm{kg/m}^2.\mathrm{s}$

E_v = Volumetric erosion, m^3/kg

E_{90} = Reference erosion rate at 90° impact angle, kg/kg

e = The energetic restitution coefficient

$eg_{i,i+1}$ = $f_{i+1} - f_i$

$F_{collision}$ = The force a particle acts on another particle due to interparticle collision, $\mathrm{kg.m}/s^2$

F_{Dc} = Particle drag force on continuous phase, $\mathrm{N/m}^3$

$F_{fluid-particle}$ = The force that the fluid acts on a particle, $\mathrm{kg.m}/s^2$

$F_{ij} =$ Tensor to account for production by system rotation, $\mathrm{kg/m.\,s^3}$

$F_{mag} =$ Magnus force, N

$F_{other} =$ Other gas-solid interaction forces (Magnus, Saffman, rotational drag), N

$F_{particle-fluid} =$ The force a particle acts on the fluid, $\mathrm{kg.\,m/}s^2$

$F_{p-p} =$ Particle-particle interaction force, N

$F_{Saff} =$ Saffman force, N

$f =$ Obtained numerical solution

$f_r =$ Curvature correction function

$\Delta_f =$ Filter size, m

$\Delta_f{}^* =$ Dimensionless filter size

$G =$ Generation, $\mathrm{kg/m.\,s^3}$

$GCI_{i,i+1}^{fine} =$ Grid convergence index, %

$g =$ Gravitational acceleration, $\mathrm{m/s^2}$

$H =$ The Hamaker constant, J

$H_d =$ Heterogeneity index

$Hv =$ Vickers hardness, GPa

$h_{p-g} =$ Gas-particle heat transfer coefficient, $\mathrm{W/m^2.\,K}$

$I =$ Stress tensor

$K_{DPM} =$ Drag coefficient (averaged for the discrete phase in a cell), $\mathrm{Ns/m^4}$

$k =$ Turbulent kinetic energy, $\mathrm{m^2/s^2}$

$k_{\Theta_s} =$ The granular diffusion coefficient, $\mathrm{kg/m}$

$k_2 =$ Velocity exponent constant

$k_3 =$ Diameter exponent constant

$L =$ The lateral displacement, m

$L_a =$ The lateral non-dimensional displacement

$l =$ Interparticle distance, m

$m =$ Mass, kg

$\dot{m}_p =$ The mass rate of particles hitting the wall, $\mathrm{kg/s}$

$N =$ Number of collisions, #

$NC =$ Number of control volume of mesh, #

$n =$ Number of particles in parcel, #

$\bar{n} =$ Mean expected number of collisions, #

$n_1 =$ Impact angle function constant

$n_2 =$ Impact angle function constant

$P =$ Collision probability

$P_{ij} =$ Stress production tensor, $\mathrm{kg/m.\,s^3}$

$Pr =$ Prandtl number

$\Delta P =$ Pressure drop, Pa

$\Delta P_0 =$ Pressure drop in particle-free case, Pa

$p =$ Pressure, Pa

$p_c =$ The yield pressure, Pa

$p_s =$ Solid phase pressure, Pa

$R =$ Cyclone main body radius, m

$Re =$ Reynolds number

$Re_k =$ Relative Reynolds number, $\frac{\rho_g d_1 |\overrightarrow{u_{p1}} - \overrightarrow{u_{p2}}|}{\mu_g}$

$Re_p =$ Particle Reynolds number

$Rg =$ $\varepsilon g_{12}/\varepsilon g_{23}$

$R_{ij} =$ Reynolds stress tensor, $\overline{u_i' u_j'}$ $\mathrm{m^2/s^2}$

$RN =$ Randomly generated number in the range [0, 1]

$\mathrm{r} =$ Radial distance from the center, m

$rg =$ Grid refinement ratio

$S =$ Source term due to additional gas-solid interaction forces, $\mathrm{N/m^3}$

$SL =$ Solid loading ratio, kg solid/kg air

$St_{rel} =$ Relative Stokes number

$T =$ Temperature, K

$t =$ Time, s

$\Delta t =$ Time step, s

$U_{crit} =$ Critical velocity, $\mathrm{m/s}$

$u =$ Instantaneous velocity, $\mathrm{m/s}$

$\bar{u} =$ Mean component of velocity or directly resolved component of velocity, $\mathrm{m/s}$

$u' =$ Fluctuating component of velocity or sub-grid component of velocity, $\mathrm{m/s}$

$\overline{u_i' u_i'} =$ RMS of velocity fluctuations, $\mathrm{m^2/s^2}$

$u_{dpm} =$ Particle velocity (averaged for the discrete phase in a cell), $\mathrm{m/s}$

$u_{slip}^* =$ Dimensionless slip velocity

$u_t =$ Terminal velocity, $\mathrm{m/s}$

$\overline{u'^2} =$ RMS value of tangential velocity fluctuations, $\mathrm{m^2/s^2}$

$V =$ Gas phase velocity, $\mathrm{m/s}$

$V' =$ Reference velocity, $\mathrm{m/s}$

$V_{cell} =$ Cell volume, $\mathrm{m^3}$

$V_{collision} =$ Collision volume, $\mathrm{m^3}$

$V_p =$ Particle velocity, $\mathrm{m/s}$

$V_{parcel} =$ parcel volume, $\mathrm{m^3}$

$v =$ Gas-phase velocity, $\mathrm{m/s}$

$v_{in} =$ Gas velocity at cyclone inlet, $\mathrm{m/s}$

$\overline{v'^2} =$ RMS value of radial velocity fluctuations, $\mathrm{m^2/s^2}$

$\overline{w'^2} =$ RMS value of axial velocity fluctuations, $\mathrm{m^2/s^2}$

$x =$ Location, m
$Y =$ Dissipation, $\mathrm{kg/m.\,s^3}$
$Y_c =$ The radial distance, m
$y^+ =$ Dimensionless wall distance
$z_0 =$ The minimum contact distance, m

Greek symbols

A = A parameter in the revised Sarkar drag model
$\alpha =$ Volume fraction
$\alpha g = \frac{r_{12}^{p} GCI_{12}^{fine}}{GCI_{23}^{fine}}$
$\beta =$ Drag coefficient, $\mathrm{kg/m^3/s}$
$\Gamma =$ Effective diffusivity, Pa.s
$\gamma =$ Impact angle, radian
$\varepsilon =$ Scalar rate of dissipation of turbulent kinetic energy, $\mathrm{m^2}/s^3$
$\varepsilon g_{i,i+1} = \frac{f_{i+1}-f_i}{f_i}$
$\varepsilon_{ij} =$ Dissipation tensor, $\mathrm{kg/m.\,s^3}$
$\eta_p =$ Collision efficiency
$\Theta_s =$ Granular temperature, $\mathrm{m^2}/s^2$
$\lambda =$ Thermal conductivity, $\mathrm{W/m.\,K}$
$\lambda_s =$ Bulk viscosity, kg/ms
$\mu =$ Viscosity, Pa.s
$\mu_s =$ Shear viscosity, kg/ms
$\mu_{s,coll} =$ Collisional viscosity, kg/ms
$\mu_{s,fric} =$ Frictional viscosity, kg/ms
$\mu_{s,kin} =$ Kinetic viscosity, kg/ms
$\mu_t =$ Turbulent viscosity, kg/ms
$\nu =$ Kinematic viscosity, $\mathrm{m^2}/s$
$\xi =$ Discrete piecewise constant function
$\Pi_{R,ij} =$ Tensor to account interaction with dispersed phase, $\mathrm{kg/m.\,s^3}$
P = A parameter in the revised Sarkar drag model
$\rho =$ Density, $\mathrm{kg/m^3}$
$\rho_w =$ Wall density, $\mathrm{kg/m^3}$
$\sigma =$ Turbulent Prandtl number
$\tau_c^t =$ Turbulent stress tensor, $\mathrm{kg/m.\,s^2}$
$\bar{\bar{\tau}}_s =$ Solid phase stress-strain tensor, Pa
$\tau_w =$ Wall shear stress, Pa
$\Upsilon_{\Theta_s} =$ Granular energy diffusion term, $\mathrm{kg/m.}\,s^2$
$\phi =$ The impact angel of two collided particles, radian

$\phi k =$ Transfer rate of kinetic energy, $\mathrm{kg/m.s^3}$
$\varphi_{ij} =$ Pressure strain tensor, $\mathrm{kg/m.s^3}$
$\omega =$ Specific dissipation rate, $1/\mathrm{s}$
$\vec{\omega} =$ Fluid angular velocity, $\mathrm{rad/s}$
$\omega_p =$ Particle rotational velocity, $\mathrm{rad/s}$

Subscripts

$c =$ Continuous/gas phase
$g =$ Gas phase
$i =$ Grid level
$i =$ ith direction
$i =$ ith particle
$\mathrm{in} =$ Inlet
$k =$ Turbulent kinetic energy
$p =$ Particle
$pi =$ ith particle
$r =$ Radial direction
$s =$ Solid phase
$w =$ Wall
$z =$ Axial direction
$\theta =$ Tangential direction
$\omega =$ Specific dissipation rate
$1 =$ Collector particle
$2 =$ Contributor particle

Abbreviation

CFD = Computational Fluid Dynamics
cc = Curvature correction
DDPM = Dense Discrete Phase Model
DEM = Discrete Element Model
DNS = Direct Numerical Simulation
DPM = Discrete Phase Model
DRW = Discrete Random Walk
EVM = Eddy Viscosity Model
FTIR = Fourier-transform infrared spectroscopy
IMF = Integrated Melting Furnace
KTGF = Kinetic Theory of Granular Flow
LDA = Laser Doppler Anemometry
LDV = Laser Doppler Velocimetry
LES = Large Eddy Simulation

PBE =	Population Balance Equation
PDE =	Partial Differential Equation
PVC =	Precessing Vortex Core
PSD =	Particle Size Distribution
RANS =	Reynolds-averaged Navier–Stokes
RMS =	Root Mean Square
RNG =	Renormalization Group
RSM =	Reynolds Stress Model
SGS =	Sub-Grid-Scale
sst =	Shear stress transport
TFM =	Two-Fluid Model

Table of contents

1 Introduction

1.1 Background and motivation

A cyclone is a stationary device in which solid particles, are separated from a gas stream as a result of centrifugal force acting on them. When a process requires particle/gas separation, a cyclone is the first device to be considered, due to its low construction and operating cost, reliability, simplicity, robustness and ability to handle a broad range of different pressure, temperature, and solids loading [1].

As shown in Figure 1-1, an ordinary cyclone consists of (1) a cylindrical vessel, (2) a conical base and (3) a tangential inlet connected to the upper part of the vessel. The solid outlet is located at the base and the gas outlet is positioned at the center of the vessel roof extending inwardly into the cyclone. The particle-laden flow is introduced tangentially, creating a swirling motion inside the cyclone. The centrifugal force caused by the swirling motion pushes particles towards the wall. The swirling flow is downward in the outer part of the swirl (the outer vortex) and upward in the center (the inner vortex). The downward flow of the outer vortex transports collected particles (those at the wall) out the bottom of the cyclone, while the gas escapes from the central outlet at the top [1].

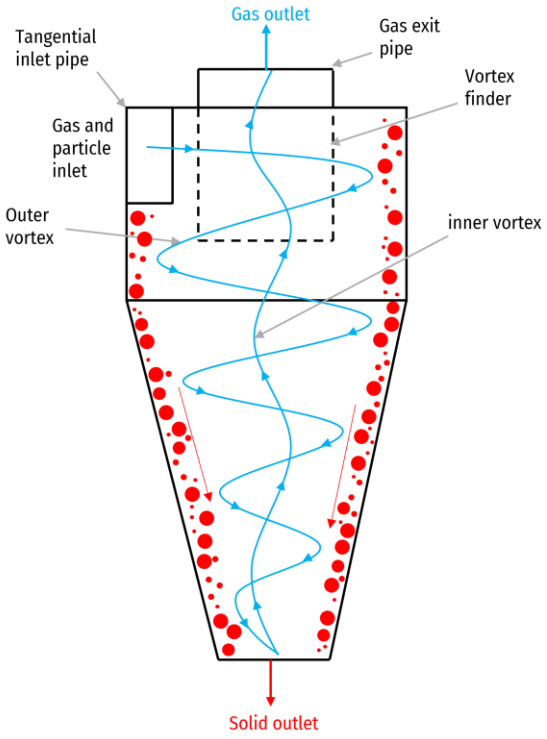

Figure 1-1. Sketch of an ordinary cyclone.

Cyclones are also commonly used as gas-solid heat exchangers (cyclone preheaters), mostly in order to preheat solid material to improve the energy efficiency of high-temperature gas-solid processes. Generally, in a cyclone preheater which normally operates at high solid loads (dense gas-solid flow), cold solid material is fed to a stream of hot gas flow (coming from a furnace/kiln/reactor) in a duct connected to the cyclone. The gas-solid heat exchange normally takes place in this duct and in the cyclone, the cooled gas and preheated particles will be separated [2].

The rapid growth of energy-intensive industries, including cement and stone wool production, demands a constant need for sustainability improvement and minimizing adverse environmental impacts in these industries. Cyclone preheaters are the key components in both cement [2–5] and stone wool production [6,7] industries as they influence the efficiency and cost of these high-temperature processes. Thereby, the design and optimization of cyclone preheaters play a role in the improvement of such processes. Industrial partners of this project, FLSmidth A/S and ROCKWOOL A/S, intend to improve the performance of cyclone preheaters in particular in terms of pressure drop and separation efficiency. ROCKWOOL A/S also aims to reduce wall erosion as it is a serious issue in their cyclone preheaters.

Despite their deceitful simplicity, cyclone preheaters are complicated to design and difficult to optimize, as the flow field within them is complex. Due to this complexity, Computational Fluid Dynamics (CFD) became, over the last two decades, an important tool in cyclone analysis and design by providing a detailed picture and understanding of the flow field inside these devices [8]. However, the complicated features of the two-phase flow in cyclones make CFD simulation of them challenging. High swirl intensity, high turbulence intensity which is anisotropic, high curvature of the streamlines, having multiphase flow and phase interaction, and being naturally unstable are a couple of these features [8].

In this PhD, the focus is on industrial cyclone preheaters operating under high solid loads. CFD simulation of these cyclones, compared to dilute or small-scale cyclones, is more challenging. It is due to e.g., higher computational expense and the infeasibility of some of the conventional models in industrial cases Furthermore, in the case of dense gas-solid flow, particle-particle collisions and interactions might play a role which are complex to model.

Most CFD models of cyclones presented in the literature are adequate only for low and moderate particle loads and for lab-scale cyclones. A few models, focused on highly loaded cyclones, mostly considered large particles where agglomeration does not play a significant role, and they were mostly implemented on lab-scale cases [9,10]. Therefore, the lack of a validated CFD model for the simulation of highly loaded large-scale cyclone preheaters applicable for the whole range of particle sizes is clear.

CFD models should preferably be validated against experimental measurements. However, the existing experimental studies of highly loaded cyclones are limited to global measurements in lab-scale devices. Local measurements of velocity or temperature profiles in highly loaded cyclones are missing, even in lab-scale geometries or ambient temperatures let alone in industrial cyclone preheaters. In the case of industrial cyclone preheaters, even global measurements are limited. Although the focus of the present study is on CFD simulation, considering the mentioned lack of experimental data, some measurement campaigns in industrial units were conducted to provide the required validation data.

This project is conducted in collaboration with FLSmidth A/S and ROCKWOOL A/S as part of the ProBu project: Process Technology for Sustainable Building Materials Production. FLSmidth A/S manufactures industrial cyclone preheaters to be operated in the cement production process where a set

of cyclone preheaters are installed upstream of the calciner and the kiln. On the other hand, in ROCKWOOL A/S, a set of cyclone preheaters are installed upstream of the melting furnace in Integrated Melting Furnace (IMF) system for stone wool production. Therefore, this PhD study mostly focuses on cyclone preheaters in the cement industry and stone wool production industry. Despite their similarity in working principle and solid loading, cyclone preheaters in the cement industry operate with considerably finer particles (0.5-300 μm with a mean diameter around 5 μm) than in the stone wool plant cyclone preheaters (50-3000 μm with a mean diameter around 375 μm). Therefore, it is required to develop a validated CFD model applicable to the whole range of particle sizes, capable of predicting important performance parameters of cyclone preheaters such as pressure drop, separation efficiency, and heat transfer rate, as well as flow pattern. Additionally, the model needs to be capable of predicting erosion in case of stone wool production cyclone preheaters.

1.2 Objectives

The overall objective of the present study is to develop a comprehensive and validated CFD model for simulation of industrial-scale cyclone preheaters with high particle load. The model shall improve the understanding of such cyclones and provide predictions of performance parameters such as pressure drop, separation efficiency, and heat transfer rate, as well as flow pattern and erosion predictions as functions of geometry, operating conditions and material properties. The developed model can then later be used by engineers in related industries as a tool to troubleshoot, optimize, and redesign industrial cyclone preheaters. The CFD model should have the following features:

- Computationally inexpensive to be used in industrial cases
- Ability to properly mimic crucial physical phenomena taking place in cyclones including turbulence, gas-particle interactions, particle-particle interactions, etc.
- Proven ability to provide reliable predictions of important performance parameters of cyclone preheaters including pressure drop, separation efficiency, and heat transfer rate
- Ability to capture the measured or expected effect of operating conditions on the performance parameters
- Proven ability to provide a validated prediction of the flow pattern and temperature profile
- Ability to provide erosion pattern predictions
- Implemented in a commercial CFD solver

1.3 Outline

After a literature survey (Chapter 2), the project is divided into three phases:

1. Investigation of the hydrodynamic of multiphase flow in iso-thermal, highly loaded cyclones by excluding heat transfer (Chapters 3, 4, and 5).

2. Inclusion of heat transfer to the model to simulate non-isothermal highly loaded industrial cyclone preheaters (Chapter 6).

3. Erosion investigation in a cyclone preheater (Chapter 7).

In **Chapter 2**, a comprehensive literature review mostly focusing on CFD simulation of cyclones is provided to help with the selection of appropriate multiphase models, turbulence model, etc., for the present case.

In **Chapter 3**, an iso-thermal highly loaded lab-scale cyclone is simulated using a set of chosen models to evaluate their validity against limited available experimental measurements. Also, the challenges and limitations of the chosen models are identified providing easier implementation of the model in large-scale cases.

In **Chapter 4**, the model developed in Chapter 3 is implemented on an iso-thermal, highly loaded pilot-scale (1.6 m in diameter) cement cyclone operating with relatively fine particles (0.5-300 μm with a mean diameter around 5 μm). Considering the presence of fine particles in this cyclone, the model is modified to account for particle agglomeration. After the modifications, the model is successfully validated by experimental measurements of pressure drop and separation efficiency.

The developed model presented in Chapters 3 and 4 consists of several sub-models, model parameters, and numerical parameters by which the performance of the model is influenced. **In Chapter 5**, to study the performance of the developed model, an extensive analysis is performed, varying one sub-model or parameter at a time, and systematically assessing the effect on the results. In addition, the impact of some operating conditions on the performance of an iso-thermal large-scale highly loaded cyclone is examined.

In **Chapter 6**, heat transfer modeling is added to the developed model to simulate a non-isothermal industrial cyclone preheater of ROCKWOOL A/S with a diameter of 1.6 m. The model is validated by experimental measurements of pressure drop, gas and particle exit temperature (heat transfer rate), local gas velocity profile and gas temperature profile.

In **Chapter 7**, the developed model is used to investigate erosion in the industrial cyclone preheater of ROCKWOOL A/S. The predictions of erosion patterns are qualitatively compared against visual inspections of the cyclone preheater interior. In addition, parametric studies on operating conditions were performed to evaluate their impacts on erosion, pressure drop, and heat transfer rate.

Finally, in **Chapter 8** the conclusions of the study and suggestions for future activities are summarized. The chapters and their relations are summarized in Figure 1-2.

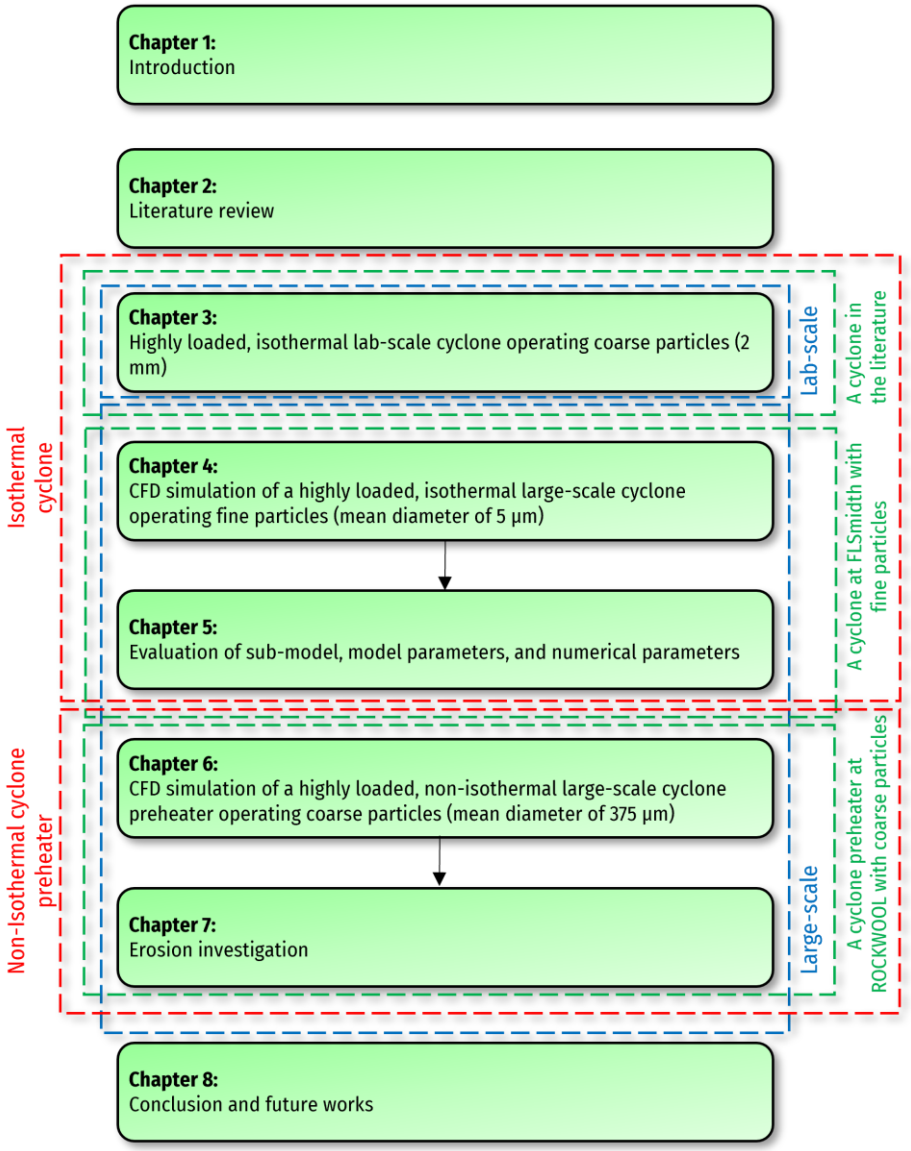

Figure 1-2. Summary of chapters of the thesis and their relations

1.4 Publications

The following journal articles are published during the PhD study regarding the studies presented in Chapters 4 and 5, respectively:

- M. Mirzaei, P.A. Jensen, M. Nakhaei, H. Wu, S. Zakrzewski, H. Zhou, W. Lin, A hybrid multiphase model accounting for particle agglomeration for coarse-grid simulation of dense solid flow inside large-scale cyclones, Powder Technol. 399 (2022) 117186. https://doi.org/10.1016/J.POWTEC.2022.117186.
- M. Mirzaei, P.A. Jensen, M. Nakhaei, H. Wu, S. Zakrzewski, H. Zhou, W. Lin, CFD-DDPM coupled with an agglomeration model for simulation of highly loaded large-scale cyclones: Sensitivity analysis of sub-models and model parameters, Powder Technol. (2022) 118036. https://doi.org/10.1016/J.POWTEC.2022.118036.

In addition, the following journal articles are under revision regarding the studies presented in Chapters 6 and 7, respectively:

- M. Mirzaei, S. Clausen, H. Wu, S. Zakrzewski, M. Nakhaei, H. Zhou, K. Jønck, P.A. Jensen, W. Lin, CFD simulation and experimental validation of multiphase flow in industrial cyclone preheaters.
- M. Mirzaei, S. Clausen, H. Wu, M. Nakhaei, H. Zhou, K. Jønck, P.A. Jensen, W. Lin, Investigation of erosion in an industrial cyclone preheater by CFD simulations.

2 Literature review

2.1 Introduction

CFD simulation of cyclones is a challenging task due to their complicated gas-solid flow field features, listed as follows, but not limited to [8]:

- High swirl intensity
- High turbulence intensity which is anisotropic due to the swirl
- High curvature of the streamlines
- Precessing vortex core (PVC)* and vortex breakdown
- Multiphase flow, phase interaction, inter-particle collisions
- Occurrence of agglomeration and breakage
- Being confined
- Being naturally unstable
- Adverse pressure gradients and recirculation zones

The gas-solid flow in industrial cyclone preheaters is even more complicated due to high solid load, high temperature, and heat transfer between gas and particles [4,11,12]. In addition, it should be noted that to resolve asymmetries and other details of the complex flow inside cyclones, full three-dimensional modelling is required. A successful simulation of cyclones needs a proper resolution of these flow features. To overcome the aforementioned challenges, some strategies and models should be considered which will be presented in the following section.

The advent of reliable and robust models and the rapid development of computers and computational fluid dynamics techniques enable detailed simulations of such a complex case. Although it is desired to mimic every physical effect in detail, this is not usually feasible or even required if the impact is minor. As a

* The inner vortex in the cyclone is unsteady and presents quasi-periodic and radially oscillations around the cyclone axis. This phenomenon is known as precessing vortex core (PVC). The PVC is representative of the positional displacement of the axis of the spinning body that precesses at a periodical frequency that raises the velocity fluctuations in the core region, and consequently a small rise in the velocity fluctuations of the outer region.

universal rule, more complex models require higher computational resources, so it is crucial to judge the balance between model complexity/accuracy and the resources required [13].

In the present study to capture the naturally unstable and fluctuating flow field, a proper turbulence model, to capture phase interaction and particle motion, a proper multiphase model accounting for potential particle-particle interactions, and to capture heat exchange between gas and particles, a proper heat transfer model are required to be applied and solved with mass, momentum, and energy conservation equations. Several turbulence models (including Reynolds Averaged Navier–Stokes (RANS), Large Eddy Simulation (LES), etc.), multiphase models (including one-way and two-way Discrete Phase Model (DPM), Discrete Element Model (DEM), Two-Fluid Model (TFM), Dense Discrete Phase Model (DDPM), etc.), and heat transfer models are developed in the literature some of which are available in commercial CFD packages. The selection of the right models depends on various factors:

- level of desired accuracy and resolution
- available computational resources
- abilities and disabilities and application range of each model, and their advantages and disadvantages over each other.

In this chapter, a short description of models used in the literature for the simulation of cyclones is provided. Furthermore, these factors for each model and the comparison of models in the simulation of cyclones are discussed to assist in a proper choice of models for the present study. This literature review is important to have a clearer understanding of the state of the art in the research of CFD simulation of cyclones.

2.2 CFD simulation of cyclones

The following are reviewed in this section:

- turbulence models, multiphase models and approaches for the gas-solid heat transfer modeling used in the literature for the CFD simulation of cyclones.
- CFD studies of cyclones categorized based on the models used.
- studies focusing on cyclones working under high temperatures or under high solid load, and studies focusing on industrial-scale cyclones or cyclone preheaters which are specific features of the cyclones in the present study.

These reviews were used as a basis for choosing appropriate models in the present study.

2.2.1 Turbulence modeling

The swirling flow in industrial-scale cyclones is highly and fully turbulent (cyclones commonly run at the range of $Re = 10^5 - 10^6$) [14]. In the principle of Direct Numerical Simulation (DNS), the entire range of turbulent flow structures is resolved using very fine grids, and Naiver–Stokes equations without using a turbulence model. At present, DNS is solely applicable for very small geometries and low Reynolds numbers, so industrial-scale equipment or even some laboratory-scale setups cannot be simulated using DNS [8]. Therefore, since the flow in cyclones is highly turbulent, it is crucial to utilize a proper turbulence model to capture the anisotropic turbulent flow inside them.

Turbulence models used in the literature to simulate cyclones can be classified into two groups based on their formulation as presented in Figure 2-1: (1) Reynolds Averaged Naiver–Stokes (RANS) turbulence models, (2) Large Eddy Simulation (LES) model. Several types of (RANS) turbulence models have been used in the simulation of cyclones which will be briefly discussed. A very short description of all these models (a more detailed description of each model can be found in CFD books [15,16]) and their advantages and disadvantages will be presented in this section, justifying the selection of the most suitable model in the present study. A more detailed explanation of the turbulence model (or models) that is chosen for this study will be presented later.

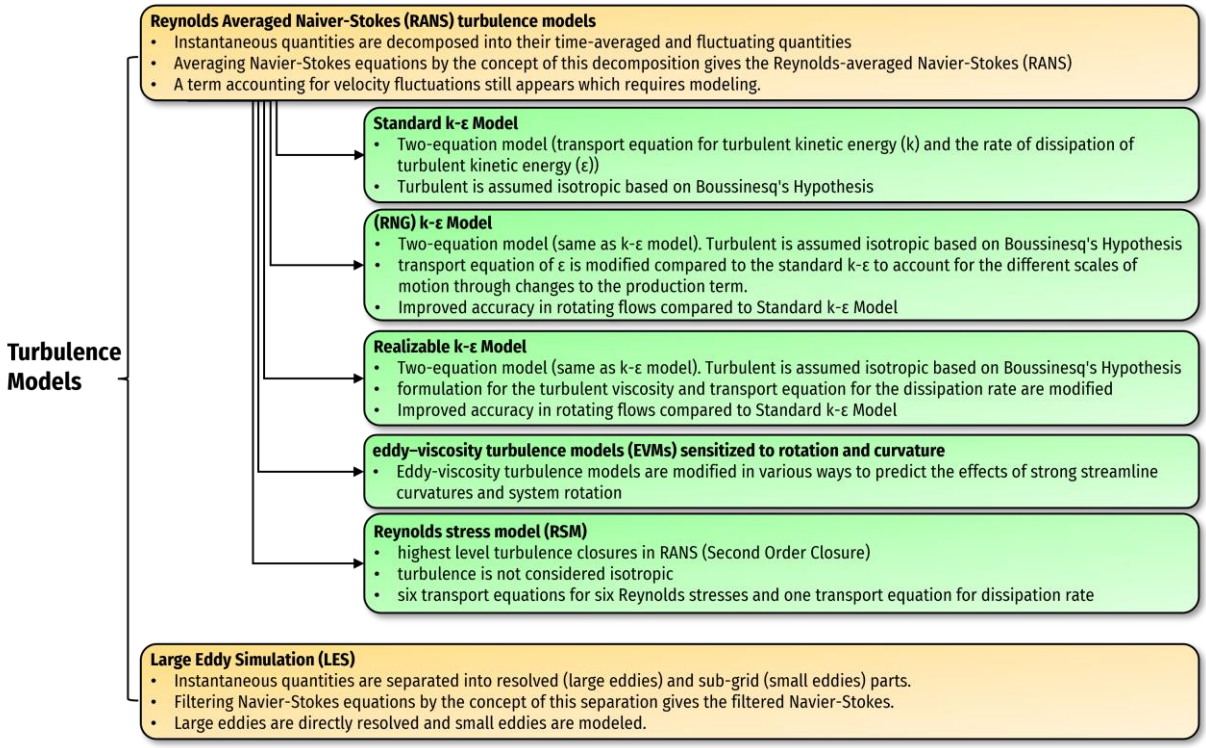

Figure 2-1. Categories of turbulence models used in the literature for the simulation of cyclones with a short description of them.

2.2.1.1 Reynolds Averaged Navier–Stokes (RANS) turbulence models

In these models, variables in Navier–Stokes equations are decomposed into the time-averaged and fluctuating components. This decomposition leads to Reynolds–averaged Navier–Stokes equations that are presented below in the Cartesian form [15,16]:

$$\frac{\partial \rho}{\partial t} + \frac{\partial}{\partial x_i}(\rho \overline{u_i}) = 0 \qquad 2\text{–}1$$

$$\frac{\partial}{\partial t}(\rho \overline{u_i}) + \frac{\partial}{\partial x_j}\left(\rho \overline{u_i}\,\overline{u_j}\right) = -\frac{\partial p}{\partial x_i} + \frac{\partial}{\partial x_j}\left[\mu\left(\frac{\partial \overline{u_i}}{\partial x_j} + \frac{\partial \overline{u_j}}{\partial x_i} - \frac{2}{3}\sigma_{ij}\frac{\partial \overline{u_k}}{\partial x_k}\right) + \frac{\partial}{\partial x_j}\left(-\rho\overline{u_i' u_j'}\right)\right] \qquad 2\text{–}2$$

here the instantaneous value (φ) is the sum of the mean value ($\bar{\varphi}$) and the fluctuating value (φ'). The stress term on the right-hand side (Reynolds stress) $R_{ij} \equiv \rho\overline{u_i' u_j'}$ is required to be modeled to close RANS

equations. RANS turbulence models are classified into several groups. The ones used in the literature for the simulation of cyclones are presented in this section.

2.2.1.1.1 Standard k-ε model

In the standard k-ε model, two transport equations for the turbulence kinetic energy and turbulence dissipation rate are solved to estimate Reynolds stress. An early attempt by Boysan et al. [17,18] which was confirmed by other authors [1,19–23] revealed that the standard k-ε turbulence model is incompetent for the simulation of swirling flows because it leads to nonsensical tangential velocities. It is due to the assumption of an isotropic turbulence structure in this model, while the turbulence inside cyclones is highly anisotropic in nature, so this model cannot suitably reflect the flow inside cyclones. However, due to its robustness and cost efficiency, it has been used to simulate cyclones in a few limited cases [24–28].

2.2.1.1.2 Renormalization Group (RNG) k-ε model

In this model, the standard k-ε model is refined to improve the model prediction accuracy in some flows. One of the aspects that is included in the RNG k-ε model is the effect of rotation on turbulence. This makes the RNG k-ε model more accurate compared to the standard model for simulation of swirling flow inside cyclones. An example of tangential velocity predictions using RNG k-ε is presented in Figure 2-2 (extracted from the study of Hoekstra et al. [29]).

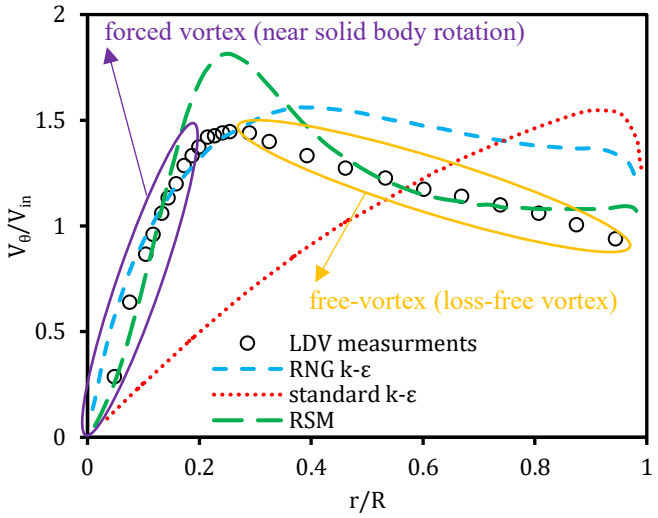

Figure 2-2. Comparison of tangential velocity profile normalized by inlet velocity obtained by standard k-ε, RNG k-ε, RSM, and LDV measurement in a Stairmand cyclone with a body diameter of 0.29 m and $Re = 2.8 \times 10^5$ provided by Hoekstra et al. [30] for a cyclone.

Although the accuracy of RNG k-ε is not comparable to more sophisticated turbulence models such as the Reynolds Stress Model (RSM) and Large Eddy Simulation (LES), the improvement compared to the standard version is clear [31–33]. While the model yet cannot predict the free vortex† distribution in some

† The flow inside an ordinary cyclone consists of an outer free-vortex (also known as near loss-free vortex) and a forced vortex (also known as near solid body rotation) at the core as shown in Figure 2-2.

cases [34] and underestimate pressure drop, it provides better prediction of flow pattern in some other cases compared to the standard version (12–20 % deviation from experimental data is reported) [35–37].

Gimbun et al. [35] noted that in simulation of cyclones at high temperatures (>850 K), only a marginal difference between RNG k-ε and more sophisticated turbulence models is observed.

2.2.1.1.3 Realizable k-ε model

In the realizable k-ε model, k-ε transport equations are modified to better capture features such as strong streamline curvature, vortices, and rotation. Thereby the model accuracy in simulation of cyclones, compared to the standard k-ε model, is improved [38].

It should be noted that none of the standard, RNG, and realizable k-ε models were designed for strongly swirling flow with high streamline curvature as in cyclones. These models are usually used when there are computational limitations or when prediction accuracy is of minor importance [39,40]. These models, which are known as conventional eddy–viscosity turbulence models (EVMs), should not be considered trustworthy for the simulation of cyclones, in particular in cyclones with a low sloid load where the swirl intensity is higher, and results from these models must always be checked with more sophisticated models and experimental data [41].

2.2.1.1.4 Eddy–Viscosity turbulence Models (EVMs) sensitized to rotation and curvature

The problem with conventional two-equation turbulence models which are known as eddy–viscosity turbulence models (EVMs) is that they fail to predict the effects of strong streamline curvatures. In fact, conventional EVMs including standard, RNG, and realizable k-ε models cannot represent the region of near loss-free rotation part observed close to the walls of swirling flows such as flow inside cyclones [8,42,43]. Despite the advances in computational power making the use of more complicated turbulence models, such as RMS and LES, more applicable, EVMs are still favored, because of their outstanding superiority in terms of robustness and computational cost. Thus, many researchers tried to modify EVMs to overcome their deficiencies.

As mentioned, one of the most serious deficiencies of EVMs is their incapability of catching the impacts of streamline curvature and system rotation which play a vital role in various turbulent flows, especially in cyclones. Thereby several approaches by several researchers [42,44–50] were proposed to make EVMs sensitized to rotation and curvature.

The approaches proposed by Smirnov et al. [47] (SSTCC model), Alahmadi et al. [42] (SSTCCM model), Zhang et al. [48] (SARCM model), and Dhakal et al. [49,50] (k-ω-υ^2 model) were used for the simulation of cyclones. A comparison of results from these models is shown in Figure 2-3 and Figure 2-4. These approaches are able to overcome weaknesses of EVMs in the simulation of cyclones and provide quite reliable results which are competitive with more complicated turbulence models while being robust and computationally cheap.

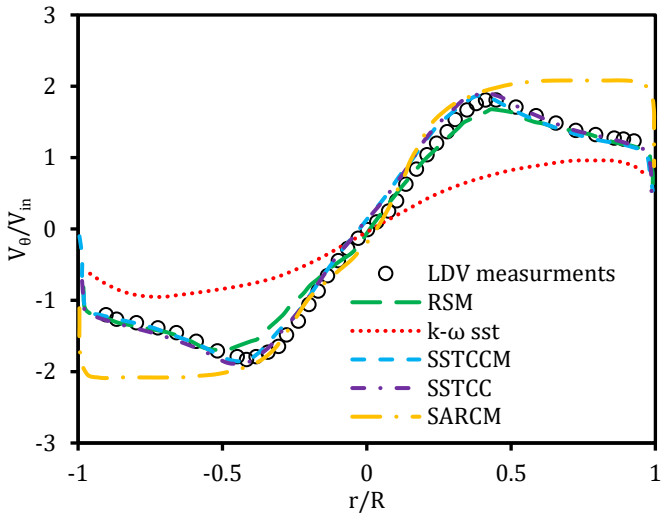

Figure 2-3. Comparison of tangential velocity profile normalized by inlet velocity obtained by RSM, k-ω sst, SSTCC, SSTCCM and SARCM turbulence models and LDV measurements in a cyclone provided by Alahmadi et al. [42]

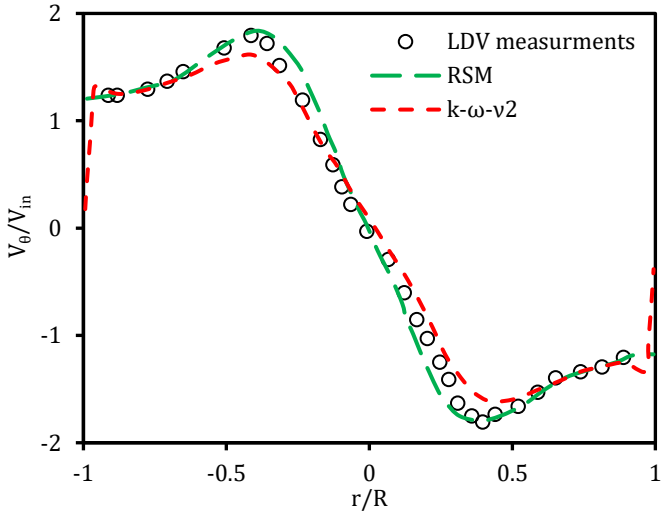

Figure 2-4. Comparison of tangential velocity profile normalized by inlet velocity obtained by RSM and k-ω-υ^2 turbulence models and LDV measurements in a cyclone provided by Dhakal et al. [49,50]

2.2.1.1.5 Reynolds Stress Model (RSM)

The most advanced RANS turbulence model is the Reynolds Stress Model (RSM), which provides better predictions in the case of complex flows where eddy–viscosity turbulence models might fail. As it was mentioned, the eddy–viscosity turbulence models (EVMs) are not able to capture the strong streamline curvatures of flow in cyclone separators. This issue is because eddy viscosity is considered isotropic in conventional EVMs based on the Boussinesq's hypothesis which might be untrue for highly swirling flows. In swirling flow inside cyclones, the tangential velocity component is roughly two orders of magnitude higher than other components, so its fluctuation levels are considerably higher meaning that the velocity fluctuations vary in each direction which is known as anisotropic turbulence. Therefore to better model the

actual complex flow inside cyclones, a turbulence model that leaves the isotropic eddy–viscosity hypothesis is required, and the Reynolds Stress Model (RSM) is one of them [51,52].

By resolution of transport equations for each of the six Reynolds stress components, RSM provides a more detailed picture of vortexes, velocity components, and pressure gradients and accounts for the impacts of swirl and stream curvature which are important parameters for simulation of cyclones. The ability of RSM in accurately modeling swirling flows with anisotropic turbulence, including cyclones, has been widely reported and confirmed in the literature [9,19,20,29,53,54].

RSM was successfully used for the simulation of cyclones working under high solid loads [9–11,55] or high temperatures [12,56–59] and for the simulation of industrial-scale cyclones [57,58,60] and preheater cyclones [26,61,62], so it is the preferred choice for the present study. RSM was coupled with various multiphase models (DPM with one-way coupling [63], DPM with two-way coupling [64,65], Eulerian–Eulerian approach [59], DEM [9,66], DDPM [10,55] and other hybrid models [11,67]) to simulate cyclones.

Including early works that were limited to EVMs due to computational limitations, our extensive literature survey shows that roughly 70 % of published works simulating cyclones have used RSM as the turbulence model, making it the most popular model in CFD simulation of cyclones. The superiority of RSM over conventional EVMs is clearly observed in Figure 2-2 and is confirmed by other authors [19,68]. RSM is reported to be able to predict not only mean values of velocity components but also fluctuations quite well which might be of importance for the simulation of the dispersed phase in cyclones [68]. It should be noted that RSM is the most complicated RANS turbulence model with high coupling between the equations, so in terms of robustness, convergence, and required computational resources, the RSM is inferior to simpler models.

Many researchers judge RSM's accuracy based on predictions of mean flow fields. However, it might be also important to predict fluctuating flow fields as the dispersed phase of a cyclone is affected by not only mean flow fields but also instantaneous fluctuating flow fields [69]. Several authors mentioned that in some cases even RSM is not able to predict fluctuating velocity profiles accurately in some regions (mainly the core region) of cyclones and profiles lie below the experimental values [53,69]. Besides, the inability of RSM to capture some characteristics of flow, such as precessing vortex core (PVC), is reported in the literature [29,34]. Regarding these issues, several points should be considered. These inabilities and inaccuracies were reported in the works that used RSM by a steady approach, while the nature of the flow and PVC (a quasi-periodic instability and a dominant characteristic of the flow) are unsteady. So, the fluctuating velocities could not be predicted precisely when a steady approach was used. In many cases, the application of an unsteady approach enabled the solver to capture the unsteady nature of PVC and solved this issue [13,53,70].

The superiority of unsteady RSM over Steady RSM in the simulation of a cyclone studied by Gronald et al. [13] is clearly observed in Figure 2-5 and is confirmed by other authors [53,70]. Although the use of an unsteady approach leads to longer run time and consequently a higher computational cost, due to the advent of high-performance computing, unsteady simulation of even large-scale cyclones seems feasible. On the

other hand, the application of a suitable discretization scheme and time step can improve the performance of RSM [53].

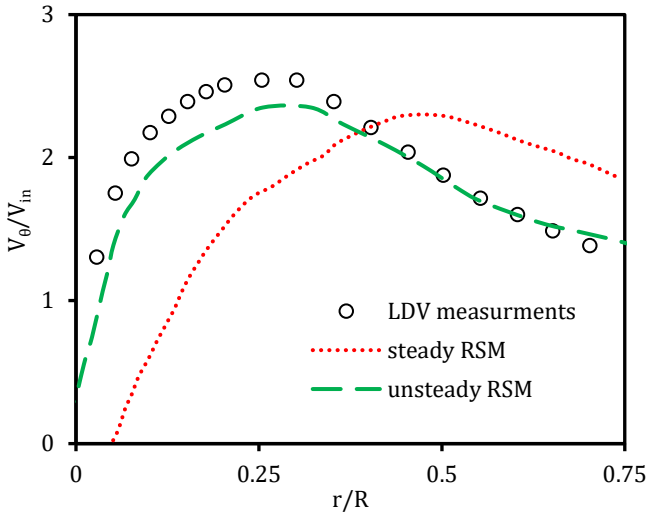

Figure 2-5. Comparison of tangential velocity profile normalized by inlet velocity obtained by steady RSM, unsteady RSM, and LDV measurement in a laboratory-scale cyclone with a body diameter of 0.4 m and $Re = 2.82 \times 10^5$ (based on the cyclone body diameter and the superficial inlet velocity) operating at ambient temperature and pressure provided by Gronald et al. [13].

2.2.1.2 Large Eddy Simulation (LES) turbulence model

Turbulent flows are defined by eddies with broad ranges of length and time scales [15,16]. In RANS turbulence models, eddies of all sizes are modelled spatially, and in DNS, eddies of all sizes are resolved directly. There is another model known as the Large Eddy Simulation (LES) turbulence model that falls between RANS and DNS; by applying a spatial filter on Navier–Stokes equations, small eddies are filtered out and modeled, while the large ones are resolved directly by solving the filtered Navier–Stokes equations. In other words, the effect of small eddies on the momentum equation is expressed as a sub-grid-scale (SGS) stress term in the filtered Navier–Stokes equations (equations 2–3 and 2–4), and this stress term ($\tau_{ij} \equiv \rho\overline{u_i'u_j'} - \rho\bar{u}_i\bar{u}_j$) requires modeling. There are different variations of LES model and some were used to model cyclones [4,13,19,52,69,71–75]. The details of each model are not discussed here. It should be considered that to directly resolve large eddies, considerably fine meshes are required for this model, in particular, close to walls where eddies are small but contain a high amount of energy. The filtered Navier–Stokes equations are written as follows:

$$\frac{\partial \rho}{\partial t} + \frac{\partial}{\partial x_i}(\rho\bar{u}_i) = 0 \qquad 2\text{–}3$$

$$\frac{\partial}{\partial t}(\rho\bar{u}_i) + \frac{\partial}{\partial x_j}\left(\rho\bar{u}_i\bar{u}_j\right) = -\frac{\partial \bar{p}}{\partial x_i} + \frac{\partial}{\partial x_j}\left[\mu\left(\frac{\partial \bar{u}_i}{\partial x_j} + \frac{\partial \bar{u}_j}{\partial x_i} - \frac{2}{3}\sigma_{ij}\frac{\partial \overline{u_k}}{\partial x_k}\right) - \frac{\partial}{\partial x_j}\left(\rho\overline{u_i'u_j'} - \rho\bar{u}_i\bar{u}_j\right)\right] \qquad 2\text{–}4$$

Where the instantaneous value (φ) is the sum of the directly resolved component ($\bar{\varphi}$) and the modelled subgrid component (φ').

Regarding velocity profile, the LES turbulence model is reported to provide slightly better predictions of single-phase cyclonic flow compared to RANS turbulence models both in terms of tangential and axial

velocities [43]. Minor superiority of LES over RANS turbulence models can be observed in Figure 2-6 provided by Slack et al. [19] and it is confirmed by other authors [13,72,73,76]. Even RSM which is the most sophisticated RANS turbulence model is reported to underpredict the peak of the mean tangential velocity. By better capturing the unsteady oscillation of flow by a precessing vortex core (PVC) leading to better prediction of flow patterns, LES is reported to be superior in the prediction of the pressure drop inside cyclones [43].

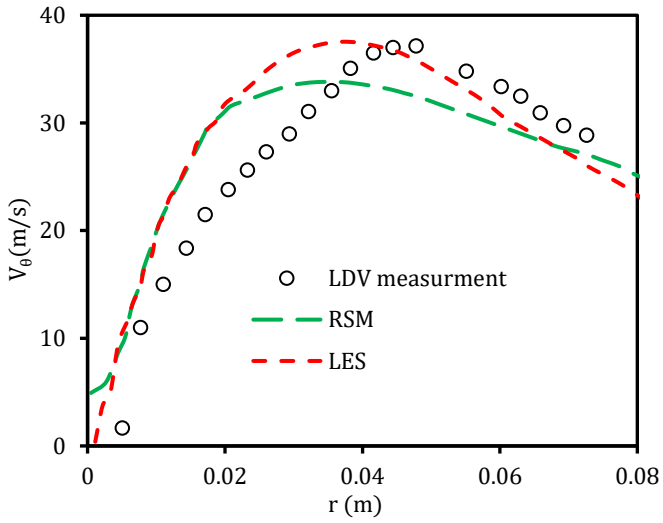

Figure 2-6. Comparison of tangential velocity LES, RSM, and LDV measurement in a Stairmand cyclone with a body diameter of 0.205 m and $Re = 2.74 \times 10^4$ (based on the cyclone body diameter and the superficial inlet velocity) operating at ambient temperature and pressure provided by Slack et al. [19].

As it was mentioned, the dispersed phase is affected by turbulence fluctuations. RANS turbulence models only provide mean velocity values and velocity fluctuations are not calculated explicitly, so the effect of turbulence fluctuations on particle motion is generally taken into account using a stochastic model such as the Discrete Random Walk Model (its detail will be presented later) which sometimes needs parameter tuning that might not be applicable for different cyclone geometries and operating conditions [52]. But in the LES turbulence model since directly resolved velocity fluctuations (that are much stronger than the sub-grid-scale fluctuations) are explicitly calculated, much less stochastic modeling of particle motion is required compared to RANS simulations. Thus, the superiority of LES over RANS becomes more sensible in the simulation of multiphase flow and estimation of separation efficiency which might be affected by velocity fluctuations [19,52].

Although the LES turbulence model seems to be superior to RANS turbulence models in different aspects, its inferiority in terms of computational cost is of great importance and should not be neglected. LES needs very fine grids to resolve large eddies. Besides, LES is an unsteady model, and it requires a comparatively long flowtime run to acquire stable statistics of the flow. In addition, since energy-containing eddies are comparatively small around the wall, LES requires very high-density mesh near walls to capture the boundary layer, so it becomes even more costly in confined geometries (practically, it cannot be used in confined geometries with very high Reynolds number) which is the case in the simulation of cyclones. Due to the necessity of fine grids, it becomes even more impractical in the simulation of industrial-scale

geometries as the use of LES for the simulation of industrial-scale cyclones has not been reported in the literature yet. Therefore, considering the above-mentioned limitations of LES, it seems that RANS turbulence models are more practical in the case of industrial-scale cyclone separators because they are computationally cheap and provide quite acceptable predictions.

2.2.1.3 Conclusions on turbulence modeling

In Table 2-1, a qualitative evaluation matrix of turbulence models used in the literature for the simulation of cyclones is provided to make a better comparison of them. Considering that sensitized EVMs, RSM, and LES at least capture the mean flow field in cyclones and the fact that LES is considerably more expensive so that its application in large-scale cases is questionable, RSM and sensitized EVMs seems to be suitable options for the simulation of cyclones in our study. Regarding the robustness of sensitized EVMs and their superiority over RSM in terms of computational cost, which is of great importance in our case, sensitized EVMs are preferred and should be tried to see whether they can provide results that are reliable enough for our case or not. If not, then RSM must be used to achieve the desired accuracy.

It should be also noted that in the CFD simulation of industrial-scale cyclones with complex geometries, it is possible to find regions with low grid quality that are challenging to repair. In such a case, EVMs that are more stable and robust, compared to RSM, and can provide stable converging solutions even with relatively low-quality grids are highly preferable.

Table 2-1. Qualitative evaluation matrix of turbulence models used in the literature for the simulation of cyclones. The signs show the level of superiority or inferiority: ++ as the highest level of superiority and -- as the highest level of inferiority.

Model	Standard k-ε	RNG k-ε	Realizable k-ε	Sensitized EVMs	RSM	LES
Capturing mean flow field in cyclones	--	-	-	++	++	++
Capturing fluctuating flow field in cyclones	--	--	--	~	+	++
Capturing anisotropy in turbulence	--	--	--	--	++	++
Sensitivity to rotation and curvature	--	~	~	++	++	++
Robustness	++	++	++	++	-	--
Resolution	--	--	--	-	+	++
Computational efficiency	++	++	++	++	~	--

2.2.2 Multiphase flow modeling

The gas-solid multiphase flow inside a cyclone is considered particle-laden flow, due to the presence of discrete particles in a continuous gas which is basically the definition of particle-laden multiphase flow. Depending on the presence or absence of considerable interaction between particles, which relies on interparticle spacing and hence solid volume fraction, particle-laden flows can be categorized into dilute and dense flows. On the other hand, Based on the solid volume fraction, the interaction between two phases can be divided into three groups: one-way, two-way, and four-way coupling interactions (see Figure 2-7) [8,77].

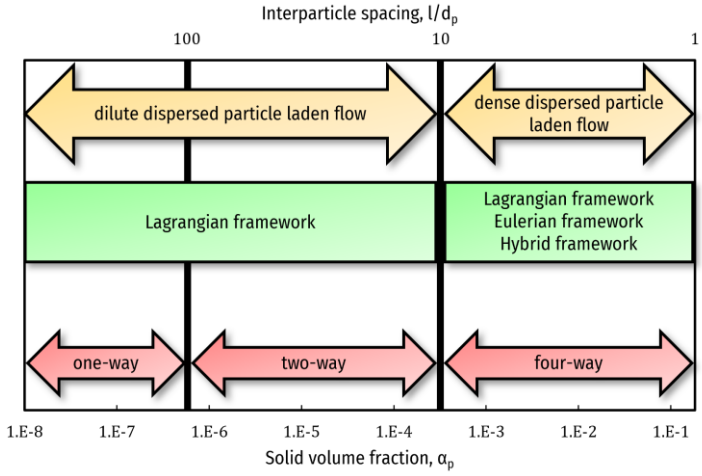

Figure 2-7. Types of interactions in particle-laden flows mapped based on the solid volume fraction and inter-particle spacing. Note that the borderlines are approximate [8,77].

For very low values of solid volume fraction (where the interparticle spacing, l/d_p, is greater than 100), the effect of particles on the fluid is negligible while the particles are dispersed by the fluid. The interaction between particles and the fluid is termed one-way coupling.

For moderate values of solid volume fraction (where $10 < l/d_p < 100$), particles and the fluid mutually influence each other, but the distance between particles is still too far that they do not influence each other. This interaction is termed two-way coupling.

For high values of solid volume fraction (where $1 < l/d_p < 10$), in addition to the two-way coupling between the particles and fluid, particles are close enough to each other so that particle-particle interactions, i.e., direct collision and indirect impact through the nearby flow field, and consequently, possible particle break-up, agglomeration and attrition, cannot be neglected. The interaction is termed four-way coupling.

Cyclones are applicable in the whole range of particle-laden flows, so depending on the value of the solid volume fraction of the studied cyclone, one-way, two-way, or four-way coupling should be considered to model multiphase interactions in cyclones [8].

Depending on the framework by which the dispersed phase is treated, multiphase modeling of particle-laden flows can be divided into two types: Lagrangian (known also as Eulerian–Lagrangian framework), and Eulerian (known also as Eulerian–Eulerian framework) [78]. Generally, to model dilute particle-laden flows where considering one-way or two-way coupling is sufficient, the Lagrangian framework is applied. On the other hand, to model dense particle-laden flows, each of the frameworks can be applied based on the polydispersity of the particles, their size and load, desired accuracy, and level of output information (whether some information such as particle location and velocity is desired or not), availability of computational resources, etc.

In the following sections, multiphase models used for CFD simulations of cyclones are categorized based on the level of coupling (summarized in Figure 2-8) and explained and reviewed briefly.

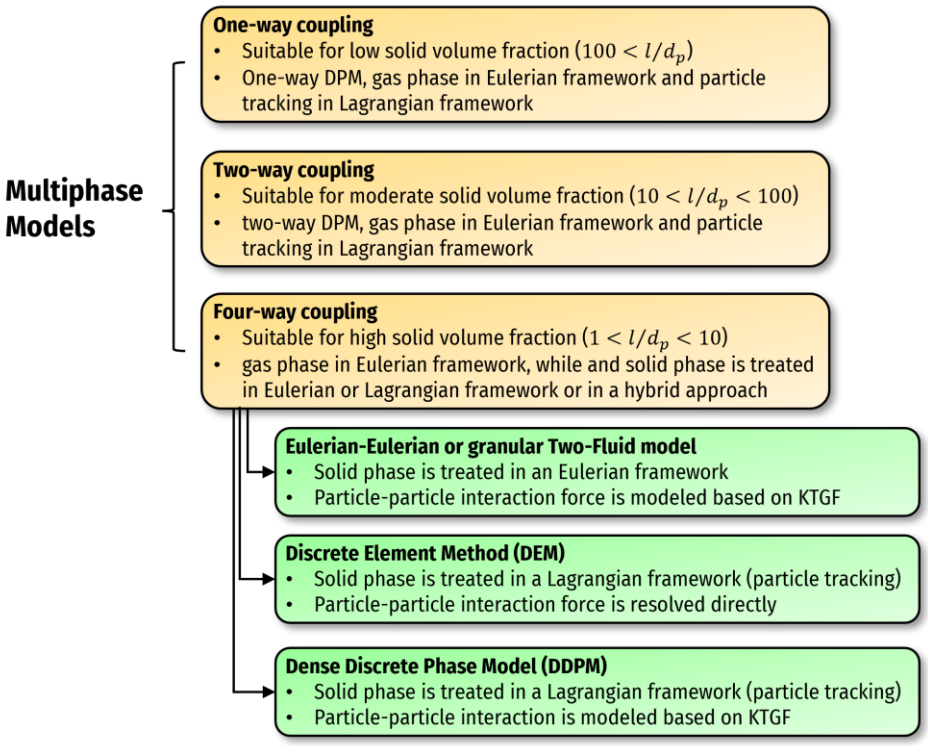

Figure 2-8. Categories of common multiphase models used in the literature for the simulation of cyclones with a short description of them.

2.2.2.1 One-way coupling

As it was stated, to model one-way coupled particle-laden flows, the Eulerian-Lagrangian approach (also referred to as one-way Discrete Phase Modeling, DPM) can be applied, where the gas flow is treated as a continuum and modeled in an Eulerian framework, and solids are tracked in a Lagrangian frame without influencing the fluid phase.

The motion of particles can be modeled by applying Newton's laws of motion for each of the particles (or parcels as representative of several particles with the same properties) in a Lagrangian framework. When the gas phase is modeled, the forces acting on particles can be calculated. Thus, a force balance on each particle can be written which leads to the calculation of particle acceleration by applying Newton's second law, and consequently, the particle can be tracked. The dispersed phase is represented by a number of computational particles whose trajectories (x_{pi}) can be computed by integrating the following equation:

$$\frac{dx_{pi}}{dt} = u_{pi} \qquad 2\text{–}5$$

Where u_{pi} can be calculated by integrating the equation of the translational motion for particle i obtained from force balance:

$$m_{pi}\frac{d\vec{u}_{pi}}{dt} = m_{pi}\frac{18\mu}{\rho_p {d_p}^2}\frac{C_D Re_p}{24}\left(\vec{u}_g - \vec{u}_{pi}\right) + m_{pi}g\frac{\rho_p - \rho_g}{\rho_p} + \vec{F}_{virtual\ mass} + \vec{F}_{Basset} + \vec{F}_{pressure\ gradient} + \vec{F}_{Thermophoretic} + \vec{F}_{Brownian} + \vec{F}_{Saffman\ Lift} + \vec{F}_{Magnus\ Lift} \quad (2–6)$$

Generally, $\vec{F}_{virtual\ mass}$, the unsteady force needed to accelerate the fluid surrounding the particle, $\vec{F}_{Basset}$, the unsteady force due to temporal delay in boundary layer development as the relative velocity varies with time, and $\vec{F}_{pressure\ gradient}$, the extra force because of the pressure gradient in the fluid become important when the density ratio of the dispersed phase to the continuous phase approaches unity. In the case of gas-solid cyclones, these terms can be neglected [79]. $\vec{F}_{Thermophoretic}$, the force due to a temperature gradient in the continuous phase, and $\vec{F}_{Brownian}$, the force due to the discrete nature of molecular motion become important when particles are very fine [79], so these terms can be neglected in the simulation of ordinary gas-solid cyclones.

On the other hand, $\vec{F}_{Saffman\ Lift}$, the lift force due to the pressure distribution established on a particle in a velocity gradient field, and $\vec{F}_{Magnus's\ Lift}$, the lift force established due to the rotation of the particle might play a role in the simulation of cyclones [75,80]. However, in most studies, these two terms were considered minimal compared to drag and body forces and were neglected. Although $\vec{F}_{Saffman\ Lift}$ can be directly computed using provided expressions, to calculate $\vec{F}_{Magnus\ Lift}$ the relative rotation of the particles and thus the angular velocity of the particles (ω_p) are required which can be obtained by an additional ODE equation for the rotational motion. This ODE can be derived from particle torque balance.

The separation process in cyclones reflects the competition between the motion of particles to the outer wall of the cyclone due to centrifugal force (due to mean tangential velocity), and the motion of particles due to the presence of velocity fluctuations (this motion is known as turbulent dispersion) that disperses the particle throughout the entire volume. Therefore, the prediction of velocity fluctuations is important. RANS turbulence models do not provide predictions of velocity fluctuations; they only provide mean velocity values and Root Mean Square (RMS) of velocity fluctuations (in EVMs estimated based on turbulent kinetic energy, k, and in RSM directly calculated). So as the value of velocity fluctuation is not available in RANS turbulence models to predict the dispersion of the particles due to the time-dependent turbulence fluctuations, a model is required which might lead to a reduction in the accuracy of separation efficiency prediction. Besides, despite its ability to reliably predict mean velocity values in cyclones, even RSM as the most sophisticated RANS turbulence model is reported in some cases (mostly steady simulations) to underpredict RMS of velocity fluctuations which intensifies this inaccuracy. On the other hand, In LES because the majority of velocity fluctuations are resolved directly, the impact of the model required to capture time-dependent minor sub-grid-scale fluctuations on particle motion is slight which makes LES superior in the prediction of separation efficiency cyclones using one-way coupling.

Considering these, a proper model to capture the effect of velocity fluctuations on the motion of particles should be applied in one-way DPM for better particle tracking. Due to its simplicity and reliable agreement with measurements in many applications, a stochastic model known as Random Walk is widely used to model particle dispersion by turbulence in cyclones [20,30,43,81,82]. In the Random walk Model,

fluctuating particle velocity can be represented in two approaches: discrete random walk (DRW) [20,43,81,82] and continuous random walk (CRW) [30,43]; the former is more frequently used for the simulation of particle motion in cyclones due to its reported validity and its availability in commercial CFD packages. DRW was used both with RANS [20,43,81,82] and LES [69,71,72] turbulence models. As it was mentioned, for LES, only the effect of sub-grid-scale turbulence is required to be modeled by a stochastic model, so in some studies, by assuming that the influence of sub-grid-scale turbulent structures on particle motion is minor, no particle dispersion model was applied [52].

2.2.2.2 Two-way coupling

As it was stated, for moderate values of solid volume fraction (where $10 < L/d_p < 100$) normally an Eulerian–Lagrangian approach that takes the momentum transfer from the particles to the fluid into account should be applied which is known as two-way coupling. The difference between one-way and two-way coupling is mainly that a force term is added in the momentum conservation equation in two-way coupling to account for the effect of the moving particles on the fluid phase flow.

A summary of the most cited CFD studies of gas-solid cyclones using one-way and two-way coupling is presented in Table 2-2 and Table 2-3 respectively. As presented in these tables, RSM and LES as the turbulence model and Ansys Fluent as the solver are more popular. It should be noted that most of the investigations were done on lab-scale cyclones.

Table 2-2. Details of most cited CFD studies on gas-solid multiphase flow in cyclones using one-way coupling approach

Author	Cyclone diameter (m)	Particle size (μm)	Turbulence model	CFD solver	Validation
Wang et al. [20]	0.2	30	RSM	Fluent	Flow pattern data, pressure drop, and separation efficiency measured by the authors
Elsayed et al. [22,70,71]	0.031	0.025–10	RSM, LES	Fluent	Flow pattern data, pressure drop, and separation efficiency measured by Hoekstra et al. [29,30] and Shukla et al. [53]
Chuah et al. [21]	0.031	0.5–4	RNG, RSM	Fluent	pressure drop and separation efficiency measured by Xiang et al. [83]
Bernardo et al. [84]	0.1, 0.29, 0.3	26	RSM	CFX	Flow pattern data measured by Yuu et al. [85], and Patterson et al. [86]
De Souza et al. [52]	0.03	0.5–6	LES	Developed	Flow pattern data measured by Hoekstra et al. [30] and separation efficiency measured by Xiang et al. [83].
Safikhani et al. [81]	not mentioned	0.026–3.4	RSM	Fluent	pressure drop and separation efficiency measured by Zhu et al. [87].
Brar et al. [88]	0.29	0.3–6.8	RSM	Fluent	Flow pattern data measured by Hoekstra et al. [30]. and separation efficiency measured by Zhao et al. [89].

Table 2-3. Details of most cited CFD studies on gas-solid multiphase flow in cyclones using two-way coupling approach

Author	Cyclone diameter (m)	Particle size (μm)	Turbulence model	CFD solver	Validation
Derksen et al. [73]	0.29	not mentioned	LES	Developed	Pressure drop measured by Yuu et al. [85]
Wan et al. [63]	0.3	1.5–18	RSM	Fluent	separation efficiency measured by the authors
Derksen et al. [69]	0.09	5	LES	Developed	Flow pattern data measured by Obermair et al. [90]
Sedrez et al. [65]	0.15	64	RSM	Fluent	Pressure drop and erosion rate measured by the authors
Zhou et al. [91]	0.2	18	RSM	Fluent	Pressure drop measured by the authors
Huang et al. [64]	0.07	2	RSM	Fluent	Pressure drop measured by the authors

2.2.2.3 Four-way coupling

As it was mentioned, in dense dispersed particle-laden flow, interparticle interactions and the indirect impact of particles on each other through the nearby flow field become important and should be modeled, i.e., four-way coupling, to have a reliable simulation. Based on the framework, by which the dispersed phase is treated, multiphase modeling of dense dispersed particle-laden flows can be divided into three types: Discrete Element Method (DEM), Eulerian–Eulerian or granular Two-Fluid model (TFM), and hybrid multiphase model. Each of these models, their applications, and their advantages and disadvantages are discussed briefly in the following subsections.

2.2.2.3.1 Eulerian–Eulerian or granular Two-Fluid model (TFM)

In contrast to the Eulerian–Lagrangian models that are based on the tracking of individual particles, the Eulerian–Eulerian model considers the multitude of the particles as an artificial continuous solids phase. In this model, both solid and gas phases are treated as interpenetrating continua each governed by conservation equations. The Kinetic Theory of Granular Flow (KTGF) approach is applied to the dispersed phase momentum equation to account for particle interaction. Because the volume of each phase cannot be also occupied by the other phases at the same time, a volume fraction for each phase is defined based on the distribution of each phase leading to a transformation of conservation equations for the gas and solid phase. The conservation equation can be written for the gas phase as follows:

$$\frac{\partial(\rho_g \alpha_g)}{\partial t} + \nabla.(\alpha_g \rho_g u_g) = 0 \qquad 2\text{–}7$$

$$\frac{\partial}{\partial t}(\alpha_g \rho_g u_g) + \nabla.(\alpha_g \rho_g u_g u_g) = -\alpha_g \nabla p_g + \nabla.\alpha_g\left[\mu_g\left(\nabla u_g + \nabla {u_g}^T\right) + \left(-\rho\overline{u_i' u_j'}\right)\right] + f_{g,drag} + f_{g,added} \qquad 2\text{–}8$$

Where $f_{g,drag}$ is the drag force applied on gas phases by the solid phase (s) and $f_{g,added}$ are other forces applied to the fluid including external body force, lift force, turbulent dispersion force and so on that might play a role in some cases. On the other hand, the conservation equation for solid phase (s) can be as follows:

$$\frac{\partial(\rho_s \alpha_s)}{\partial t} + \nabla.(\alpha_s \rho_s u_s) = 0 \quad 2\text{–}9$$

$$\frac{\partial}{\partial t}(\alpha_s \rho_s u_s) + \nabla.(\alpha_s \rho_s u_s u_s) = -\alpha_s \nabla p_s + \alpha_s \rho_s g + \nabla.\alpha_s \bar{\bar{\tau}}_s + f_{s,drag} + f_{s,added} \quad 2\text{–}10$$

In the granular TFM it is assumed that some energy is transferred from the mean flow toward chaotic fluctuations of the particles due to interparticle collisions, so to model interparticle interaction, the behavior of the kinetic energy of these fluctuations should be described which is done by an additional transport equation for the granular temperature [92]. The addition of this transport equation results in additional terms in momentum conservation for the solid phase such as granular pressure force or the solids stress tensor which are meant to account for interparticle interactions. In addition to this transport equation, some modeling and equations are required for $f_{s,drag}$ (due to gas-solid interaction) and $f_{s,added}$ terms to close the momentum conservation for the solid phase. A more detailed description of this approach and details of these additional terms and equations can be found in the literature [93,94].

This approach has been widely used for the simulation of gas-solid multiphase flow in many applications, especially for the simulation of fluidized beds where its suitability has been proven [93,95]. This approach cannot treat different particle sizes in one solid phase, so every size class must be considered as a distinct phase meaning that each representative particle diameter needs an additional mass and momentum conservation equation which leads to a significant increase in the required computational recourses and solution instabilities. Therefore, applying this approach to multiphase flow with ploy-dispersed particle size distributions which is the case in most cyclone separators is quite hard. Furthermore, this approach demands noticeably fine grids since the minimum stable sizes of cells are around ten particle diameters [96]. Besides, this model does not provide particle trajectories which in some cases, such as the study of erosion in cyclones, is crucial. Another deficiency of this approach is that it neglects the impact of particle rotation which might play a role in some cases. Considering all these advantages and disadvantages, this approach has been used for the simulation of cyclone working at high solid loads [26–28,59,97]. A summary of CFD studies of gas-solid cyclones using this approach is presented in Table 2-4; the following points are drawn from this table:

- Ansys Fluent is not the dominant solver as in one-way and two-way coupling.
- Simpler turbulence models (compared to the ones used in one-way and two-way coupling) are used to stabilize the solution.
- In some cases, only one solid phase is considered which makes the predictions, especially separation efficiency predictions, questionable.
- Large-scale cases have been investigated by this method.

Table 2-4. Details of CFD studies on gas-solid multiphase flow in cyclones using the Eulerian–Eulerian four-way coupling approach

Author	Cyclone diameter (m)	Particle size (μm)	Solid volume fraction	Turbulence model	Number of solid phases	CFD solver	Validation
Meier et al. [94]	0.315	1430	0.000003	k-ε	1	Developed	-
Vegini et al. [97]	0.3	6	0.000002	k-ε	1	Developed	Separation efficiency and pressure drop measured by Zhao et al. [98]
Cristea et al. [59]	Industrial scale	1–192	around 0.0007	RMS	4	Fluent	separation efficiency and pressure drop measured by the authors
Mariani et al. [26,27]	6	30–120	around 0.00012	RSM	1	Star-CCM	Heat transfer rate measured by the authors
Luciano et al. [28]	1	4–15	up to 0.0007	k-ε	5	Developed	Pressure drop measured by the authors

2.2.2.3.2 Discrete Element Method (DEM)

In DEM multiphase model, unlike the TFM model, only the gas phase is treated in the Eulerian framework and the solid phase is treated in the Lagrangian framework. Therefore, regarding the considerable volume of the solid phase, the governing equations of gas-phase are the same as those used in granular TFM (equations 2–7 and 2–8). The difference between two-way DPM and DEM in particle tracking is that extra force terms are added in the momentum conservation equation in DEM coupling to account for the effect of particle-particle interactions (see equation 2–11). Unlike, one-way and two-way coupling where f_{drag} depends only on the relative velocity between the particle and fluid, here it also depends on the presence of neighboring particles, so it is also a function of solid volume fraction which can be expressed by a correlation.

$$m_{pi}\frac{d\vec{u}_{pi}}{dt} = f_{drag} + f_{body} + \vec{F}_{virtual\,mass} + \vec{F}_{Basset} + \vec{F}_{pressure\,gradient} + \vec{F}_{Thermophoretic} + \vec{F}_{Brownian} + \vec{F}_{Saffmans\,Lift} + \vec{F}_{Magnus\,Lift} + \sum_{j=1}^{N}\vec{F}_{collision,ij} \quad 2\text{–}11$$

The concept behind DEM modeling which was first introduced by Cundall and Strack [99] is to model particle-particle and particle-wall interactions by accounting for the forces resulting from the collisions. To model these interactions, particles are considered as soft spheres (soft-particle collision method) which are allowed to have a small overlap when colliding with each other instead of having physical deformation. Accordingly, based on the overlapping distance, repulsive interparticle normal and tangential contact forces are defined. In addition to contact forces, normal and tangential viscous damping forces are also defined to model the energy loss due to the collision. Thus, $\vec{F}_{collision}$ is defined as in equation 2–12 where normal and tangential contact and viscous damping forces can be calculated by existing models [79].

$$\vec{F}_{collision,ij} = \vec{F}_{\text{normal contact},ij} + \vec{F}_{\text{tangential contact},ij} + \vec{F}_{\text{normal damping},ij} + \vec{F}_{\text{tangential damping},ij} \quad 2\text{–}12$$

The Discrete Element Method (DEM) has been extensively used for the simulation of gas-solid flows [100–102] in general and the simulation of cyclones working at high solid loads in particular. summary of CFD studies of gas-solid cyclones using this approach is presented in Table 2-5; the following points are drawn from this table:

- Ansys Fluent is the dominant solver. In some cases, it is coupled with another software for better DEM calculation.
- Unlike in the Eulerian–Eulerian model where simple two-equation turbulence models are commonly used to stabilize the solution, in DEM, more complex turbulence models (RSM and LES) are commonly used.
- Since DEM is computationally expensive, the studies are limited to lab-scale cases and large particles (the finer particles, the more particles to be tracked, and the more computationally expensive).

Table 2-5. Details of CFD studies on gas-solid multiphase flow in cyclones using DEM four-way coupling approach

Author	Cyclone diameter (m)	Particle size (μm)	Solid volume fraction	Turbulence model	Solver	Validation
Chu et al. [9]	0.2	2000	Up to 0.0012	RSM	Fluent	Single-phase flow pattern data measured by Yuu et al. [85] and pressure drop measured by the authors
Wei et al. [66]	0.3	2000	Up to around 0.0086	RSM	Fluent coupled with EDEM	Pressure drop measured by the authors and estimated by empirical correlation
Wang et al. [51]	0.2	2200	Very low	RSM	Fluent coupled with EDEM	Flow pattern data, pressure drop, and separation efficiency measured by Hoekstra et al. [29,30]
Fulchini et al. [103]	0.04	200–500	Up to around 0.0001	not mentioned	Fluent coupled with EDEM	No validation
Zhou et al. [104]	0.29	2000–2800	Up to 0.0001	RSM	Fluent	Single-phase flow pattern data measured by Hoekstra et al. [29,30] and pressure drop measured by the authors
Sgrott et al. [74]	0.29	0.5–60	Up to 0.0001	LES	OpenFOAM	Single-phase flow pattern data measured by Hoekstra et al. [29,30]

As it was mentioned, this approach is usually used for high solid loads multiphase flows where the number of particles is comparatively too high. In this model, the interparticle interaction of each two particles must be calculated, so a considerable computational resource is required. As the solid load increases or particle size decreases, this becomes more intensified so that it might not be applicable for very high solid loads or very fine particles or industrial-scale simulations which are the case in the present study. Although, applying the concept of parcels (coarse-graining) might improve computational efficiency, still, in many cases, a very large number of parcels (grains) are required to model practical systems. However, it should be mentioned that, unlike granular TFM which has difficulties in modeling polydispersed particles, DEM can

easily handle such particles. Besides, unlike granular TFM, this model can provide dynamic information about particles, such as the trajectories and forces acting on them, which are very valuable in some studies as sometimes such information is not even accessible by experimental measurements [105]. Another advantage of this model compared to granular TFM and also the Hybrid multiphase model (which will be discussed in the following section) is that here fewer closure models are required for the solid phase meaning that the particle motion is more directly resolved (particle flow is resolved down to the particle level) leading to more accurate multiphase simulation.

2.2.2.3.3 Hybrid Eulerian–Lagrangian framework

Methods described in the two previous sections are known as conventional four-way coupling methods where the solid phase is treated either in an Eulerian or Lagrangian framework. As it was mentioned, both these approaches have their advantage and disadvantage. Considering all these advantages and disadvantages, a hybrid Eulerian–Lagrangian treatment of solid phase benefiting the advantages of both frameworks and avoiding their disadvantages as much as possible can be a great solution for the simulation of highly loaded particle-laden flows. For this purpose, several authors have developed various hybrid models in which the solid phase is treated in a hybrid Eulerian–Lagrangian framework (the fluid phase is still treated in an Eulerian framework).

Hybrid Eulerian–Lagrangian models can be divided into three groups [106]: (1) Lagrangian-based hybrid model where particle trajectories and interparticle interactions are indirectly estimated, (2) Eulerian-based hybrid model where the effect of poly-disparity on the conservation equations of mass and momentum of solid phase can be included by tracing passive Lagrangian particles, and (3) domain decomposition method where the granular TFM model could cover dense particle regions because in that region inter-particle collisions tend to be dominant while the Lagrangian model might be applied to dilute particle regions.

A summary of CFD studies of gas-solid cyclones using a hybrid approach is presented in Table 2-6; the following points are drawn from this table:

- Ansys Fluent is the dominant solver in the hybrid method as well.
- The Lagrangian-based hybrid model is more common than the other two.
- Hybrid models can be easily coupled with complex turbulence models such as RSM.
- Large-scale cases and cases operating fine particles have been investigated by this method.

Since one of the hybrid Eulerian–Lagrangian multiphase models known as the Dense Discrete Phase Model (DDPM) is more developed compared to others and is available in Ansys Fluent as a commercial CFD package and is also used for other applications than cyclones, this approach will be discussed in more detail in the following section.

Table 2-6. Details of CFD studies on gas-solid multiphase flow in cyclones using Hybrid Eulerian–Lagrangian four-way coupling approach. The ones marked with * studied industrial-scale cyclones.

Author	Cyclone diameter	Particle size (μm)	Solid volume	Turbulence model	Hybrid type	Solver	Validation
Pirker et al. [67]	0.3	2–100 monodispersed	around 0.0038	RSM	domain decompositio	Fluent	No validation
Pirker et al. [108]*	1.6	1–100	up to 0.0038	RSM	Eulerian based	Implemented to Fluent	Pressure drop, separation efficiency, grade efficiency measured by the authors and estimated by correlations of Muschelknautz [107]
Schellander et al. [80]	0.3	0.55–6.15	up to 0.0012	not mentioned	Eulerian based	Developed	Grade efficiency measured by the authors and estimated by correlations of Muschelknautz [107]
Schneiderbauer et al. [11]*	2.5	0.6–500	0.0001	RSM	Lagrangian based	Fluent	Grade efficiency measured by the authors
Cristea et al. [109]*	4.12	1–192	0.0003	RSM	Lagrangian-based	Fluent	Pressure drop, separation efficiency, and heat transfer rate measured by the authors
Kozołub et al. [55]	0.2	40–80	up to around	RSM	Lagrangian-based	Fluent	Pressure drop measured by the authors
Cristea et al. [58]*	not mentioned	1–192	around 0.0007	RSM	Lagrangian-based	Fluent	Pressure drop, separation efficiency, and heat transfer rate measured by the authors
Hwang et al. [10]	0.2	2000	up to 0.001	RSM	Lagrangian-based	Fluent	Pressure drop measured by Chu et al. [9]

A hybrid Eulerian–Lagrangian multiphase model: Dense Discrete Phase Model (DDPM)

The Dense Discrete Phase Model (DDPM) is a Lagrangian-based hybrid model applicable to both dilute and dense particle-laden flows. DDPM is similar to DEM as in both the particle phase is treated in a Lagrangian framework, however, unlike DEM where particle-particle interactions are directly resolved, in DDPM particle-particle interaction is modeled based on the Kinetic Theory of Granular Flow (KTGF) taken from the TFM model. in other words, Unlike DEM where the collision forces in equation 2–11 are directly resolved by equation 2–12, in DDPM, these collision forces are modeled based on the gradient of the solids phase granular pressure, similar to what is done in TFM. Applying a model instead of directly resolving of particle-particle interaction makes the DDPM model a computationally cheaper model compared to DEM. This approach has recently been used for the study of cyclones working under high solid loads [10,55,58,109]. Although DDPM might be less accurate than DEM as it does not directly resolve particle-particle interactions, it seems to be a suitable option for the present case because of its considerable superiority in terms of computational cost [10]. This superiority is of great importance in the present study where large-scale cases are to be simulated. Moreover, DDPM is superior to TFM in terms of its ability to provide trajectories and handle wide particle size distributions common in cyclones.

2.2.2.4 Cyclones working under high solid loads

Cyclones studied in the present work are partly different from many cyclones studied in the literature, in the following areas:

- having industrial-scale geometry
- working under a high solid load
- working under high temperature
- used for the purpose of preheating

As far as the authors are aware, there is only one research work which studied a cyclone having all these aspects, but there are several works which studied cyclones having one (or two) of them. In this section, research works focusing on cyclones working under high solid load, i.e., overall solid volume fraction higher than 0.0001 which is the case in the present study, simulated using four-way coupling multiphase models (DEM, TFM, hybrid) will be briefly reviewed. Some of the studies are listed in Table 2-4, Table 2-5, and Table 2-6.

There are several works [9,66,103] that used DEM as the multiphase model for cyclones working under high solid loads, however, due to the limitation of computational resources, these studies are limited to small-scale cyclones (up to the cyclone diameter of 0.2 m) and comparatively large particle sizes (coarser than 200 μm). Chu et al. [9], in their DEM simulation, could capture some important phenomena in cyclones including the formation of the strands of particle flow, and the decrease of pressure drop and tangential velocity due to the increase in solid load. Wei et al. [66] applied DEM on a cyclone working under higher solid loads compared to Chu et al.'s study [9] and observed that although at low solid loads, pressure drop decreases as the solid load is increased, at higher solid loads, the pressure drop is not much dependent on solid load. They also observed that at higher solid loads, the formation of particle strands becomes clearer.

Contrary to what was observed in Chu et al.'s study [9], Wei et al. [66] observed that the particle-wall interaction is the dominant force in particle motion, not the particle-particle interaction.

Some limited research works used TFM as the multiphase model for cyclones working under high solid load. Mariani et al. [27], Cristea et al. [59], and Luciano et al. [28] applied it to multiple cyclones in series to analyze the effect of geometry and operational conditions on cyclone's performance to optimize the performance of cyclones working under high solid loads.

The application of hybrid multiphase models for the simulation of cyclone working under high solid loads started since 2006. Since then, various research groups [11,67,80,108] proposed different novel models or applied existing ones for cyclones. The theory behind each model was quite different, but in all of them, the goal was to benefit from mentioned advantages of both conventional models and avoid their disadvantages as much as possible and it was achieved to different levels as claimed by the authors. Cristea et al. [58,109] applied it on multiple cyclones in series and achieved acceptable engineering accuracy for separation efficiency and pressure drop. Kozołub et al. [55] studied the effect of solid loading on the performance of cyclones by applying different sub-model parameters in DDPM. They reported that although this model can reproduce the reduction in the cyclone pressure drop due to the presence of solid particles qualitatively, it underpredicts the pressure drop in the studied cyclone which is claimed to be due to the selected model parameters value. Hwang et al. [10] attempted to compare the result of the DDPM model with the result of DEM obtained by Chu et al. [9] and reported acceptable agreement with experimental data for pressure drop for DDPM, though DEM provided a better fit (see Figure 2-9).

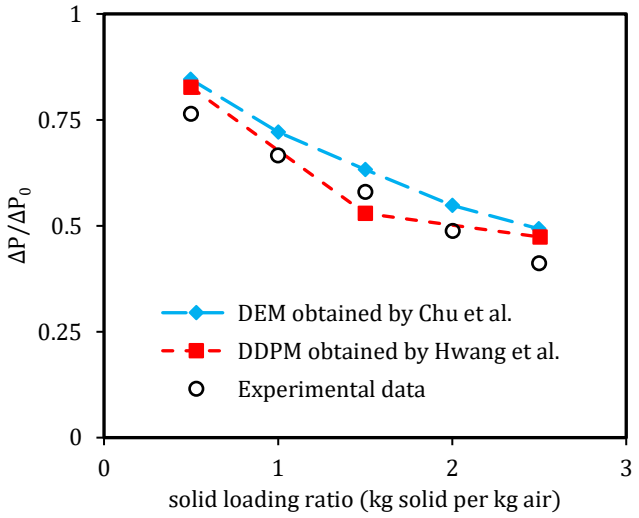

Figure 2-9. Comparison of the pressure drops obtained from DDPM, DEM, and experiments at different solid loading ratios provided by Hwang et al. [10].

2.2.2.5 Conclusions on multiphase modeling

As it was stated, choosing between one-way coupling, two-way coupling, and four-way coupling should be based on the value of solid volume fraction. The overall solid volume fractions of several CFD studies of cyclones are presented in Figure 2-10 and compared with the categorization proposed by Elghobashi [77].

In some studies [4,37,60,84,88,110–114] one-way coupling multiphase model was used, when the solid volume fraction of the studied case lies in the region of two-way coupling, which makes the results questionable. When the solid volume fraction of the studied case is in the region of two-way coupling not very close to the four-way coupling region (i.e., volume fraction lower than 1e-4), the two-way coupling multiphase model can be used with confidence and there is no need to account for particle-particle interaction as it was done in some studies [63,64,91]. However, in some studies [97], the authors were cautious, and even though the solid volume fraction is in the region of two-way coupling and not close to the four-way region, the four-way coupling multiphase model was used to take minor particle-particle interactions into account to be more accurate.

Because in cyclones, particles are mostly concentrated in the near-wall region, the local solid volume fraction might be much higher than the overall value, therefore when the solid volume fraction of the studied case is in the region of two-way coupling and close to the four-way coupling region, there will be some regions where particle-particle interaction might play an important role, so a four-way coupling multiphase model should be used to be cautious as it was done in several studies [11,27,103]. However in some cases [65,69], even though the solid volume fraction is close to the four-way coupling region, two-way coupling was used.

When the overall solid volume fraction of the studied case is in the region of four-way coupling, particle-particle interaction plays an important role, so a four-way coupling multiphase model should be used as it was done in several studies [9,10,28,55,58,59,66].

The region of the overall solid volume fraction of industrial cyclone preheaters that are supposed to be simulated in the present study (cyclone preheaters at FLSmidth A/S and ROCKWOOL A/S) is presented in Figure 2-10. As it can be observed the solid volume fraction in the present study is in the region of two-way coupling and close to the four-way coupling region. Therefore, as it was explained, due to the concentration of particles in the near-wall region and the formation of strands, particle-particle interaction might play a role and a four-way coupling multiphase model should be used in the present study. However, the two-way coupling multiphase model can be applied to assess the importance of considering particle-particle interaction.

In Table 2-7, a qualitative evaluation matrix of TFM, DEM, and DDPM models is provided to assess the feasibility of these models for simulations in the present study. Due to the inability of TFM to easily handle polydispersed particles, and to be used for the investigation of erosion which both are important in the present study and other disadvantages, the TFM model seems not to be an interesting option.

On the other hand, in the comparison between DEM and DDPM, although DEM directly resolves some phenomena leading to probably more accurate results, its computational inefficiency, especially for the industrial-scale cases and very fine particles, makes DEM an infeasible option in the present study.

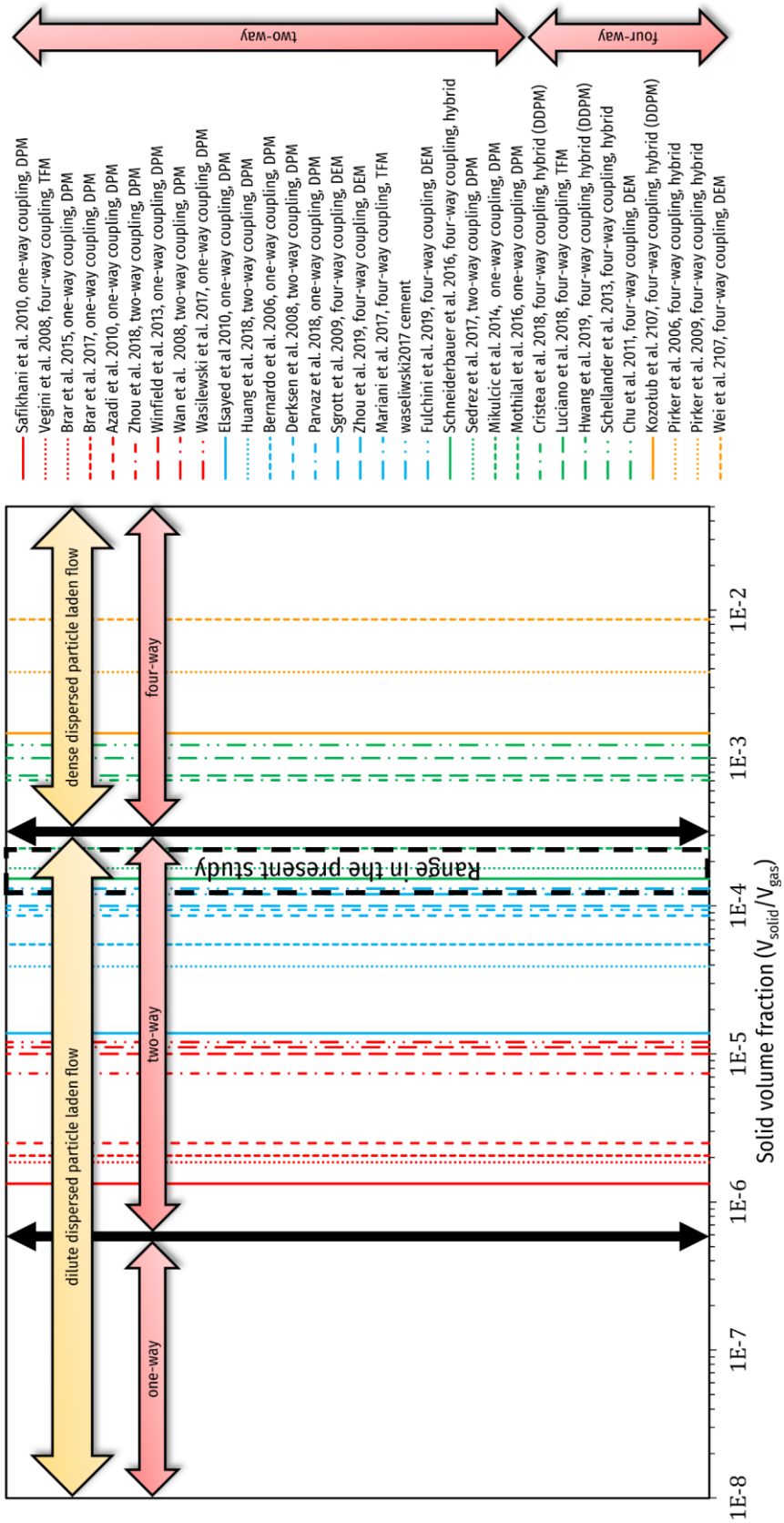

Figure 2-10. The overall solid volume fraction of several CFD studies of cyclones compared with the ranges of one-way coupling, two-way coupling, and four-way coupling proposed by Elghobashi [77]. It should be noted that these values are the highest value used in each study.

Table 2-7. Qualitative model evaluation matrix of three available four-way coupling multiphase models. The signs show the level of superiority or inferiority: ++ as the highest level of superiority and -- as the highest level of inferiority.

Model	TFM	DEM	DDPM
Particle-particle interaction	+	++	+
Particle rotation	--	++	+
Effect of wall roughness	--	+	+
Particle trajectory	--	++	++
Erosion investigation	-	++	++
Handling polydispersity of particles	-	++	++
Solid phase resolution	+	++	+
Computational cost	-	--	+

Although DDPM might not be as accurate as DEM, its ability to model particle-particle interactions, particle rotation, the effect of wall roughness, its ability to provide particle trajectories and erosion information, its ability in handling polydispersed particles, and its very crucial superiority over DEM in term of computational efficiency make DDPM an ideal option at least as the first trial. Therefore, DDPM is chosen as the first option in the present work to be tested to see whether its predictions are validated by the experimental results or not.

2.2.3 Heat transfer modeling

In the present study, a specific kind of cyclone known as cyclone preheater is studied. In cyclone preheaters, the purpose of the operation is not just to separate the particles from the gas, but the main purpose is to make heat exchange between hot gas (usually leaving from a reactor, furnace, calciner, kiln, etc.) and cold particles. So, to simulate cyclone preheaters an approach for accounting heat exchange and heat transfer should be applied. In general, in particle-laden flows, depending on whether the dispersed phase is treated in the Eulerian or Lagrangian framework, two different approaches can be applied.

If the dispersed phase is treated in an Eulerian framework (including TFM multiphase model) a separate enthalpy equation (energy conservation equation) including a term for heat exchange between gas and solid phase is written for each phase. On the other hand, if the dispersed phase is treated in the Lagrangian framework (including one-way DPM, two-way DPM, and DEM) energy conservation equation is applied differently for each phase. For the dispersed phase, to examine the change in thermal energy of a particle the heat transfer from the continuous phase to the dispersed phase is modeled using a simple heat balance to relate the particle temperature, to the convective heat transfer and the absorption/emission of radiation at the particle surface (if present) assuming that there is not considerable internal resistance to heat transfer. While for the continuous phase, an energy conservation equation is considered including a term for the source or sink of energy accounting for heat exchange with the dispersed phase (source or sink of energy is the negative value of heat received by the particles in each computational cell).

It should be noted that the form of the energy conservation equation varies depending on the multiphase model. In general, when there is heat transfer in the studied system, the physics of multiphase flow and its CFD simulation become more complex as the gas density and viscosity cannot be considered as constant

anymore. Besides extra transport equation(s) for energy which is coupled with other existing PDEs must be solved.

There are several CFD studies of cyclones simulating gas-solid heat exchange which are summarized in Table 2-8. As can be observed, EVMs are more common in the simulation of non-isothermal cyclones than isothermal ones. Another point to mention is that the validation of CFD simulations in terms of local velocity and temperature profile is clearly lacking in these cases.

Table 2-8. Details of CFD studies on gas-solid multiphase flow in cyclones investigating gas-solid heat exchange. The ones marked with * studied industrial-scale cyclones used for the purpose of preheating.

Author	Cyclone diameter (m)	Temperature range (K)	Solid volume fraction	Turbulence model	Multiphase model	Validation
Cristea et al. [59]*	Industrial scale	300–1200	around 0.0007	RSM	TFM	Pressure drop and separation efficiency measured by the authors were used for the validation.
Mikulcic et al. [4]*	6	900–1200	0.0002	LES	one-way DPM	Pressure drop and heat transfer rate measured by the authors were used for validation.
Mothilal et al. [39,115]	0.1	300–500	up to around 0.0002	RNG	one-way DPM	Pressure drop measured by Hoekstra et al. [30] and the heat transfer rate measured by the authors.
Wasilewski et al. [2]*	3.5	300–900	around 0.0002	RSM	two-way DPM	The heat transfer rate measured by the authors.
Mariani et al. [26,27]*	6	600–850	around 0.0001	k-ε	TFM	The heat transfer rate measured by the authors.
Cristea et al. [58,109]*	industrial scale	900–1100	around 0.0007	RSM	DDPM	Separation efficiency, pressure drop, and heat transfer rate measured by the authors

2.2.3.1 Cyclones working under high temperatures and cyclones used for the purpose of preheating

As mentioned, the cyclones studied in the present study operate under high temperatures and are used for the purpose of material preheating, which makes them somewhat different from the majority of other cyclones studied in the literature. CFD studies focusing on cyclones used for the purpose of preheating are summarized in Table 2-8 (the ones marked with *).

In CFD studies focusing on cyclones working under high temperatures, the calculations are carried out by either including heat transfer (which are summarized in Table 2-8) or considering the isothermal condition. In several research works [35,57,97,116,117], to avoid the complexity which arises when an energy conservation equation is added, simulations are carried out at a fixed high temperature. In these studies, both gas and solid have the same high temperature, so the energy conservation equation and gas-solid heat exchange and heat transfer are not required and consequently not included. These studies were done to study how the performance of cyclones is affected by the increase in temperature. It is observed in [12,35,117] and experimental studies [86,118,119] that in general, in constant gas volumetric flow rate, an increase in temperature leads to a reduction of swirl intensity and turbulence in cyclones due to an increase in gas viscosity and a decrease in gas density which leads to a lower Reynolds number and swirl intensity.

It should be noted that if this reduction is considerable, turbulence models which were considered inaccurate due to high swirling motion inside cyclones might be sufficient for cyclones working under high temperatures. Gimbun et al. [35] showed that under operating temperatures higher than 800 K, RSM and RNG k-ε provide nearly the same pressure drop in the studied cyclone which is also in agreement with the experimental data, although under lower temperatures a discrepancy between results of two turbulence models is observed. The reduction in swirl and turbulence due to the increase in temperature is reported to reduce the cyclone's pressure drop. Contrary, this leads to lower separation efficiency which can be partly explained by the occurrence of two phenomena: (1) the drag force applied to the particles is intensified as a consequence of increased gas viscosity due to an increase in temperature, and (2) the reduction in the swirl intensity leads to a weaker centrifugal effect on the particles, which both cause reduction in the separation efficiency [86].

2.3 Other aspects of CFD simulation

The size distribution of particles in industrial cement cyclones, which is one of the two main focuses of the present study, includes very fine (even sub-micron) so that it is classified as Geldart C type of particle (based on Geldart's particle classification [120]); and known as cohesive particles which are very prone to agglomeration. When a particle-laden system includes such particles, particle agglomeration is an important mechanism [51,52], especially in cyclones where the separation efficiency is highly sensitive towards the particle size. On the other hand, in the case of industrial cyclones in stone wool material production, which is the other focus of the present study, wall erosion is a serious issue to be investigated. Therefore, in this section, other aspects of CFD simulations that are of interest in the present study including agglomeration modeling and erosion modeling are discussed briefly. Moreover, in general, there are some challenges in the CFD simulation of industrial-scale multiphase systems that will be addressed briefly in this section. In addition, an overview of available and required validation data will be presented at the end.

2.3.1 Agglomeration modeling

When particles collide with each other, they might tend to stick together to form bigger particles. This phenomenon which is known as agglomeration might play a key role in the motion of particles and consequently in the performance of cyclones in some cases, especially cyclones handling fine particles as Van der Waals force becomes more dominant. This was observed in some experimental studies of cyclones [1,74,121]. In fact, when larger and smaller particles agglomerate, the separation of finer particles from gas becomes more likely. Therefore, to better describe the particle behavior in cyclones in such cases, agglomeration should be included in the modeling.

Particle agglomeration is a complex phenomenon and needs considerable modelling effort. The approach used for the modeling of agglomeration depends on whether the solid phase is treated in an Eulerian framework or a Lagrangian framework. So far, in CFD simulation of cyclones, agglomeration modeling was just included in multiphase models that treat the particle phase in a Lagrangian framework.

Research works investigating CFD simulation of cyclones including agglomeration modeling can be divided into two approaches: (1) an approach based on the model introduced by Sommerfeld et al. [122] which was used by Paiva et al. [123], Ho et al. [124], and Sgrott Junior et al. [74], and (2) an approach

based on the well-known population balance equation (PBE) which was used by Schneiderbauer et al. [11]. In all these studies, it is claimed that including agglomeration in the model can improve the estimation of the fractional separation of the sub-micro particles in cyclones which shows the importance of proper agglomeration modelling.

The approach based on the model introduced by Sommerfeld et al. [122] consists of three steps: (1) looking for a possible collision between two particles, (2) The evaluation of whether the collision results either in a rebound of particles, or they may stick together making a new bigger agglomerate, and (3) describing the result of the collision to define how the new agglomerate is treated concerning the size and the velocity. On the other hand, in the approach based on the population balance equation (PBE), the distribution of particle diameter classes due to the agglomeration will be described by a transport equation [11,125]. In both these models, particle tracking is required.

Considering the importance of agglomeration in the present study, in particular in cases with fine particles, including an agglomeration model can be considered as a potential solution if predictions deviate from experimental measurements.

2.3.2 Erosion modeling

Erosion which is defined as the loss of material due to the impact of solid particles on walls might cause harsh operational and economic issues during the operation of particle-fluid systems including cyclones. Erosion depends on the particle-wall impact angle, particle impact velocity, frequency of particle-wall collision, and particle and wall properties [126]. The particle-wall impact angle, particle impact velocity, and frequency of particle-wall collision can be estimated by Multiphase CFD models that provide particle trajectories (one-way and two-way DDP, DEM, and DDPM). Therefore, by implementing an erosion model to the multiphase CFD model, the erosion rate can be estimated in the studied multiphase system. Erosion models are used together with CFD simulations, for example, in elbows [127], pipes [128,129], valves [130] and recently cyclones [65,75,114,131–133].

In Table 2-9 a summary of CFD studies of gas-solid cyclones investigating erosion based on such models is provided. There are several erosion models based on different theories assuming different simplifications. DNV [134] and Oka [135,136] have been more commonly used for the study of erosion in cyclones. As can be observed from the table, as far as the author is aware, there is only one study available in the literature reporting quantitative measurements of erosion in a cyclone [65].

Sedrez et al. [65] by doing both experimental and numerical studies, showed that the erosion rate is dependent on gas inlet velocity; an increase in gas flow rate intensifies erosion. It was also shown (based on the measurements) that an increase in the solid loading ratio decreases erosion. The decrease due to an increase in solid loading ratio (which was not investigated numerically) might be attributed to the "shielding" effect of particles meaning that not all particles can hit the wall because some particles just collide with the particles bouncing back after hitting the wall which leads to less particle-wall interaction and consequently lower erosion rate. This effect has also been observed in other studies [9].

Table 2-9. Details of CFD studies on gas-solid multiphase flow in cyclones investigating erosion

Author	Multiphase model	Erosion model	Solid volume fraction	Solver	Validation
Sedrez et al. [65]	two-way DPM	DNV [134], Oka [135,136]	up to 0.0002	Fluent	Pressure drop and erosion measurement by the authors
Parvaz et al. [114]	one-way DPM	DNV	up to 0.00009	Fluent	Flow pattern data and pressure drop measured by Hoekstra et al. [30], separation efficiency measured by Zhao et al. [89], and erosion measurement by Sedrez et al. [65]
Mazyan et al. [133]	two-way DPM	not mentioned	not mentioned	Fluent	Separation efficiency measured by Ji et al. [137].
Tofighian et al. [75]	one-way DPM	Oka	0.000002	OpenFOAM	Flow pattern data measured by Hoekstra et al. [30], separation efficiency measured by Zhao et al. [89], and erosion measured by Sedrez et al. [65]

It should be noted that erosion models are known to only provide qualitative validation against experimental erosion data in cyclones meaning that they can be used for identifying locations where the erosion is more severe not for accurate estimation of eroded mass. In addition to the limitations of erosion models, this inaccuracy has also been reported to be due to not implementing an accurate particle-wall rebound coefficient [114] and not taking into account the wall roughness effect [75].

2.3.3 Challenges in industrial-scale CFD simulation of cyclones

Cyclones investigated in the present study differ from most cyclones studied in the literature in part due to their industrial-scale geometry. Moving from stimulation of small-scale to large-scale cyclones might arise the following concerns:

1. Required computational resources will be increased because of the need for more computational cells to achieve sufficient grid resolution, as well as an increased number of computational particles residing inside the domain
2. Due to the scaling which leads to a change in volume-to-surface ratio, models validated at lab-scale cyclones may not be necessarily suitable for the simulation of large-scale cyclones and should be carefully tested.
3. The use of coarse grids which is inevitable to reduce computational cost in industrial-scale CFD simulations might cause neglecting small (unresolved) scales which might lead to inaccuracy in simulation.

For the third concern, the drag force must be accurately predicted as the dominant force influencing particle motion in cyclones in order to make a reliable prediction of the performance parameters of cyclones [11]. Numerous studies have shown that when multiphase models are used with coarse grids, using common homogeneous drag models (such as Wen-Yu and Gidaspow drag models) might lead to inaccurate predictions of multiphase flow hydrodynamics [138,139]. This inaccuracy is due to the erroneous prediction of drag caused by the inability of coarse grids to resolve mesoscale structures (such as particle strands in

cyclones) [11,138–146]. To overcome the shortcomings of homogeneous drag models for industrial-scale simulations, heterogeneous drag models (also called sub-grid drag models) are suggested as a solution to be used to incorporate the influence of small mesoscale and heterogeneous structures on the drag correlations [11,138–146]. Among research works simulating industrial-scale cyclones, only Schneiderbauer et al. [11] addressed the effect of sub-grid structures on gas-solid flow by using sub-grid modifications to the drag force in a coarse grid hybrid Eulerian–Lagrangian multiphase model. To the author's knowledge, in the rest of the existing simulation studies of industrial-scale cyclones, homogenous drag models are used.

Although none of the existing literature sub-grid drag models is derived for cyclones where the flow rotation is dominant, several heterogeneous drag models such as Sarkar [138], Pirker [142], and Igci [141] validated in different fluidization regimes are available in the literature and can be tested in the present study.

A summary of research works simulating industrial-scale cyclones can be found in the works summarized in Table 2-6 and Table 2-8 (the ones marked with *).

2.3.4 Availability of experimental data for model validation

To verify any CFD simulation, reliable experimental measurements (validation data) are required. These experimental measurements can be divided into two categories:

1. Overall measurements of performance parameters such as pressure drop, separation efficiency, and temperature changes over the whole system in the case of cyclone preheaters
2. Local detailed measurements (e.g., gas velocity and temperature)

These local [20,29,30,53,85–87,90,111] and overall [20,29,30,63–65,83,85,87,89,91,111] measurements can be found in the literature in the case of lab-scale cyclones working under low solid loads and ambient temperature. Limited studies are available that focus on overall measurements in the case of highly loaded or large-scale cyclones, but local measurements in such cases are missing. Generally, regarding industrial-scale cyclones or highly loaded cyclones, the lack of experimental measurements is clear. To the author’s best knowledge, local measurements in highly loaded cyclones are totally missing in the literature, even in lab-scale geometries or ambient temperatures let alone in industrial cyclone preheaters. In general, the few existing experimental literature studies of cyclone preheaters [2,4,26,27,58,109] or cyclones working under high solid loads [9,11,28,55,59,66,80,98,104,108], are limited to overall measurements.

Therefore, as the local measurements of gas velocity and temperature in industrial-scale highly loaded cyclone preheaters are missing, providing such data in the present study can fill this gap. Such measurements in addition to overall measurements of pressure drop, separation efficiency and temperature changes over the whole system in the case of industrial cyclones planned to be investigated in the present study will enable us to validate the developed CFD model.

2.4 Conclusions

Based on the literature survey, a relatively novel multiphase model known as Dense Discrete Phase Model (DDPM), introduced by Ansys Fluent, is promising for its computational cost efficiency and its ability to

handle polydispersity of particles which are important in the present case. Regarding turbulence models, RSM and EVMs sensitized to rotation and curvature seem to be promising options.

Due to the relative novelty of DDPM, These sets of models have not been extensively investigated, in particular, in cyclones, therefore their challenges such as instabilities, computational expenses, issues in solution convergence and how to overcome them are not clear yet and should be investigated. Also, these models contain several sub-models, model parameters, and numerical approaches which require investigations to decide what to use in the present case.

To test this set of models, it is a good idea to first focus on the hydrodynamics of multiphase flow in isothermal cases. Then, if they work properly, heat transfer can be added on top to simulate non-isothermal cyclone preheaters. Based on this literature survey, agglomeration modeling and heterogeneous drag models (also called sub-grid drag models) which are not usually available in commercial CFD tools are suggested as two potential solutions if modifications are required.

The literature survey also clearly shows the lack of experimental measurements, in particular, local measurement of flow patterns, meaning that measurement campaigns should be held in the present study to provide validation data.

3 CFD simulation of an isothermal lab-scale cyclone operating under high solid loads

3.1 Introduction

Based on the literature review in Chapter 2, considering the computational cost efficiency of the DDPM multiphase model (introduced by Ansys Fluent), its capability of accounting for particle-particle interactions which is of importance in the present study, and other mentioned superiorities, this model is chosen as the first candidate of multiphase model to simulate highly loaded cyclones. Before applying the model to industrial-scale cyclone preheaters, which is the ultimate goal of the present study, the model was first used to simulate a lab-scale generic cyclone, to validate the model against available experimental data in the literature, and to evaluate the capability of the model in the prediction of performance parameters of highly loaded cyclones.

This generic cyclone was studied experimentally and numerically by other authors Chu et al. [9] and Hwang et al. [10] under solid loads similar to industrial-scale cyclone preheaters planned to be investigated in the present study. In addition to the validation, simulation of this lab-scale cyclone using the DDPM would help identifying the challenges and limitations of the model as well as the special treatments required for numerical convergence. DDPM is a relatively new multiphase model, and such knowledge is scarce in the literature, and thereby should be investigated. Furthermore, this investigation will help an easy implementation of the model in large-scale cases late on. On the other hand, any future potential modification to the models or solver settings can be tested more easily in a small geometry.

As discussed in the literature review, RSM and EVMs sensitized for flow rotation are feasible and reliable turbulence models for simulation of highly loaded cyclones. In the lab-scale cyclone, where high-quality structured grids can be generated, a relatively unstable turbulence model such as RSM can be used. However, this might be a challenge in large-scale cases where achieving a high-quality mesh is difficult. Therefore, a comparison between these two turbulence models can be done in a lab-scale cyclone simulation. If a sensitized EVM works more or less the same as RSM, it can be used with more confidence for the simulation of large-scale cases where RSM might not be applicable.

The experimental data from high solid load cyclones are scarce in the literature. Chu et al. [9] investigated a lab-scale cyclone operating under solid loads in the range of 0-2.5 kg solid/kg air. The influence of solid loads on the pressure drop of the cyclone was studied. The obtained experimental data were used for the validation of a CFD-DEM simulation by the same authors [9]. Moreover, another research group simulated this cyclone using the DDPM multiphase model [10]. Chu's data were used in this study. In addition to the evaluation of the validity of the model, the simulation predictions can be compared with the results obtained from CFD-DEM as a more expensive multiphase model with a higher level of resolution. In both published studies [9,10], the RSM turbulence model was used, however, in the present study in addition to RSM, an EVM (k-ω sst) sensitized to rotation and curvature is tested for comparison.

3.2 Case description

A typical Lapple cyclone with a height (H) of 0.8 m and a diameter (D) of 0.2 m shown in Figure 3-1 was considered in the study by Chu et al. [9]. In the present work, a dust bin is added to the end of the dipleg (where separated particles leave the cyclone), and also inlet and gas outlet were extended. These were done to first mimic the original experimental rig and to avoid reverse flow issue in the simulations, and to ensure that the final results are not affected by the type of boundary condition at the outlet. Details of the cyclone dimensions can be found in Table 3-1. The operating conditions of experiments conducted on this cyclone and applied in the present CFD simulation study are summarized in Table 3-2.

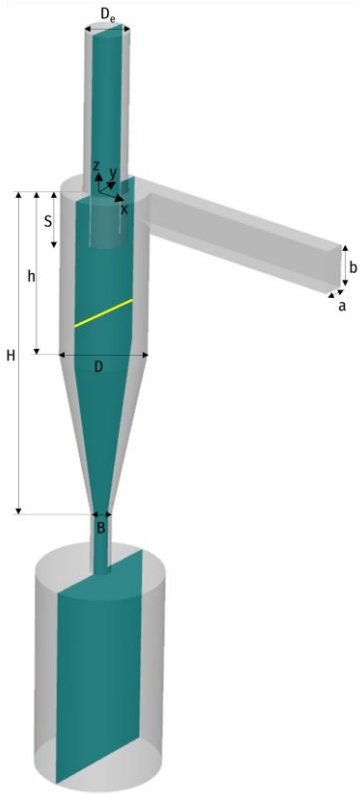

Figure 3-1. 3D view of the geometry of the cyclone (adopted from [9]). The origin is located at the center of the circle roof. The cyan plane and yellow line (0.3 m away from the roof) are the plane of contours and line of profiles in the results and discussion section.

Table 3-1. Cyclone dimensions where D (cyclone diameter) is 0.2 m [9].

a/D	b/D	D_e/D	S/D	h/D	H/D	B/D
0.25	0.5	0.5	0.625	2.0	4.0	0.25

Table 3-2. Summary of operating conditions taken from [9]

Particle diameter (m)	0.002	Gas inlet velocity (m/s)	20
Particle density (kg/m3)	2500	Gas viscosity (kg/m/s)	1.8e-5
Particle inlet velocity (m/s)	3	Operating temperature	Ambient
Gas material	Air	Solid load ratios (kg solid/kg air)	0.5, 1, 1.5, 2, and 2.5
Gas density (kg/m3)	1.225	Solid flow rates (kg/s)	0.061, 0.122, 0.184, 0.245, and 0.306

3.3 Grid generation

Structured hexahedral mesh aligned with flow direction is superior to other mesh types, in minimizing numerical diffusion and consequently providing more accurate results. This was proven in our preliminary single-phase simulations of a lab-scale cyclone. Therefore, for the present cyclone, structured hexahedral grids were generated using ICEM CFD. As it can be observed in Figure 3-2 (a), the geometry excluding the inlet duct was covered using several layers of O-grid blocks to maximize mesh quality (minimizing skewness and non-orthogonality). Blocks in the region where the inlet duct meets the cylindrical body was cut to avoid low angel cells (which might make numerical instability, especially in the RSM turbulence model) at the tangential connection (see Figure 3-2 (b)).

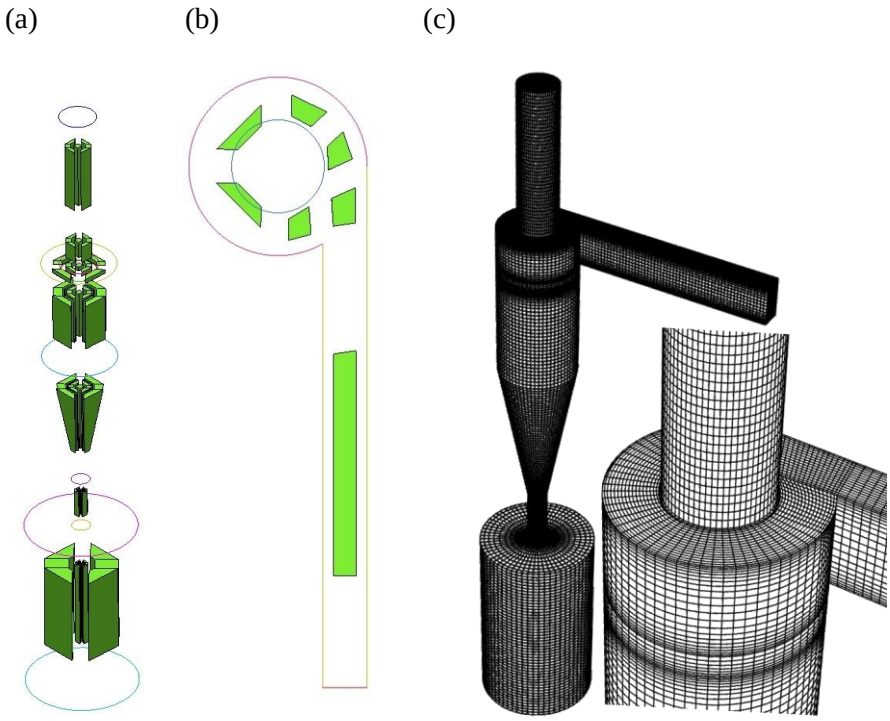

Figure 3-2. (a, b) Blocks used for the generation of a structured hexahedral mesh using ICEM CFD. (c) 3D view of CFD grids (480 000 cells).

Five levels of grids (157k, 275k, 480k, 563k, and 705k cells) were provided for the mesh independence study. In all generated grids at all zones near walls, the grids are finer to capture potential sharp changes in the near-wall region. To ensure y^+ values remain in the valid range of used turbulence models and used near-wall treatment methods (y^+ must be below 300 [147]) first cell height was kept below 0.002 m (except in the bin region). To avoid numerical instability in the solution, the cell growth rate (expansion rate) was kept below or equal to 1.2. One of the generated grids is shown in Figure 3-2 (c) as an example.

3.4 Computational method

In the present case, DDPM was coupled with RSM and k-ω sst cc (k-ω sst sensitized for curvature and implemented on the lab-scale cyclone using Ansys Fluent 2019 R3 solver. DDPM, RSM and k-ω sst cc include several sub-models. The details of these models and sub-models can be found in the Ansys Fluent theory guide [147].

DDPM is a hybrid Eulerian-Lagrangian multiphase model which implicitly models particle-particle interaction by employing the Kinetic Theory of Granular Flow (KTGF). The gas phase is resolved in an Eulerian framework where the Navier–Stokes equations incorporating phase volume fraction are solved and the particle/solid phase is resolved in a Lagrangian framework for particle tracking. A brief description of the model is presented in this section.

3.4.1 Gas-phase (continuous phase) mathematical modeling:

The continuity and momentum conservation equations for the continuous phase (gas phase) in DDPM in combination with dispersed versions of turbulence models (dispersed RSM and dispersed k-ω sst cc) can be expressed as follows:

$$\frac{\partial}{\partial t}(\alpha_c \rho_c) + \nabla.(\alpha_c \rho_c \bar{u}_c) = 0 \qquad 3\text{–}1$$

$$\frac{\partial}{\partial t}(\alpha_c \rho_c \bar{u}_c) + \nabla.(\alpha_c \rho_c \bar{u}_c \bar{u}_c) = -\alpha_c \nabla p + \nabla.\left[\alpha_c \mu_c \left(\nabla \bar{u}_c + \nabla \bar{u}_c{}^T\right)\right] + \nabla.\tau_c^t + F_{Dc} + S + \alpha_c \rho_c g \qquad 3\text{–}2$$

F_{Dc} reflects the force particles apply on the fluid due to drag and is described as follows:

$$F_{Dc} = K_{DPM}\left(u_{dpm} - \bar{u}_c\right) \qquad 3\text{–}3$$

The Wen-Yu drag model [148] is used to calculate K_{DPM}.

3.4.1.1 DDPM coupled with dispersed RSM

In the case of dispersed RSM, the turbulent stress tensor, τ_c^t, is defined by equation 3–4 and is directly resolved by solving six transport equations for the Reynolds stresses ($R_{c,ij}$), together with an equation for the dissipation rate (ε).

$$\tau_c^t = -\alpha_c \rho_c R_{c,ij} \qquad 3\text{–}4$$

In the case of dispersed RSM, transport equations for the Reynolds stresses ($R_{c,ij}$) is described by equation 3–5.

$$\frac{\partial}{\partial t}\left(\alpha_c \rho_c R_{c,ij}\right) + \frac{\partial}{\partial t}\left(\alpha_c \rho_c \bar{u}_c R_{c,ij}\right) = P_{ij} + D_{L,ij} + D_{T,ij} + \varphi_{ij} - \varepsilon_{ij} + F_{ij} + \Pi_{R,ij} \quad 3–5$$

In addition to terms on the left-hand side, some terms on the right-hand side including P_{ij}, $D_{L,ij}$, and F_{ij} are exact equations meaning that they do not require modeling. However, other terms including $D_{T,ij}$, φ_{ij}, ε_{ij}, and $\Pi_{R,ij}$ requires modeling. Sub-models used to close these terms are summarized in Table 3-3. How each of these terms is defined and modeled and details of each model can be found in the Ansys Fluent theory guide [147].

Table 3-3. Summary of details in turbulence models used in the present study

RSM	Dispersed model	
	Pressure-Strain (φ_{ij})	Linear, Gibson and Launder [149], Fu et al. [150], and Launder [151]
	Turbulent diffusion ($D_{T,ij}$)	The simplified model of Daly and Harlow [152]
	Dissipation tensor (ε_{ij})	Sarkar [153]
	Wall treatment	Enhanced method neglecting pressure gradient effects
	Model constants	Ansys Fluent defaults
k-ω sst cc	Dispersed model	
	CCURV (curvature correction factor)	1
	Model constants	Fluent defaults

The scalar dissipation rate in the continuous phase, ε_c, which is required for the calculation of some terms is determined using a transport PDE similar to that used in the standard k-ε model.

$$\frac{\partial}{\partial t}(\alpha_c \rho_c \varepsilon_c) + \frac{\partial}{\partial t}(\alpha_c \rho_c \bar{u}_c \varepsilon_c) = \nabla.\left(\alpha_c \left(\mu_c + \frac{\mu_{t,c}}{\sigma_\varepsilon}\right)\nabla \varepsilon_c\right) + \alpha_c \frac{\varepsilon_c}{k_c}\left(C_{1\varepsilon} G_{k,c} - C_{2\varepsilon}\rho \varepsilon_c\right) \quad 3–6$$

Where turbulence kinetic energy, k_c , is obtained by taking the trace of the Reynolds stress tensor:

$$k_c = \frac{1}{2}\overline{u_\iota{}' u_\iota{}'} \quad 3–7$$

And G_k which is the turbulence kinetic energy generation is defined as follows:

$$G_k = -\rho \overline{u_\iota{}' u_\jmath{}'} \frac{\partial \bar{u}_j}{\partial x_i} \quad 3–8$$

3.4.1.2 DDPM coupled with dispersed k-ω sst cc

In the case of the dispersed k-ω sst cc, turbulent stress tensor, τ_c^t, is approximated using the Boussinesq hypothesis (3–9).

$$\tau_c^t = -\alpha_c \rho_c R_{c,ij} = -\alpha_c \left[-\frac{2}{3}\left(\rho_c k_c + \mu_{t,c} \nabla. u_c\right)\delta_{ij} + \mu_{t,c}\left(\nabla \bar{u}_c + \nabla \bar{u}_c{}^T\right)\right] \quad 3–9$$

to determine k_c and $\mu_{t,c}$ and subsequently, turbulent stress tensor, τ_c^t, two transport equations (one for k and one for ω) need to be solved:

$$\frac{\partial}{\partial t}(\alpha_c \rho_c k_C) + \frac{\partial}{\partial x_i}(\alpha_c \rho_c \bar{u}_c k_C) = \frac{\partial}{\partial x_j}\left(\alpha_c \Gamma_k \frac{\partial k_C}{\partial x_j}\right) + \alpha_c f_r G_k - \alpha_c Y_k \quad 3\text{–}10$$

$$\frac{\partial}{\partial t}(\alpha_c \rho_c \omega_C) + \frac{\partial}{\partial x_i}(\alpha_c \rho_c \bar{u}_c \omega_C) = \frac{\partial}{\partial x_j}\left(\alpha_c \Gamma_\omega \frac{\partial k_C}{\partial x_j}\right) + \alpha_c f_r G_\omega - \alpha_c Y_\omega \quad 3\text{–}11$$

Detailed definitions of terms and parameters in these equations, as well as how the curvature correction function (f_r) is modeled can be found in the Ansys Fluent theory guide [147]. Briefly, f_r (the curvature correction function) is modeled by a revised version of an empirical function suggested by Spalart and Shur [44] to take the effects of streamline curvature and system rotation into account.

3.4.2 Solid-phase (dispersed phase) mathematical modeling

In DDPM multiphase model, the equation of motion of each parcel (as a representative of several particles with the same property) is expressed in equation 3–12. Details of the particle tracking approach are summarized in Table 3-4. It should be noted that in gas phase conservation equations, α_c is updated each time step by mapping particle location to the Eulerian framework.

$$m_{pi}\frac{d\vec{u}_{pi}}{dt} = m_{pi}\frac{18\mu_c}{\rho_p {d_p}^2}\frac{C_D Re_p}{24}\left(\vec{u}_c - \vec{u}_{pi}\right) + m_{pi} g \frac{\rho_p - \rho_c}{\rho_p} + F_{p-p} + F_{other} \quad 3\text{–}12$$

Table 3-4. Summary of particle tracking approach used in the present study

particle tracking	Unsteady, by flow time
Tracking scheme	implicit
Averaging method	Node based averaging
Particle injection velocity (m/s)	3 (as stated in the experimental study)
Particle diameter (m)	0.002 (as stated in the experimental study)
Particle injection flow rate (kg/s)	0.0612, 0.122, 0.184, 0.245, and 0.306
Drag law	Wen-Yu [148]
Turbulent dispersion	DRW (with random eddy lifetime; 0.3 as time scale constant in case of RSM turbulence model and 0.15 in case of k-ω sst cc turbulence model)
Parcel release method	Constant mass (1 mg so parcels are smaller than the smallest cell size as required by DDPM multiphase model)

The Wen-Yu model [148] is used for C_D calcualtion:

$$C_D = \begin{cases} \frac{24}{Re_p}{\alpha_g}^{-2.65}\left(1 + 0.15{Re_p}^{0.687}\right) & Re_p \le 1000 \\ 0.44{\alpha_g}^{-2.65} & Re_p > 1000 \end{cases} \quad 3\text{–}13$$

F_{p-p}, particle-particle interaction force, is described by a model based on the Kinetic Theory of Granular Flow (KTGF). KTGF models average particle interactions instead of resolving all collisions between particles. The particle-particle interaction force is obtained by the solids stress tensor ($\bar{\bar{\tau}}_s$) defined as follows:

$$F_{p-p} = -m_{pi}\frac{1}{\rho_p}\nabla.\bar{\bar{\tau}}_s \quad 3\text{–}14$$

$$\bar{\bar{\tau}}_s = \alpha_s\left(\lambda_s - \frac{2}{3}\mu_s\right)\nabla u_s + \alpha_s\mu_s(\nabla u_s + \nabla {u_s}^T) \quad 3\text{–}15$$

For the evaluation of solids stress tensor ($\bar{\bar{\tau}}_s$), shear viscosity (μ_s) and bulk viscosity (λ_s) are needed to be models. In addition, to evaluate shear viscosity collisional, kinetic, and optional frictional viscosity must also be modeled.

$$\mu_s = \mu_{s,col} + \mu_{s,kin} + \mu_{s,fric} \quad 3\text{–}16$$

Estimation of these viscosities (bulk, collisional, kinetic and frictional) can be done using different closure models (details can be found in the Ansys Fluent theory guide [147]). In short, granular viscosity, granular bulk viscosity, solid pressure, granular temperature, frictional viscosity, frictional pressure, and radial distribution terms must be modeled using closure models.

Closure models used in the present work for each term are listed in Table 3-5. It should be noted that in the simulated cases in the present work, the solid volume fraction never exceeded the limit for including frictional viscosity, so it was not included in the present work. To model these viscosities, granular temperature defined in the Kinetic Theory of Granular Temperature (KTGF) is required which can be obtained by solving a transport equation (algebraic or PDE) of granular temperature.

$$\frac{2}{3}\left[\frac{\partial}{\partial t}(\alpha_s\rho_s\Theta_s) + \nabla.(\alpha_s\rho_s u_s\Theta_s)\right] = (-p_s I + \tau_s):\nabla u_s + \nabla.\left(k_{\Theta_s}\nabla\Theta_s\right) - \Upsilon_{\Theta_s} + \phi k \quad 3\text{–}17$$

Table 3-5. Summary of sub-models in DDPM used in the present study

Granular temperature model	Phase property
Granular viscosity	Gidaspow [93] model
Collisional viscosity	Gidaspow et al. [93] and Syamlal et al. [154]
Kinetic viscosity	Gidaspow et al. [93]
Granular bulk viscosity	Lun-et-al [155] model
Frictional viscosity	None
Granular temperature	Algebraic model
Solid pressure	Lun-et-al [155] model
Radial distribution	Lun-et-al [155] model
Packing limit	0.63
Transition factor	0.75

By assuming that the granular fluctuation energy is in local equilibrium and its production and dissipation are balanced locally, the convection and diffusive terms in the transport equation 3–17 can then be neglected. Under this assumption, the PDE transport equation of granular temperature can be expressed in an algebraic form (equation 3–18).

$$0 = (-p_s I + \tau_s) : \nabla \widetilde{u_s} - \Upsilon_{\Theta_s} \qquad 3\text{–}18$$

Where the collisional dissipation of energy, Υ_{θ_s}, can be represented by the expression derived by Lun et al.[155]. In the present case, the algebraic form is used as done by the other research group [10].

In the case of the DDPM coupled with dispersed k-ω sst cc, six PDEs (continuity and momentum equations and two transport equations of k and ω) and in the case of DDPM coupled with dispersed RSM eleven PDEs (continuity and momentum equations, six transport equation for Reynolds stresses, and one transport equation for ε) together with one ODE for each particle/parcel equation of motion should be solved.
Details of boundary conditions and solver settings used in the present study are summarized in Table 3-6 and Table 3-7 respectively.

Table 3-6. Summary of boundary conditions used in the present study

Gas inlet	Velocity inlet (20 m/s as stated in the experimental study)
Gas outlet	Pressure outlet for gas. Escaped for particles.
walls	No slip for the gas phase. Reflect for particles (rebound coefficient = 0.8) for all walls except dust bin walls which traped boundary condition is used

Table 3-7. Summary of solver settings used in the present study

Pressure-velocity	Phase coupled SIMPLE
Gradient discretization	Least squares cell-based
Pressure discretization	PRESTO!
Momentum discretization	Second-order upwind
Volume fraction discretization	QUICK
Turbulent kinetic energy discretization	Second-order upwind
Turbulent dissipation rate discretization	Second-order upwind
Reynolds stresses	Second-order upwind
Under relaxation factor	Fluent defaults except for pressure (0.7) and momentum (0.3)
Time step (s)	2e-4

3.5 Simulation strategy

After solving convergence issues, finding suitable sub-models, constants (time step and parcel mass), and solver settings, a mesh independency study was performed. Then, for each of the five desired solid loads (0.5, 1, 1.5, 2, and 2.5 kg solid/kg air) two cases were simulated; One using k-ω sst cc turbulence model and another using RSM (10 simulations in total). All simulation runs continued until the quasi-steady-state condition was achieved. Several parameters including pressure drop, velocity magnitude at several points, the maximum and average values of y+, the mass of particles in the cyclone main body, and gas-phase mass imbalance were tracked with time. The maximum and average values of y+ were also tracked to ensure that near-wall treatment for turbulence modeling works properly and first cell height is fine enough.

As an example, changes in the mass of particles in the cyclone main body (the parameter that converges slower than other parameters) with flow time for the case with 1.5 kg solid/kg air is shown in Figure 3-3. As can be observed in the case of k-ω sst cc convergence is achieved after almost 1.6 s and in the case of RSM convergence is achieved after almost 3.5 s (in the case of RSM first 1.6 s of the simulation was proceeding using k-ω sst cc).

For all solid loads, first, simulations started with k-ω sst cc and ran until convergence was achieved. Then, simulations were stopped, and the turbulence model was switched to RSM and then continued again until all tracked parameters converged. The time step (2e-4 s) was chosen to ensure convergence in each time step and to ensure that the courant number is kept below 2 in all cells. With this time step adequate drop of residuals (by order of 1e-3) was achieved in all time steps (after 15 inner iterations at worst).

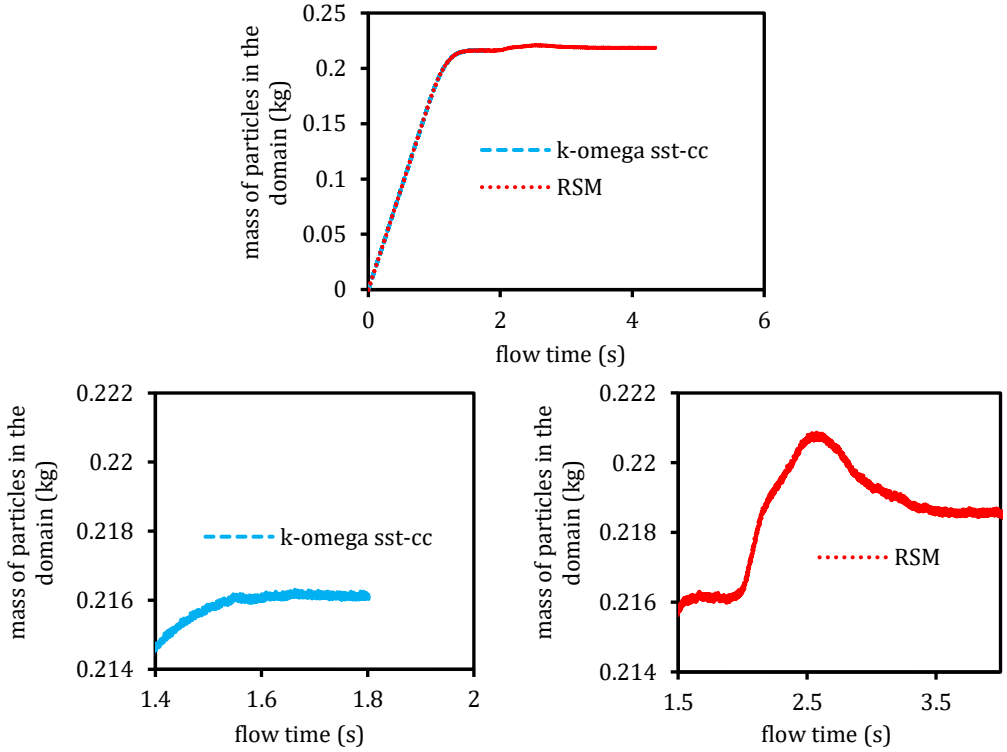

Figure 3-3. Changes in the mass of particles in cyclone main body with flow time for the case with a solid load of 1.5 kg solid/kg air. Figures on the bottom are showing the same as on top but zoomed on the converging part.

In the simulation, several challenges were faced, which were overcome by special treatments and procedures. In appendix A, some of these challenges and the way how they were overcome are addressed.

3.6 Mesh independency study

To find the mesh-independent solution, a mesh independency study was carried out. Five structured hexahedral grids with different numbers of cells (157k, 275k, 480k, 563k, and 705k) were generated for this purpose. Simulations were carried out using these grids for one of the solid loads (1.5 kg solid/kg air), and the results (most importantly pressure drop as an important performance parameter of cyclones and as a parameter that is experimentally measured in this case) were compared to ensure predictions are mesh

independent. As can be observed in Figure 3-4, in both cases of RSM and k-ω sst cc, variations of pressure drop with the number of cells are negligible.

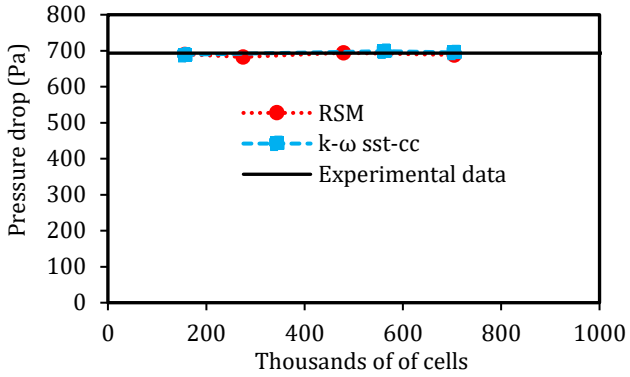

Figure 3-4. Mesh independency study; variation of cyclone pressure drop with the number of cells used for the case with a solid load of 1.5 kg solid/kg air.

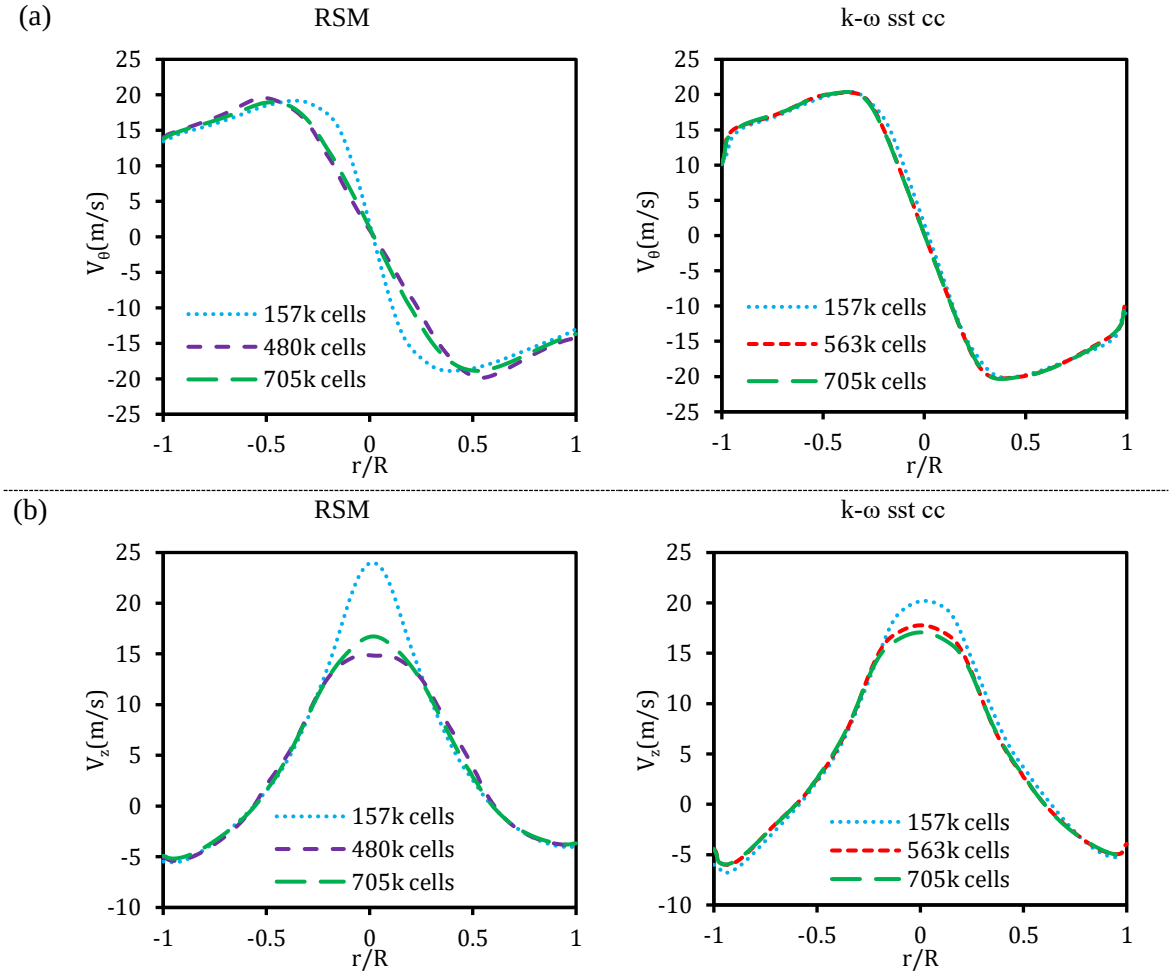

Figure 3-5. Radial profiles of (a) tangential velocity and (b) axial velocity for RSM (left), and k-ω sst cc (right) obtained using different grids at z = 0.3 m (0.3 m below the roof).

3.7 Validation

Since the pressure drop is the only experimental data in the studied cyclone, these data were used to validate present CFD simulations. Pressure drops obtained by CFD simulation in the present work for different solid loads and both used turbulence models were compared with pressure drop measured experimentally by Chu et al. [9] in Figure 3-6. Moreover, in Figure 3-6, the present predictions are also compared with the predictions of the CFD-DEM simulation reported by Chu et al. [9] and also the predictions of the CFD-DDPM simulation by Hwang et al. [10].

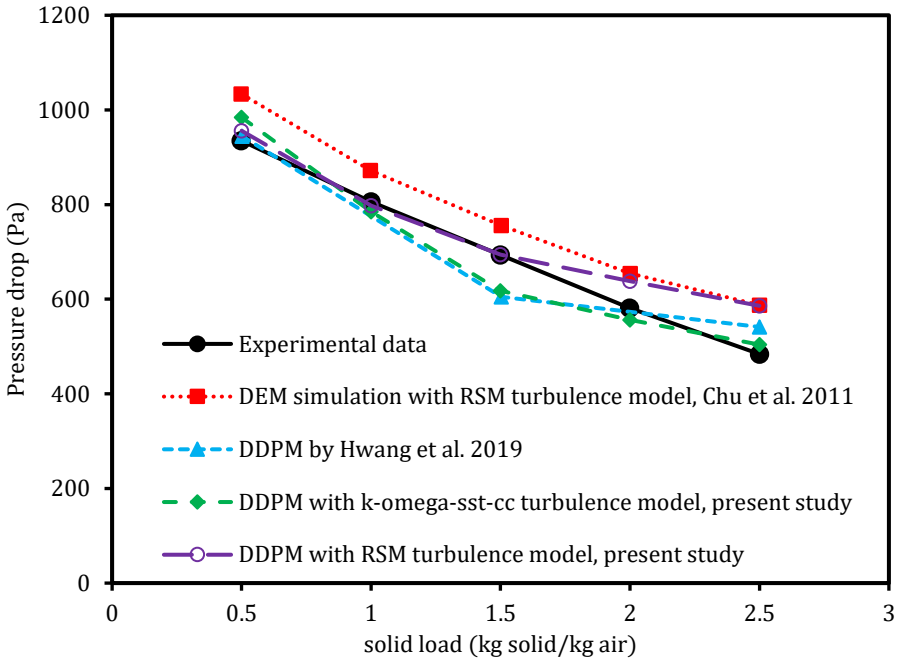

Figure 3-6. Comparison of the pressure drop obtained from DDPM and two turbulence models (present study), DEM (published by chu et al.[9]), DDPM published by Hwang et al.[10] and experiments at different solid loading ratios.

From Figure 3-6, a quite reasonable agreement between predictions obtained in the present study and experimental measurements can be observed. In particular, for solid loads below 1 kg solid/kg air, the agreement is very good, which is important because the industrial cyclone preheaters, to be investigated in this thesis, operate with solid loads below 1 kg solid/kg air. Although RSM seems to provide better predictions, the result obtained by k-ω sst cc is acceptable as well. Under all solids loads and even with k-ω sst cc, the results obtained in the present study using DDPM multiphase model seem to be as well as DEM multiphase model. This is of importance as DEM multiphase model directly resolves particle-particle interactions and is way more expensive compared to DDPM; a similar level of accuracy is obtained using a multiphase model which is less computationally expensive. In general, Figure 3-6 shows that at least in terms of pressure drop (as the only available measured parameter to be compared), the DDPM multiphase model is capable of predicting the performance of a cyclone working under high solid loads which shows the validity of DDPM in such cases.

As discussed in section 2.2.1, k-ω sst cc is superior to RSM in terms of robustness and stability (even in cases with low-quality grids, it is fairly well stable). k-ω sst cc seems to be a promising option for the simulation of industrial-scale highly loaded cyclones where high-quality grids might not be feasible and

therefore solution stability and robustness are of importance. It is because predictions of k-ω sst cc shown in Figure 3-6 are in acceptable agreement with experimental measurements and are comparable with the predictions of RSM.

3.8 Result and discussion

In Figure 3-7, the contours of tangential velocity for different solid loading ratios obtained by both turbulence models are presented. As expected [1,9,10,73,85,156,157], an increase in solid load leads to a reduction in the swirling motion of gas; this tendency is predicted by both turbulence models. This dampening of swirling motion looks more severe in the lower region of the cyclone. Although a minor discrepancy can be observed, both turbulence models provide quite similar distributions of tangential velocity which again confirms the capability of k-ω sst-cc for the prediction of flow pattern in highly loaded cyclones.

Compared to RSM which is a more accurate turbulence model, it seems that k-ω sst-cc slightly overpredicts the magnitude of minimum and maximum tangential velocities, which is demonstrated more obviously in Figure 3-8. In Figure 3-8, the radial distribution of tangential gas velocity at a specific height (0.3 m away from the cyclone roof) for both turbulence models and various solid loads are compared which more clearly shows the agreement of flow pattern predictions obtained by the two turbulence models. The reduction in swirl due to the increase in solid load can be clearly seen in Figure 3-8.

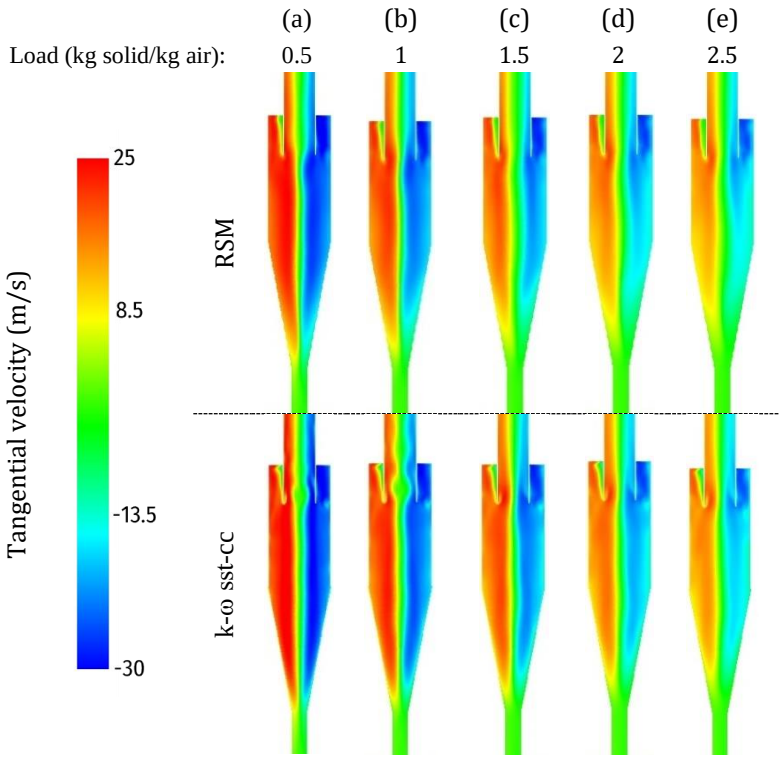

Figure 3-7. Tangential velocity (m/s) distributions at the central section parallel to the cyclone inlet obtained from the RSM turbulence model (up) and k-ω sst-cc turbulence model (down) under different solid loading ratios: (a) 0.5, (b) 1, (c) 1.5, (d) 2, and (e) 2.5 kg solid/kg air.

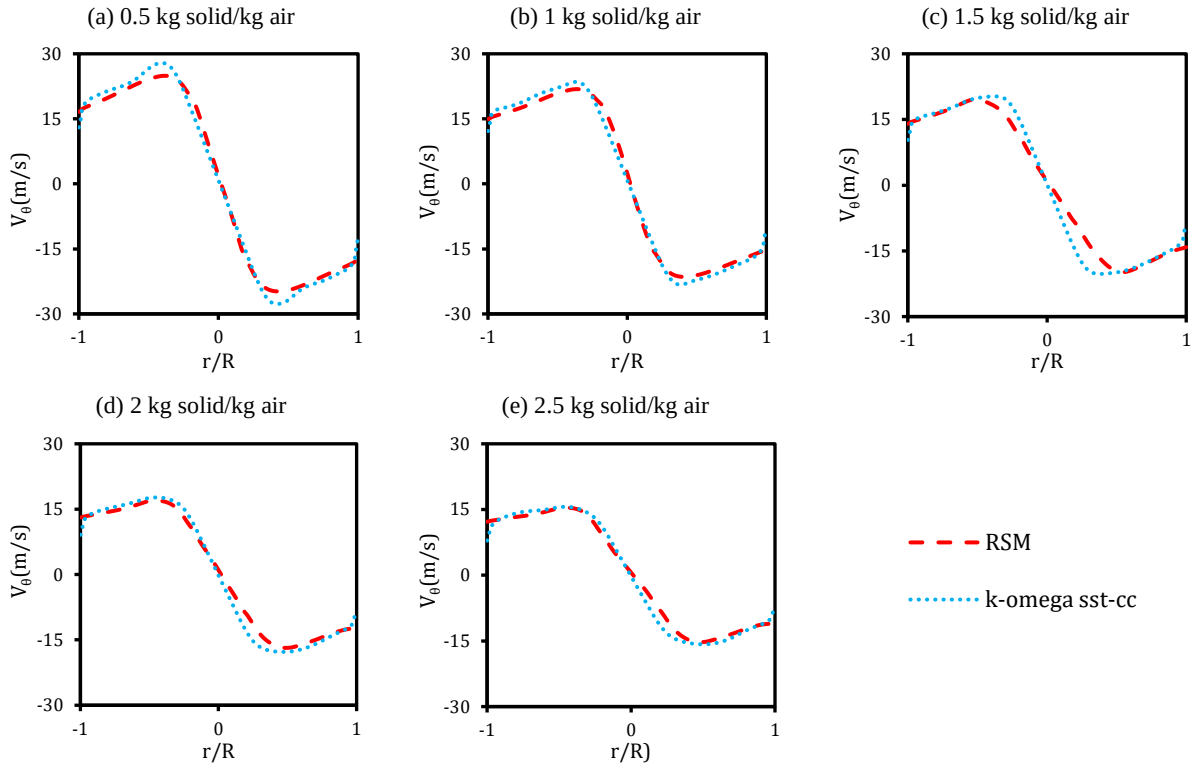

Figure 3-8. Profiles of tangential gas velocity (m/s) at a specific height (0.3 m away from cyclone roof) evaluated for different solid loading ratios: (a) 0.5, (b) 1, (c) 1.5, (d) 2, and (e) 2.5 kg solid/kg air.

Figure 3-9 shows the contours of axial velocity for different solid loading ratios obtained by both turbulence models. It can be observed that the high axial velocity region (reddish part) shrinks and move upwards as the solid load is increased. Unlike tangential velocity distribution, a visible discrepancy between axial velocity profiles obtained by the two turbulence models can be observed. However, the discrepancy becomes less intense as the solid load is increased. This discrepancy might lead to a discrepancy in the prediction of performance parameters of cyclones such as pressure drop and separation efficiency obtained from these two turbulence models. However, the results of the present study indicate that this discrepancy is minor, at least in terms of pressure drop.

As expected, the axial velocity increases in the direction from the wall to the centre and reaches its maximum at the cyclone axis. The axial gas velocity in the near-wall region is negative, meaning that the gas flow is swirling down and carry particles concentrated in the near-wall region downwardly towards the dust bin. On the other hand, far from the walls, around the centre, the axial gas velocity is positive, meaning that the gas flow is swirling up in the centre as expected. Figure 3-10 compares the radial distribution of axial gas velocity at a specific height (0.3 m away from the cyclone roof) for both turbulence models and various solid loads, which shows the mentioned discrepancy of predictions between the two turbulence models.

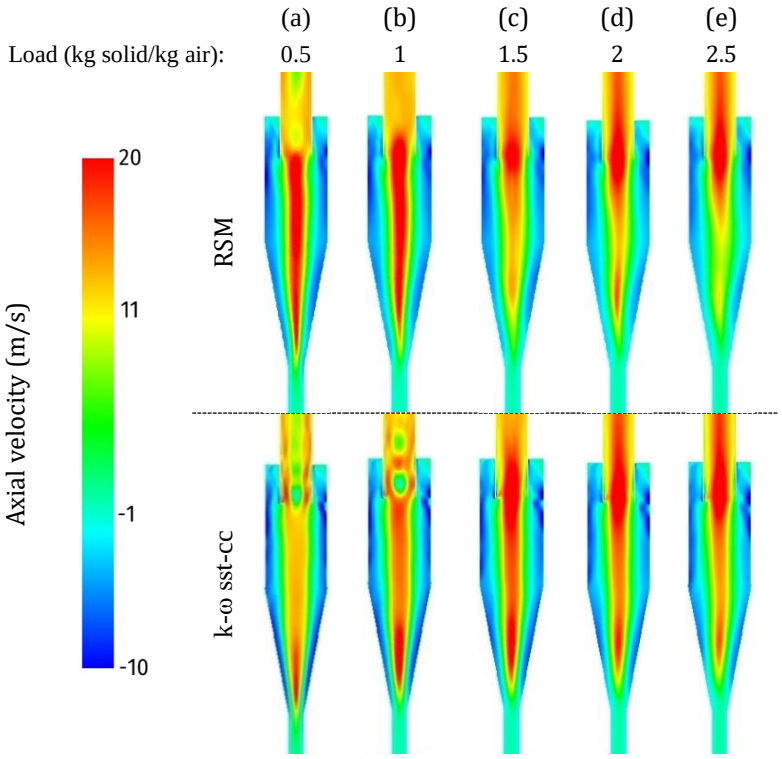

Figure 3-9. Axial velocity (m/s) distributions at the central section parallel to the cyclone inlet obtained from the RSM turbulence model (up) and k-ω sst-cc turbulence model (down) under different solid loading ratios: (a) 0.5, (b) 1, (c) 1.5, (d) 2, and (e) 2.5 kg solid/kg air.

As can be observed from Figure 3-10, this discrepancy diminishes as the solid load is increased. It should also be noted that, although k-ω sst-cc might not predict maximum axial velocity accurately, the width of the downward and upward swirling motion is predicted almost as well as RSM, which is of importance for predicting particles fate (whether a particle is separated or escaped). In the present study, it is meaningless to study the effect of the turbulence model on predicting the fate of particles because only comparatively large particles (2 mm) are injected which all are separated into the dust bin independent of operating conditions or used turbulence model (in all simulated cases separation efficiency is 100%).

Figure 3-11 shows static pressure distributions at the central section under different solid loading ratios obtained from both turbulence models used. As expected from cyclones, high-pressure regions are observed close to the cyclone wall; in all cases, the static pressure decreases in the direction from the wall to the center. An increase in solid load leads to shrinkage of the negative pressure core.

Figure 3-12 shows the distributions of solid volume fraction for the case with a solid loading ratio of 1.5 kg solid/kg air as an example. Distributions obtained from both turbulence models are quite similar suggesting that quite similar particle motion is obtained by each turbulence model. It can be observed that as expected from cyclones, particles are concentrated in the near-wall region.

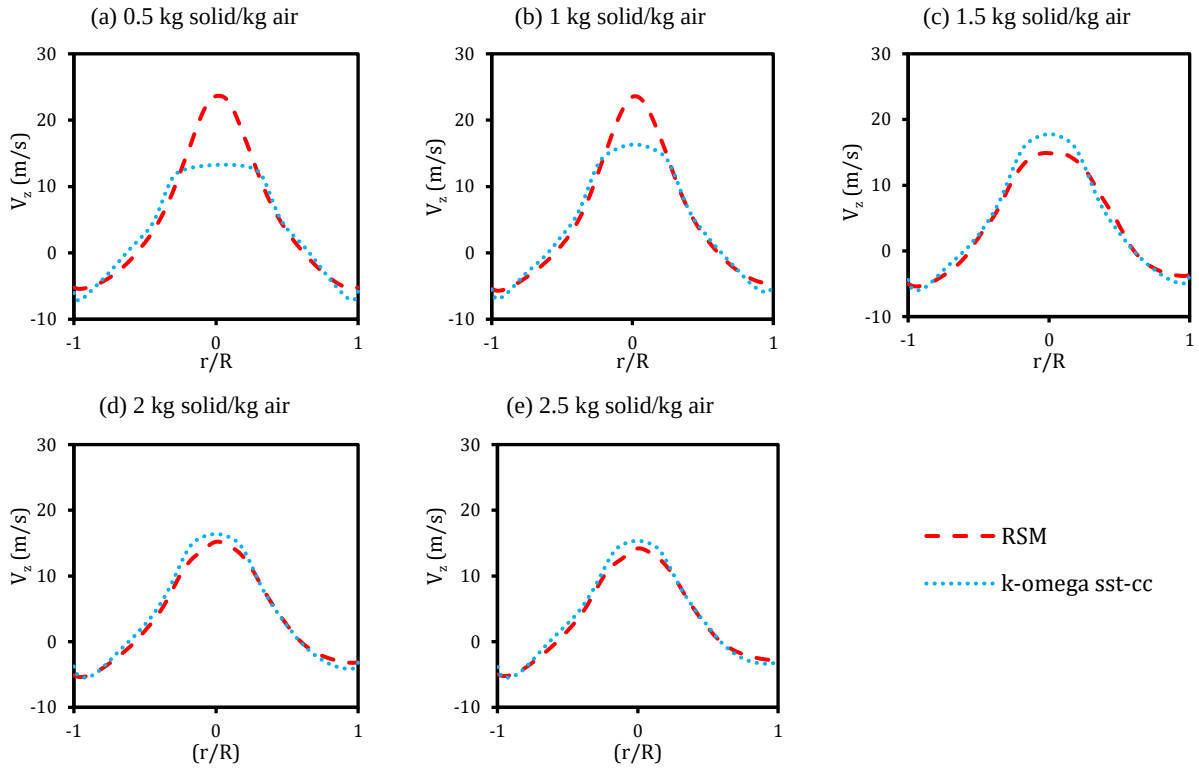

Figure 3-10. Profiles of axial gas velocity (m/s) at a specific height (0.3 m away from cyclone roof) evaluated for different solid loading ratios: (a) 0.5, (b) 1, (c) 1.5, (d) 2, and (e) 2.5 kg solid/kg air.

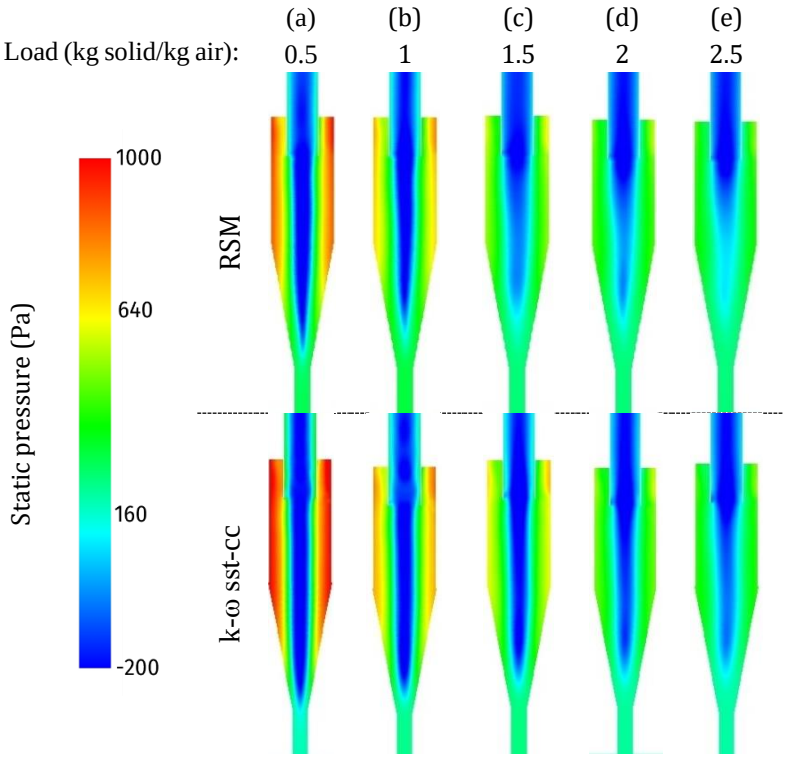

Figure 3-11. Static pressure (Pa) distributions at the central section parallel to the cyclone inlet obtained from the RSM turbulence model (up) and k-ω sst-cc turbulence model (down) under different solid loading ratios: (a) 0.5, (b) 1, (c) 1.5, (d) 2, and (e) 2.5 kg air/kg air.

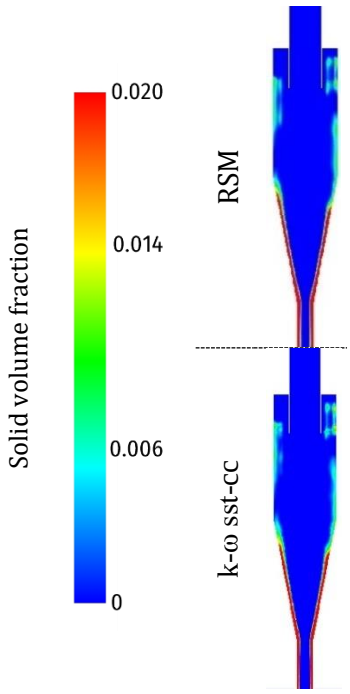

Figure 3-12. Solid volume fraction distributions at the central section parallel to the cyclone inlet obtained from the RSM turbulence model (up) and k-ω sst-cc turbulence model (down) under a solid loading ratio of 1.5 kg solid/kg air.

In addition to these comparisons, velocity fluctuations obtained from the two turbulence models were also compared. This comparison is presented in Appendix A.

3.9 Conclusions

By comparing results obtained from the DDPM multiphase model with experimental data of pressure drop of a lab-scale cyclone with high solid loads, it can be concluded that, at least, in terms of prediction of pressure drop, this model coupled with either RSM or k-ω sst-cc is capable to simulate cyclones working under high solid loads. Predictions obtained from DDPM are similar to predictions obtained from a more expensive multiphase model (DEM). The model is well able to capture the reduction in pressure drop and swirling motion due to an increase in solid flow rate. In addition to similar prediction of pressure drop, two tested turbulence models provide similar and reasonable flow pattern predictions as well; the discrepancies observed in the predicted flow patterns are minor so that it does not affect the pressure drop predictions as an important performance parameter of cyclones. Although noticeable discrepancies in the prediction of the velocity fluctuations from two tested turbulence models are observed, in the near-wall region where the velocity fluctuations are of more importance the predictions are in better agreement.

In general, by having this validation, the model can be used with more confidence for simulation of industrial-scale cyclone preheaters as the ultimate goal of the project. Despite minor discrepancies between the predictions of two tested turbulence models, considering the superiority of the k-ω sst-cc turbulence model in terms of computational cost and stability, and considering its acceptable prediction in reasonably good agreement with experimental data and comparable with predictions of RSM, the k-ω sst-cc turbulence model can be used on industrial-scale cyclones where the application of RSM might not be feasible.

Although the used models worked quite well in the prediction of pressure drop of a highly loaded lab-scale cyclone, its capability in terms of prediction of separation efficiency, as another important performance parameter of cyclones, should be investigated as well. The problem to do so was that as far as the author is aware, there was not a published suitable experimental study on a cyclone working under our desired solid load that provides separation efficiency measurements to be used as validation data.

After validation of the model on a lab-scale cyclone (at least in the prediction of pressure drop), to move to larger-scale cases, a pilot-scale, isothermal, highly loaded cyclone at FLSmidth (Dania Research and Development (R&D) centre) tested under industrial conditions and ambient temperature was simulated. Details of this simulation will be discussed in Chapter 4.

4 CFD simulation of an isothermal large-scale cyclone operating under high solid loads

This chapter is a reprint of the manuscript “A hybrid multiphase model accounting for particle agglomeration for coarse-grid simulation of dense solid flow inside large-scale cyclones” published in Powder Technology [158].

4.1 Abstract

A hybrid multiphase model (Dense Discrete Phase Model, DDPM) coupled with an agglomeration model and a sub-grid drag model was developed for simulation of industrial-scale cyclones with high solid loading. The model is validated by experimental results of pressure drop and separation efficiency from a pilot-scale cyclone with a diameter of 1.6 m. Key trends such as improvement in separation efficiency and reduction in pressure drop of cyclone due to an increase in particle load are well captured by the model. It is concluded that including the agglomeration model is crucial in particular in cases involving very fine particles (d_p < 15 μm) for accurate predictions of pressure drop and separation efficiency, while using the sub-grid drag modification improves the prediction of separation efficiency.

4.2 Introduction

Industrial cyclones operating under high solid loads (greater than 0.1 kg solid/kg air) are widely used as a key component in building material industries such as cement production and also in processes employing Circulating Fluidized Beds (CFB). However, there is still a lack of consensus on the key mechanisms involved in the operation of highly-loaded cyclone separators, considering the limited number of experimental and modeling studies focusing on them. While conducting informative experiments might be unfeasible on industrial cyclones, a reliable CFD model may provide better knowledge on the mechanisms occurring in such industrial cyclones and thereby help for better scaling-up, design, optimization and troubleshooting.

Cyclones are applicable in the whole solid volume fraction range of particle-laden flows. Depending on the value of solid load of the studied cyclone, one-way [20–22,52,70,71,81,84,88,111], two-way [63–65,69,73,91], or four-way [9–11,26–28,51,55,58,59,66,67,74,80,94,97,103,104,108,109] coupling were considered to model multiphase interactions in them. Considering the relatively high solid load of cyclones used in building material industries and CFB units (typically above 0.3 kg solid/kg air and can be on the

order of 10-100 kg solid/ kg air [159]), which are the focus of the present work, and the fact that the particles are mostly concentrated in the near-wall region, the four-way coupling is required to be applied to correctly model the dense particle-laden flow.

Based on the framework by which the dispersed phase is treated, four-way coupling multiphase modeling of dense dispersed particle-laden flows is conventionally divided into two types: Discrete Element Method (DEM) [99], and Eulerian–Eulerian or granular Two-Fluid Model (TFM) [93]. In addition to these two, a more novel type, known as the hybrid multiphase model [11], was developed to benefit from the advantages of the two conventional types and avoid their disadvantages. All these three types have been used for the simulation of dense particle-laden flow in cyclones [9–11,26–28,55,58,66,67,74,80,94,97,103,104,108,109,160]. A version of the hybrid multiphase model introduced by Ansys Fluent, known as the Dense Discrete Phase Model (DDPM), seems to be a good option for simulation of industrial-scale highly loaded cyclones. DDPM is computationally affordable for industrial dense particle-laden flows as it models particle-particle interactions, unlike DEM which directly resolves them. In addition, unlike TFM, DDPM easily handles polydispersed particles which is crucial for the hydrodynamics and the performance (separation efficiency) of cyclones. However, DDPM requires some modifications for simulation of highly loaded industrial cyclones working with fine particles.

Accurate prediction of drag force as the dominant force that governs particle motion in cyclones is vital if reasonable predictions of performance parameters of cyclones are desired [11]. It is widely reported that when multiphase models based on the Kinetic Theory of Granular Flow (KTGF) (and the DDPM is one of them) are used with coarse grids, then using common homogeneous drag models leads to failure in the prediction of the multiphase flow hydrodynamics [138,139]. This failure is due to the unrealistic prediction of drag force caused by the inability of coarse grids to resolve mesoscale structures (such as particle strands in cyclones) [11,138–146]. To overcome the deficiencies of homogeneous drag models for industrial-scale simulations heterogeneous drag models (also called sub-grid drag models) should be used to account for the effect of small mesoscale and heterogeneous structures on the drag correlations [11,138–146].

The size distribution of particles in industrial cyclones often includes very fine (even sub-micron) particles. When a particle-laden system includes very fine particles (usually finer than 10 μm) particle agglomeration is an important mechanism [161,162], especially in cyclones that the separation efficiency is highly sensitive towards the particle size. In fact, through agglomeration, larger particles (agglomerates) are formed from fines, which are separated more easily from the gas and thereby the separation efficiency of the cyclone is improved [11,121,123,137]. In addition, the improvement in separation efficiency with increased solid load may be adequately explained by the agglomeration phenomenon in cyclones. This explanation proposed by Mothes et al. [163] and supported by others [121,137] elaborates that higher particle load leads to more particle collisions and consequently more agglomeration and larger agglomerates. This phenomenon is believed to be significant enough to cause the observed increase in the overall separation efficiency in the cyclone [1]. It is worth mentioning that in some gas-solid dispersed cases particle breakage/attrition should be considered in addition to agglomeration, however, it is not the case in the present study. First, among the cyclone theories available in the literature, none uses attrition/breakage to explain the separation process [121,164], however, there are theories based on particle

agglomeration [163]. This suggests that particle attrition/breakage generally tends to be minor when compared with agglomeration in the case of cyclones. In addition, particle breakage/attrition in cyclones is only addressed in the literature in the case of cyclones processing catalyst particles in fluid catalytic cracking (FCC) [121,165] (at least as far as the authors are aware it is not addressed in the case of mineral processing cyclones [164]). That is because mineral particles are way less attritable so that particle attrition/breakage does not affect the performance of cyclones considerably [164]. Therefore, although in the case of catalyst particles, particle attrition/breakage might play a minor role, in the case of mineral processing cyclones (that are studied in the present work) it is negligible and can be ignored [121,164].

Another well-known observation called “fish-hook” behavior; the observation of minima in the grade efficiency curve of the cyclone at an intermediate particle size (meaning that finer particles are more easily separated compared to intermediate-size particles) can be explained by the agglomeration phenomenon. Finer particles are more prone to agglomeration compared to intermediate-size particles, so they make more and larger agglomerates and have high separation efficiency. The observation of such minima in many experimental studies [1,121,123,166–168] indicates the significance of the agglomeration phenomenon.

It is worth mentioning that the observation of such minima in the grade efficiency curve is usually interpreted as evidence of agglomeration, however, occurring of agglomeration in a cyclone does not guarantee to have a minimum in the curve [121,123]. The presence or absence of a minima and its location (particle size and fractional efficiency where minima are observed) depends on the operating conditions (most importantly gas and solid flow rate), the geometry of the cyclone, and the properties and size distribution of particles; therefore, such a minimum might not be observed in all cyclone cases even though agglomeration is occurring in them [121,123].

Considering the aforementioned reasons, if a reliable prediction of separation efficiency in the simulation of cyclones is desired, including a model to account for particle agglomeration is necessary. This becomes more important in cyclones operating with very fine particles as such particles are more likely to agglomerate. Also, in cyclones operating under high solid loads where particle collision is more frequent, particle agglomeration plays a more important role.

Most CFD models of cyclones presented in the literature are adequate only for low and moderate loaded and lab-scale cyclones as they neglect particle-particle interaction and particle agglomeration and use quite fine mesh which is inapplicable in industrial cases. A few models focused on highly loaded cyclones mostly considering large particles [9,10,160] where agglomeration does not play a significant role, and they were mostly implemented on lab-scale cases [9,10,55,97] with fine grids where homogeneous drag models are adequate. In addition, there is a lack of validation of models in the prediction of separation efficiency and the effect of solid load on the performance of cyclones.

In order to provide a better understanding of phenomena occurring inside highly loaded cyclones operating under industrial conditions, a pilot-scale cyclone running with limestone particles is simulated in this work. A hybrid Eulerian-Lagrangian multiphase model (DDPM) combined with a stochastic model to account for particle agglomeration is used with a sub-grid drag model to account for the effect of small structures not resolved by a coarse grid. The simulations are carried out using Ansys Fluent 2019R3 and validated against

measurements of separation efficiency and pressure drop conducted under several operating conditions of the pilot-scale cyclone and thereby evaluating the reliability, and predictive capability of the proposed model.

4.3 Experimental study for model validation

Figure 4-1 shows the configuration of a pilot-scale cyclone (1.6 m in diameter) located in FLSmidth R&D Center Dania tested under industrial operating conditions (particle load, material, and size, and hydrodynamic conditions are as the industrial cyclones but the setup works at room temperature) to provide validation data for the present CFD study. The configuration is made up of a cyclone-like swirl maker (2), the cyclone (5) with a dust bin (7) and the outlet pipe, a riser (4) connecting the swirl maker to the cyclone, and a particle injection pipe (3). The swirl maker is designed to mimic the actual flow pattern (swirling motion in the riser) in industrial configurations of cascades of cyclones. The gas stream is introduced to the swirl maker to have a swirling motion, then the particles are injected into the riser where the upward swirling motion of gas carries all the particles to the cyclone.

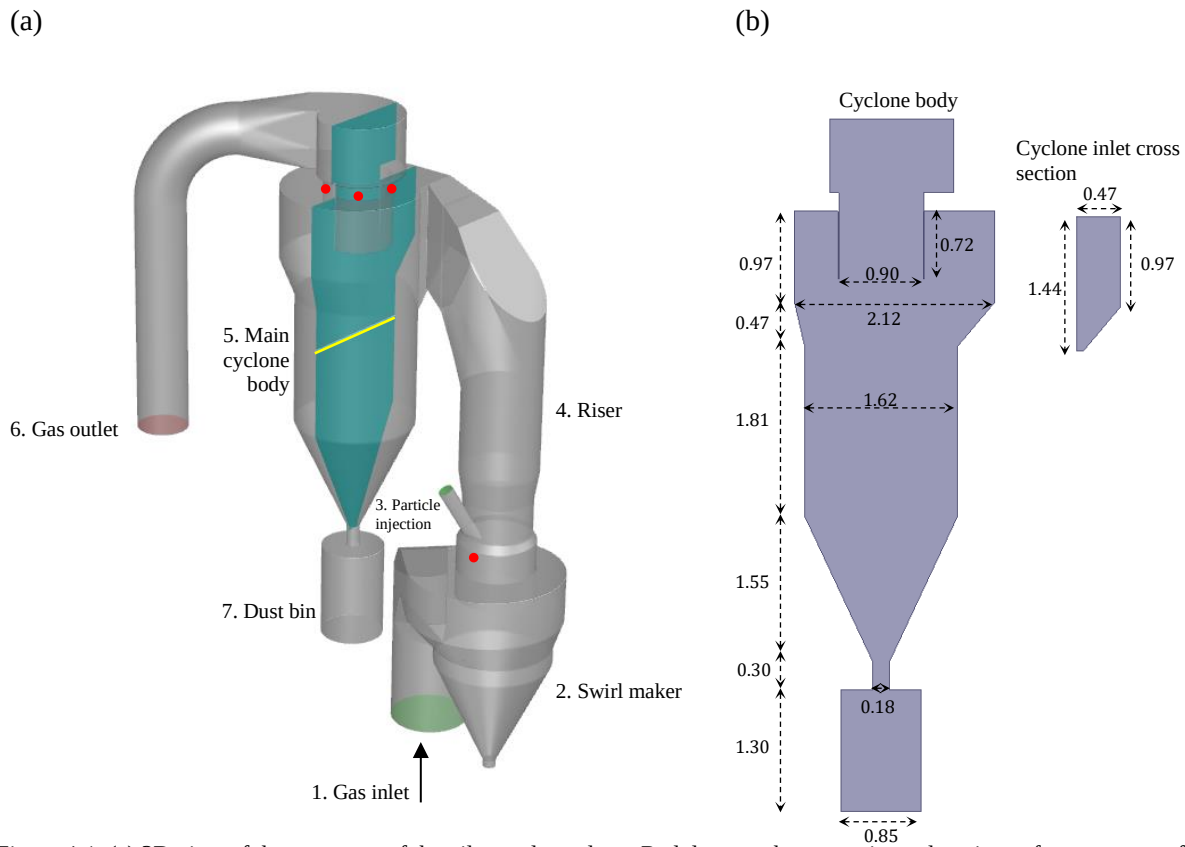

Figure 4-1. (a) 3D view of the geometry of the pilot-scale cyclone. Red dots are the approximate locations of pressure taps for measuring static pressure drop. The cyan plane and yellow line are the plane of contours and line of profiles in the results and discussion section (4.5). (b) 2D view of cyclone main body with dimensions (dimensions are in meter).

The particles (mineral raw meal used for cement production mostly comprised of limestone and clay) used in the experiments had a wide PSD (Particles Size Distribution) similar to the PSD used in cement plants. It is seen in Figure 4-2 that most particles are between 1 and 100 µm. The particles had a sauter mean diameter of 5.0 µm with a density of 3100 kg/m^3, which is classified as Geldart C type of particle (based

on Geldart's particle classification [120]); and known as cohesive particles which are very prone to agglomeration.

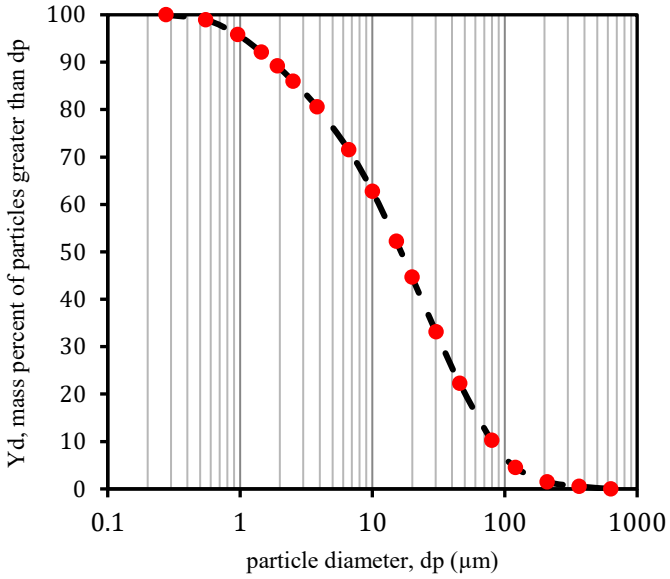

Figure 4-2. PSD of injected meal used for the experimental measurements. The analysis was performed using a Malvern mastersizer 2000 with a Hydro 2000S wet dispersion unit.

Table 4-1. Operating conditions of conducted tests on the pilot-scale cyclone. The cases are named in a way to present the main operating conditions of the case (e.g., in Case-1 G8.2-S3.7, gas flow rate and solid flow rate are 8.2 kg/s, 3.7 kg/s respectively).

Parameter	Case-1 G8.2-S3.7	Case-2 G8.2-S4.7	Case-3 G8.2-S5.4	Case-4 G9.4-S3.2	Case-5 G9.4-S4.2	Case-6 G9.4-S5.8	Case-7 G10-S5.1
Air flow rate (kg/s)	8.2	8.2	8.2	9.4	9.4	9.4	10.0
Solid flow rate (kg/s)	3.7	4.7	5.4	3.2	4.2	5.8	5.1
Solid loading ratio (kg solid / kg air)	0.45	0.57	0.66	0.34	0.45	0.62	0.51
solid volume fraction (m^3/m^3)	0.0002	0.0002	0.0003	0.0001	0.0002	0.0002	0.0002
Average gas velocity at cyclone inlet, v_{in} (m/s)	12.0	12.0	12.0	13.7	13.7	13.7	14.7
Average gas velocity in the riser (m/s)	7.6	7.5	7.6	8.7	8.6	8.6	9.3
Measured pressure drop (Pa)	1038	953	949	1357	1323	1302	1543
Measured separation efficiency (%)	93.4	95.6	95.8	90.8	93.5	95.4	94.1
Temperature (˚C)	24						
Particle density (kg /m^3)	3100						
Air density (kg/m^3)	1.187						
Air viscosity (kg/(m.s))	1.83×10^{-5}						

Static pressure was measured at locations (red dots) illustrated in Figure 4-1 to measure the pressure drop over the riser and cyclone. The separation efficiency was also measured based on the variation of accumulated mass in the dust bin, and the variation of mass in the silo connected to the particle injection pipe. Both parameters were measured and recorded for 5-7.5 minutes to ensure the stability of the operation.

The experiments were conducted at various operating conditions with different gas flow rates and solid flow rates (covering overall volume fraction of 0.0001 to 0.0003 as the common load in industrial cement cyclone preheaters, corresponding to solid load ratio from 0.34 to 0.66 kg solid/ kg air). Seven of these operating conditions are used in the present study as validation data. In Table 4-1, the operating conditions of these seven cases in addition to measured separation efficiency and pressure drop are summarized.

4.4 Model description

The hybrid Eulerian–Lagrangian multiphase model used in the present study (DDPM) is a Lagrangian–based hybrid model that implicitly approximates particle-particle interaction using the Kinetic Theory of Granular Flow (KTGF). In DDPM, the gas phase is treated in an Eulerian framework where the Navier–Stokes equations including phase volume fraction are solved. The particle phase is treated in a Lagrangian framework while the particle-particle interaction is modeled based on the Kinetic Theory of Granular Flow (KTGF) [169]. This approach was recently used for the study of cyclones working under high solid loads [10,55,58,109,160]. The equations describing this model including continuous phase and dispersed phase equations can be found in the literature [10]. To evaluate the solids stress tensor required in DDPM for modeling particle-particle interactions this model uses several closure law equations based on the KTGF to estimate some required parameters such as bulk, collisional, kinetic and frictional viscosities. the ones used in the present study (summarized in Table B-1 in Appendix B) were the same as other studies [10,55,160] in the literature using DDPM to simulate cyclones.

Regarding turbulence modeling, in addition to Reynolds Stress Model (RSM) [9,19,20,29,51–54] and Large Eddy Simulation (LES) [4,13,19,52,69,71–75] as widely accepted turbulence models in the literature for simulation of cyclones, a novel Eddy Viscosity Models (EVMs) sensitized to flow rotation and curvature such as the one available in Ansys Fluent (k-ω sst-cc) have attracted attention recently. Such sensitization can overcome weaknesses of EVMs in the simulation of cyclones providing quite reliable results, competitive with more complicated turbulence models [42,47–50]. LES requires very fine girds that is unfeasible in industrial-scale cases. On the other hand, EVMs are way more computationally efficient and robust compared to RSM that is crucial in simulation of industrial cases. These make k-ω sst-cc an optimal option for simulation of turbulence in cyclones. The equations describing the turbulence model used in the present work (a dispersed version of k-ω sst turbulence model sensitized to rotation and curvature) can be found in Ansys Fluent theory guide [147].

In the present study, for particle tracking, in addition to translational particle motion, rotational particle motion including a rotational drag force [170] was considered to provide more realistic particle motion in a cyclone as suggested by several authors [9,74,75,104,106]. Also, the Magnus force was added to the translational particle motion by using the Oesterle-Bui-Dinh correlation [171].

The particle-wall collision was modeled by normal and tangential reflection coefficients (i.e. the ratio between particle rebound velocity to particle impact velocity) of 0.8 as used by many others in cyclones. Moreover, considering the proven impact of wall roughness in particle motion in confined cases such as cyclones [1,8] a rough wall model [172–174] available in Ansys Fluent with roughness parameters of a wall with ISO no. 12 (ISO 4287) was used to obtain more realistic particle trajectories.

4.4.1 Drag model

Various drag models were designed and validated for different flow regimes and unit operations, but none of them was designed or validated in cyclones. However, a model known as the revised Sarkar et al. drag model [138] successfully verified and validated for a wide range of applications such as bubbling fluidized bed, turbulent fluidized bed, dense circulating fluidized bed, dilute circulating fluidized bed [138], dual-circulating fluidized bed [146], CFB risers [175,176], and FCC riser [177] seems to be a suitable option to be tested in cyclones as well.

Although none of the sub-grid drag models available in the literature was intended for the cyclones where the flow rotation is dominant, in addition to its wide range of verified applications, the reason that the revised Sarkar et al. drag model [138] was chosen over others was that it provided reliable predictions in pre-tests simulations. The revised Sarkar et al. drag model [138] provided predictions in slightly better agreement with experimental results when compared with other tested sub-grid drag models such as Pirker et al. [142], Radl et al. [143], and Igci et al. [141]. In particular, it better captured the trend of improvement in the separation efficiency when the solid load is increased.

Sub-grid drag models basically formulate a drag reduction resulting from sub-grid level structures such as clustering effects that leads to a more accurate prediction of drag force in coarse-gird simulation. Normally a heterogeneity index H_d, accounting for the hydrodynamic disparity between homogeneous and heterogeneous drag is defined based on a specific homogeneous drag model. In the present model heterogeneity index is defined based on the Wen-Yu drag model in equation 4–1:

$$H_d = \frac{CD_{revised-Sarkar}}{CD_{Wen-Yu}} = \frac{\beta_{reivsed-Sarkar}}{\beta_{Wen-Yu}} \qquad 4\text{–}1$$

In the revised Sarkar et al. drag model [138], the heterogeneity index H_d is formulated as follows by equation 4–2 to 4–11:

$$H_d = \frac{\beta_{revised-Sarkar}}{\beta_{Wen-Yu}} = \begin{cases} 1 - 0.95\left(1 - e^{-\mathrm{A}\left(u_{slip}^{*} - u_0\right)^{\mathrm{P}}}\right) & u_{slip}^{*} > u_0 \\ 1 & u_{slip}^{*} \le u_0 \end{cases} \qquad 4\text{–}2$$

$$CD_{Wen-Yu} = \begin{cases} \frac{24}{Re_p}\alpha_g{}^{-2.65}\left(1 + 0.15 Re_p{}^{0.687}\right) & Re_p \le 1000 \\ 0.44\alpha_g{}^{-2.65} & Re_p > 1000 \end{cases} \qquad 4\text{–}3$$

$$\beta_{Wen-Yu} = \frac{3}{4}\frac{\alpha_g(1-\alpha_g)\rho_g|u_g - u_p|}{d_p} CD_{Wen-Yu}\alpha_g{}^{-2.65} \qquad 4\text{–}4$$

$$Re_p = \frac{\alpha_g \rho_g d_p |u_g - u_p|}{\mu_g} \qquad 4\text{–}5$$

$$\mathrm{P} = (a_{14} + a_{15}\alpha_s + a_{16}\alpha_s{}^2)\left(1 + \frac{a_{17}}{\Delta_f{}^*} + \frac{a_{18}}{(\Delta_f{}^*)^2}\right) \qquad 4\text{–}6$$

$$\mathrm{A} = \frac{(a_1 + a_2\alpha_s + a_3\alpha_s{}^2 + a_4\alpha_s{}^3 + a_5\alpha_s{}^4)(1 - e^{-300\alpha_s})}{1 + e^{100(\alpha_s - 0.55)}}\left(1 + \frac{a_6}{\Delta_f{}^*} + \frac{a_7}{(\Delta_f{}^*)^2}\right)\left(1 + \frac{a_8}{(u_{slip}^{*})^2}\right) \qquad 4\text{–}7$$

$$u_0 = \frac{a_9 + a_{10}\alpha_s}{0.01 + {\alpha_s}^{a_{11}}}\left(1 + \frac{a_{12}}{{\Delta_f}^*} + \frac{a_{13}}{({\Delta_f}^*)^2}\right) \quad 4\text{–}8$$

$${\Delta_f}^* = \max\left(\frac{g\Delta_f}{{u_t}^2}, 0.5\right) \qquad \Delta_f = 2(V_{cell})^{1/3} \quad 4\text{–}9$$

$$u^*_{slip} = \frac{\left|u_g - u_p\right|}{u_t} \qquad u_t = \frac{g{d_p}^2(\rho_p - \rho_g)}{18\mu_g} \quad 4\text{–}10$$

$$a_{1-18} = \{0.75597773, 2.73931487, -5.60196497, -1.65853820, 16.70299223, -0.44145335, 0.18195034, -0.01827347, 0.28441799, -1.943573770, 0.22177961, 0.31175890, -0.15971960, 0.47750002, 0.062794180, 5.13011673, 0.67680355, -0.54535726\} \quad 4\text{–}11$$

As a point of clarification, a_{1-18} values in equation 4–11 were obtained by fitting data from fine-grid kinetic theory-based two-fluid model (Eulerian–Eulerian model) simulations in periodic 3D domains using algebraic expressions (equations 4–2 to 4–10) [138]. Note that using sub-grid drag models constituted based on Eulerian–Eulerian simulations (such as the revised Sarkar et al. drag model) in an Eulerian–Lagrangian model (such as DDPM in present work) is an approximation as the particle information needs to be mapped to the Eulerian grid before using the correlations [144,178]. An approximation of this kind is reasonable and the drag models deduced for Eulerian–Eulerian simulations can be used in Eulerian–Lagrangian simulations (such as DDPM) and the other way around [144,178] (Particularly, the revised Sarkar et al. drag model has been used successfully in Eulerian–Lagrangian models in the literature [146,175]).

The filter-to-grid ratio of 2 ($\Delta_f = 2(V_{cell})^{1/3}$) was suggested in the revised Sarkar model [138]. In general, when using sub-grid drag models that are a function of the filter size, the predictions might be affected by filter-to-grid ratio so that in those cases the ratio should be optimized [179–181] or instead more novel models that make H_d independent of filter size should be used [182]. However, the sensitivity analysis of the filter-to-grid ratio (the common values of 1, 2, and 3 were tested) conducted for case-2 of operating conditions of the present study showed that the predictions are not affected by the filter-to-grid ratio considerably (the variation of pressure drop and separation efficiency from is less than 2% and 1% respectively), so the suggested value of 2 could be used.

The revised Sarkar et al. drag model was implemented to the Ansys Fluent solver using "DEFINE DPM DRAG" user-defined function. It should be noted that the Wen-Yu drag model is also tested in the present work for comparison.

4.4.2 Agglomeration model

The agglomeration was described by a stochastic Lagrangian inter-particle collision model proposed by Sommerfeld [122,161], assuming that two particles may collide only if they are located in the same Eulerian cell. The model is based on the algorithm of O'Rourke [183] to efficiently reduce the computational cost.

The calculation algorithm of the agglomeration model is summarized in Figure 3 and details of the model equations are listed in Table 4-2. The probability of two parcels in a cell colliding N times in a time step Δt, $P(N)$, can be estimated using equations 4–12 and 4–13. Considering that the probability of not having any collision at all is $P(0) = \exp(-\bar{n})$, to at least have one probable collision a randomly generated number

RN in the range [0, 1] must be greater than $P(0)$ (equation 4–14). On the other hand, the collision efficiency, η_p, defined as the ratio of the number of particles hitting the collector to the number which would strike it if the streamlines were not diverted by the collector can be estimated using equations 4–15 and 4–16. A collision is only occurring if the lateral displacement L (defined using a random process in equation 4–17) is smaller than the value of Y_c (the radial distance defined in equation 4–18) plus the small particle radius (equation 4–19). To have a collision both criteria in equations 4–14 and 4–19 must be met.

Table 4-2. List of equations for agglomeration modeling.

$\bar{n} = \frac{n_2 \frac{\pi}{4}(d_1 + d_2)^2 \lvert\overrightarrow{u_{p1}} - \overrightarrow{u_{p2}}\rvert \Delta t}{V_{cell}}$		4–12
$P(N) = \exp(-\bar{n})\frac{\bar{n}^N}{N!}$		4–13
$RN > P(0)$		4–14
$\mathrm{St}_{rel} = \frac{\rho_p d_2 \lvert\overrightarrow{u_{p1}} - \overrightarrow{u_{p2}}\rvert \Delta t}{18\mu_g d_1}$		4–15
$\eta_p = (\frac{\mathrm{St}_{rel}}{\mathrm{St}_{rel} + a})^b$	a and b are functions of a relative Reynolds number Re_k [162]	4–16
$L_a = \frac{2L}{d_1 + d_2} = \sqrt{XX^2 + ZZ^2}$	XX and ZZ are randomly generated numbers in the range [0, 1] so that $L_a < 1$	4–17
$\eta_p = (\frac{2Y_c}{d_1})^2$		4–18
$L < Y_c + 0.5 d_2$		4–19
$U_{crit} = \frac{\sqrt{1 - e^2}}{e^2} \frac{H}{\pi d_2 {z_0}^2 \sqrt{6 p_c \rho_p (1 + d_2/d_1)}}$	Constants are summarized in Table 4-3; values proposed by Sommerfeld [161]	4–20
$\lvert\overrightarrow{u_{p1}} - \overrightarrow{u_{p2}}\rvert \cos(\phi) \leq U_{crit}$	$\phi = \arcsin(L_a)$ is the impact angel of two collided particles	4–21

Table 4-3. Particle properties for calculation of the critical impact velocity

Parameter	Value
Hamaker constant H (J)	5×10^{-19}
Minimum contact distance z_0 (m)	4×10^{-10}
Yield pressure p_c (Pa)	5×10^{9}
Energetic restitution coefficient e	0.7

When a collision takes place, two collided particles either stick (and form an agglomerate) or rebound. Only the van der Waals force was considered as the interparticle force. The possibility of particles sticking or rebounding can be evaluated using a critical velocity based on an energy balance, which is given in equation 4–20. When the normal relative velocity of two colliding particles is lower than this critical velocity, the restitution energy after the impact does not exceed the van der Waals energy between collided particles, and agglomeration will occur (equation 4–21).

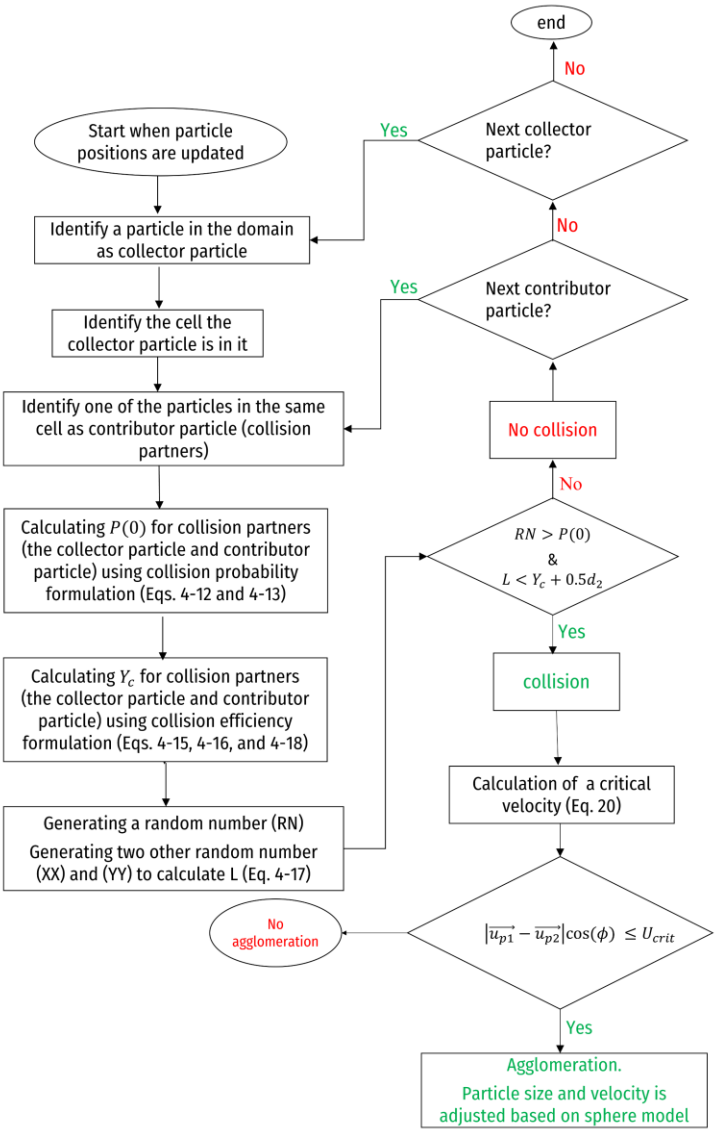

Figure 4-3. Calculation algorithm of the agglomeration model

When two collided particles form an agglomerate, the size of the agglomerate and its velocity were calculated based on mass and momentum conservation. To simplify, spherical agglomerates (with the mass of two collided particles) without any void (which is referred to as the sphere model [74]) were considered as the outcome of the agglomeration process. The assumption and derivation of the equations are described in detail in the literature [122,161].

This algorithm was implemented to the Ansys Fluent solver using “DEFINE DPM SPRAY COLLIDE” user-defined function and was called whenever particle positions were updated.

4.5 Results and discussion

The suggested model performs numerically stable and provides reasonable flow pattern, particle motion, and pressure drop and separation efficiency predictions that will be discussed in detail in the following sections.

4.5.1 Mesh independence

The mesh independence study was performed for two of the operating conditions (case-4 and case-6) using seven levels of mesh resolution (polyhedral mesh with prism layers described in more detail in Appendix B). Some information about these seven levels of mesh including the average cell volume, grid resolution, and grid-to-parcel size ratio are presented in Table 4-4. It is worth mentioning that considering the values of $\sqrt[3]{\overline{V_{cell}}}/\overline{d_p}$ being in order of 10^3, the present study is considered a coarse-grid simulation (normally when the grid size is significantly greater than 10 particle diameters, the simulation is referred to as coarse-grid simulation [96]).

Table 4-4. Levels of grids in mesh independence study. $\overline{d_p}$ is the sauter mean diameter of particles and equals 5×10^{-6}m. Level 3 is used for the rest of simulations.

Grid	Number of cells (million)	$\overline{V_{cell}} = Average\ of\ cell\ volume$ (m^3)	$\sqrt[3]{\overline{V_{cell}}}/\overline{d_p}$ grid dimensionless resolution	$\overline{V_{cell}}/(parcel\ volume)$ grid to parcel size ratio
Level 7	0.5	63.6×10^{-6}	7982	4926
Level 6	1.1	61.0×10^{-6}	7873	4728
Level 5	1.7	5.99×10^{-6}	7826	4643
Level 4	2.9	13.5×10^{-6}	4758	1044
Level 3	**4.2**	$\mathbf{9.6\times10^{-6}}$	**4254**	**746**
Level 2	5.5	5.3×10^{-6}	3485	410
Level 1	7.5	5.0×10^{-6}	3426	390

The two cases were selected as two cases with the same gas flow rate (9.4 kg/s) but with different solid loads (case-4 with a loading ratio of 0.3 kg solid/kg and case-6 with a loading ratio of 0.6 kg solid/kg) to investigate whether grid size could influence trends of cyclone performance parameters when the solid load is increased, in particular the improvement in separation efficiency.

Predicted pressure drop and separation efficiency obtained from these levels are compared in Figure 4-4 and Figure 4-5. As can be observed from these figures the predictions did not deviate considerably from the prediction of the finest mesh when 4.2 million cells or finer were used; The deviations were less than 1% in the case of separation efficiency and less than 2% in the case of pressure drop, suggesting that predicted results were independent of the characteristics of the mesh size if at least 4.2 million computational cells were used. In addition, the improvement in separation efficiency when the solid load was increased from case-4 to case-6 as a well-known trend also observed in our measurements could just be captured if at least 4.2 million cells were used while coarser girds were unable to capture such an improvement. Therefore, the rest of the simulations and studies were done using this mesh resolution.

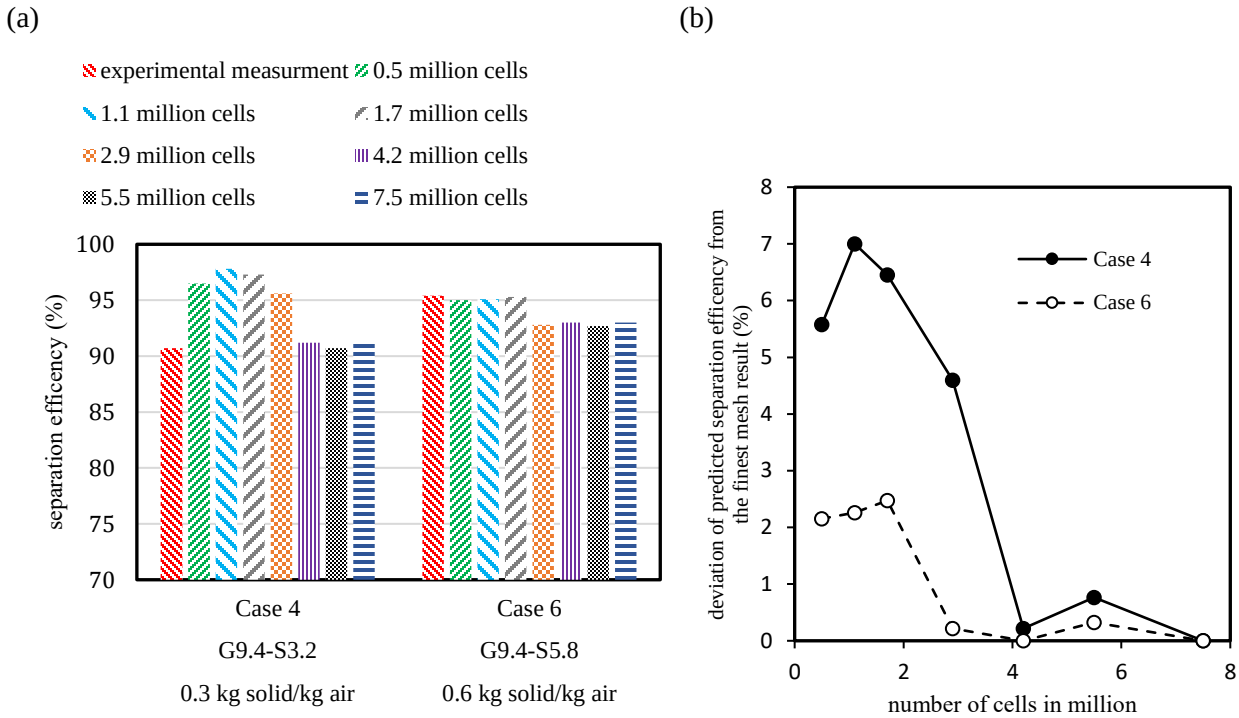

Figure 4-4. (a) Comparison of predicated separation efficiency obtained from seven levels of mesh for two operating conditions (case-4 and case-6). (b) Deviation of predicted separation efficiencies from the one predicted using the finest mesh.

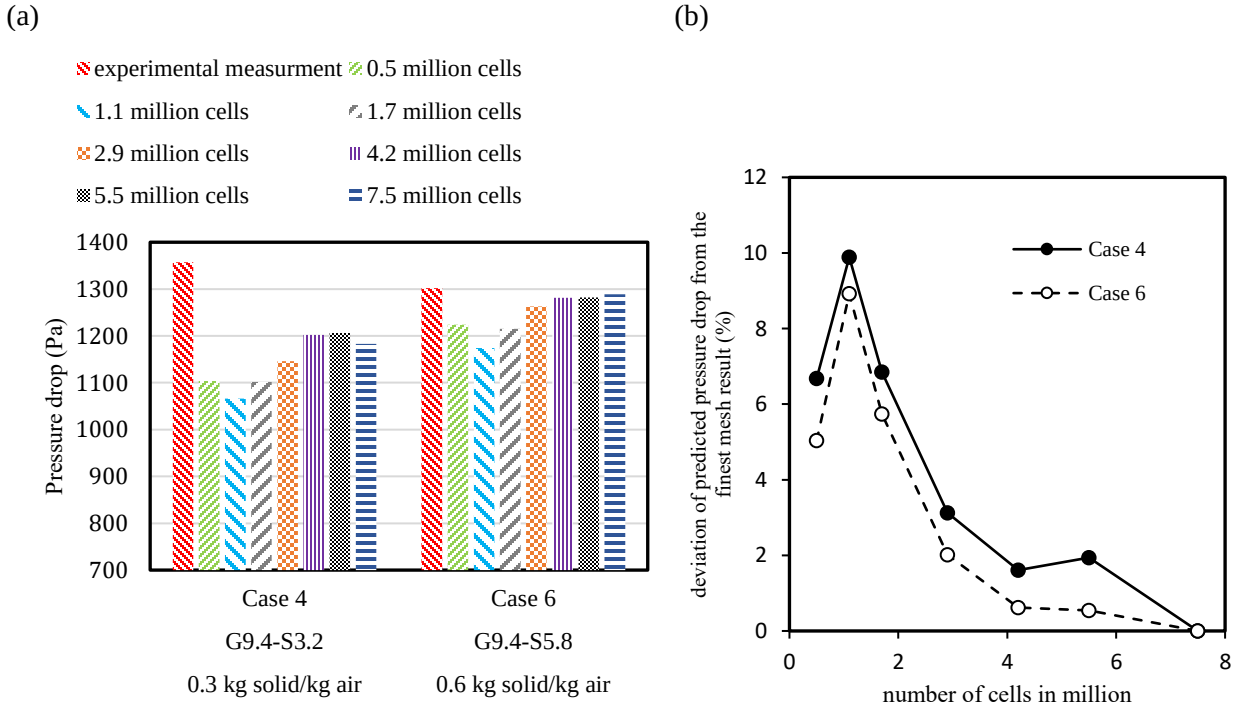

Figure 4-5. (a) Comparison of predicated pressure drop obtained from seven levels of mesh for two operating conditions (case-4 and case-6). (b) Deviation of predicted pressure drops from the one predicted using the finest mesh.

Also, to quantitatively evaluate the grid convergence and the error due to grid resolution [184], convergence calculations for the three finest grid levels using the approach suggested by Roache [185,186] are presented in Table 4-5. The formulation can be found in the referenced papers. As the values for α are close to unity,

it can be concluded that the solution is within the asymptotic range of convergence. Using these calculations, the values when the grid spacing vanishes can be estimated based on the Richardson extrapolation [185] with an error band (for example the pressure drop in case 4 is estimated to be 1211 Pa with an error band of 2.979%).

Table 4-5. Grid convergence calculations using the GCI method for the three finest grid levels. $i = 0$ is the value at zero grid space

		i	Ng_i ($\# \times 10^6$)	f_i	$rg_{i,i+1}$	$eg_{i,i+1}$	$\varepsilon g_{i,i+1}$	$GCI_{i,i+1}^{fine}$ %	Rg	αg
Case 4	Pressure drop (Pa)	0		1211						
		1	7.5	1183						
					1.109	23	0.019	2.979		
		2	5.5	1206					-5.862	1.019
					1.094	-4	-0.003	0.538		
		3	4.2	1202						
	Separation efficiency (%)	0		87.7						
		1	7.5	91.4						
					1.109	-0.7	-0.008	5.058		
		2	5.5	90.7					-1.389	0.992
					1.094	0.5	0.006	4.132		
		3	4.2	91.2						
Case 6	Pressure drop (Pa)	0		1281						
		1	7.5	1289						
					1.109	-7	-0.005	0.799		
		2	5.5	1282					6.962	0.995
					1.094	-1	-0.001	0.121		
		3	4.2	1281						
	Separation efficiency (%)	0		94.9						
		1	7.5	93.0						
					1.109	-0.3	-0.003	2.493		
		2	5.5	92.7					-0.997	0.997
					1.094	0.3	0.003	2.906		
		3	4.2	93.0						

Furthermore, the comparison of flow pattern distributions in seven levels of mesh presented in Figure 4-6 shows minor differences in flow patterns obtained by different grids. These differences were mainly in the core region and in quantifying the peak of velocities. However, in the near-wall region, the region with the greatest impact on the performance of a cyclone, very similar patterns were obtained by different grids. Variations in flow patterns explain the minor variation in predicted pressure drop and separation efficiency.

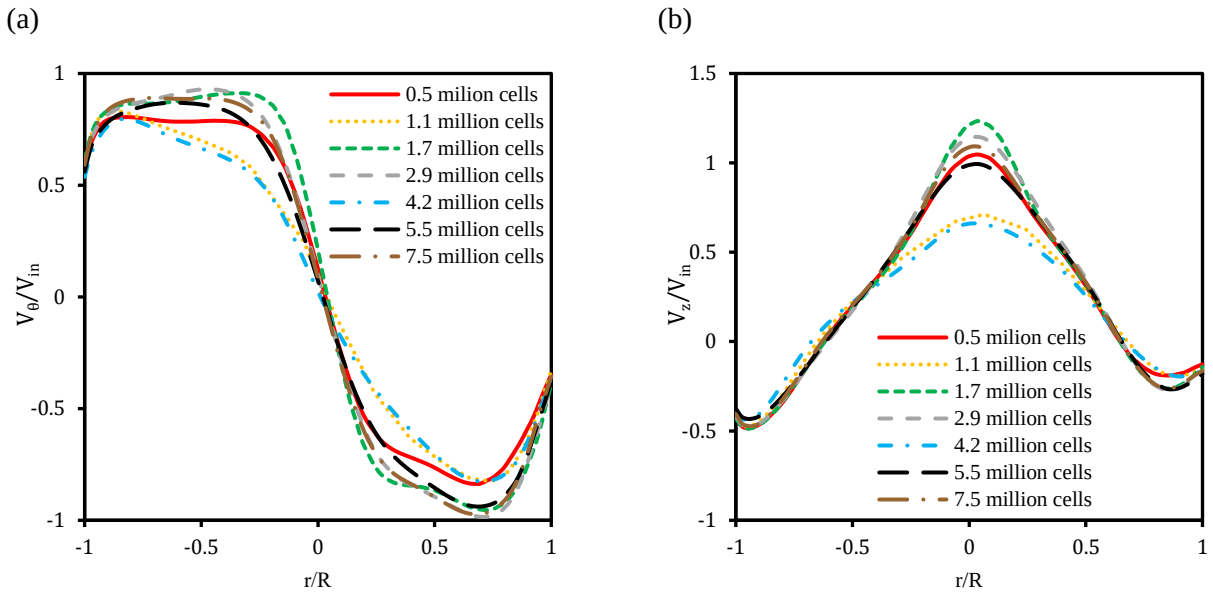

Figure 4-6. Comparison of flow pattern distributions in seven levels of mesh for case-4 (G9.4-S3.2) at a specific height (2 m below cyclone roof shown in Figure 4-1); (a) tangential velocity, (b) axial velocity.

In the present study, the strategy of coarse-graining was to have the same parcel size (same parcel mass) for different particle sizes. Three parcel sizes (1, 2 and 4 micrograms) were tested to perform parcel size independence. The deviations of results were negligible (below 0.5% for both pressure drop and separation efficiency).

In DDPM, the use of relatively large time steps (up to 0.1 s) is reported [10,187], however, time step size independence with the smallest time step of 1 ms was performed. Five courant numbers of 25 (0.001 s), 50 (0.002 s), 100 (0.004 s), 200 (0.008 s), and 400 (0.015 s) were tested showing that the results were independent of time step size in the studied range (the variation of both pressure drop and separation efficiency was less than 2%).

The results presented in this study were obtained from the parcel size of 4 micrograms and the courant number of 200 (to keep the simulations as fast as desired) ending up to having approximately 560, 670, 760, 430, 550, 750, and 690 thousand parcels in the domain in case-1 to case-7 respectively and a time step size of 5×10^{-3} s when convergence is achieved.

Details of solver settings used in the present work are summarized in Appendix B. Simulations were carried out on a Linux cluster using 32 processors (Intel(R) Xeon(R) Gold 6226R @ 2.90 GHz and 64 GB RAM with high-speed Infiniband network connection). For chosen mesh, parcel size, and time step, it took less than 2.5 hours to have 1 s progress in time (meaning that it will not take longer than 3 days to ensure steady results; tracking parameters show that 20-30 s of flow-time guarantee the steady condition, however, simulations continued up to 50 s). Therefore, considering available computational resources, the presented model is easily applicable and affordable for industrial-scale cyclone simulation.

4.5.2 Importance of agglomeration model

To show the significance of including an agglomeration model in the simulation of a highly-loaded cyclone, three of the cases were also simulated without implementing the proposed agglomeration model. The results are presented in Figure 4-7 and Figure 4-8 and are compared with experimental measurements and also model predictions where the agglomeration model was included. As shown in Figure 4-8 if an agglomeration model is not included, the separation efficiency will be highly under-predicted as very fine particles with low inertia remain in the domain which mostly escape from the cyclone vortex finder. Without agglomeration, particles enter the cyclone with a lower mean size ending up with a lower separation efficiency compared to the case with agglomeration.

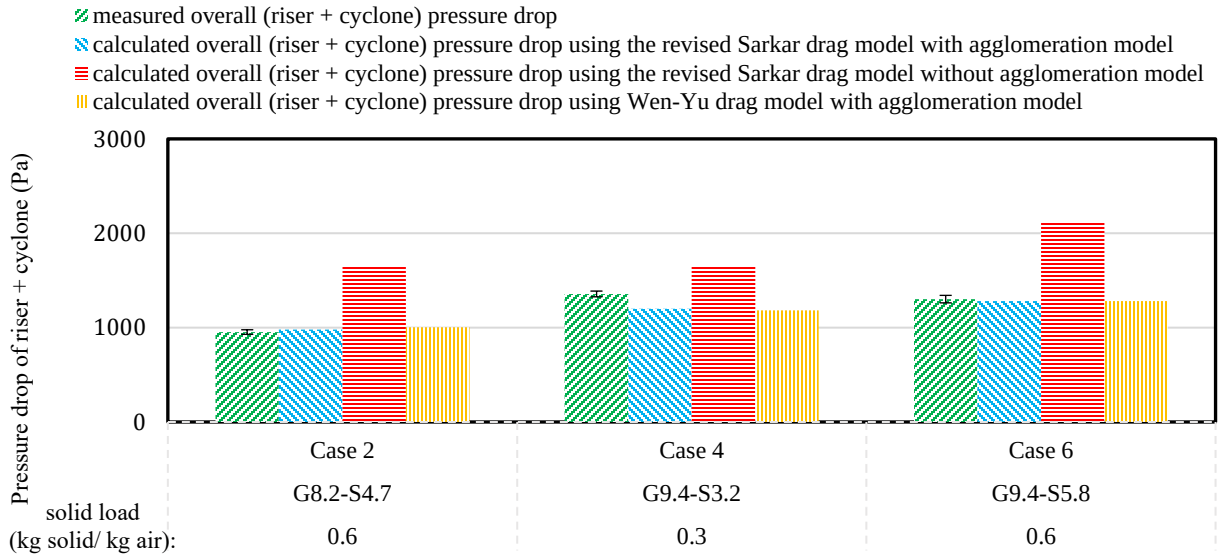

Figure 4-7. Comparison of calculated overall pressure drop obtained from (1) the revised Sarkar drag model with agglomeration model, (2) the revised Sarkar drag model without agglomeration model, and (3) Wen-Yu drag model with agglomeration model. Error bars are the standard deviation of measured overall pressure drop

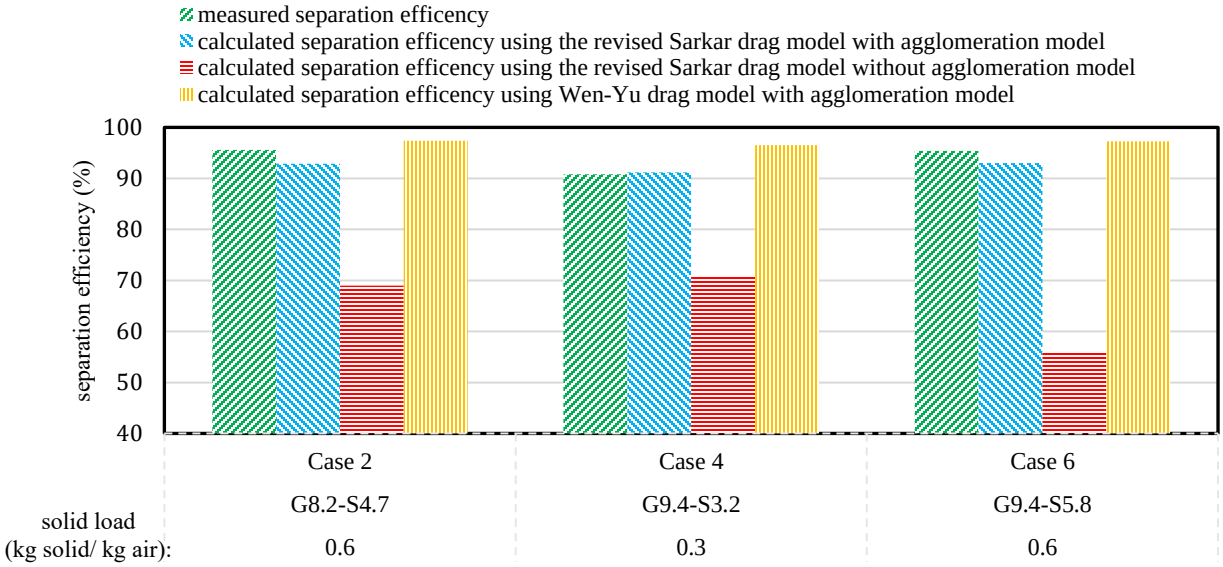

Figure 4-8. Comparison of calculated separation efficiency obtained from (1) the revised Sarkar drag model with agglomeration model, (2) the revised Sarkar drag model without agglomeration model, and (3) Wen-Yu drag model with agglomeration model.

Without an agglomeration model the improvement in separation efficiency due to an increase in solid load cannot be captured (comparing case-2 and case-4). An increase in solid load dampens swirling motion and consequently lower the centrifugal force acting on particles while PSD is not altered as agglomeration is not included, so separation efficiency predictions will be lower when the solid load is increased.

In addition to separation efficiency predictions, the prediction of pressure drop is also erroneous when agglomeration is neglected. Without agglomeration, the gas phase must carry particles finer than the actual size of particles (that experience agglomeration) which leads to more energy loss as finer particles need more energy to be carried as they experience a greater drag force. While measurements and simulation with the agglomeration model did not report a significant change in overall pressure drop when the solid load is increased (comparing case-2 and case-4), without agglomeration, the model predicted a considerable increase in overall pressure drop.

It is also worth mentioning that excluding the agglomeration model, led to unphysical particle motion so that accumulation of particles in the cyclone was observed.

Overall, as can be observed in Figure 4-7 and Figure 4-8 to accurately predict separation efficiency and pressure drop, and to observe important trends such as improvement in separation efficiency when the load is increased, including the agglomeration model is crucial.

4.5.3 Importance of sub-grid drag model

Studying the importance of using a heterogamous drag model instead of a homogeneous one was done by simulating three cases once with the presented sub-grid drag model (the revised Sarkar drag model [138]) and once using a homogeneous drag model (the Wen-Yu drag model [148]). The results are compared in Figure 4-7 and Figure 4-8. It should be noted that in both cases the agglomeration model is included. Although apparently the overall pressure drop predictions were not significantly affected by using either drag models (see Figure 4-7), when the Wen-Yu drag model is used the separation efficiency was over-predicted (greater than 96.5% in all cases) due to over-prediction of drag force as shown in Figure 4-8. Using Wen-Yu drag model led to deviation of predicted separation efficiency from the measured value up to 6%, while by using the revised Sarkar drag model this deviation did not exceed 3%.

In addition to this over-prediction, the Wen-Yu drag model was also inferior to the revised Sarkar model in capturing the trend of improvement in separation efficiency due to an increase in solid load (see Figure 4-8); the measurements reported a 4.6% increase in separation efficiency when the solid load is increased from 0.3 kg solid/kg air in case-4 to 0.6 kg solid/kg air in case-6, while the revised Sarkar model and Wen-Yu drag model predicted a 1.8% and a 0.8% increase in separation efficiency respectively. Although none of the models captured the exact trend, the revised Sarkar model performed better.

Therefore, although pressure drop prediction can be achieved with the same level of accuracy by using the homogeneous Wen-Yu drag model, for accurate prediction of separation efficiency, and consequently better-observing of improvement in separation efficiency when the load is increased, including a sub-grid drag model (the revised Sarkar drag model) is helpful.

In Figure 4-9, a snapshot of a converged solution of case-2 showing particles colored with heterogeneity index $H_d = \frac{\beta_{Sarkar}}{\beta_{Wen-Yu}}$ is presented; the lower value of heterogeneity index, the higher over prediction of the drag force by the Wen-Yu drag model compared to a more realistic prediction of the revised Sarkar drag model. Having many particles with heterogeneity index values smaller than one shows an extent of drag overprediction by the Wen-Yu drag model and this illustrates the importance of including a sub-grid drag model.

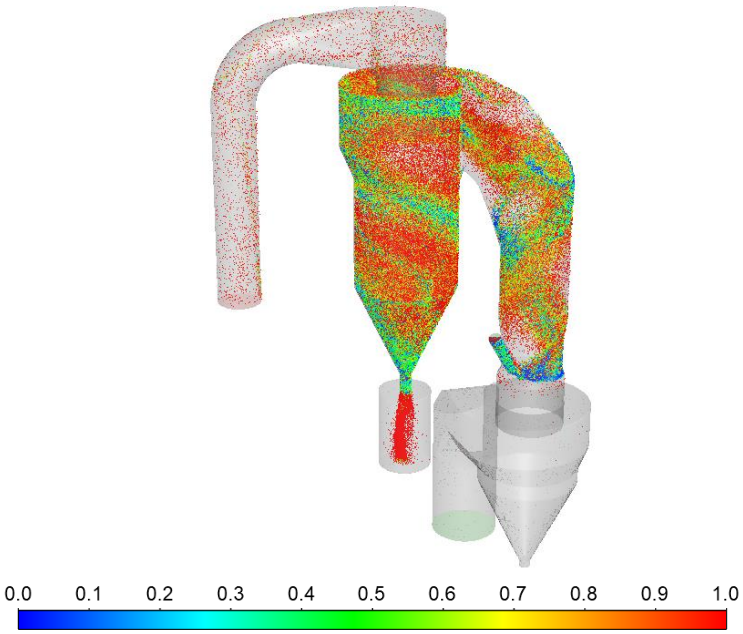

Figure 4-9. A snapshot of a converged solution of case-2 showing particles colored with heterogeneity index H_d value

Simulations and results presented in the following sections were obtained by including the agglomeration model and the revised Sarkar drag model. It should be noted that these models were also included in the mesh independence study.

4.5.4 Pressure drop

In Figure 4-10, pressure drops obtained from simulations are compared with the measurements for all seven cases; the model predicts the overall pressure drops in a reasonable agreement with experimental measurements, as the predicted values did not deviate more than 12% from the measurements.

Experimental measurements showed that the overall (riser + cyclone) pressure drop is more sensitive towards the gas flow rate than the solid flow rate, and the same was observed in the simulations. Considering case-1, case-2, and case-3 that have identical gas flow rates, varying the solid load did not affect the overall pressure drop significantly; measurements showed a slight reduction as the solid load was increased while the simulations predicted a slight increase. The same trend was observed in case-4, case-5, and case-6. The reason that the overall pressure drop is not affected significantly by the solid load is that the pressure drop in the riser and in the cyclone change differently with increasing the solid load so that they are cancelled out to some level. As the solid load is increased, the pressure drop of the cyclone is reduced due to the

dampening of swirling motion (the way this dampening leads to a reduction in pressure drop which seems counter-intuitive is discussed in detail in the literature [1]), while the pressure drop in the riser is increased as the gas needs to carry more particles leading to more loss of energy. The model can picture these well-known increases of pressure drop in the riser and reduction of pressure drop in the cyclone due to an increase in the solid load (see calculated pressure drops in the riser and the cyclone in case1 to case-3 and case-4 to case-6 in Figure 4-10).

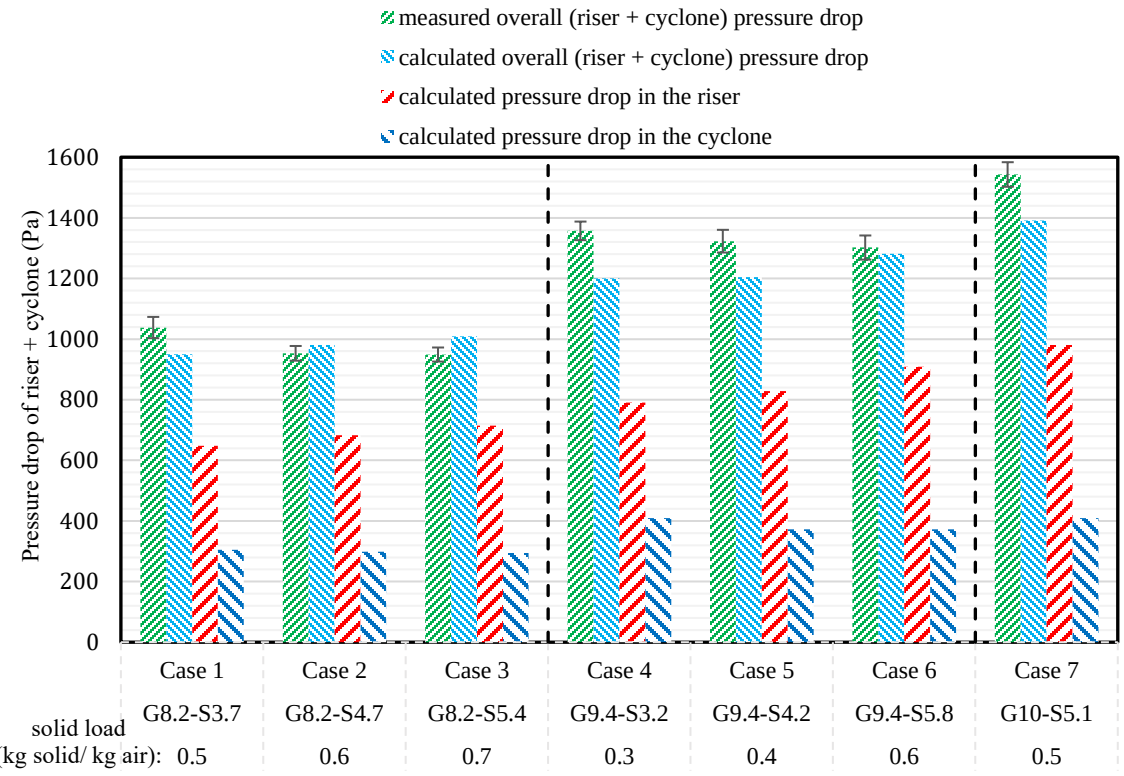

Figure 4-10. Comparison of measured and calculated overall pressure drops for all operating conditions. Error bars are the standard deviation of the measured overall pressure drop. The measured pressure drop referred to as the overall pressure drop is the summation of the pressure drop in the cyclone and in the riser (values obtained from the simulations are taken from the same positions shown in Figure 4-1).

Overall, considering all cases, as observed by both the measurements and the simulations, an increase in gas flow rate leads to a greater pressure drop. To see just the effect of gas flow rate case-2 and case-6 which have an identical solid load (0.6 kg solid/kg air) can be compared. An increase in the gas flow rate from 8.2 m^3/s in case-2 to 9.4 m^3/s in case-6 led to a considerable increase in the overall and also both the riser and the cyclone pressure drop.

4.5.5 Separation efficiency

Overall separation efficiencies achieved from simulations are compared with the measurements for applied operating conditions in Figure 4-11. Clearly observed from Figure 4-11, the model estimates the overall separation efficiency quite accurately as the predicted values matched well with experimental measurements with small deviations (the deviations did not exceed 3%).

Unlike pressure drop, the separation efficiency seems to be more sensitive towards solid flow rate than gas flow rate. Such an observation was seen both in experimental measurements and simulations when comparing different operating conditions. Measurements showed that with a constant gas flow rate (case-1 to case-3 and case-4 to case-6), an increase in solid load leads to a measurable improvement in separations efficiency; such improvement is also widely reported in the literature. The presented model is well able to predict such improvement with comparable trends as can be observed in Figure 4-11.

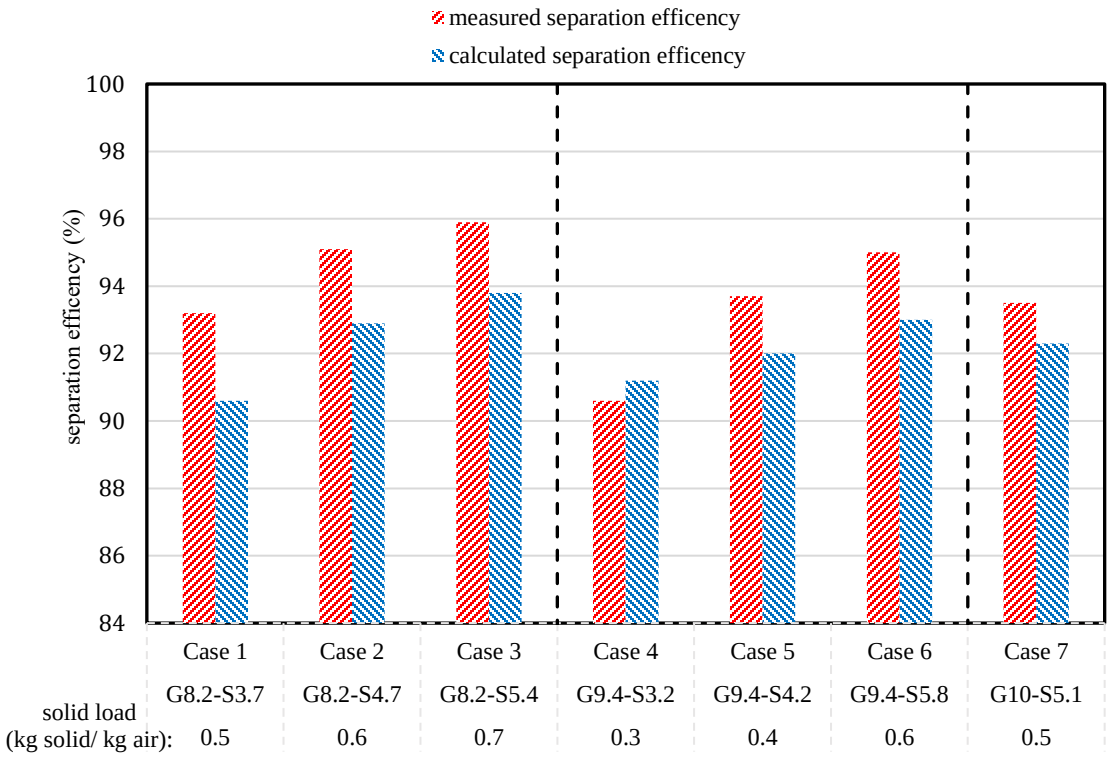

Figure 4-11. Comparison of measured and calculated overall separation efficiency for all operating conditions.

An increase in the solid load dampens the swirling motion in the cyclone so that particles experience less centrifugal force towards the wall and consequently are more likely to escape from the vortex finder to the outlet. However, the impact of the increase in particle agglomeration due to an increase in particle load is apparently significant enough to compensate for this dampening.

Higher particle load leads to more particle collisions and consequently, more agglomeration and overall larger agglomerates that experience greater centrifugal force compared to overall smaller agglomerates in lower load although the swirling velocity is dampened. This will lead to improvement in the overall separation efficiency despite the dampening of swirling motion. In addition, an increase in the solid load attenuates the turbulence (turbulent kinetic energy is reduced) which might improve the separation of particles as particles will be less dispersed by the turbulence. To see such a trend, accurate simulation of flow patterns and accurate modeling of agglomeration phenomenon are required, and the current model is accurate enough to do so.

Comparing case-2 with case-6 that have a similar solid load (0.6 kg solid/kg air) shows that increasing the gas flow rate while the solid load is maintained constant (by increasing solid flow rate) will not lead to a

measurable change in separation efficiency of the cyclone. This means that the separation efficiency is more governed by solid load than gas flow rate. Such a trend was observed both in simulations and measurements.

4.5.6 Flow pattern

Figure 4-12 presenting contours of gas tangential velocity, axial velocity, pressure and solid volume fraction averaged over 5 seconds after convergence for one of the operating conditions (case-4) shows typical flow characteristics expected in cyclones; the rotational features of the cyclone flow (Figure 4-12 (a)), ascending flow in the inner vortex and descending in the outer vortex (Figure 4-12 (b)), drop in the pressure in the direction from the wall to the center (Figure 4-12 (c)), and concentration of particles in near-wall region and formation of particle strand (Figure 4-12 (d)).

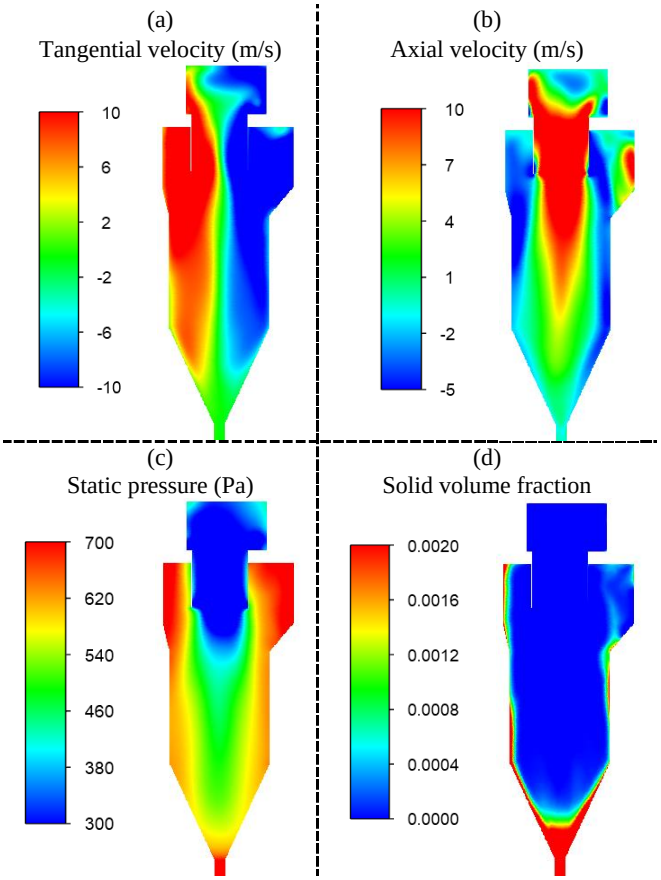

Figure 4-12. Mean flow pattern contours in case-4 (G9.4-S3.2): tangential velocity (a), axial velocity (b), static pressure (c), and solid volume fraction (d)

To provide a picture of the flow pattern in the cyclone and how it is affected by operating conditions, contours of tangential velocity and axial velocities, are presented in Figure 4-13 and Figure 4-14 respectively for three operating conditions; Case-2 (G8.2-S4.7), (b) Case-4 (G9.4-S3.2), and (c) Case-6 (G9.4-S5.8) (case-2 and case-6 have same solid loading ratio but different gas flow rate, while case-4 and case-6 have same gas flow rate but different solid loading ratio). In addition, radial profiles at a specific height (2 m below the cyclone roof, the location is shown with a yellow line in Figure 4-12) are provided to better show the variation of the gas flow field inside the cyclone. Although local measurements were not

conducted for the studied pilot-scale cyclone, the provided flow pattern is in qualitative agreement with what is expected from cyclones.

The expected swirling motion in cyclones can be observed in Figure 4-13. The radial distribution of tangential velocity is well-matched with expectations; an increase in the magnitude of tangential velocity as going far away from the center up to a region close to the wall where a sharp reduction in the magnitude of tangential velocity is observed. It can be observed that as expected an increase in the solid load from 0.3 kg solid/kg air in case-4 to 0.6 kg solid/kg air in case-6 while the gas flow rate is kept constant leads to a reduction in the swirling motion of the gas phase. This dampening of swirling motion is more severe in the lower region of the cyclone where the particles are concentrated (see Figure 4-12 (d)). In cyclones, it is generally believed that such a reduction in swirling motion due to an increase in solid load will lead to a reduction in pressure drop, as observed in the present simulation (reduction in cyclone pressure drop from case-4 to case-6 in Figure 4-10).

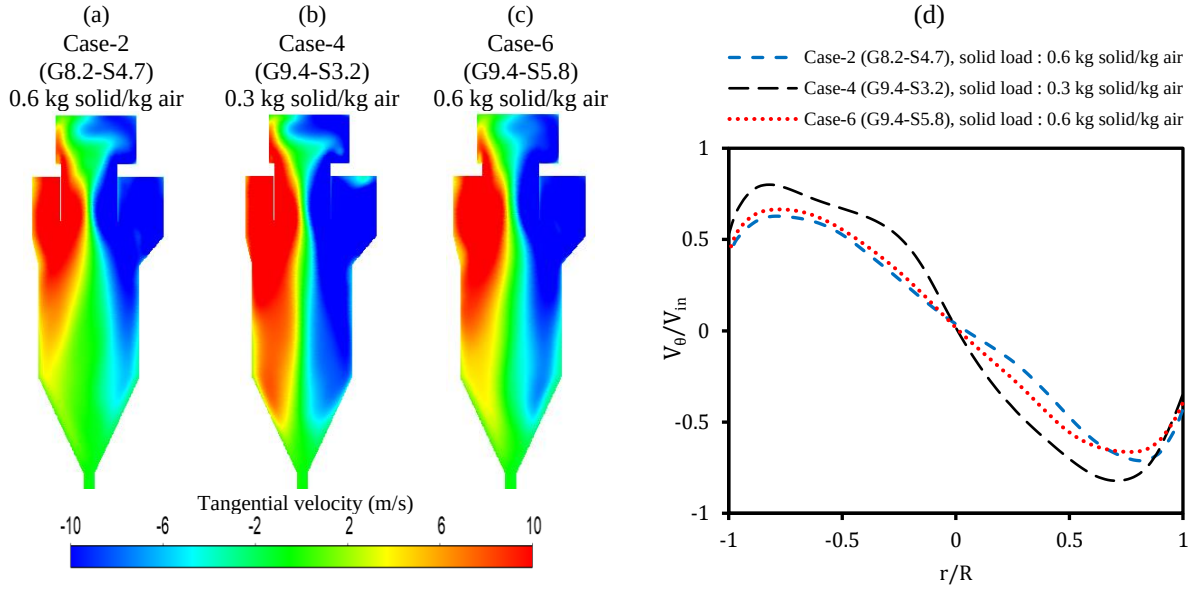

Figure 4-13. Tangential velocity (m/s) distributions at a central cross-section of cyclone main body: (a) Case-2 (G8.2-S4.7), (b) case-4 (G9.4-S3.2), and (c) Case-6 (G9.4-S5.8). (d) The radial profile of tangential velocity at a specific height (2 m below the cyclone roof shown in Figure 4-1).

As shown in Figure 4-12 (c), high-pressure regions are observed close to the cyclone wall. The pressures reduce as moving towards the center which is a typical feature of a swirling motion. A lower radial gradient of static pressure is observed when the solid load is increased due to the dampening of swirling motion.

Figure 4-14 shows that the axial velocity profile is negative (descending) near the walls, meaning that the gas flow is swirling down (outer vortex) carrying particles concentrated in the near-wall region towards the dust bin as expected. On the other hand, far from the walls, around the center, the axial gas velocity is positive (ascending), meaning that the gas flow is swirling up (inner vortex) in the center as expected. It was observed that the width of the inner vortex is not sensitive to solid load or gas flow rate. As can be observed in Figure 4-14 (d), the axial gas velocity increases in the direction from the wall to the center and

reaches its maximum at the center. It can be observed that the high axial velocity region shrinks and move upwards as the solid load is increased.

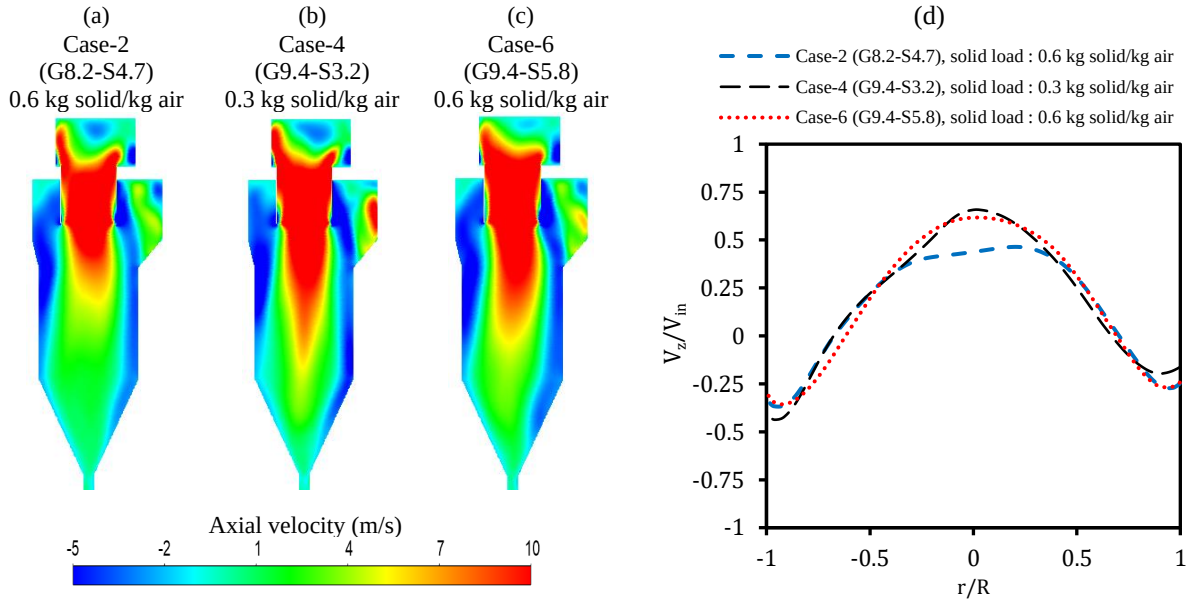

Figure 4-14. Axial velocity (m/s) distributions at a central cross-section of cyclone main body: (a) Case-2 (G8.2-S4.7), (b) Case-4 (G9.4-S3.2), and (c) Case-6 (G9.4-S5.8). (d) The radial profile of axial velocity at a specific height (2 m below the cyclone roof shown in Figure 4-1).

Figure 4-12 (d) shows that the particles are concentrated in the near-wall region as expected from cyclones; higher particle concentration in the direction from the center to the wall reaching the maximum on the wall. A concentration of particles was also observed at the conical end of the cyclone due to having a very thin dipleg.

In Figure 4-15, magnitudes of tangential and axial velocity in the case of a particle-free cyclone and in the case of a highly-loaded cyclone (case-2, SL=0.6 kg solid/kg air) are compared. In the particle-free case, the magnitude of the tangential velocity is significantly greater than the axial velocity, and therefore the fluctuations in the tangential direction are considerably greater than in the other directions. This means that in the particle-free case, the turbulence is anisotropic [188]. Therefore, in particle-free cases (and also in ordinary cyclones with very low solid load) assuming the isotropic eddy–viscosity hypothesis (which is the basis of the EVMs turbulence model) might be erroneous and the turbulence model used in the present study might not be sufficient. However, as it can be observed in Figure 4-15 (b), in the case of a highly loaded cyclone the magnitudes of tangential and axial velocity are comparable, so the fluctuations in different directions are comparable as well, therefore isotropic eddy–viscosity hypothesis assumed in k-ω sst turbulence model used in the present work is credible. In other words, although in case of cyclones with low solid load, turbulence models leaving the isotropic eddy–viscosity hypothesis such as RSM or LES are required, in case of a highly loaded cyclone where the swilling motion is dampened so that velocity components are in the same order, using turbulence models assuming the isotropic eddy–viscosity hypothesis such as k-ω sst turbulence model used in the present work is sound and sufficient.

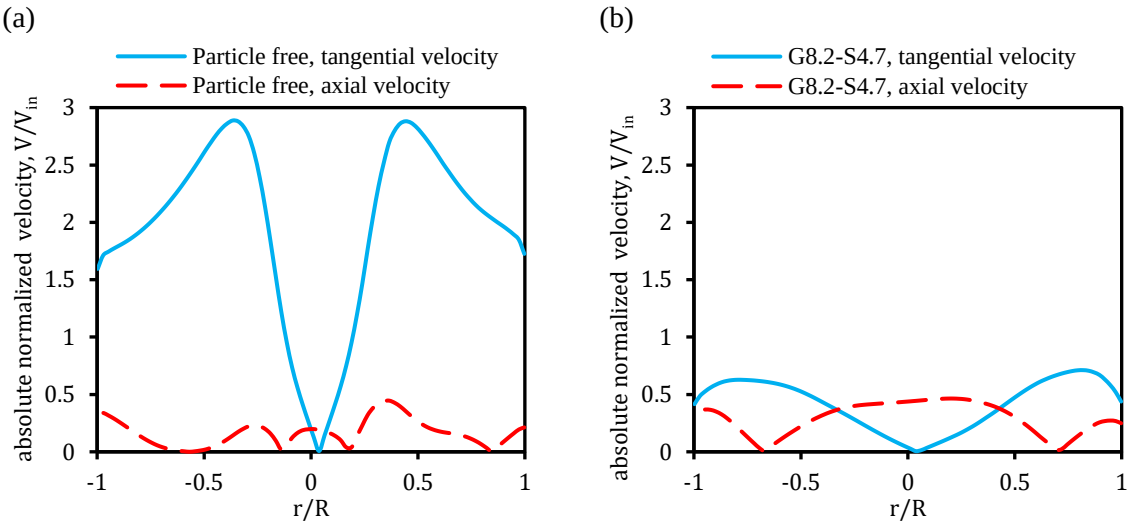

Figure 4-15. Comparison of the magnitude of tangential and axial velocity at a specific height (2 m below cyclone roof shown in Figure 4-1) in case of (a) particle-free cyclone (SL=0) and (b) Case-2 (G8.2-S4.7).

4.5.7 Grade efficiency

The grade efficiency curves obtained from CFD simulations for three operating conditions are present in Figure 4-16. The "fish-hook" behaviour is observed in all cases as there is at least one minimum in each grade efficiency curve in the range of 1-10 µm. Such grade efficiencies (an overall increase of fractional efficiency as particle size become bigger with local minima) were reported in cyclones with high solid loading [189]. As expected and reported, an increase in solid load led to an upward shift in the grade efficiency curve. It should be noted that case-2 and case-6 which have identical solid loads are presenting similar grade efficiencies suggesting that the separation efficiency is more controlled by the solid load than the gas flow rate in the present case and applied operating conditions. As can be observed in Figure 4-16, fractional efficiencies of particles finer than 15 µm were more sensitive to the solid load while the larger particles appeared to be less affected by the solid load level. Apparently, particles bigger than 50 µm were almost totally separated in the studied cyclone at the applied operating conditions.

High values of fractional efficiency for sub-micron particles can be only justified by the effect of solid load and particle agglomeration as cyclones with low solid loads present very low values of fractional efficiencies for sub-micron particles (in some cases 0% fractional efficiency) since agglomeration does not play a role when the solid load is too low.

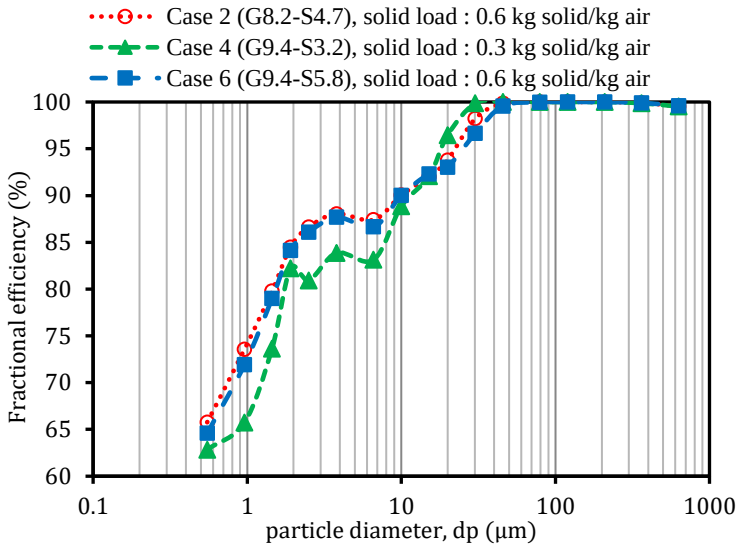

Figure 4-16. Grade efficiency curve for case-2, case-4, and case-6.

In addition to grade efficiency curves, to better see the impact of the formation of agglomerates, the PSD of particles leaving the domain (after agglomeration) are presented for these three cases in Figure 4-17 and are compared with the PSD of injected particles. The significant difference between the PSD of particles leaving the domain and the PSD of particles injected into the domain shows the importance of the agglomeration phenomenon. As the solid load is increased, overall larger particles are formed as the curve is shifted to the right which is explained by the fact that a higher load leads to more particle collision and agglomeration and larger clusters. Although around 30% of injected particles are finer than 6 µm, almost all particles leaving the domain were bigger than 6 µm as they all had formed agglomerates inside the domain. In case-2 and case-6 which have similar solid loads, the PSDs of particles leaving the domain were similar suggesting that in the studied case the agglomeration is mostly governed by the solid load.

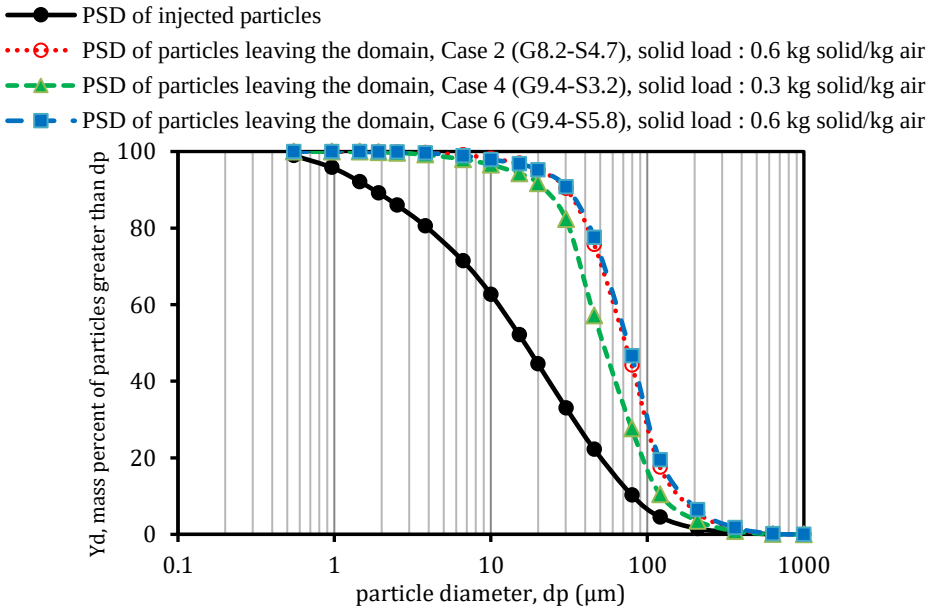

Figure 4-17. PSD of particles (after agglomeration) leaving the domain (the particles collected in the dust bin + the particles escaped to the gas outlet) for case-2, case-4, and case-6 compared with PSD of injected particles.

In Figure 4-18, the PSDs of particles in six cross sections of the domain are shown to see how the PSD vary in the device and where agglomeration takes place more frequently. The most significant change in the PSD between consecutive planes occurs between the injection plane and plane 1 meaning that the agglomeration mostly occurs in the injection pipe. Comparing the PSD in planes 1 and 2 shows that agglomeration is still occurring up to plane 2 as the PSD varies considerably. It seems that the agglomeration is almost complete by plane 2 and not occurring in the volume between planes 2 and 3 (the riser) as the PSDs in these planes are quite the same. From plane 3 to plane 4 and to the particle exit plane the PSD change slightly which can be either due to further agglomeration of particles and that more fine particles escape to the vortex finder as going down in the cyclone.

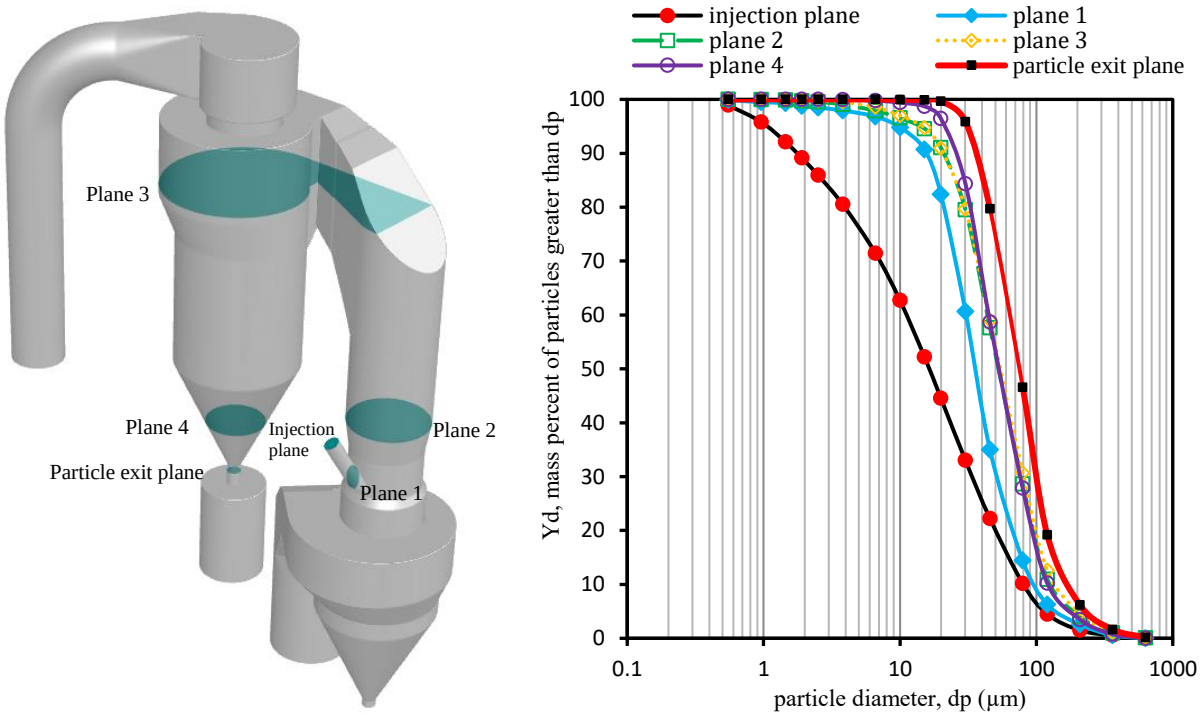

Figure 4-18. Variation of PSD in six planes in the domain

4.6 Conclusions

In the present study, a hybrid multiphase model coupled with an agglomeration model based on a stochastic Lagrangian inter-particle collision and a sub-grid drag modification based on the revised Sarkar et al. drag model [138] was developed for simulation of industrial cyclones with high particle load. The model was implemented in Ansys Fluent to simulate a pilot-scale cyclone operating under industrial cement plant conditions. The suggested model performs numerically stable converging in a reasonable duration using available resources making it applicable and affordable for simulation of industrial-scale cyclones. The model provides reasonable flow pattern, particle motion, and pressure drop and separation efficiency predictions. This model was validated against experimental measurements (separation efficiency and pressure drop) under different gas and solid flow rates. The measurements were done on a pilot plant cyclone with an internal diameter of 1.6m and solid loading ratio of 0.34-0.66 kg solid/ kg air. Reasonable

agreement with experimental pressure drops and separation efficiencies were achieved proving the capability of the model in capturing important phenomena occurring inside such a device.

The following points are drawn from the present study as the main conclusions:

- In addition to accurate prediction of pressure drop and separation efficiency, the presented model can also capture the influence of changes in operating conditions observed in our experiments. The model well predicts the improvement in separation efficiency, reduction in the pressure drop of the cyclone body and increase in the pressure drop of the riser when the solid load is increased. The model is also capable of predicting the increase in the pressure drop of both the cyclone and the riser when the gas flow rate is increased.
- Including the agglomeration model for simulation of highly loaded cyclones is vital if reasonable predictions of overall and fractional separation efficiencies and also pressure drop are desired, in particular in cases including fine particles (finer than 15 μm). Without such an agglomeration model, the separation efficiency is highly under predicted while the pressure drop is highly overpredicted by the model. In addition, the important trend of improvement in separation efficiency when the solid load is increased cannot be captured unless the agglomeration model is implemented. With the agglomeration model inclusion, the well-known "fish-hook" behavior (a minimum in grade efficiency curve) in cyclones can be captured by the CFD simulations.
- The Wen-Yu homogenous drag model over-predicts the separation efficiency when using coarse grids in a large-scale cyclone showing the necessity to use a sub-grid drag modification for the simulation of large-scale cyclones. However, the Wen-Yu drag model might be sufficient for the prediction of pressure drop in cyclones as it provides similar predictions as a heterogeneous drag model.
- The applied sub-grid drag model called the revised Sarkar et al. drag model [138] that has previously been tested successfully for a wide range of applications is now also verified and validated for simulation of highly loaded industrial-scale cement plant cyclones. The model provides reliable predictions of important performance parameters of the setup in agreement with experimental measurements. We believe this model can be used with confidence for the prediction of drag in such a device.

Since there is not a specific sub-grid drag model intended for the cyclones in the literature, as future work, a sensitivity analysis on other drag models (both heterogeneous and homogeneous) and also a sensitivity analysis on other models and parameters used in the present work can be conducted to investigate how they could influence predictions of performance parameters in cyclones. This investigation is done thoroughly in Chapter 5.

In addition to the four-way coupling simulations (DDPM) presented in this chapter, the present case was also simulated using the two-way coupling method for comparison. This comparison is presented in Appendix C (C.1). It concludes that in the present case with relatively fine particles, the two-way coupling method seems to be insufficient.

The case studied in the present chapter was an isothermal cyclone in the cement industry. A hypothetical non-isothermal cyclone preheater with the geometry and the PSD presented in this chapter was also simulated to show the ability of the developed model in the simulation of cyclone preheaters in the cement industry. The results are briefly presented in Appendix E. In addition, a simplified, isothermal CFD simulation of another cyclone in the cement industry with a diameter of 6.6 m is investigated in Appendix G to evaluate and show the ability of the developed model in simulation of larger-scale cases.

5 Sensitivity analysis of sub-models and model parameters

This chapter is a reprint of the manuscript “CFD-DDPM coupled with an agglomeration model for simulation of highly loaded large-scale cyclones: Sensitivity analysis of sub-models and model parameters” published in Powder Technology [190].

5.1 Abstract

The Dense Discrete Phase Model coupled with an agglomeration model is developed and validated for the simulation of industrial cyclones with high solid loads. The performance of the model is influenced by sub-models, model parameters, and numerical parameters. To optimize the performance of the present CFD model, an extensive sensitivity analysis was performed, varying one sub-model or parameter at a time, and systematically assessing the effect on the results through comparisons with measured pressure drop and separation efficiency of a highly loaded pilot-scale cyclone. The investigation shows that the turbulence model and particle-particle restitution coefficient have the strongest influence. This study concludes with the recommendation of a set of sub-models, model parameters, and numerical parameters providing the best prediction of the hydrodynamics of large-scale highly loaded cyclones. In addition, the impact of some operating conditions on the performance of a large-scale highly loaded cyclone were examined

5.2 Introduction

Cyclones operating with high solid loads are a vital part of building material industries such as cement production [2–5], stone wool production [6,7] and also processes employing circulating fluidized beds (CFB) [160,191], and Fluid Catalytic Cracking applications [156]. The geometrical simplicity and the low costs in construction, operation, and maintenance have made cyclones the first option when gas-particle separation and/or heat exchange is required.

CFD simulation of such a device has become an invaluable tool for optimizing cyclone design and operation [28,110,192]. Despite the simplicity of highly loaded cyclones, the complex particle-particle and gas-particle interactions, highly turbulent flow, and particle agglomeration, make the CFD simulation quite complicated [11]. It becomes even more complicated in the simulation of large-scale cyclones where the use of coarse grids (that might be unable to resolve mesoscale structures) is inevitable due to the limitation of computational resources [11].

Conventionally there are two common strategies to model multiphase flow in CFD simulation of dense dispersed gas-solid flow: (1) Two Fluid Method (TFM) [93], and (2) coupling of CFD with the Discrete Element Method (DEM) [11]. Both strategies treat the gas phase as a continuum medium in an Eulerian framework while they are different in how the particles are treated: as a continuum in the Eulerian framework in the TFM method, and as discrete particles in the Lagrangian framework in CFD-DEM. However, they have limitations in the simulation of highly loaded large-scale cyclones. CFD-DEM is limited to lab-scale cases due to its limitation in coarse-graining, the number of grains to contain, and its necessity to simulate with very small time steps to capture particle-particle collisions that make it unfeasible for simulation of highly loaded large-scale cyclones [193]. On the other hand, TFM cannot easily handle the polydispersity of particles which is crucial for the simulation of the hydrodynamics of cyclones and the prediction of their performance [93].

A more recent strategy called Dense Discrete Phase Model (DDPM) was developed to avoid these issues [106,147]. DDPM is a cost-effective solution for industrial dense particle-laden flows. Unlike DEM which directly resolves particle-particle interactions, DDPM models these interactions based on the Kinetic Theory of Granular Flow (KTGF) so that larger time steps and larger grain-to-particle ratio can be applied to accelerate the calculations tremendously [10,187,194,195]. In addition, DDPM can easily handle polydispersed particles [158]. However, there is a lack of criteria in the open literature to guide a proper choice for the particle-particle interaction forces modeling in DDPM, time step size, and grain-to-particle ratio in particular for the simulation of a highly loaded large-scale cyclone.

Widely accepted turbulence models for cyclones (Reynolds Stress Model [9,29,51] and Large Eddy Simulation [69,74,75]) are unfavored in case of industrial-scale cyclones due to their high computational costs and instability in case of unstructured mesh that is commonly used for large-scale simulations [158]. In addition to RSM and LES as widely accepted turbulence models for cyclones, novel Eddy Viscosity Models (EVMs) sensitized to rotation and curvature have attracted much attention recently due to their superiority over LES and RSM in terms of computational cost and robustness. It was proven in several research works [42,47–50,158] that this sensitization can overcome weaknesses of EVMs in the simulation of cyclones so that they can provide quite reliable results which is competitive with more complicated turbulence models, while these sensitized models are more robust and require much less computational resources [42,47–50]. Considering the industrial scale of the studied case, and the fact that in LES, very fine girds are required to resolve large eddies, in particular, in near-wall regions, LES is not favored. On the other hand, regarding the robustness of EVMs and their superiority over RSM in terms of computational cost which are of great importance in our case (industrial-scale geometry), and its proven ability to capture mean flow field in cyclones when sensitized for flow rotation and curvature, EVMs are preferred. All available EVMs (standard, RNG, RNG, and realizable versions of k-ε and standard and shear stress transport (sst) versions of k-ω) can be sensitized to flow rotation and curvature, but which perform better under highly loaded cyclones and how significant is the effect of this sensitization have yet to be studied.

With multiphase models based on the Kinetic Theory of Granular Flow (KTGF), such as the DDPM, using conventional homogeneous drag models in coarse grids, as is required in large-scale simulations, fails to adequately capture the hydrodynamics of multiphase flow [138,139]. For this reason, heterogeneous drag

models (also known as sub-grid drag models) that take into account mesoscale and heterogeneous structures are recommended [11,138,139,141,143,146]. However, none of the sub-grid drag models presently available in the literature has been developed for cyclones, and there is a lack of guidance in choosing a suitable drag model for the simulation of highly loaded cyclones among the available drag models.

Agglomeration is a vital phenomenon in particle-laden systems with very fine particles e.g. in cyclones. Thus, a model accounting for agglomeration is essential if a valid prediction of cyclones is desired [161,162]. Furthermore, it is crucial to investigate the parameters affecting agglomeration extent, such as the particle-particle restitution coefficient, and how they impact simulation predictions.

The impact of particle-wall interaction modeling parameters on the performance of low-loading cyclones has been reported to be minor [69,75,196], but the extent to which it affects highly loaded cyclones has not been investigated. In addition, no criteria are provided in the literature to help determine whether including particle rotation, Saffman force, Magnus force, and particle turbulent dispersion is crucial for the simulation of highly loaded cyclones or not, while their relevance has been noted in the case of low loading cyclones [75,80,104,108,197–199].

In the present work, sensitivity analyses were performed on sub-models (models for particle-particle interaction force calculation, turbulence models, drag models and other gas-particle interactions), model parameters (particle-particle restitution coefficient and particle-wall rebound coefficient), and numerical parameters (parcel/grain size, time step size and order of discretization) of a hybrid multiphase model developed and validated for simulation of large-scale highly loaded cyclones. The purpose of the sensitivity analysis is to assess the significance of each of the sub-models, model parameters, and numerical parameters, to clarify their impact, and to optimize the performance of the numerical model. In addition, the effect of some operating conditions, such as solid loading, particle size distribution and gas underflow on the performance of a highly loaded large-scale cyclone were studied.

5.3 Numerical model description

In the present work, a hybrid Eulerian–Lagrangian multiphase model, Dense Discrete Phase Model (DDPM) is used. The model implicitly approximates particle-particle interaction using the Kinetic Theory of Granular Flow (KTGF) and is coupled with an agglomeration model [122,161]. The gas phase is treated in an Eulerian framework where the Navier–Stokes equations including phase volume fraction are solved. The particle phase is treated in a Lagrangian framework while the particle-particle interaction is modeled based on the Kinetic Theory of Granular Flow (KTGF) [169]. The model is described as follows:

5.3.1 Gas phase

The continuity and momentum conservation equation for the continuous phase (gas phase) in DDPM multiphase modeling coupled with dispersed turbulence models are as follows:

$$\frac{\partial}{\partial t}(\alpha_c \rho_c) + \nabla.(\alpha_c \rho_c \bar{u}_c) = 0 \qquad 5\text{–}1$$

$$\frac{\partial}{\partial t}(\alpha_c \rho_c \bar{u}_c) + \nabla.(\alpha_c \rho_c \bar{u}_c \bar{u}_c) = -\alpha_c \nabla p + \nabla.\left[\alpha_c \mu_c \left(\nabla \bar{u}_c + \nabla \bar{u}_c{}^T\right)\right] + \nabla.\tau_c^t + F_{Dc} + S + \alpha_c \rho_c g \qquad 5\text{–}2$$

F_{Dc} accounts for the force particles apply on fluid due to the drag and is modeled as follows:

$$F_{Dc} = K_{DPM}\left(u_{dpm} - \bar{u}_c\right) \quad 5\text{–}3$$

5.3.1.1 Turbulence modeling

In the present work, we tested different versions of k-ε and k-ω turbulence models in their dispersed form: standard, RNG, RNG for swirl dominate flow, and realizable versions of k-ε and standard and shear stress transport (sst) versions of k-ω. In most cases, the used turbulence models included a term to sensitize the model for curvature correction and rotation. Here the turbulence model used as the base case (sst version of k-ω turbulence model sensitized for curvature correction, k-ω sst cc) is presented while details of other tested turbulence models can be found in the Ansys Fluent theory guide [147].

5.3.1.1.1 Dispersed form of k-ω sst sensitized for curvature correction (k-ω sst cc)

In the case of the dispersed k-ω sst-cc, turbulent stress tensor, τ_c^t, is approximated using the Boussinesq hypothesis as follows:

$$\tau_c^t = -\alpha_c \rho_c R_{c,ij} = -\alpha_c \left[-\frac{2}{3}\left(\rho_c k_c + \mu_{t,c} \nabla . \bar{u}_c\right)\delta_{ij} + \mu_{t,c}\left(\nabla \bar{u}_c + \nabla \bar{u}_c{}^T\right)\right] \quad 5\text{–}4$$

to calculate k_c and $\mu_{t,c}$ and consequently, turbulent stress tensor, τ_c^t, two transport equations (one for k and one for ω) must be solved:

$$\frac{\partial}{\partial t}(\alpha_c \rho_c k_C) + \frac{\partial}{\partial x_i}(\alpha_c \rho_c \bar{u}_c k_C) = \frac{\partial}{\partial x_j}\left(\alpha_c \Gamma_k \frac{\partial k_C}{\partial x_j}\right) + \alpha_c f_r G_k - \alpha_c Y_k \quad 5\text{–}5$$

$$\frac{\partial}{\partial t}(\alpha_c \rho_c \omega_C) + \frac{\partial}{\partial x_i}(\alpha_c \rho_c \bar{u}_c \omega_C) = \frac{\partial}{\partial x_j}\left(\alpha_c \Gamma_\omega \frac{\partial k_C}{\partial x_j}\right) + \alpha_c f_r G_\omega - \alpha_c Y_\omega \quad 5\text{–}6$$

Definitions of terms and parameters in these equations and how curvature correction function (f_r) is modeled can be found Ansys Fluent theory guide [147]; in short, f_r(curvature correction function) is modeled by a modified version of empirical function suggested by Spalart and Shur [44] to account for streamline curvature and system rotation effects.

5.3.2 Solid/particle phase

In DDPM multiphase model, the equation of motion of each parcel is expressed as follows:

$$m_{pi}\frac{d\vec{u}_{pi}}{dt} = m_{pi}\frac{18\mu_c}{\rho_p {d_p}^2}\frac{C_D Re_p}{24}\left(\vec{u}_c - \vec{u}_{pi}\right) + m_{pi} g \frac{\rho_p - \rho_c}{\rho_p} + F_{p-p} + F_{other} \quad 5\text{–}7$$

where F_{p-p} is modeled based on the Kinetic Theory of Granular Flow (KTGF). In the KTGF model, instead of resolving all particle collisions, the interactions are averaged for the solid-gas flow. Note that α_c in gas phase conservation equations are updated each time step by mapping particle location obtained from equation 5–7 (Lagrangian framework) to the Eulerian framework.

In addition to the translational particle motion equation, a particle rotation equation can be considered as follows:

$$\frac{d\vec{\omega}_{pi}}{dt} = \frac{15}{16\pi}\frac{\rho}{\rho_p}C_\omega\left(\frac{1}{2}\nabla\times\vec{u}_c - \vec{\omega}_{pi}\right) \quad 5\text{–}8$$

5.3.3 Particle-particle interactions

5.3.3.1 Particle-particle interaction force based on KTGF

The particle-particle interaction forces are obtained by the solids stress tensor ($\bar{\bar{\tau}}_s$) as defined in equations 5–9 and 5–10.

$$F_{p-p} = -m_{pi}\frac{1}{\rho_p}\nabla.\bar{\bar{\tau}}_s \quad 5\text{–}9$$

$$\bar{\bar{\tau}}_s = \alpha_d\left(\lambda_s - \frac{2}{3}\mu_s\right)\nabla u_s + \alpha_d\mu_s(\nabla u_s + \nabla {u_s}^T) \quad 5\text{–}10$$

To evaluate solids stress tensor ($\bar{\bar{\tau}}_s$) shear viscosity (μ_s) and bulk viscosity (λ_s) are required. On the other hand, to evaluate shear viscosity collisional, kinetic, and optional frictional viscosity are required to be modeled.

$$\mu_s = \mu_{s,col} + \mu_{s,kin} + \mu_{s,fric} \quad 5\text{–}11$$

Estimation of these viscosities (bulk, collisional, kinetic and frictional) can be done using different closure models details of which can be found in the Ansys Fluent theory guide [147]. In short, granular viscosity, granular bulk viscosity, solid pressure, granular temperature, frictional viscosity, frictional pressure, and radial distribution terms must be modeled using a closure model. Closure models tested in the present work for each of these terms can be found in Table 5-1.

Table 5-1. Base case model description and tested options for all the varied parameters and models.

	Parameter/Model	Base case model	Other tested parameters/models
Gas phase modeling	Turbulence model	k-ω sst	k-ω standard, k-ε standard, k-ε RNG, k-ε RNG swirl dominant flow, k-ε Realizable
	Curvature correction	included	Not included
Particle-particle interaction force modeling	granular viscosity	Gidaspow [93]	syamal-obrien [154], set to zero
	granular bulk viscosity	Lun [155]	set to zero
	solid pressure	Lun [155]	syamal-obrien [154], set to zero
	granular temperature	algebraic	none
	frictional viscosity	Schaeffer [200]	Set to zero
	frictional pressure	based ktgf	Set to zero
	radial distribution	Lun [155]	syamlal-obrien [154], ma-ahmadi [201], set to 0
Gas-solid interactions modeling	Drag	Sarkar[138]	Wen-Yu [148], Gidaspow [202], TGS [203], BVK [204], DiFelice [205], Pirker [142], Igci [141]
	Filter-to-grid ratio	2	1, 3
	Particle rotation	included	Not included
	Rotational drag	Dennis et al. [170]	Not included
	Saffman force	included	Not included
	Magnus force	Oesterle-Bui-Dinh [171]	Not included
Model parameters	Particle-particle restitution coefficient	0.7	0.5, 0.6, 0.8, 0.9, 0.95
	Particle-wall rebound coefficient	0.8	0.5, 0.6, 0.7, 0.9, 1
Numerical parameters	Courant number (Time step (s))	300 (0.012 s)	25 (0.001 s), 50 (0.002 s), 100 (0.004 s), 200 (0.008 s), 400 (0.015 s), 600 (0.02 s), 800 (0.03 s) 3200 (0.1 s)
	Parcel mass (kg)	0.00004	0.00001, 0.00002, 0.00008, 0.00032, 0.00064, 0.00128
	Discretization method	Second order	First order

5.3.3.2 Agglomeration

In addition to particle-particle interaction force modeling based on KTGF, particle agglomeration that was found to be crucial in the case of cyclones handing very fine particles (d < 15 μm) [161,162] was modeled based on a stochastic Lagrangian inter-particle collision model proposed by Sommerfeld [122,161]. Details of the agglomeration model can be found in Chapter 4. In short, whether two particles in a cell collide or not is judged based on calculated collision probability and efficiency, and whether two collided particles agglomerate or rebound is judged by comparing the relative velocity of the particles with a critical velocity (agglomeration occurs if $\left|\overrightarrow{u_{p1}} - \overrightarrow{u_{p2}}\right|\cos(\phi) \leq U_{crit}$). This critical velocity is defined as follows:

$$U_{crit} = \frac{\sqrt{1-e^2}}{e^2} \frac{H}{\pi d_2 {z_0}^2 \sqrt{6 p_c \rho_p (1 + d_2/d_1)}} \qquad 5\text{–}12$$

5.3.4 Gas-solid interactions

5.3.4.1 Drag force

To close the momentum conservation equation (equation 5–2) and for particle tracking (equation 5–7) the drag force between fluid and particles must be modeled. In dense systems such as highly loaded cyclones, the drag force is influenced by the presence of other nearby particles which makes its modeling quite complex. In such cases, drag modeling is mainly based on empirical observations, and has limited ranges of validation.

Therefore, since in the literature, there is not a model designed specifically for highly loaded cyclones, to find the best-suited drag model, in the present work, a set of models has been tested. This set includes five homogeneous drag models (Wen-Yu [148], Gidaspow [202], TGS [203], BVK [204], DiFelice [205]) and three heterogeneous drag models (Sarkar [138], Pirker [142], Igci [141]). Except for Wen-Yu and Gidaspow, all other models were implemented to Fluent using UDFs.

The heterogeneous drag models are reported to be superior in the case of coarse-grid simulation of large-scale cases as they account for the effect of small mesoscale and heterogeneous structures on the drag correlations [11,138–146].

5.3.4.2 Other gas-solid interaction forces

5.3.4.2.1 Magnus force

Rotating particles in a fluid generate a Magnus lift force due to pressure differential along their surfaces as follows [79]:

$$F_{mag} = \frac{1}{2} A_p C_{RL} \rho_g \frac{\left|\vec{u}_{pi} - \vec{u}\right|}{\left|\vec{\omega}_{pi} - \vec{\omega}\right|} \left[\left(\vec{u}_{pi} - \vec{u}\right) \times \left(\vec{\omega}_{pi} - \vec{\omega}\right)\right] \qquad 5\text{–}13$$

where C_{RL} is the rotational lift coefficient and is modeled based on Oesterle-Bui-Dinh[171] expression in the present work.

5.3.4.2.2 Saffman force

Particles with low Reynolds numbers, especially particles finer than 1 μm, experience a Saffman lift force as a result of shear that is modeled by the following expression [206]:

$$F_{Saff} = m_p \frac{5.188 v^{0.5} \rho_g d_{ij}}{\rho_p d_p (d_{lk} d_{kl})^{0.25}} \left(\vec{u} - \vec{u}_{pi}\right) \qquad 5\text{–}14$$

5.3.4.2.3 Rotational drag force

An additional drag force is generated for rotating particles represented as C_ω in the particle rotation equation which is modeled by a function of the rotational Reynolds number [170].

The effect of these three additional gas-solid interaction forces on the gas phase is summarized as a source term (S) in the momentum conservation equation (equation 5–2) and their effect on the particle phase is summarized as F_{other} in particle motion equation (equation 5–7).

5.4 Experimental setup and simulation details

The experimental setup described in Chapter 4 was simulated in the present study; a pilot-scale cyclone (1.6 m in diameter) shown in Figure 5-1 (a) tested under industrial operating conditions (particle load, material, and size shown in Figure 5-1 (b)) and room temperature.

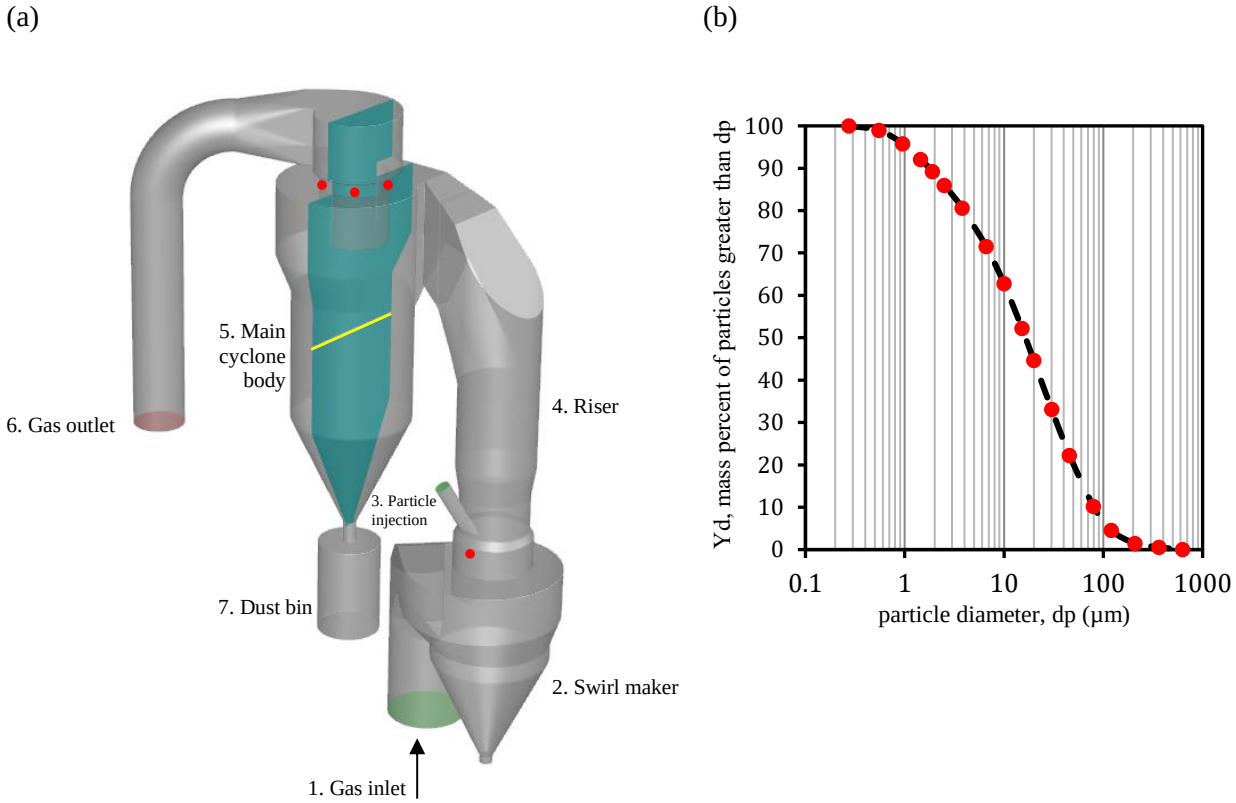

Figure 5-1. (a) 3D view of the geometry of the pilot-scale cyclone. Red dots are approximate locations of pressure taps for measuring static pressure drop. The cyan plane and yellow line are the plane of contours and line (at 2 m below the roof) of profiles in the results and discussion section. (b) PSD of injected solid material used for the experimental measurements obtained by a Malvern mastersizer 2000 with a Hydro 2000S wet dispersion unit.

The experiments were conducted at various operating conditions with different gas flow rates and solid flow rates. Three of these operating conditions are used in the present study. In Table 5-2, the operating conditions of these three cases in addition to measured separation efficiency (defined in cyclones as separation efficiency (%) $= (1 - \frac{\text{solid flow rate escaped to the gas outlet}}{\text{solid flow rate injected to the cyclone}}) \times 100)$) and pressure drop are summarized. Unless it is specifically mentioned, the case-1 (base case) operating condition is used in sensitivity analyses.

It is worth mentioning that highly loaded cyclones refer to cyclones with a dense gas-solid two-phase flow to be distinguished from low solid load cyclones (dilute gas-solid two-phase flow) [1]. The approximate borderline between dilute and dense flow is a solid volume fraction of 0.001 [8,77], and since in the cyclone studied here the solid volume fraction in regions close to the wall is greater than 0.001, the cyclone is considered as a highly loaded cyclone.

In the present study, 4.2 million polyhedral cells with prism layers were used to discretize the geometry. This grid was found to provide mesh-independent predictions in the present model and geometry. The solver employed in the present work was Ansys Fluent 2019R3; details of the solver, numerical methods, and mesh independency study is discussed in detail in Chapter 4.

Table 5-2. Operating conditions of conducted tests used in the present study. Unless it is mentioned case-1 (base case) operating condition is used in sensitivity analyses. The cases are named in a way to present the main operating conditions of the case (e.g., in Case-1 G8.2-S4.7, gas flow rate and solid flow rate are 8.2 kg/s, 4.7 kg/s respectively).

Parameter	Case-1 G8.2-S4.7 (base case)	Case-2 G9.4-S3.2	Case-3 G9.4-S5.8
Air flow rate (kg/s)	8.2	9.4	9.4
Solid flow rate (kg/s)	4.7	3.2	5.8
Solid loading ratio (kg solid / kg air)	0.57	0.34	0.62
Measured overall pressure drop (Pa)	953	1357	1302
Measured separation efficiency (%)	95.6	90.8	95.4
Temperature (˚C)	24		
Particle density (kg /m^3)	3100		
Air density (kg/m^3)	1.187		
Air viscosity (kg/(m.s))	1.83×10^{-5}		

To find out the best-suited sub-models, model parameters, and numerical parameters of the developed model (DDPM coupled with agglomeration modeling) for the simulation of highly loaded large-scale cyclones, several sensitivity analyses were performed. Sensitivity analyses include particle-particle interaction modeling (based on KTGF), turbulence models, drag models, particle-particle restitution, particle-wall rebound coefficient, discretization method, grain-to-particle size ratio, grid-to-parcel size ratio, and time step size.

Table 5-1 summarizes the set of base case models and parameters chosen based on preliminary simulations. Starting from this set, one of them was varied at a time and its effect on the results was assessed. In addition to models and parameters in the base case, all other tested models and parameters are summarized in Table 5-1. To analyze the results, mainly pressure drop, and separation efficiency predictions were compared with experimental measurement and the predictions in the using base case model.

5.5 Results and discussion

The results obtained from sensitivity analyses on sub-models, model parameters, numerical parameters, and operating conditions are presented in this section. Note that throughout the study if the deviation of a predicted parameter from the base case is below 2.5%, the effect is considered minor.

5.5.1 Sub-models

5.5.1.1 Turbulence modeling

The sst (shear stress transport) version of the k-ω turbulence model sensitized for curvature correction (k-ω sst cc) has been validated for simulation of highly loaded large-scale cyclones [158] where the use of

more complicated turbulence models such as RSM or LES is not feasible due to their instability and computational cost. In addition, in a study of a highly loaded lab-scale case (discussed in Chapter 3), the sst version of the k-ω turbulence model was proven to perform as well as RSM, capable of predicting performance parameters of a lab-scale highly loaded cyclone in agreement with experimental measurements (at least for pressure drop predictions that measurements were available). Therefore, this turbulence model was chosen as the base case in the present study.

In the sensitivity analysis of turbulence modeling in the present study, different versions of the k-ε turbulence model (standard, RNG, RNG for swirl dominate flow, and realizable) sensitized for curvature correction, the standard version of k-ω turbulence model sensitized for curvature correction, and sst version of k-ω turbulence model without curvature correction term were tested. The results were then compared with the base case (k-ω sst cc) and experimental measurements of pressure drop and separation efficiency (see Figure 5-2). The following can be drawn from the comparison in Figure 5-2:

- The use of the curvature correction term to sensitize the turbulence flow for rotation is crucial as excluding it leads to highly under prediction of separation efficiency.
- The sst version of the k-ω turbulence model is superior to the standard version as the standard version highly underpredicts the separation efficiency.
- Among k-ε turbulence models, only two RNG versions provide reasonable predictions while the other two highly underpredict the separation efficiency.

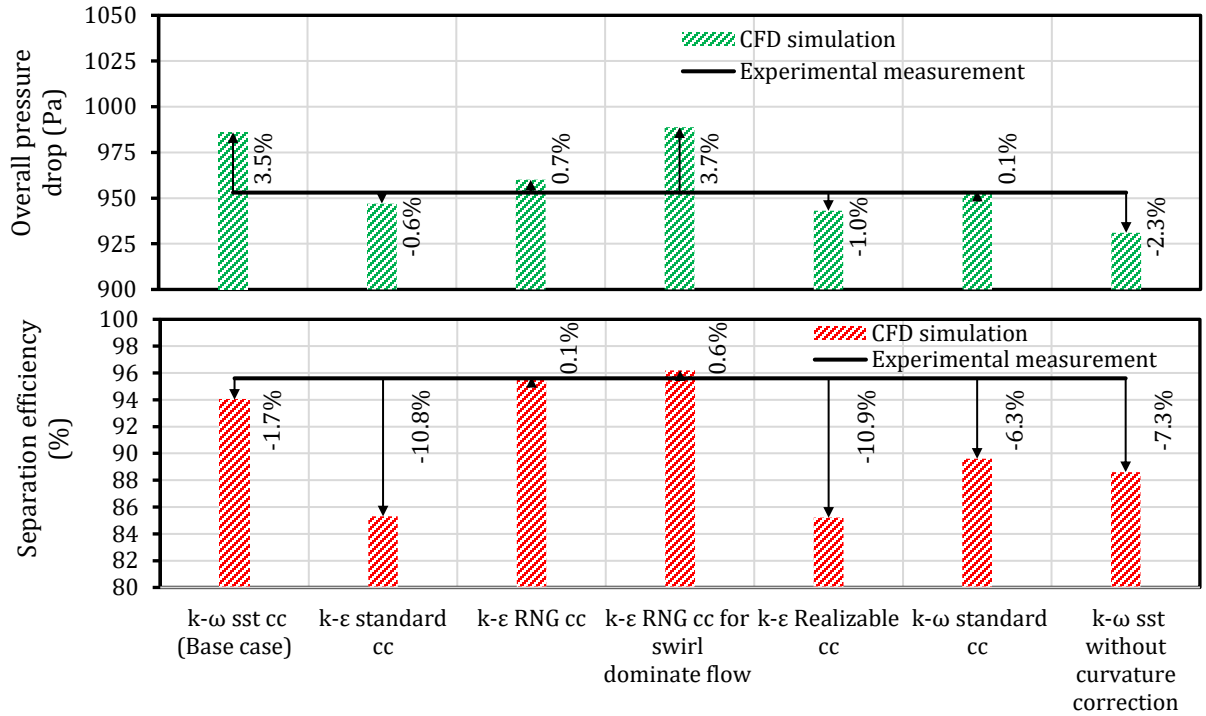

Figure 5-2. Effect of turbulence model on the overall pressure drop and separation efficiency. Arrows and corresponding percentages show the difference between CFD simulation and experimental measurement.

The comparison in Figure 5-2 shows that only k-ε RNG cc and k-ω sst cc provide reasonable predictions in particular in the prediction of separation efficiency. The sensitization of EVMs for flow rotation and

curvature was reported to overcome weaknesses of EVMs in the simulation of cyclones [42,47–50], and the presented results confirm it in the case of the k-ω sst turbulence model as the one with the correction provides quite reliable predictions, unlike the version without curvature correction. Also, The RNG version of k-ε was originally designed to include the effect of swirl on turbulence in k-ε and to improve accuracy for swirling flows and the presented results show that its impact is significant; unlike the standard version, the RNG provides good predictions.

To further compare these models they were tested for two other operating conditions (operating conditions 2 and 3 with the same gas flow rates and different solid flow rates). As shown in Figure 5-3, unlike k-ω sst cc, k-ε RNG cc is unable to capture the trend of improvement in separation efficiency when the solid load is increased (reported in the literature and observed in the measurements) that makes k-ω sst cc the superior turbulence model among all tested models. Even the other version of k-ε RNG cc that is modified for swirl dominate flows is not able to capture such a trend. In addition, it is worth mentioning that k-ω sst cc is almost 3 times faster than k-ε RNG as it requires fewer iterations to reach convergence in each time step.

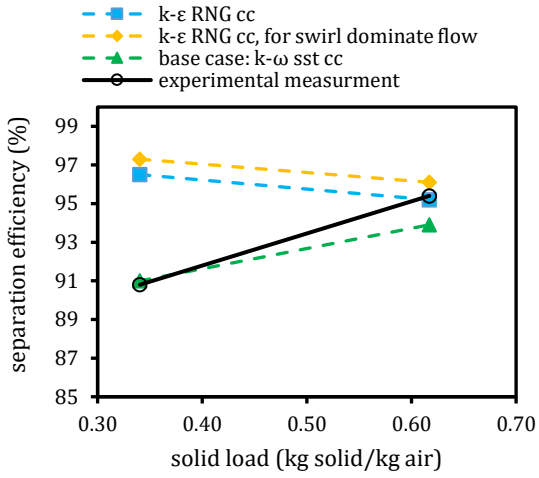

Figure 5-3. Comparison of turbulence models in capturing the trend of improvement in separation efficiency when the solid load is increased.

The flow pattern in the cyclone obtained from each of the tested turbulence models are presented and compared in Figure 5-4 and Figure 5-5. Although all models capture the overall flow in cyclones (swirling down outer vortex and swirling up inner vortex), different models provide considerably different flow patterns, especially in the conical part of the cyclone. Flow pattern (tangential and axial velocity profiles) measurements of highly loaded cyclones that are not available for now can facilitate further comparison of turbulence models.

It is worth mentioning that due to both instability and limited computational resources, RSM and LES have not been included in the present study but can be investigated in the future to further study the effect of turbulence modeling in highly loaded industrial-scale cyclones.

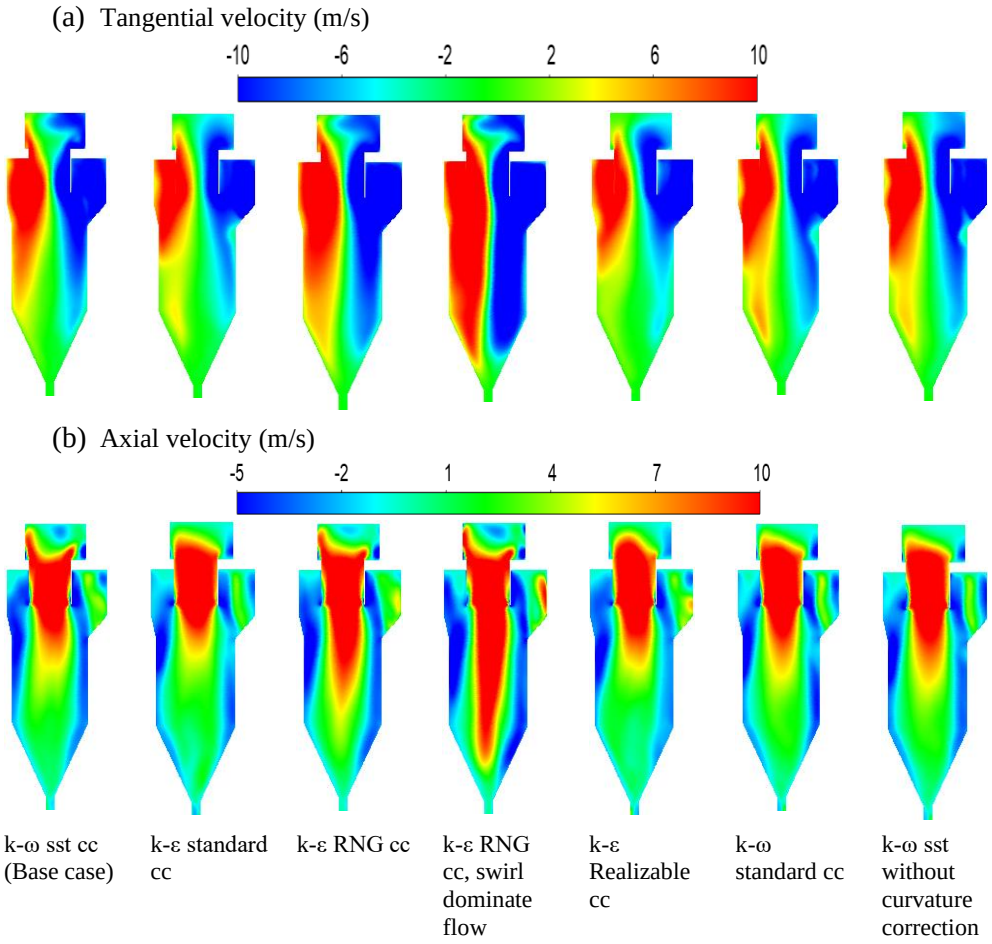

Figure 5-4. Effect of turbulence model on the flow pattern (contours at a central cross-section of cyclone main body); (a) Tangential velocity, (b) Axial velocity.

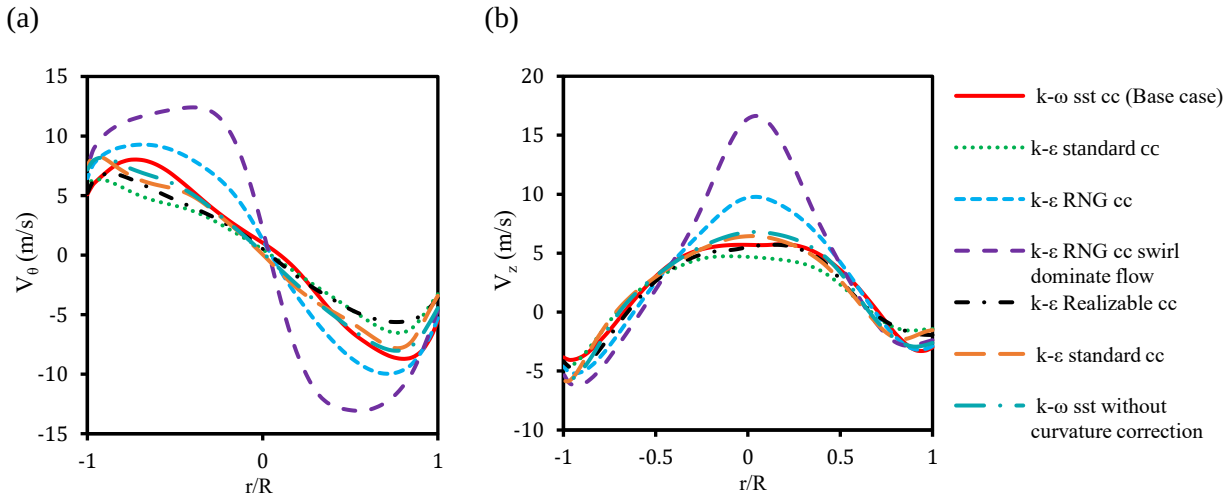

Figure 5-5. Effect of turbulence model on the flow pattern in the cyclone (profiles at a specific height, 2 m below cyclone roof); (a) Tangential velocity, (b) Axial velocity.

5.5.1.2 Particle-particle interaction modeling

As mentioned in the model description, several terms (granular viscosity, granular bulk viscosity, frictional viscosity, solid pressure and radial distribution) are required to be modeled to predict particle-particle interaction force and there are a few available options for each of these terms. Although the effect of using different models for each term was studied for different fluidization systems in the literature [207–209], such a study was missing for highly loaded cyclones. Therefore, a sensitivity analysis on each of these terms was done to figure out which model is more suitable and how they would affect the predictions in the case of highly loaded cyclones.

Simulation settings of cases used for particle-particle interaction force sensitivity analysis are summarized in Table 5-3, and the predictions of pressure drop and separation efficiency with different settings are compared in Figure 5-6. The results show that the effect of using different closure models for each of the terms is minor both in the prediction of pressure drop and separation efficiency (less than 1% effect on pressure drop and less than 2% effect on separation efficiency). Even excluding the particle-particle interaction force (by deactivating all terms in the particle-particle interaction force modeling) did not affect the predictions considerably, therefore, choosing between different available options to model particle-particle interaction force is not critical for the simulation of highly loaded cyclones (at least in the range studied in the present work <1 kg solid/kg air).

Table 5-3. Simulations settings for particle-particle interaction force analysis.

Case name	Granular viscosity	Granular bulk viscosity	Solid pressure	Frictional viscosity	Radial distribution	The rest of the models
Base case	**Gidaspow**	**Lun**	**Lun**	**Schaeffer/based ktgf**	**Lun**	The same as the base case model
granular viscosity: syamal-obrien	syamal-obrien	Lun	Lun	Schaeffer/based ktgf	Lun	
granular bulk viscosity: not included	Gidaspow	set to 0	Lun	Schaeffer/based ktgf	Lun	
solid pressure: not included	Gidaspow	Lun	set to 0	Schaeffer/based ktgf	Lun	
solid pressure: syamlal-obrien	Gidaspow	Lun	syamlal-obrien	Schaeffer/based ktgf for frictional pressure	Lun	
frictional viscosity: not included	Gidaspow	Lun	syamlal-obrien	set to 0	Lun	
frictional viscosity: schaeffer model without frictional pressure	Gidaspow	Lun	syamlal-obrien	schaeffer model without frictional pressure	Lun	
radial distribution: syamlal-obrien	Gidaspow	Lun	Lun	Schaeffer/based ktgf	syamlal-obrien	
radial distribution: ma-ahmadi	Gidaspow	Lun	Lun	Schaeffer/based ktgf	ma-ahmadi	
all set to zero	set to 0	set to 0	set to 0	set to 0	set to 0	

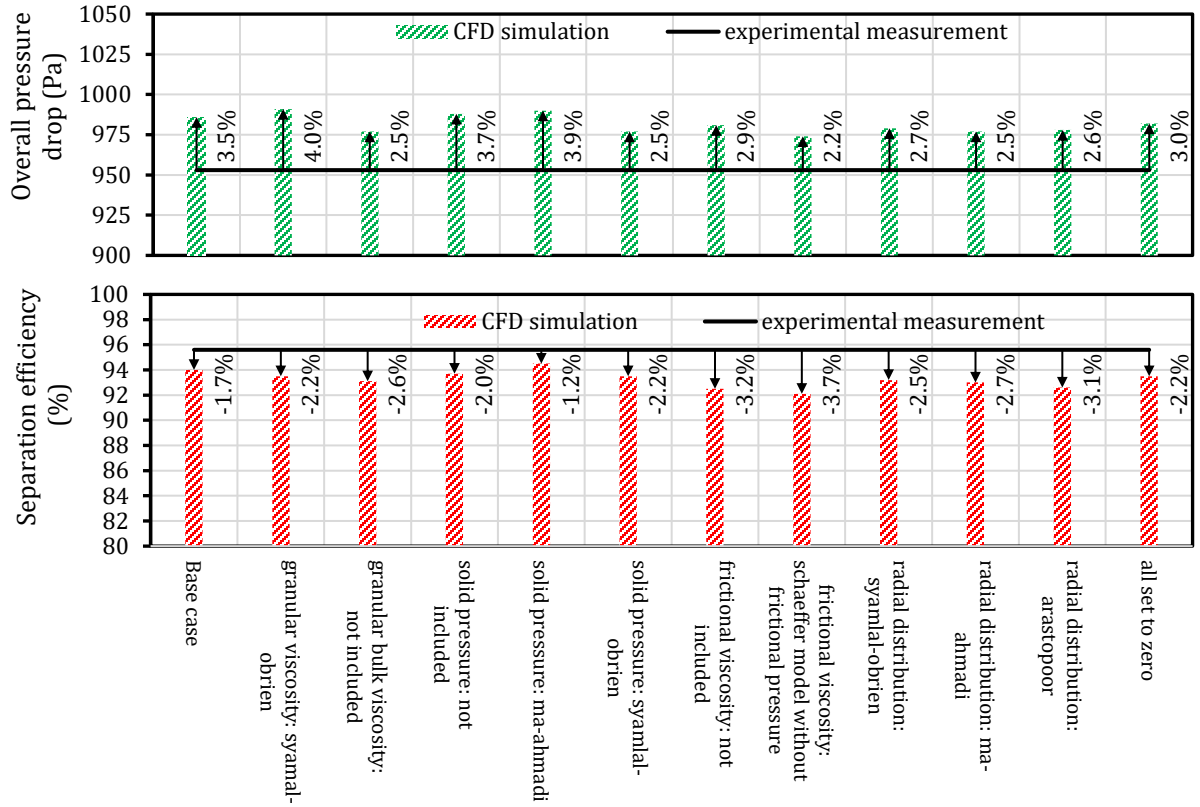

Figure 5-6. Effect of using various options for particle-particle interaction modeling on the overall pressure drop and separation efficiency. Arrows and corresponding percentages show the difference between CFD simulation and experimental measurement.

The solid volume fraction in near-wall regions exceeds 0.001 (The approximate borderline between dilute and dense flow) meaning that we have dense gas-solid flow there, so it was expected that particle-particle interaction forces be considerable and play a role in hydrodynamics multiphase flow. However, the presented results suggest that particle-particle interaction forces (even if they are considerable) do not affect the performance parameter of highly loaded cyclones and their predictions as excluding them from the model did not affect the predictions notably.

In the present case, particle-particle interaction force calculations were not a computational load compared to other calculations, however, in cases where several solid phases are required to be included (e.g. using DDPM for polydispersed particles including energy conservation that requires additional solid phases to achieve energy balance), excluding particle-particle interaction force can speed up the computation significantly without affecting the predictions considerably.

5.5.1.3 Drag model

Several drag models including five homogeneous drag models (Wen-Yu, Gidaspow, TGS, BVK, and DiFelice) and three heterogeneous drag models (Sarkar, Pirker, and Igci) were examined. Comparisons of predictions of pressure drop and separation efficiency are presented in Figure 5-7. The predicted pressure drop seems to be not affected by the drag model significantly (less than 2%), but the separation efficiency predictions are more sensitive (up to 4%). Except for the Sarkar drag model which is the base case model in the present work, all other drag models over-predict the separation efficiency.

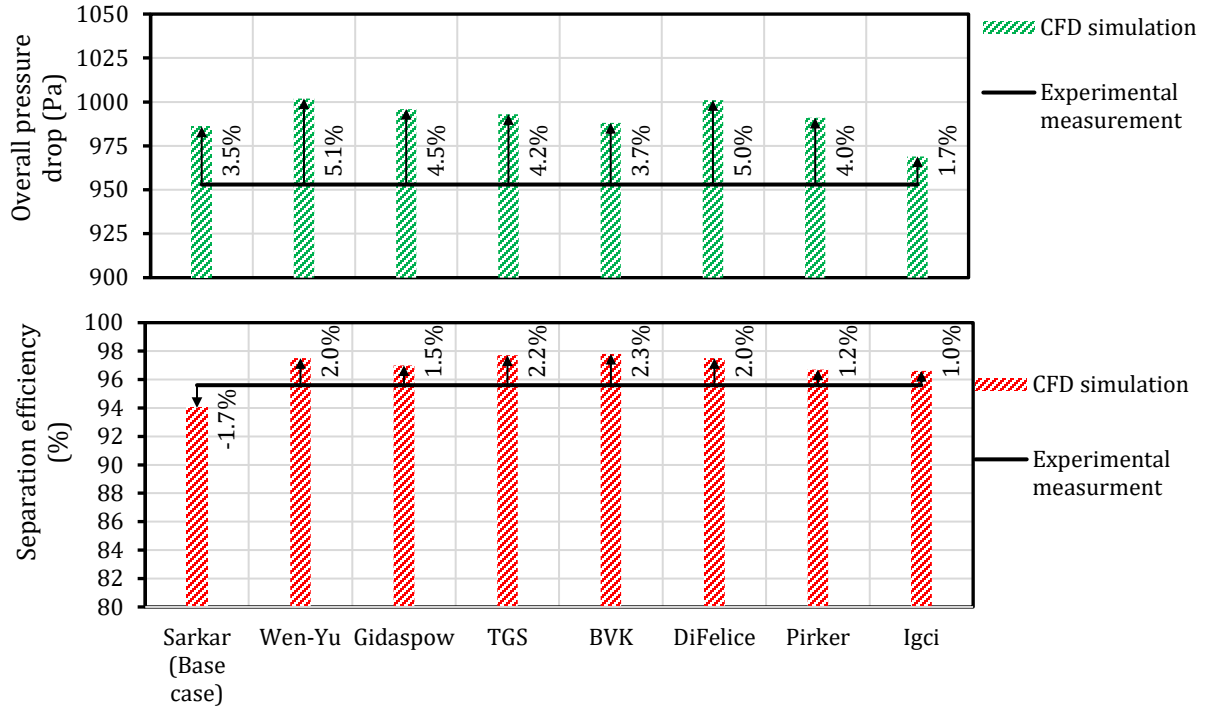

Figure 5-7. Effect of drag model on the overall pressure drop and separation efficiency. Arrows and corresponding percentages show the difference between CFD simulation and experimental measurement.

The flow patterns in the cyclone obtained from each of the tested drag models are presented and compared in Figure 5-8 and Figure 5-9. Except for the Sarkar drag model, all other drag models provide similar flow patterns in the cyclone. Although all drag models provide reasonable flow patterns matched with expectations from cyclones, without flow pattern measurements (that are not available at the moment in case of highly loaded cyclones) it is impossible to comment on which model does a better job.

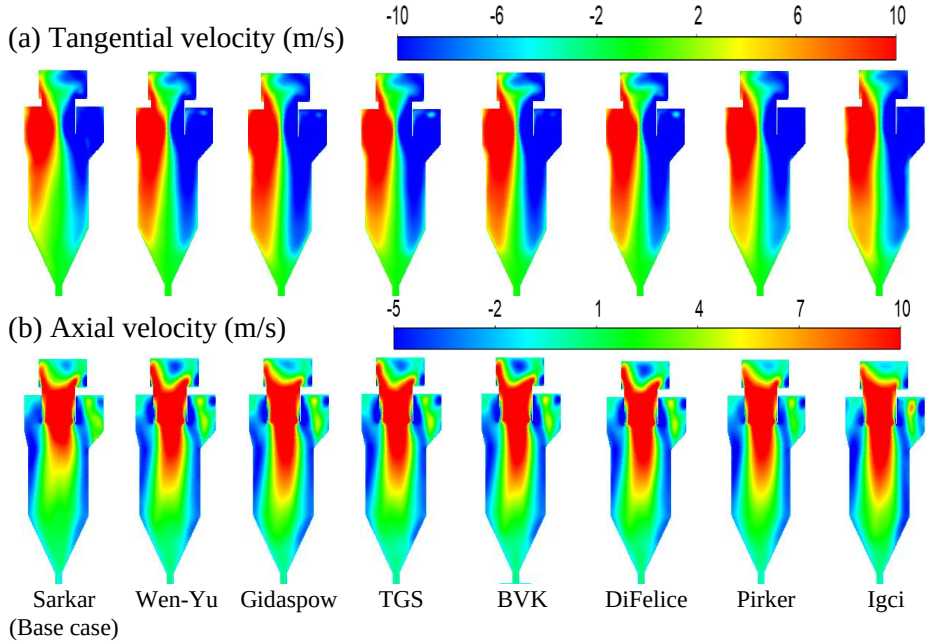

Figure 5-8. Effect of drag model on the flow pattern (contours at a central cross-section of cyclone main body); (a) Tangential velocity, (b) Axial velocity.

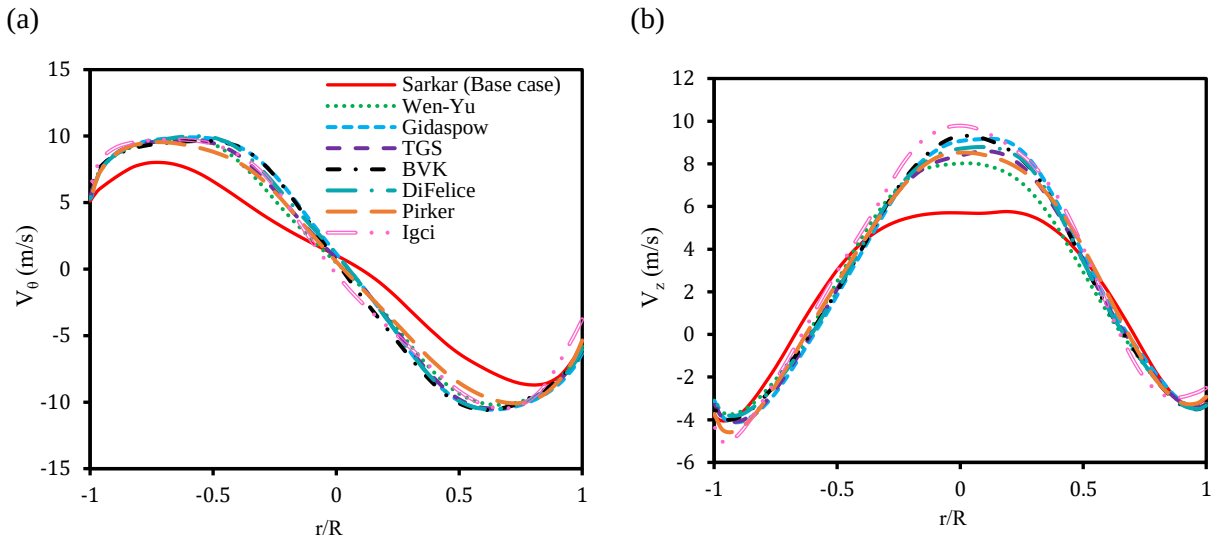

Figure 5-9. Effect of drag model on the flow pattern in the cyclone (profiles at a specific height, 2 m below cyclone roof); (a) Tangential velocity, (b) Axial velocity.

To further compare these models, they were tested for two other operating conditions (operating conditions 2 and 3 with the same gas flow rates and different solid flow rates). As shown in Figure 5-10, although all models except the Sarkar drag model overpredict the separation efficiency, they all are able to capture the trend of improvement in separation efficiency when the solid load is increased. The extent of improvement is not the same in all models (see Figure 5-10 (b)). The Igci drag model predicts the greatest improvement in the separation efficiency (closest to experimental measurement).

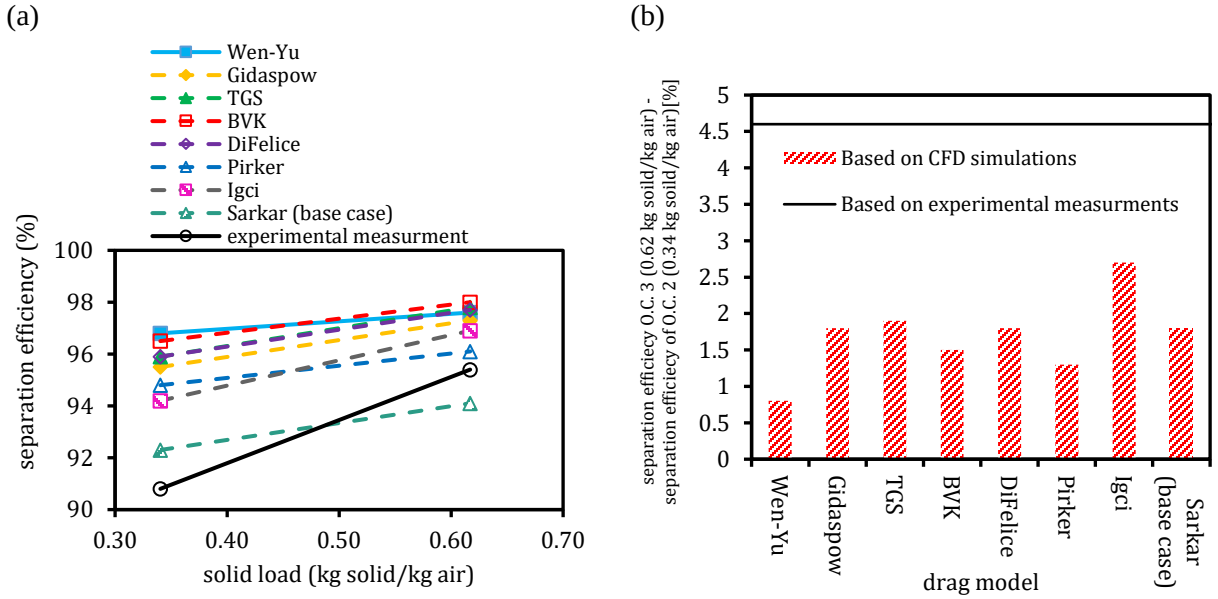

Figure 5-10. Comparison of drag models in capturing the trend of improvement in separation efficiency when the solid load is increased.

It is widely reported that in coarse-grid multiphase modeling based on the Kinetic Theory of Granular Flow (KTGF) (as it is done in the present study) using common homogeneous drag models leads to failure in the

prediction of the multiphase flow hydrodynamics [11,138–146]. However, the result presented here shows that the effect of unrealistic prediction of homogeneous drag force (caused by the inability of coarse grids to resolve mesoscale structures such as particle strands in cyclones) is not strong enough to influence predictions of performance parameters of highly loaded cyclones or even the flow pattern in a notable manner.

To show how each drag model deviates from the Wen-Yu drag model which is the common drag model used for simulation of highly loaded cyclones, snapshots of converged solution showing particles colored with the value of $\frac{\beta}{\beta_{Wen-Yu}}$ obtained from different tested drag models are presented in Figure 5-11. Note that in heterogeneous drag models $\frac{\beta}{\beta_{Wen-Yu}}$ equals the H_d, i.e., heterogeneity index, value. It is widely reported that when multiphase models based on the Kinetic Theory of Granular Flow (KTGF) are used with coarse grids, then using common homogeneous drag models, such as Wen-Yu, overpredict the drag force and that is why heterogeneous drag models should be used to overcome this over-prediction. Having a significant number of particles with $\frac{\beta}{\beta_{Wen-Yu}}$ value of greater than 1 (yellow, orange, and red particles in Figure 5-11) in BVK and TGS drag models show that they are even worse than the Wen-Yu drag model. DiFelice drag model has values close to 1 which makes it similar to Wen-Yu which overpredicts the drag. However, heterogeneous drag models (Pirker, Sarkar, and Igci) have various amounts of particles with $H_d = \frac{\beta}{\beta_{Wen-Yu}}$ values lower than 1 (blue particles in Figure 5-11) compensating for the overestimation of drag to different extents (among heterogeneous drag models, Pirker has the lowest number of particles with H_d value lower than 1 and Sarkar has the highest).

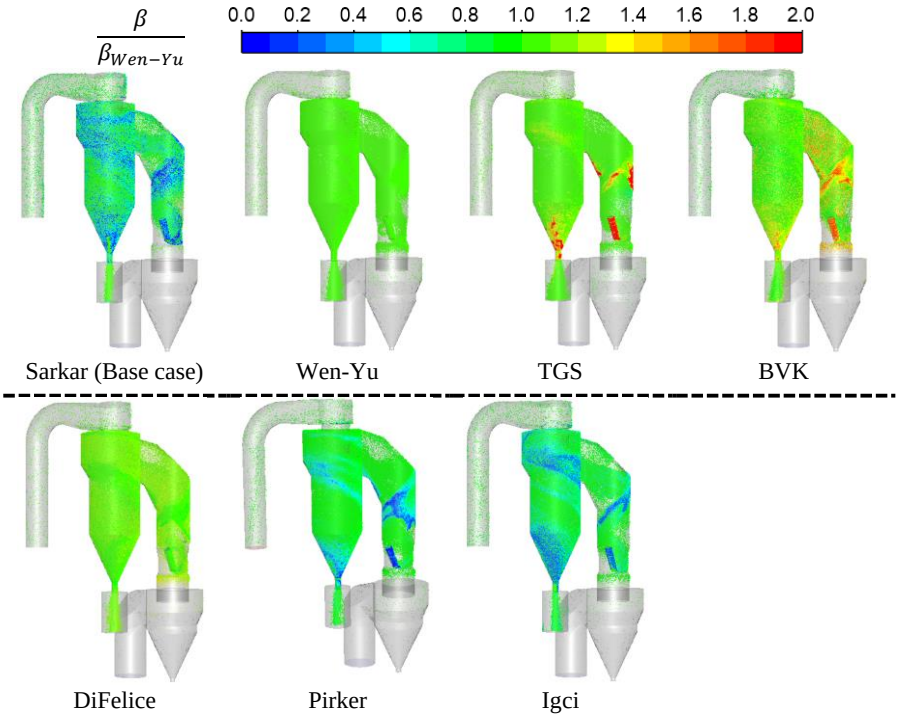

Figure 5-11. Comparison of snapshots of converged solution showing particles colored with the value of $\frac{\beta}{\beta_{Wen-Yu}}$ obtained from different drag models.

When using sub-grid drag models that are a function of the filter size, the predictions might be affected by the filter-to-grid ratio so that in those cases the ratio should be optimized [179–181] or instead more novel models that make H_d independent of filter size should be used [182]. For the base case drag model (Sarkar), a sensitivity analysis of the filter-to-grid ratio (the common values of 1, 2, and 3 were tested) was conducted showing that predictions are not affected by the filter-to-grid ratio considerably (see Figure 5-12; the variation of pressure drop and separation efficiency is less than 1%), so the suggested value of 2 can be used with confidence.

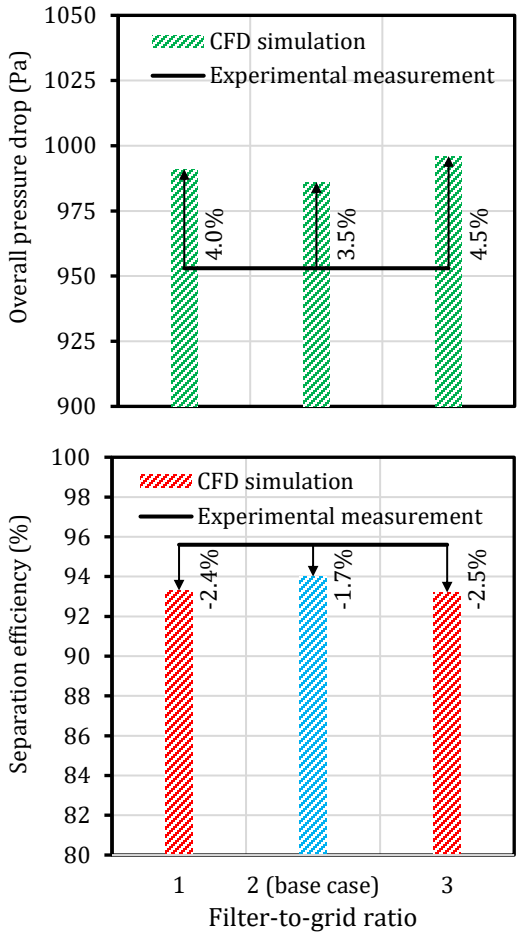

Figure 5-12. Effect of Filter-to-grid ratio in Sarkar drag model on the overall pressure drop and separation efficiency. Arrows and corresponding percentages show the difference between CFD simulation and experimental measurement.

5.5.1.4 Particle rotation, Saffman force, Magnus force, particle turbulent dispersion

Particle rotation [9,51,75,80,104,108,197–199], Saffman force [75,80,104,108,197–199], Magnus force [75,104,108,197,198], and particle turbulent dispersion [37,43,61,74,75,81,197,210] were included in several CFD models for simulation of cyclones in order to make particle motion and predictions of performance parameters more accurate. For the same reason, these terms were included in the base case model of the present work. However, considering the dominance of drag force and low value of gas to particle density (minimizing Saffman force) the significance of these terms needs to be investigated. In

addition, these terms were mostly included in cyclones with low solid loads, while in the present case of a highly loaded cyclone other phenomena such as agglomeration might be more relevant to include.

To find out the extent of the effect of these terms in the present case, the same simulations but with the exclusion of one of these terms (models) at a time were performed and the predictions are compared in Figure 5-13. The comparison shows that none of these terms has a major impact on the prediction of performance parameters of highly loaded cyclones. Unlike Particle rotation, Saffman force, and Magnus force which have been neglected in several CFD simulation studies in the literature for their minor impact, particle turbulent dispersion has been included almost in all CFD simulation studies of cyclones with low solid loading supposedly for its considerable contribution. However, as observed in the present study, in the case of highly loaded cyclones, the contribution of particle turbulent dispersion is also minor (at least compared to other factors such as drag and agglomeration) and can be neglected.

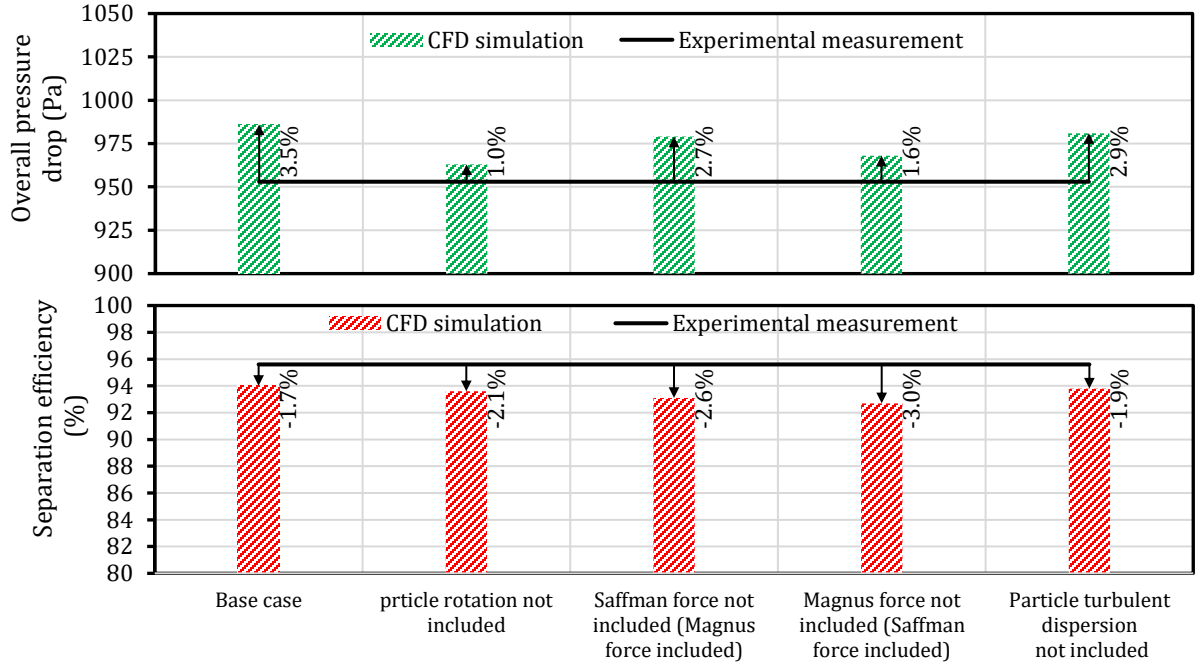

Figure 5-13. Effect of excluding particle rotation, Saffman force, and Magnus force on the overall pressure drop and separation efficiency. Arrows and corresponding percentages show the difference between CFD simulation and experimental measurement.

Therefore, these sub-models can be dropped from the model to accelerate the calculations. Particularly, excluding particle rotation which necessitates one ODE to be solved at each time step for each parcel in the domain can effectively cut down on the computational load without altering the predictions much.

The results indicate that the drag force is the dominant force for highly loaded cyclones, compared to Magnus, Saffman, and particle-particle interaction force.

5.5.2 Model parameters

5.5.2.1 Particle-particle restitution coefficient

Particle-particle restitution coefficient appears in some terms for particle-particle interaction force equations of KTGF (for estimation of some of the parameters in equations 5–10 and 5–11) and in the

agglomeration model for calculation of critical velocity. Although particle-particle interaction force was found to have a minor effect and therefore particle-particle restitution coefficient in its terms would not be of importance, this coefficient plays an important role in agglomeration modeling as the critical velocity and therefore the possibility of colliding particles making agglomerates is a direct function of its value. In other words, the extent of agglomeration is governed and can be adjusted by the particle-particle restitution coefficient.

Higher values of the coefficient lead to lower critical velocities so only particles colliding with smaller relative velocities would make agglomerates ($|\overrightarrow{u_{p1}} - \overrightarrow{u_{p2}}|\cos(\phi) \leq U_{crit}$), also higher values of the coefficient mean higher particle rebound velocity and energy, reducing the chance of making agglomerates. On the other hand, lower values lead to higher critical velocity so more colliding particles would satisfy the condition for making agglomerates. It is worth mentioning that in the present case, the agglomeration mostly occurs in the injection pipe which can be observed by investigating how the PSD of particles is changing throughout the domain (it is discussed in more detail in Chapter 4).

To see how the particle-particle restitution coefficient affects the predictions, a range of values (0.5-0.95) were tested and compared in Figure 5-14. As expected, lower values lead to more agglomeration and consequently larger agglomerates in the cyclone leading to higher separation efficiency. In addition, since larger particles require less energy to be carried by gas, lower values of particle-particle restitution coefficient and consequently larger agglomerates lead to lower pressure drop as can be observed in Figure 5-14. Although such a trend was already expected, the extent of these changes is now confirmed for the PSD studied in the present work.

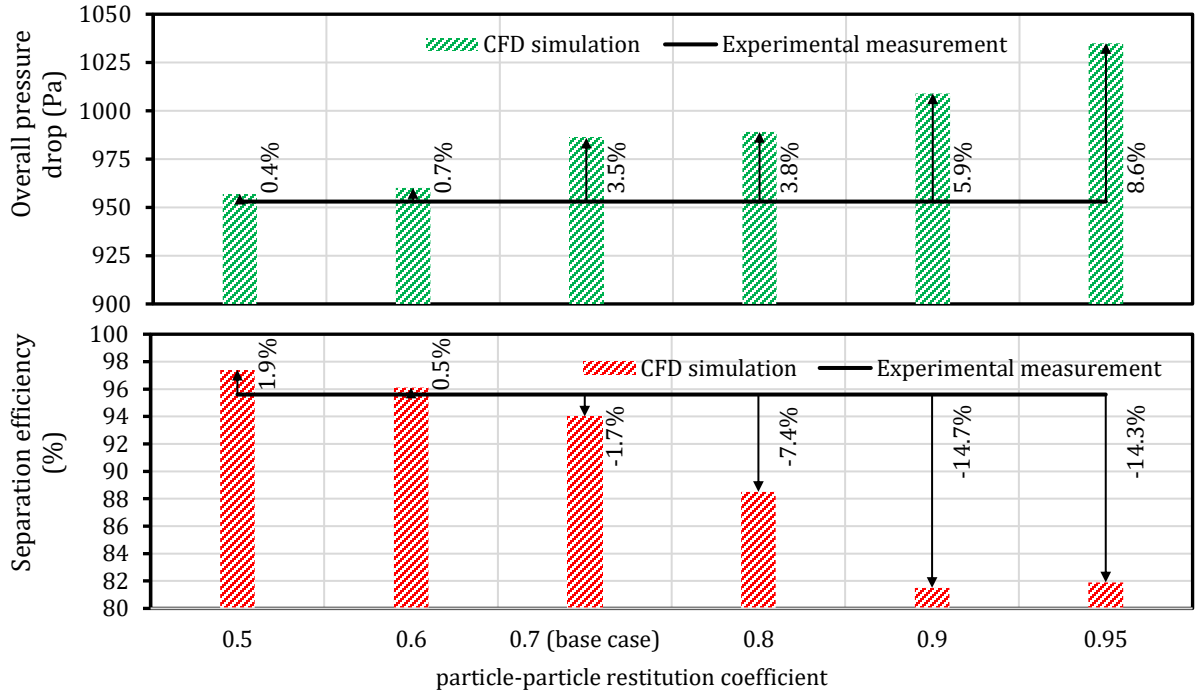

Figure 5-14. Effect of particle-particle restitution coefficient on the overall pressure drop and separation efficiency. Arrows and corresponding percentages show the difference between CFD simulation and experimental measurement.

It should be noted that the extent of the effect of the particle-particle restitution coefficient on the predictions strongly depends on the operation conditions of the cyclone. For example, in a cyclone with larger particles where agglomeration is less intense, weaker dependency is expected, while in a cyclone with finer particles where agglomeration is more intense, stronger dependency is expected. Therefore, it should be noted that the level of dependency reported here is only valid for the present operating conditions.

As can be observed, separation efficiency is significantly influenced by the particle-particle restitution coefficient (or any other parameter defining the extent of agglomeration). Therefore, to see which value would better capture the trend of improvement in separation efficiency when the solid load is increased, different values of particle-particle restitution coefficient were tested and compared for two other operating conditions (operating conditions 2 and 3 with the same gas flow rates and different solid flow rates).

The comparison shown in Figure 5-15 shows that in the case of using the Sarkar drag model, the value of 0.7 for particle-particle restitution coefficient provides the best predictions; a better match with experimental measurement of separation efficiency and the highest (the closest to the experimental measurement) improvement in separation efficiency due to an increase in the solid load. Lower values of particle-particle restitution coefficient lead to over-prediction of separation efficiency and diminishing of the extent of improvement in separation efficiency due to an increase in solid load. On the other hand, higher values are unable to capture such an improvement.

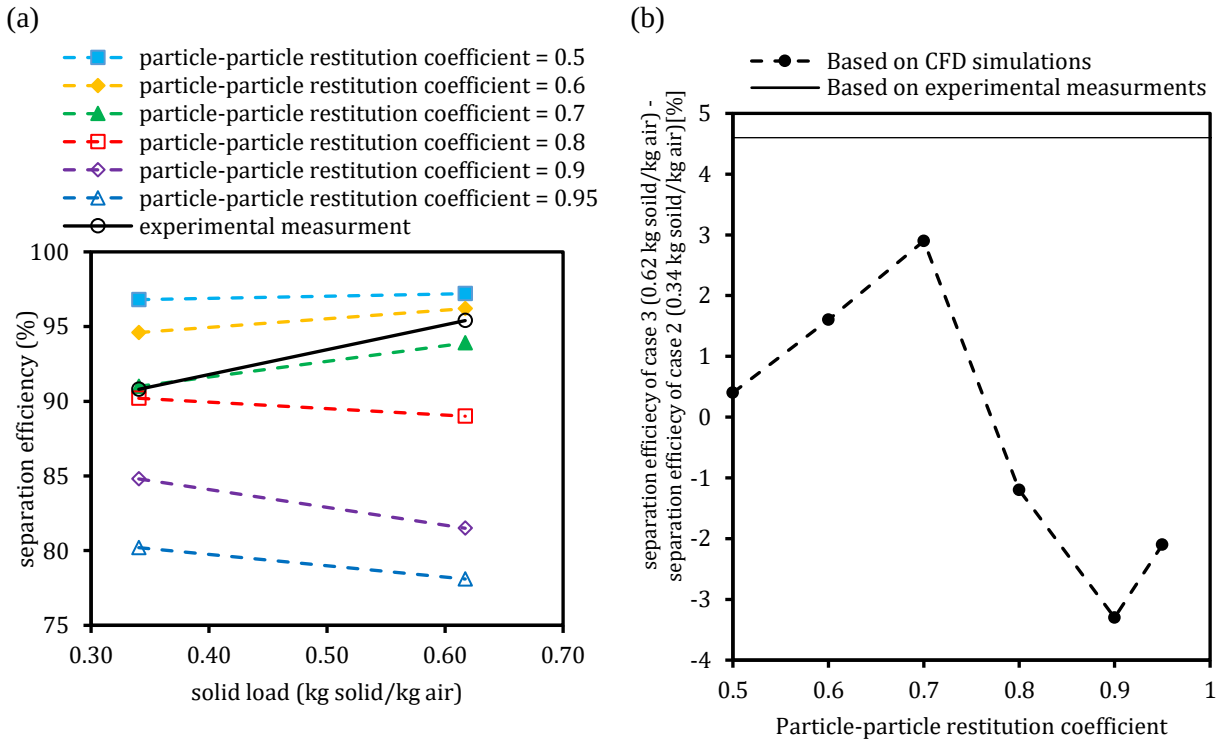

Figure 5-15. Comparison of different values of particle-particle restitution coefficient in capturing the trend of improvement in separation efficiency when the solid load is increased in the case of Sarkar drag model simulations.

Since the Igci drag model showed promising performance in capturing the trend of improvement in separation efficiency (better than all other drag models as can be observed in Figure 5-10), a similar

comparison (testing different values of particle-particle restitution coefficient for operating conditions 2 and 3 with the same gas flow rates and different solid flow rates) is done for this drag model as well (see Figure 5-16). By increasing the particle-particle restitution coefficient to 0.8 the over-prediction of separation efficiency by the Igci drag model observed in Figure 5-7 is reduced, also the extent of improvement in separation efficiency is slightly improved.

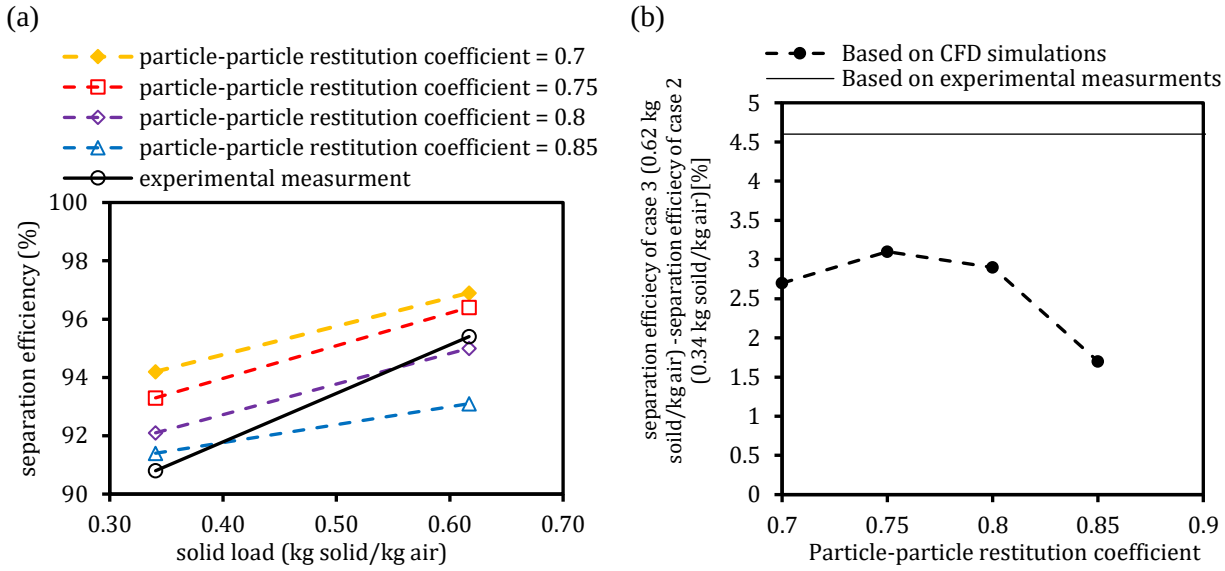

Figure 5-16. Comparison of different values of particle-particle restitution coefficient in capturing the trend of improvement in separation efficiency when the solid load is increased in the case of Igci drag model simulations.

Overall, as presented in Figure 5-17, using the Sarkar drag model combined with a particle restitution coefficient of 0.7 and using the Igci drag model combined with a particle restitution coefficient of 0.8 provide the best predictions of separation efficiency and the best trend of improvement in separation efficiency when the solid load is increased. As both Sarkar and Igci drag models provide accurate predictions, further comparison of these drag models requires flow pattern measurements since they provide considerably different axial and tangential velocity profiles (see Figure 5-8 and Figure 5-9).

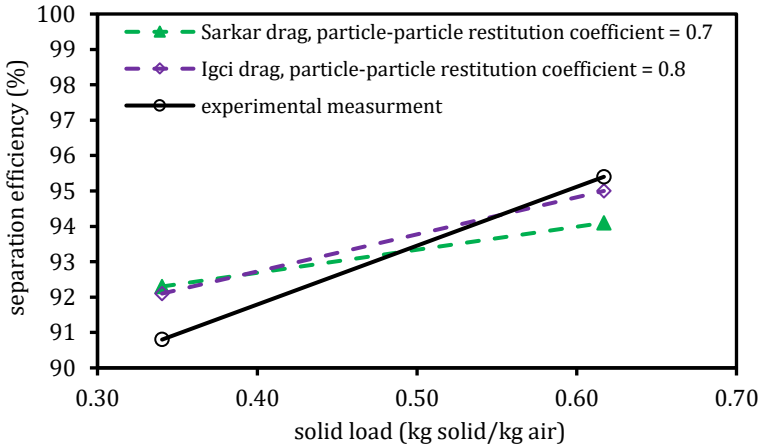

Figure 5-17. Comparison of using the Sarkar drag model combined with a particle restitution coefficient of 0.7 and using the Igci drag model combined with a particle restitution coefficient of 0.8 in the prediction of separation efficiency and in capturing the trend of improvement in separation efficiency when the solid load is increased.

Although the effect of drag modeling is minor, Igci and Sarkar drag models provided slightly better predictions as discussed. Their superiority over homogeneous drag models (Wen-Yu, Gidaspow, TGS, BVK, and DiFelice) is simply explained by the fact that homogeneous drag models are inferior in capturing the hydrodynamics of multiphase flow when used in coarse grids as they do not account for small-scale and heterogeneous structures present in the system. On the other hand, their superiority over the Pirker drag model (the other tested heterogeneous drag model), might be explained by the fact that Igci and Sarkar drag models and their equations are derived from simulations in a periodic domain (which is generic two-phase systems), while Pirker drag model was derived from simulations in a specific two-phase system (bubbling fluidized bed). Therefore, Igci and Sarkar drag models are more likely to perform better in a wider range of units (including cyclones) as they were derived from a generic case while the Pirker drag model is more likely to perform better for the specific unit that it was derived from.

Considering that properties such as particle restitution coefficient, are not available or easy to measure for a specific solid material, its value can be adjusted in a valid range (dependent on the physical properties of the solid material) to improve the predictions.

The effect of the particle-particle restitution coefficient on the grade efficiency curve of the cyclone is presented in Figure 5-18 (a). The well-known “fish-hook” behavior in highly loaded cyclones (the observation of minima in the grade efficiency curve) [189] is observed in all particle-particle restitution coefficients (except for 0.5) as there is at least one minimum in each grade efficiency curve in the range of 1-10 μm. Lower values of restitution coefficient lead to more agglomeration and consequently higher grade efficiencies. The number of these minima and their locations (particle size and fractional efficiency where a minimum is observed) depend on the solid properties (particle-particle restitution coefficient). Note that in all cases, particles larger than 45 μm are fully separated while the grade efficiencies of particles finer than 45 μm are dependent on the restitution coefficient meaning that up to this particle size agglomeration is playing a role in the performance of the studied cyclone.

Taking samples of the particles that escaped and separated from the cyclone to obtain the experimental grade efficiency can be valuable to have an understanding of the level of agglomeration happening in the cyclone and can help to choose an appropriate particle-particle restitution coefficient value as different values provide different grade efficiency curves.

In addition to grade efficiency curves, to better see the effect of particle-particle restitution coefficient on the formation of agglomerates, the PSD of particles leaving the domain (after agglomeration) are presented for all tested restitution coefficients in these three cases in Figure 5-18 (b) and are compared with PSD of injected particles. As the restitution coefficient decreases, overall larger particles are formed as the curve is shifted to the right. The lower value of the restitution coefficient, the more significant difference between the PSD of particles leaving the domain and the PSD of particles injected into the domain due to more agglomeration.

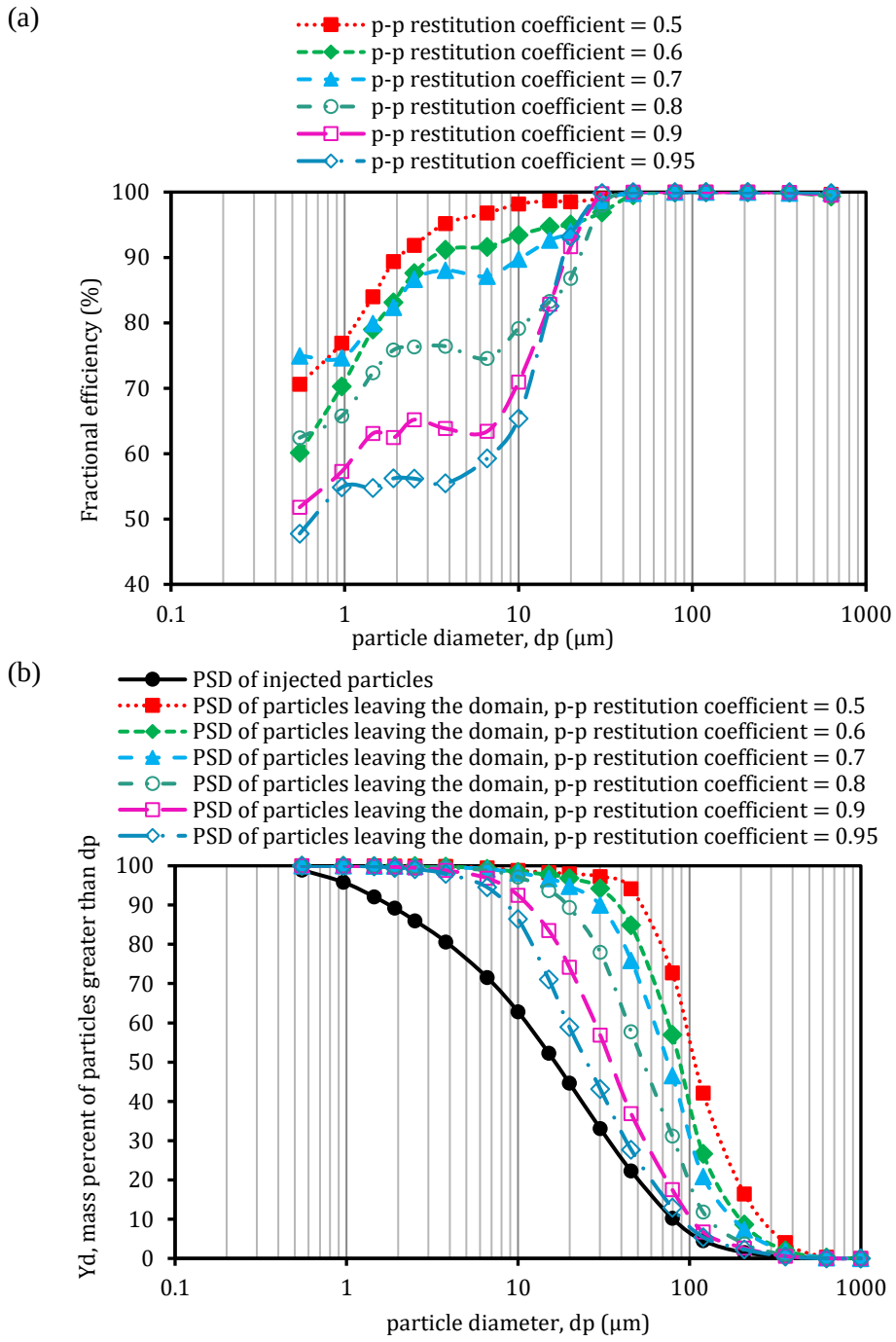

Figure 5-18. Effect of particle-particle restitution coefficient on (a) grade efficiency curve, and (b) PSD of particles (after agglomeration) leaving the domain (the particles collected in the dust bin + the particles escaped to the gas outlet).

5.5.2.2 Particle-wall rebound coefficient

The particle-wall collision was modeled by normal and tangential rebound coefficients (i.e., the ratio between particle rebound velocity to particle impact velocity) that is a property dependent on particle and wall material (and collision angle). Like the particle-particle restitution coefficient, the particle-wall rebound coefficient is not available in the literature for various wall and particle materials and is not easy

to measure. Therefore, a sensitivity analysis was done for this parameter in the range of 0.5-1 to see how it affects predictions of important performance parameters in the case of highly loaded cyclones.

As shown in Figure 5-19, its impact on the pressure drop prediction is minor. However, the impact on the separation efficiency can be divided into two ranges; (1) 0.5-0.8 where the impact is minor, and (2) 0.8-1 where an increase leads to a reduction in separation efficiency up to 10%. Higher values of particle-wall rebound coefficient mean higher particle rebound velocity and a higher chance of passing the descending outer vortex and reaching ascending inner vortex (especially in the conical part of the cyclone where the outer vortex is thin) and eventually a higher chance of escaping with gas that leads to a reduction in separation efficiency. Although values in the range of 0.9-1 might be unphysical, the rebound coefficient can be adjusted in the range of 0.8-0.9 to improve separation efficiency predictions slightly, in particular, in cases where pressure drop predictions are fine (in cases where both separation efficiency and pressure drop are off from experiments, adjusting particle-particle restitution coefficient seems more reasonable as it affects both separation efficiency and pressure drop).

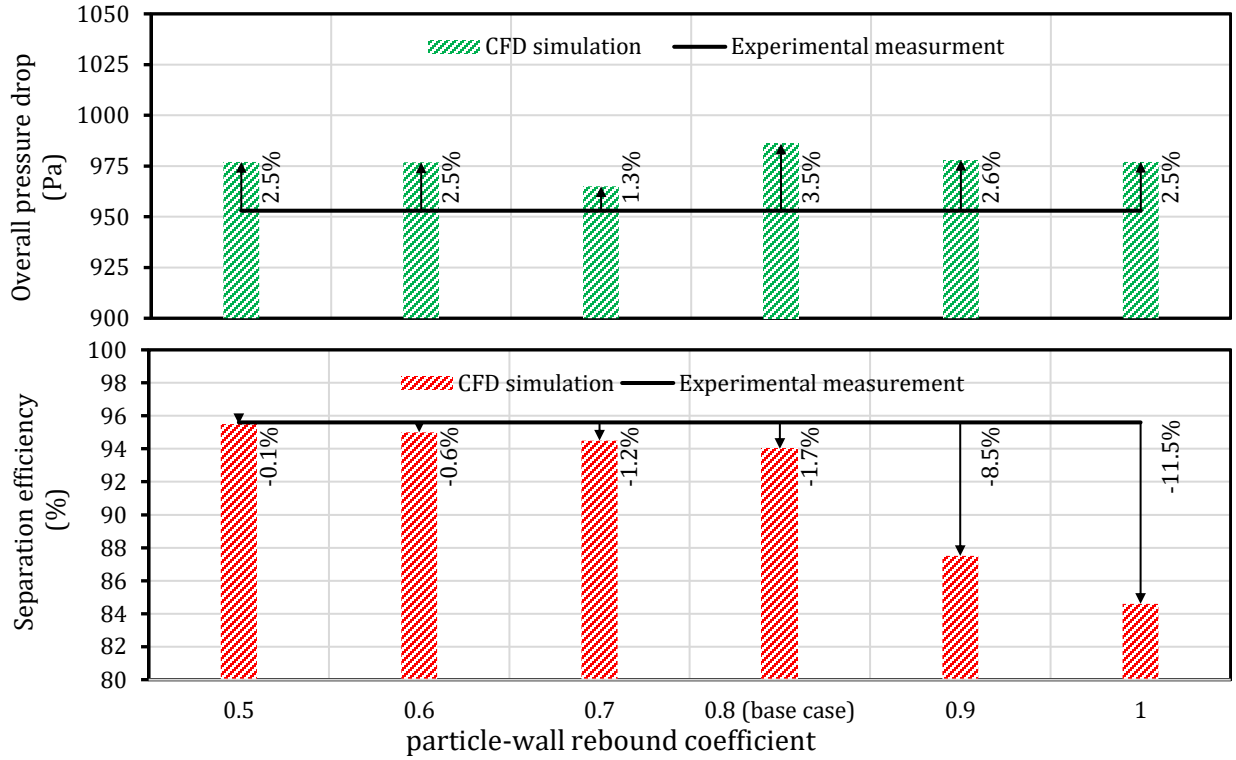

Figure 5-19. Effect of particle-wall rebound coefficient on the overall pressure drop and separation efficiency. Arrows and corresponding percentages show the difference between CFD simulation and experimental measurement. Note that both tangential and normal rebound coefficients are changed at the same time.

In the present study, more complex (and more accurate) particle-wall models that relate the rebound coefficient to the angel of collision have not been investigated because the constants in such models are dependent on the physical properties of the wall and the particles and are not available in the literature for the present case.

5.5.3 Numerical parameters

5.5.3.1 Time step

One important superiority of DDPM over other common multiphase models such as DEM and TFM is that it can simulate with relatively large time steps [10,187] which makes this model a feasible option for simulation of large-scale systems. However, unlike DEM and TFM, in DDPM due to its relative novelty, there is no recommendation to decide the time step size. Also, to speed up calculations, it is important to find out how large the time step size can be in DDPM without affecting the predictions at least in the case of highly loaded cyclones. Therefore, a sensitivity analysis is done covering 1-100 ms of time steps.

In this study, the time step is controlled by a courant number to make the analysis less dependent on the case and meshing. As shown in Figure 5-20, in the range of 1-12 ms (courant number 25-300) the predictions are not notably sensitive to the time step size (deviations from the base case are below 2%), while for larger time steps, the predictions especially the separation efficiency start to deviate. Therefore, it can be concluded that 12 ms (courant 300) is the largest time steps providing results independent time step size so it is used for all other simulations in the present work as it is the least computationally expensive.

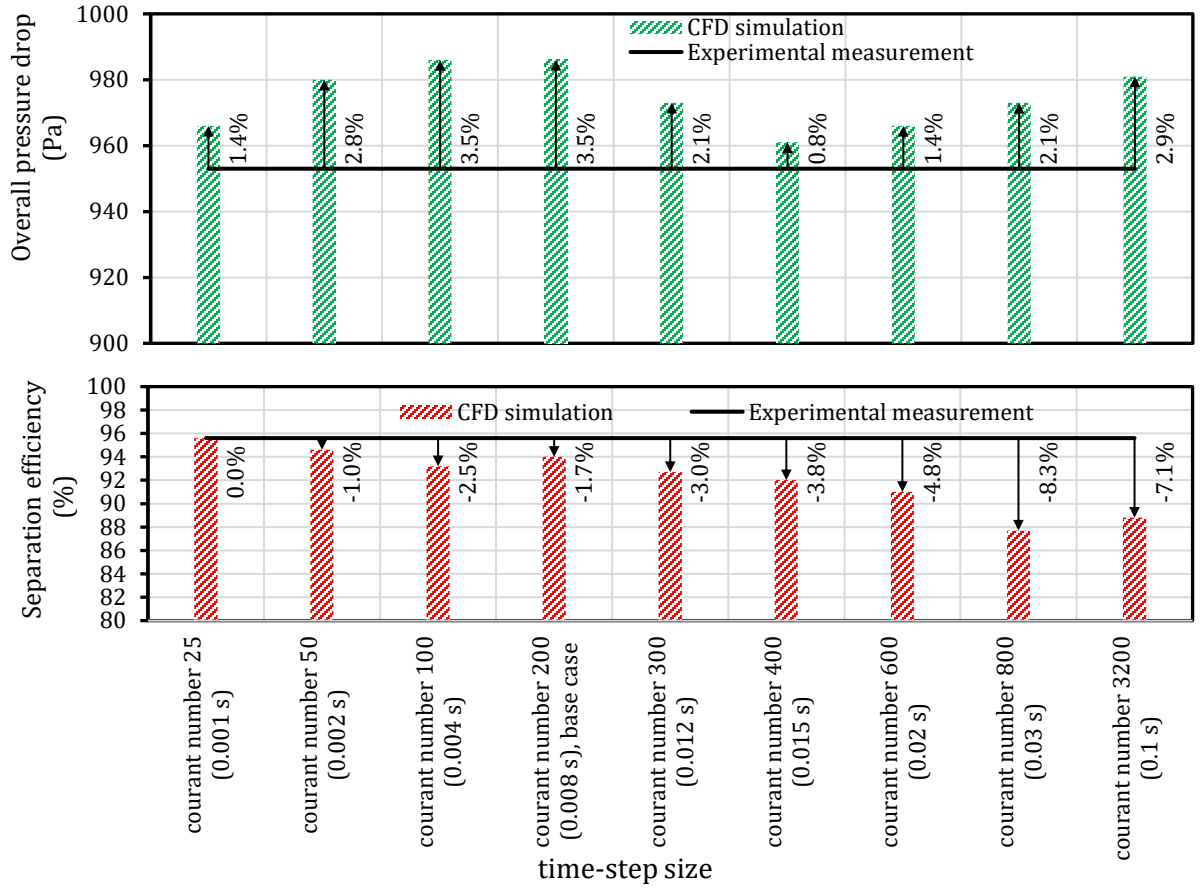

Figure 5-20. Effect of courant number (time step size) on the overall pressure drop and separation efficiency. Arrows and corresponding percentages show the difference between CFD simulation of experimental measurement.

The present study confirms that, unlike other conventional multiphase models such as TFM which requires 0.1-1 ms time steps to have a converging solution, DDPM can be run with greater time steps without

affecting the predictions which makes this model an interesting option for simulation of large-scale cases. Although the size of the time step is case-dependent, the present study suggests a range (around a courant number of 300) as a starting point for future studies in other cases.

5.5.3.2 Parcel (grain) size

In the present study, the strategy of coarse-graining was to have the same parcel size (same parcel mass) for different particle sizes. In DDPM, to ensure convergence of gas-phase calculations, it is required to have parcel (grain) size finer than cell size to avoid zero gas volume fraction in conservation equations that leads to solution divergence. On the other hand, the largest size of the grain is desired, to have fewer grains in the domain to track and have faster particle tracking. It was found that the solver can handle having a minor fraction of cells smaller than the parcel size without causing a convergence issue for the solver, but the limit of this fraction is case-dependent and is not clear. Therefore, a sensitivity analysis on parcel size is done to find this limit for the present case and the parcel size that provides the fastest solution predicting parameters of interest similar to when finer parcels are used.

Seven parcel masses were tested and compared in Figure 5-21 showing that up to a parcel mass of 80 mg, the predictions are not sensitive to the parcel size while larger parcels provide notably diffident predictions. It can be observed that in the case of 320 mg parcels, the convergence is lost in a few time steps (even with 100 iterations in each time step), and there are more of these time steps (with no convergence) in cases with larger parcels. Therefore, it can be concluded that as far as convergence in each time steps is achieved, the predictions are independent of parcel size.

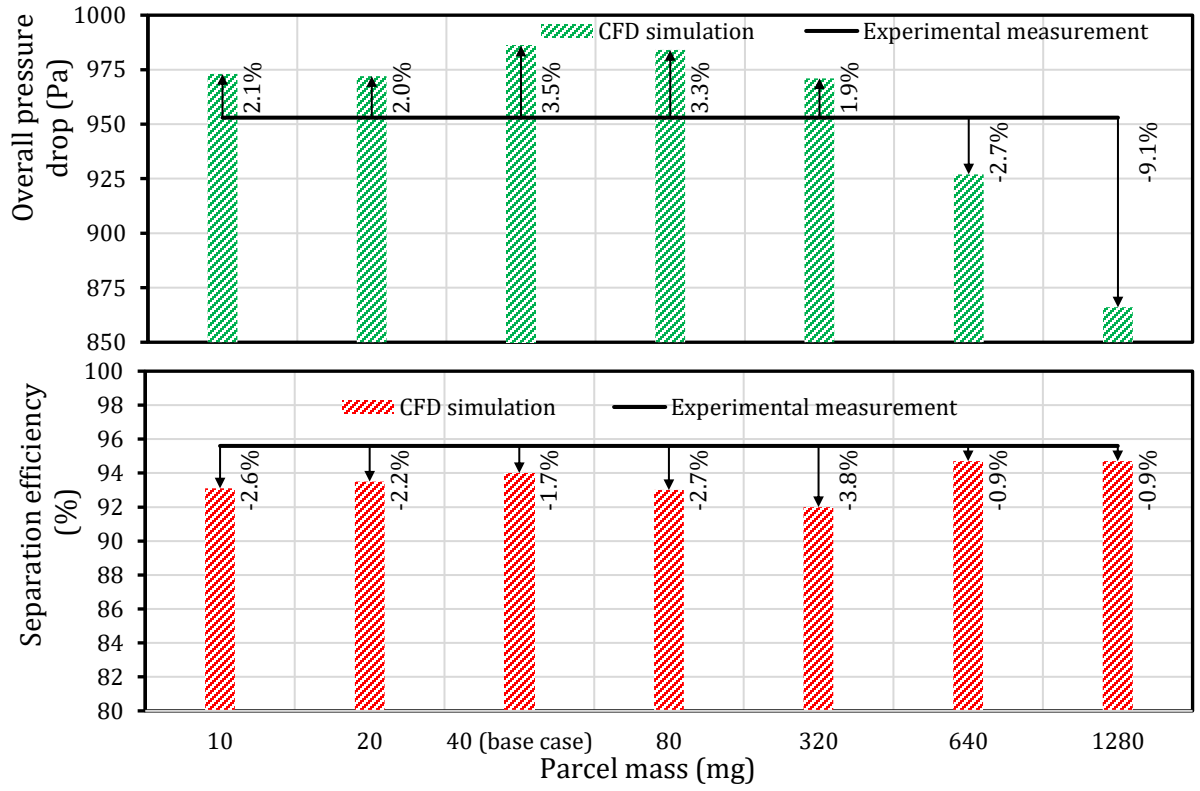

Figure 5-21. Effect of parcel size (parcel mass (kg)) on the overall pressure drop and separation efficiency. Arrows and corresponding percentages show the difference between CFD simulation and experimental measurement.

In the case of 80 mg parcel mass (the largest tested parcel with no convergence issue and providing parcel size independent predictions), only 10k cells out of 4.2M cells (0.2%) are smaller than parcel size (80 mg), while in the case of 320 mg parcel mass (finest tested parcel with convergence issue), 36k cells (0.9%) are smaller than parcel size (320 mg). Therefore, it seems that having up to 0.2% of cells smaller than the parcel size is the limit and can be handled by the solver.

It should be noted that although larger parcel size leads to faster particle tracking, it does not always speed up the whole calculations as when larger parcels are used, in some cases more iterations in Eulerian calculations will be needed to converge the solution. In the present study, among cases that provide parcel size independent predictions (10, 20, 40, 80 mg parcel) the one with 40 mg provides the fastest solution while it has more parcels in the domain to track compared to the case of 80 mg parcel. Therefore, a parcel size of 40 mg is chosen as the base case to be used for all other simulations.

The present study confirms that DDPM (as it implicitly approximates particle-particle interaction forces) can be run with a larger parcel size compared to DEM (that directly resolves these forces). In the specific case of the present work which turned out that particle-particle interaction forces have a minor effect, the parcel size can be enlarged without affecting the predictions to the limit that solution convergence is achieved. However, this conclusion is limited to the present case, as in other DDPM CFD simulations where particle-particle interaction forces might be important, smaller parcels might be needed.

5.5.3.3 Discretization method

Another way to speed up calculations is to use lower-order discretization methods to have the convergence of the solution with fewer iterations. However, as lower-order discretization means lower accuracy, the significance of its impact should be investigated. In the CFD solvers using finite volume formulation such as Ansys Fluent, there are different discretization schemes available for interpolation of each variable from the cell center to control volume surfaces. In the present work, two different sets of discretization schemes summarized in Table 5-4 (one referred to as 1st order as most of the variables are discretized by First Order schemes and the other referred to as 2nd order as most of the variables are discretized by Second Order scheme) are tested and compared in Figure 5-22.

Table 5-4. Summary of tested discretization schemes.

Case name	Gradient	Pressure	Momentum	Volume fraction	Turbulent kinetic energy	Specific dissipation rate
2nd order (base case)	Least Squares Cell Based	PRESTO!	Second Order Upwind	QUICK	Second Order Upwind	Second Order Upwind
1st order	Least Squares Cell Based	PRESTO!	First Order Upwind	First Order Upwind	First Order Upwind	First Order Upwind

As it can be observed, the impact is significant; unlike quite accurate predictions of the 2nd order scheme (base case), the 1st order scheme highly underpredicts both pressure drop and separation efficiency by 27% and 10% respectively. Therefore, although 2nd order scheme is more computationally expensive (it requires almost 1.5 times the number of iterations to converge), it is necessary to have accurate enough predictions.

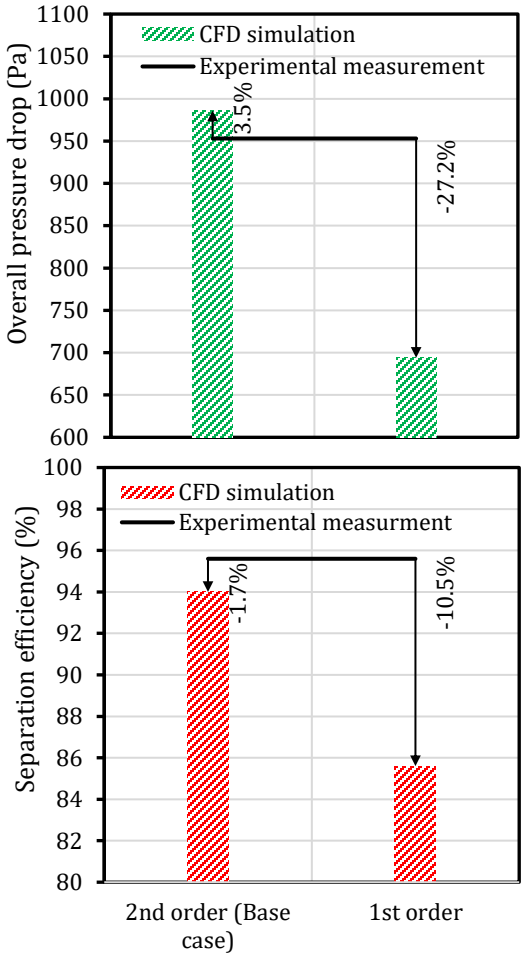

Figure 5-22. Effect of the discretization method on the overall pressure drop and separation efficiency. Arrows and corresponding percentages show the difference between CFD simulation and experimental measurement.

5.5.4 Operating conditions

5.5.4.1 Particle size distribution

It is known that the performance (pressure drop and separation efficiency) of a cyclone is directly dependent on the PSD of solid material. Although the measurements were conducted with one specific PSD (D_{32} = 6 µm, base case), to see the effect of PSD on the performance parameters of a highly loaded cyclone, five other PSDs (D_{32} = 1, 2, 6, 16, 39, and 98 µm) presented in Figure 5-23 were tested in CFD simulations and the predictions were compared in Figure 5-24.

As expected, the higher the mean particle size, the higher the separation efficiency and the lower the pressure drop (as larger particles require less energy to be carried by gas). It can be observed that the predictions are highly dependent on the PSD, so it is important to measure the PSD of the injected particle as accurately as possible.

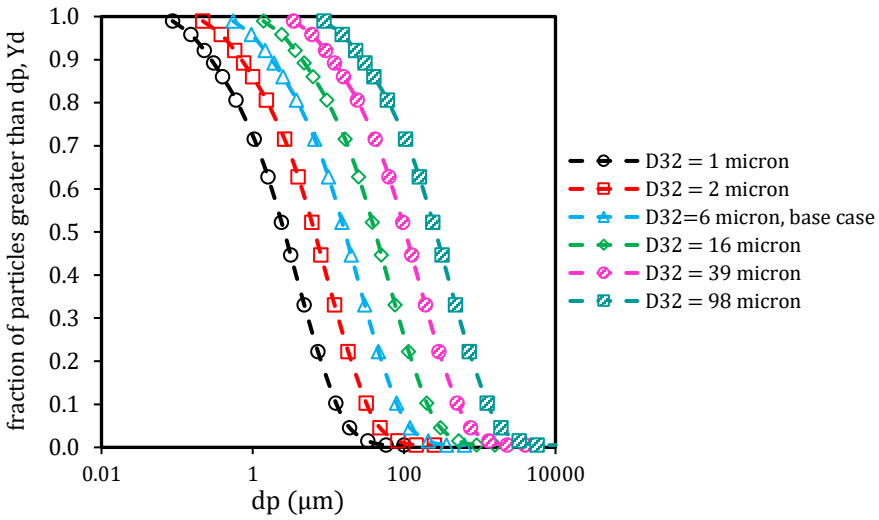

Figure 5-23. PSD of injected particles in the study of the effect of PSD.

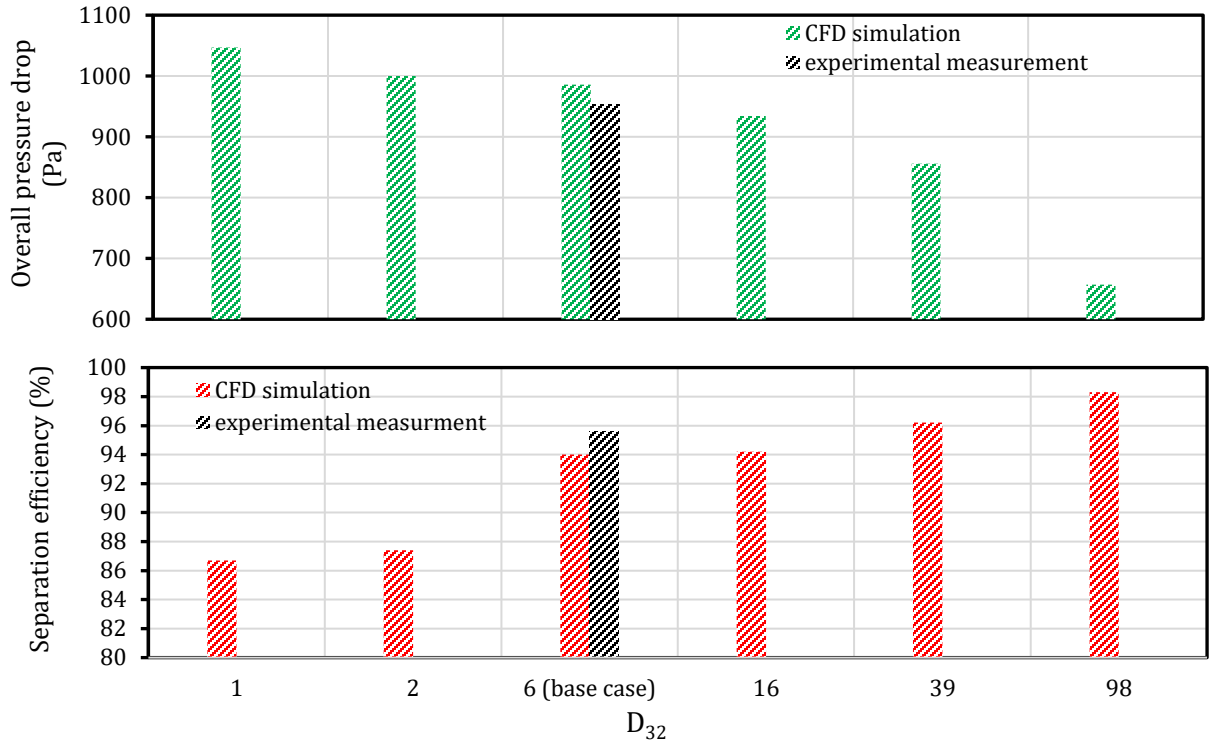

Figure 5-24. Effect of the particle size on the overall pressure drop and separation efficiency.

In Figure 5-25 (a), for each of these tested mean particle sizes, the PSD of injected particles are compared with the PSD of particles leaving the domain (after agglomeration). For finer particles (e.g., D_{32} = 1 µm) greater differences between PSD of injected and leaving particles are observed showing that the effect of agglomeration is more significant when finer particles are operated. While for larger particles (e.g., D_{32} = 98 µm) the difference between the PSD of injected and leaving particles becomes minor compared to cases with finer particles as the agglomeration becomes less crucial.

(a)

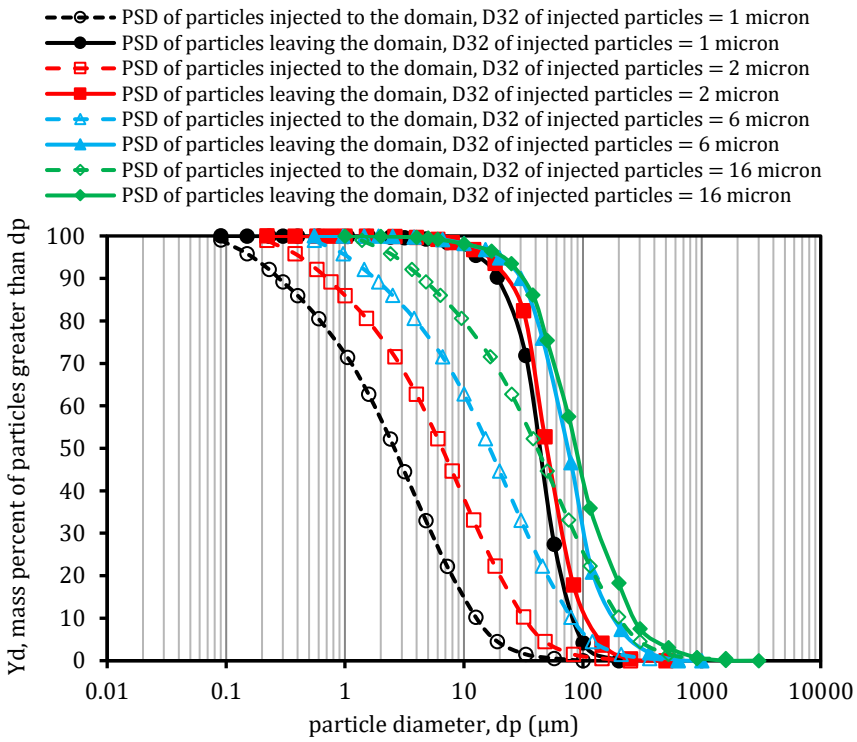

(b)

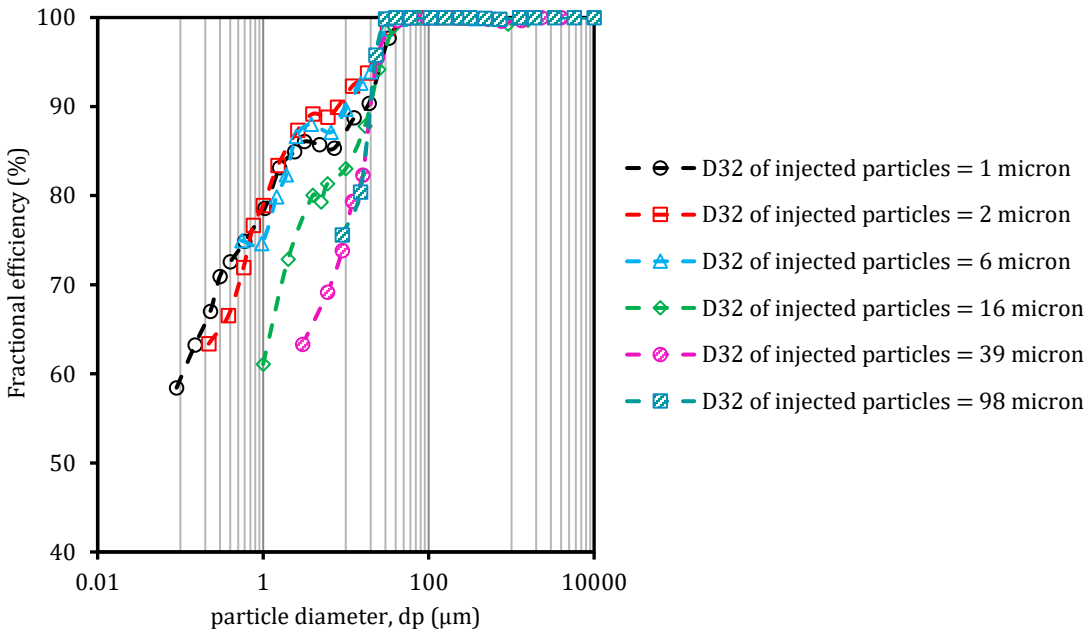

Figure 5-25. Effect of PSD of injected particles on (a) grade efficiency curve, and (b) PSD of particles (after agglomeration) leaving the domain (the particles collected in the dust bin + the particles escaped to the gas outlet).

In addition, grade efficiency curves obtained for each of these tested mean particle sizes are compared in Figure 5-25 (b). The larger the mean particle size, the harder to observe minima (fish-hook behavior) in the grade efficiency curve (no minimum observed in case of D_{32} = 39 and 98 µm) as such behavior is due to agglomeration and with larger particles the impact of agglomeration becomes minor. Note that in all cases that the minima were observed it was located in the range of 1-10 µm. Another point to mention is that even

in the case of D_{32} = 1 μm, the grade efficiency curve does not go below 50% showing the high performance of the studied cyclone.

5.5.4.2 Solid load

In addition to PSD, another operating condition affecting the performance of cyclones is solid loading. The experiments in the present study were done in the range of 0.3-0.6 kg solid/kg air, but the range was extended in the CFD simulations to lower solid loadings (down to 0.001 kg solid/kg air) and the predictions were compared with well-known analytical models valid in the range. Also, to highlight the significance of agglomeration and the importance of including it in the calculations, the predictions of CFD simulation and analytical models are compared with the predictions of CFD simulation excluding the agglomeration modeling.

The analytical model used for the prediction of separation efficiency in the cyclone is developed by Muschelknautz and co-workers [1,107,211] that uses an approach known as an equilibrium balance. The geometrical and operational (including solid load) features of the cyclone are both considered in this model. On the other hand, for the pressure drop a universal model accounting for four types of major losses in the cyclone (expansion loss at the cyclone inlet, contraction loss at the entrance of the outlet tube, swirling loss and dissipation loss of the gas dynamic energy in the outlet) proposed by Chen [212] that considers the effect of solid loading. It should be noted that, although the Chen model is reported to highly over-predict the pressure drop [191] (the over-prediction is also observed in the present work), the trends are reliable.

The effect of solid loading in the range of 0.001-0.65 kg solid/kg air on the prediction of separation efficiency, overall (cyclone + riser) pressure drop, and cyclone pressure drop are presented in Figure 5-26. As expected, in the whole range, with an increase in the solid load the separation efficiency is improved, and the pressure drop is reduced which are observed both in the analytical models and the CFD simulation only when the agglomeration model is included. The analytical models suggest that the separation efficiency and pressure drop are more sensitive to the solid load at lower loadings, and the CFD model (with agglomeration) is capturing the same.

Another point to mention is that at low solid loads, the deviation of CFD predictions with and without agglomeration is minor compared to higher loads (deviation increases with an increase in the solid load) suggesting that agglomeration plays a more important role at high solid loads as expected.

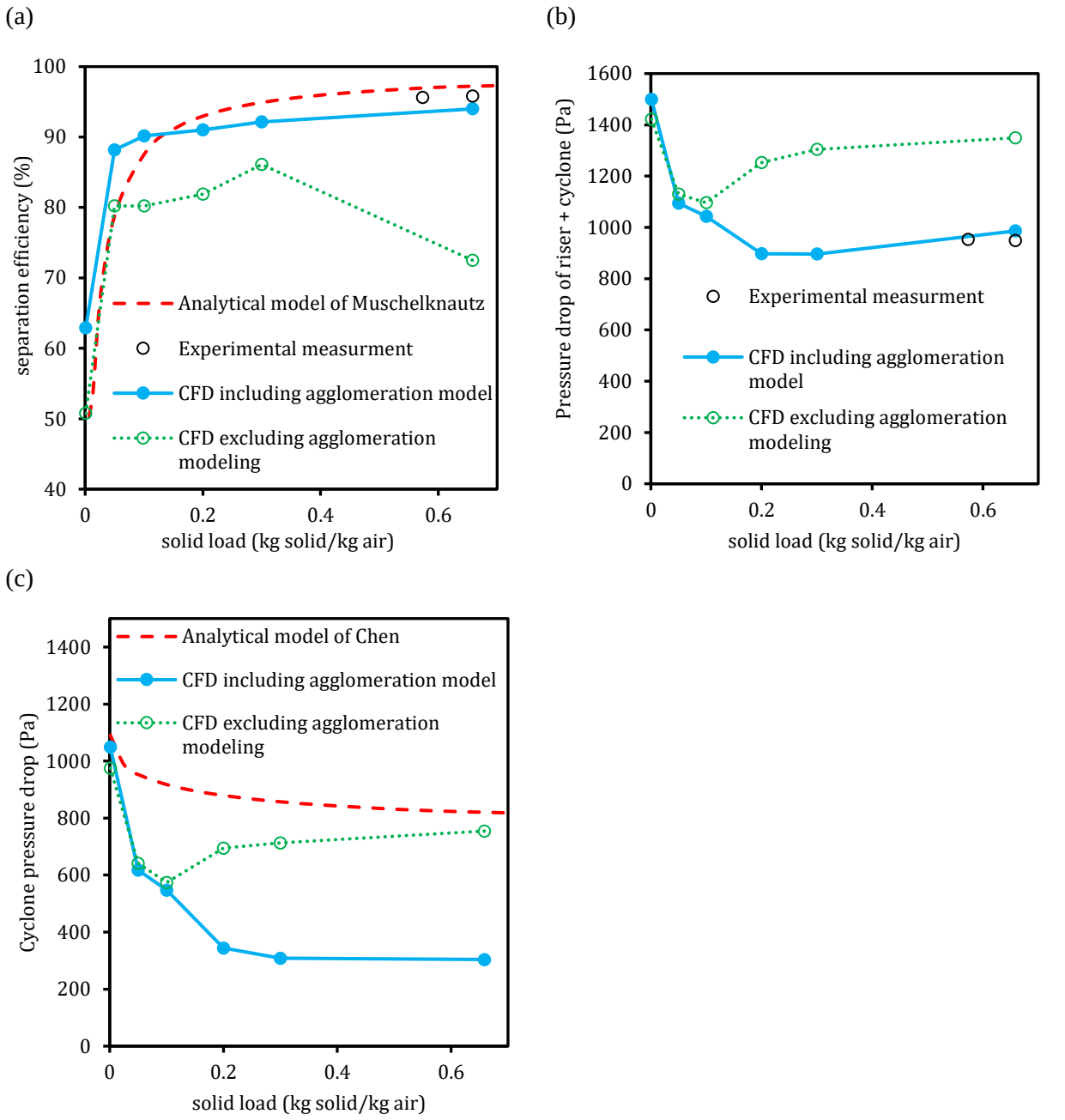

Figure 5-26. Effect of solid load on the prediction of (a) separation efficiency, (b) overall (cyclone + riser) pressure drop, and (c) cyclone pressure drop; the predictions are compared with experimental measurements and predictions of analytical models when applicable.

5.5.4.3 Gas underflow

In the present experimental setup, the dipleg was connected to a dust bin, which is supposed to have no leakage. However, in the case of industrial cyclones, in the usual cascade arrangement or cyclones in CFB units, a minor amount of gas might leave the cyclone with separated particles (a few percentages, below 5%, of inlet gas flow rate flowing downward in the dipleg) [191]. It is worth mentioning that in some industrial applications, the opposite might also happen (some gas might come to the cyclone from the dipleg

due to the pressure difference) that is not studied here. To see how this underflow would affect the performance parameters of a highly loaded cyclone, a simulation case assuming 5% gas underflow was done and compared with a case with no gas underflow as the base case in the present study (see Figure 5-27). The comparison shows that the impact of gas underflow is relatively notable as it affects the pressure drop and separation efficiency predictions by 3.9% and 3% respectively; gas underflow leads to higher separation efficiency and lower pressure drop.

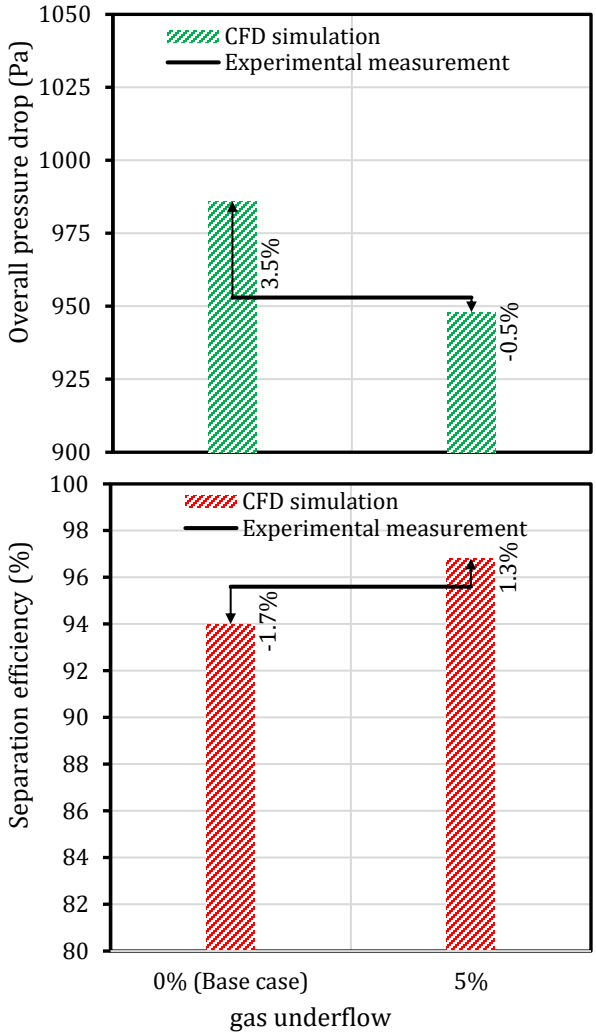

Figure 5-27. Effect of gas underflow on the overall pressure drop and separation efficiency. Arrows and corresponding percentages show the difference between CFD simulation and experimental measurement.

5.6 Conclusions

In the present study, sensitivity analyses of sub-models, model parameters, and numerical parameters on a hybrid multiphase model coupled with an agglomeration model developed for the simulation of industrial highly loaded cyclones were performed. Different options for particle-particle interaction modeling (based on KTGF), several turbulence models, and several drag models (five homogeneous drag models and three heterogeneous drag models) were examined. Additionally, the particle-particle restitution coefficient (that affects particle agglomeration), and particle-wall rebound coefficient were studied. Several numerical

parameters/schemes were investigated in this work, including the discretization method, grain-to-particle size ratio, grid-to-parcel size ratio, and time step size. In addition, the effect of operating conditions including solid loading, PSD, and gas underflow were examined. We believe that the results of this study provide some guidelines that are valuable for future CFD simulations on large-scale cyclones with high solid loadings.

The following points are drawn from the present study as the main conclusions:

- Regarding sub-models, turbulence modeling is the most crucial one. Including curvature correction term to sensitize the turbulence model for rotation is vital. The sst version of the k-ω turbulence model provides the most reliable predictions that captures the important trend of improvement in separation efficiency when the solid load is increased. The realizable and standard version of the k-ε model and the standard version of the k-ω model are not able to predict the separation efficiency accurately. Although the RNG version of the k-ε model provides more or less reasonable predictions, it is unable to capture the trend of improvement in separation efficiency when the solid load is increased.
- Particle-particle interaction force modeling is not crucial and can be excluded to speed up calculations
- Particle rotation, Saffman force, Magnus force, and particle turbulent dispersion can be excluded from the calculation as their impact is minor
- Although the effect of drag modeling is minor compared to turbulence modeling or particle-particle restitution coefficient, Igci and Sarkar drag models provided the best predictions.
- Regarding model parameters, the particle-particle restitution coefficient (directly affecting the extent of agglomeration) is the most crucial one.
- Although the particle-particle restitution coefficient affects both separation efficiency and pressure drop in the whole range, only the separation efficiency is sensitive to the particle-wall rebound coefficient just in the range of 0.8-1.
- The time step corresponding to a courant number of 300 is the largest (the fastest) time step providing independent results.
- Parcel size can be enlarged to the limit that the solution has no convergence issue without affecting the predictions. It seems that (at least in the present case and mesh) having 0.2% of cells being smaller than the parcel size is fine.
- 2nd order discretization scheme is essential to have sufficiently accurate predictions.
- The finer the mean particle size and the higher the solid load, the more significant the effect of particle agglomeration.
- Considering that different combinations of drag models and particle-particle restitution coefficients provide reasonable predictions of pressure drop and separation efficiency, LDA measurement providing flow patterns in a highly loaded cyclone is needed for further evaluation of drag models.

6 CFD simulation of a non-isothermal industrial cyclone preheater

This chapter is a reprint of the manuscript "CFD simulation and experimental validation of multiphase flow in industrial cyclone preheaters" which has been submitted for publication [213].

6.1 Abstract

A hybrid multiphase model (Dense Discrete Phase Model, DDPM) coupled with a k-ω sst turbulence model, which includes gas-solid heat exchange was developed for the simulation of industrial-scale cyclone preheaters operating under high solid loadings. The model results are validated by experimental measurements from an industrial cyclone preheater with a diameter of 1.6 m, with respect to the pressure drop, gas and particle exit temperature, local gas velocity profiles, measured using the LDA, and gas temperature profiles, measured using thermocouple and FTIR. Reasonable agreement between the data from experiments and simulations was obtained. In addition, the major trends, such as changes in the pressure drop, overall heat transfer rate, and flow pattern, caused by the changes in the operating parameters can be captured accurately by the model.

6.2 Introduction

Cyclones, primarily utilized for particle separation, are often used in high-temperature processes. In addition to their straightforward design and affordability, their ability to adapt to high-temperature conditions, especially over 900˚C, make cyclones the most applied gas-particle separator in high-temperature processes [62]. Drying, decarburization, solidification, coal pyrolysis, gasification, combustion of solid fuels, and fluid catalytic cracking applications are some of the high-temperature processes where cyclone units play a critical role [3]. Cyclones are also commonly used as heat exchangers (cyclone preheaters) mostly in order to preheat solid material to improve the energy efficiency of high-temperature processes. Cyclone preheaters are key components in several processes such as cement production [2–5] and stone wool production [6,7] and are mostly operated at high solid loads (dense gas-solid flow).

CFD simulation of cyclone preheaters (or in general cyclones operating at elevated temperatures) have been reported in the literature including different levels of coupling of particle and gas phases and resolution: single-phase calculation [117,214], one-way coupling [12], two-way coupling [2,4], and four-way coupling [26,27,58,97].

Considering that in cyclones, particles are mostly concentrated close to the walls, in the case of highly loaded cyclones, particle-particle interactions might play a significant role in the hydrodynamics of multiphase flow. Therefore a four-way coupling method should be considered [9–11,27,28,51,55,66,74,103,104]. However, conventional four-way coupling models namely the Discrete Element Method (DEM) model and the Eulerian–Eulerian model might not be suitable options. DEM is too expensive to be implemented in industrial-scale simulations, and the Eulerian–Eulerian model cannot easily handle the polydispersity of particles which is quite crucial in the performance of cyclones. On the other hand, a more novel hybrid multiphase model, the Dense Discrete Phase Model, that has been successfully validated for the simulation of hydrodynamics of multiphase flow in a highly loaded large-scale cyclone in our previous work [158,190] (presented in Chapters 4 and 5) is a promising and feasible model.

In general, the existing experimental studies of cyclones operating at high temperatures, particularly in the case of highly loaded cyclone preheaters are limited to overall measurements of pressure drop, separation efficiency and temperature changes over the whole cyclone system in lab-scale devices. Local measurements of velocity or temperature profiles in highly loaded cyclones are missing in the literature, to the best of the authors' knowledge, even in lab-scale geometries or ambient temperatures let alone in industrial cyclone preheaters. In the case of industrial cyclone preheaters which is the focus of the present study, even the overall measurements are limited.

In the limited existing experimental studies, in the case of cyclones at high temperatures, a reduction in both the pressure drop and separation efficiency has been reported when gas temperature is elevated (at a fixed volumetric gas-flow rate) [118,119]. In the case of cyclone preheaters, the overall heat transfer rate is reported to increase with increasing solid and gas flow rates, and decreasing particle size [215,216]. The improvement with the increase in the solid flow rate is attributed to the reduction in the amount of gas bypassed to the vortex finder due to the reduced radial gas velocity observed when the solid load is increased. On the other hand, the improvement with an increase in the gas flow rate is explained by the increased driving factor for gas-solid heat exchange which is due to the greater availability of hot gas to transfer heat to the particles. Although the heat transfer coefficient is reduced with the decrease in the particle size, the improvement in the heat transfer rate is due to the increase in the gas-particle heat exchange surface area. Correlations for the prediction of the overall heat transfer coefficient in cyclone preheaters are reported in the limited experimental studies in lab-scale cyclone preheaters [215,216].

Regarding the limited availability of the experimental data, to obtain the lacking knowledge to bridge the gaps of understanding of what is happening inside cyclone preheaters, a CFD model with detailed validation of flow and temperature distribution, to be utilized with confident for simulation of highly loaded industrial cyclone preheaters is missing. To simulate highly loaded industrial cyclone preheaters, gas, solid, and gas-solid heat transfer modeling need to be added to the model developed for the simulation of hydrodynamics of multiphase flow presented in Chapters 4 and 5.

The main objective of the present work is to suggest a CFD model for the simulation of highly loaded industrial cyclone preheaters with detailed validation to improve understanding of gas-solid separation and heat transfer in this kind of device. For this purpose, gas-particle heat transfer modeling has been incorporated into a hybrid Eulerian–Lagrangian multiphase model (DDPM) coupled with a dispersed

version of the k-ω sst turbulence model sensitized for flow rotation for simulation of the present cyclone preheater. The simulations are performed using Ansys Fluent 2021R1 and were validated by measurements of pressure drop, gas exit temperature, heat transfer rate, and also local flow and temperature patterns conducted under several operating conditions. The local measurements were provided by conducting water-cooled probe measurements on an industrial cyclone preheater with a diameter of 1.6 m. This validation assesses the credibility and accuracy of the proposed model.

6.3 Experimental study for model validation

6.3.1 Case description

Experiments were performed in an industrial cyclone preheater with a diameter of 1.6 m for validation of the CFD model, which is a part of the Integrated Melting Furnace (IMF) system [6], operated by Rockwool A/S. The IMF system melts mineral solid feed and then converts melted material into mineral wool and eventually insulation material. In the IMF system, there are two cyclone preheaters in cascade configuration and the top one is studied in the present work. A 3D view of the studied cyclone preheater is illustrated in Figure 6-1. The experiments were done at various operating conditions (i.e., various particle feed loads, gas flow rates, and gas inlet temperatures). There are four main components in this system: the main cyclone body (4), the dust bin (6), the riser (3), and the particle feeding pipe (2). Mineral particles are injected into the riser, where they are carried up to the cyclone by the upward flow of the gas stream.

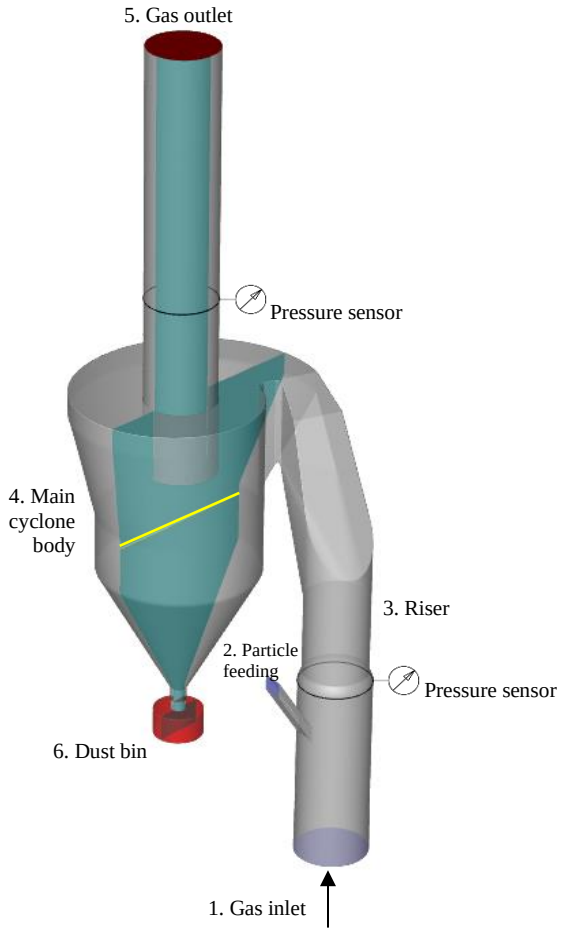

Figure 6-1. A 3D view of the geometry of the cyclone. The locations of pressure taps for measuring static pressure drop are shown. The cyan plane and yellow line are the plane of contours and line of profiles in the results and discussion section.

A PSD (Particles Size Distribution) of particles used during the experiments is obtained from sieving analysis and is presented in Figure 6-2. The particles had a Sauter mean diameter of 375 µm with an approximate density of 2700 kg/m^3, which is classified as a Geldart B type of particle, based on Geldart's particle classification [120]. The particles are a mixture of natural rock materials [6]. Two slightly different mixtures of natural rock materials were used throughout the experiments (the composition was slightly changed due to the company production line demand). The two

types of materials were tested in a DSC (NETZSCH model STA 449) and show slightly different heat capacities, which are presented in Figure 6-3.

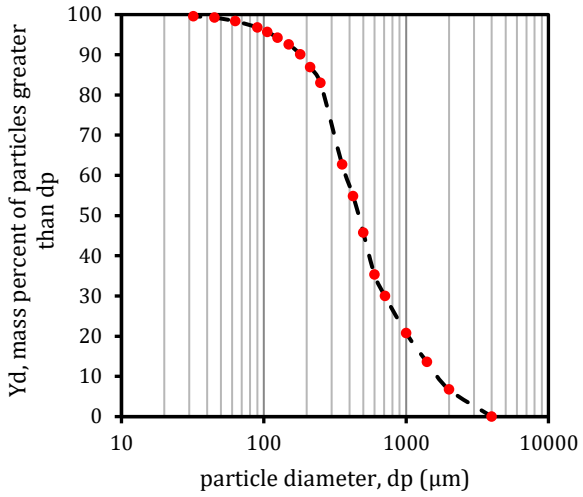

Figure 6-2. PSD of the natural rock materials used during the measurement campaigns by sieving analysis. This PSD is measured for Rock material 1; Rock material 2 has a similar PSD.

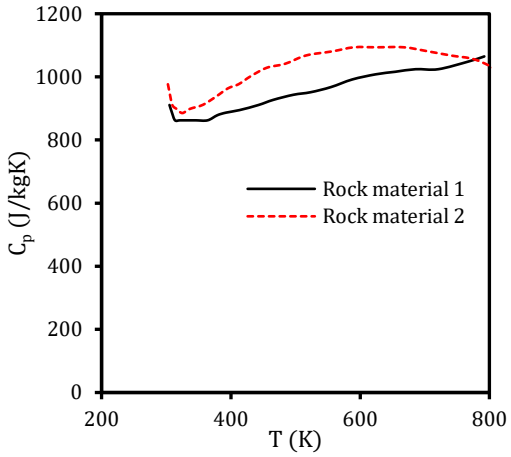

Figure 6-3. Comparison of the specific heat capacity of the two mixtures used in campaigns as a function of temperature measured by an STA (NETZSCH model STA 449).

The experiments were conducted at 10 different operating conditions with varied gas and solid flow rates and slightly different gas inlet temperatures to provide validation data for the CFD study. Table 6-1 summarizes the operating conditions (gas and solid flow rates, and gas and solid inlet temperatures), and types of measurements conducted in these 10 cases.

Table 6-1. Operating conditions of conducted tests. The cases are named in a way to present the main operating conditions of the case (e.g., in Case-1 G5.9-S3.2-T960, gas flow rate, solid flow rate, and gas inlet temperature are 5.9 kg/s, 3.2 kg/s, and 960 K respectively).

Parameter	**Case-1 G5.9-S3.2-T960**	**Case-2 G6.1-S3.1-T971**	**Case-3 G6.6-S2.9-T974**	**Case-4 G7.0-S2.9-T975**	**Case-5 G6.3-S2.9-T969**	**Case-6 G6.8-S2.9-T991**	**Case-7 G7.2-S2.9-T999**	**Case-8 G6.8-S3.4-T975**	**Case-9 G5.8-S3.3-T1035**	**Case-10 G5.3-S3.2-T1040**
Measurement	LDA (velocity profile)	LDA (velocity profile)	LDA (velocity profile)	Temperature profile	No local measurement	No local measurement	No local measurement	No local measurement	LDA (velocity profile)	Temperature profile
Gas flow rate, (kg/s)	5.9	6.1	6.6	7	6.3	6.8	7.2	6.8	5.8	5.3
Solid flow rate, (kg/s)	3.2	3.1	2.9	2.9	2.9	2.9	2.9	3.4	3.3	3.2
Solid loading ratio, (kg solid / kg air)	0.5	0.5	0.4	0.4	0.5	0.4	0.4	0.5	0.6	0.6
Gas inlet Temperature (K)	960	971	974	975	969	991	999	975	1035	1040
Particle inlet Temperature (K)	298									
Particle	Rock material 1								Rock material 2	
Pressure drop										
Gas and particle exit temperature										

The experimental data in the present study can be categorized into two groups: plant operation data and data from measuring campaigns.

6.3.2 Plant operation data

Plant operation data includes online measurements of pressure drop (difference measured by two plant's pressure sensors shown in Figure 6-1), gas inlet and exit temperature and particle exit temperature (using a thermocouple in a pile of particles accumulated in the dust bin). Furthermore, gas and solid flow rates are measured online.

6.3.3 Data from measuring campaigns

Flow pattern measurements and temperature profile measurements were conducted in measuring campaigns. Details of these measurements are presented as follows:

6.3.3.1 Flow pattern measurements

A fiber optic laser Doppler anemometer (LDA) system with a BSA processor (series F60) from Dantec Dynamics was used to perform 2D velocity measurements to provide axial and tangential velocity profiles in the cyclone main body (along the yellow line in Figure 6-1). A commercial (Dantec Dynamics) 2D fiber optic LDA head mounted in a water-cooled probe with a protection window that can be inserted through the measurement port for mapping flow profiles was used in the present study [217]. The LDA head had a diameter of 27 mm diameter and a focal length of 160 mm. The LDA head was connected to a transmitter unit with a fiber-optic cable. The transmitter unit was a Dantec model 60X41 using a 300-mW air-cooled argon-ion laser (Stellar-Pro-L Select 300). Data was typically collected over 60-120 s for each measurement point using BSA processor series F60.

The LDA head is sensitive to temperature and damage to the optical lens. As Dantec recommends keeping the temperature of the LDA head below 45°C, i.e., water-cooling was required for measurements inside the hot cyclone. Furthermore, in the studied cyclone preheater with fast-moving large particles, the fragile coated lens of the LDA head must be protected against erosion from particles moving towards the LDA optics during measurements. A tilted quartz window with a diameter of 25 mm and thickness of 3 mm was used as a protection window in front of the LDA head. Furthermore, a minor purge flow is used to avoid penetration of small gas-borne particles into the probe.

The gas velocity can be approximated by the LDA particle velocities measured. The LDA measurement volume dimensions in the present setup are 0.074 mm in diameter and 1.57 mm long at 488 nm wavelength, with a fringe spacing of 5.2 µm and a total volume of approximately 0.007 mm^3. The number of detected particles per mm^3 is approximately 2 for an LDA data rate of 5 kHz and a velocity of 20 m/s, i.e., LDA signals in the cyclone are mainly generated by many fine particles that follow the gas flow. The data rate was fairly constant across the 1.6 m diameter of the cyclone which confirms that large particles contribute very little statistically to the obtained data. Thus, the gas velocity can be approximated well by the LDA particle velocities measured. High sampling rates were obtained in all positions across the cyclone, indicating that LDA signals mainly come from high-concentration fine particles.

As with any industrial-scale measurement, flow access and maintaining steady operation represent major challenges in this work rather than the operation of the LDA system under industrial conditions. Repeated LDA velocity measurements for 60-120 s give the same result under stable operating conditions of the

preheater cyclone. However, it was difficult to control fully the operation conditions over time for a complex industrial production facility.

6.3.3.2 Temperature profile measurements

Two types of measurements were done to provide a gas temperature profile in the cyclone main body (along the yellow line in Figure 6-1): Thermocouple measurement and FTIR measurement.

6.3.3.2.1 Thermocouple measurement

Thermocouple measurements were performed with a 3.0 mm diameter thermocouple of type N (Nickel-alloy thermocouple) connected to an Agilent data acquisition/data logger switch unit (Agilent 34970A). The thermocouple was mounted in a probe made of a stainless-steel tube and Swagelok fittings at the tip for a gas-tight seal. The inner part of the probe was filled with insulation material to avoid airflow movements inside the tube.

6.3.3.2.2 FTIR measurement

In FTIR measurement (infrared IR fiber-optic spectroscopic method [34]) the local gas temperature in front of the probe tip was extracted from the measured FTIR thermal emission spectrum; it can be found from FTIR thermal emission from CO_2 at around 2350 cm^{-1} by scaling with Planckian curve. Details of the developed system can be found in the literature [218,219]. A portable blackbody was used for calibration before and after the cyclone measurements to capture any problems with unstable measurements due to dirt or particles on optics. Measurements at each point were in general made over several minutes. Data were analyzed and oscillations with a period of 5.4 s of the gas temperature were clearly seen in the FTIR measurements and weakly in thermocouple measurements due to the slow response time.

Preliminary measurements showed that an uncooled probe should be used instead of a water-cooled one as water-cooling offsets temperature measurements. It should be noted that the two methods provided similar average gas temperatures.

6.4 Model description

In the present work, a hybrid Eulerian–Lagrangian multiphase model, Dense Discrete Phase Model (DDPM) in Ansys Fluent 2021R1 solver coupled with a dispersed version of the k-ω sst turbulence model sensitized to rotation and curvature is used. This model was successfully validated for the simulation of hydrodynamics of a highly loaded large-scale cyclone in Chapters 4 and 5. It was found that the revised Sarkar drag model [138] provides slightly better predictions of important performance parameters of highly loaded large-scale cyclones. Therefore, this drag model is also used in the present work. Unlike the case in Chapters 4 and 5, the particles in the present case are relatively large such that the agglomeration does not play a role and therefore is excluded in this study.

A PDE (Partial Differential Equation) for energy conservation equation is added on top of six PDEs for multiphase and turbulence modeling in the Eulerian framework for gas phase calculation for modeling the gas-solid heat transfer. A term for the heat exchange between gas and particle appears in the energy conservation equation in the Eulerian phase (gas phase) calculation as follows:

$$Q_{p-g} = h_{p-g} A_p (T_p - T_g) \quad 6\text{–}1$$

where h_{p-g} is the heat transfer coefficient between the gas and particle and is modeled in the present work by Ranz-Marshall correlation by assuming iso-thermal particles in the system.

$$Nu_p = \frac{h_{p-g} d_p}{\lambda_g} = 2 + 0.6 Re^{1/2} Pr^{1/3} \quad 6\text{–}2$$

While a simple heat balance is used in the Lagrangian (particle) calculation to update particle temperature as follows:

$$m_p C_p \frac{dT_p}{dt} = h_{p-g} A_p (T_g - T_p) \quad 6\text{–}3$$

6.4.1 The necessity to have one solid phase for each particle size class

Preliminary simulations showed that in the way the energy conservation equation and gas-particle heat exchange is implemented in the DDPM multiphase model in Ansys Fluent 2021R1, in cases with poly-dispersed particles, to have energy balance in the system, a specific procedure must be implemented. The procedure is to have one exclusive solid phase assigned for each particle size class present in the system. For example, if four particle sizes of 200, 250, 750, and 3000 µm are present in the system, four solid/dispersed phases are needed each to be assigned to one of the size classes to have an overall closed energy balance in the system. While if only one solid phase is used, a huge energy imbalance will be observed as shown in Figure 6-4‡.

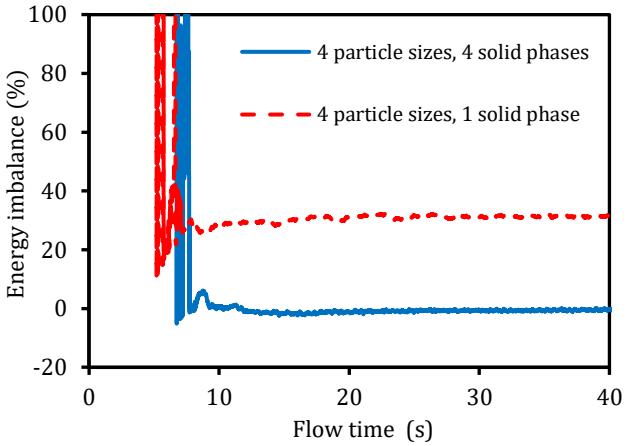

Figure 6-4. Comparison of the extent of energy imbalance in the DDPM model in a case including 4 particle sizes with and without assigning each particle size one exclusive solid phase. The comparison presented here was done for the present cyclone preheater system under the operating of Case-1 (G5.9-S3.2-T960).

6.4.2 The effect of polydispersity of particles

To achieve energy balance in the system, one exclusive solid phase is needed for each particle class included in the model in DDPM, as discussed. On the other hand, a greater number of solid phases results in heavier and more expensive numerical calculations. Therefore, it is important to find the minimum number of

‡ The procedure presented here provides energy balance in the case of relatively coarse particles of the case studied in the present chapter. However, in the case of fine particles present in the cement industry (the case investigated in Chapters 4 and 5) this procedure turned out to be insufficient. Up to version 2022R1, Ansys Fluent had only one option to model the gas-particle heat exchange. Since this approach would cause the mentioned energy imbalance in cases with fine particles, in Ansys Fluent 2022R2, a new feature was introduced to resolve the issue. The results obtained from this new feature and how it resolves the issue in the case of fine particles are presented in Appendix D.

particle sizes required to adequately represent the actual PSD in the studied case. For this purpose, a study was designed where a various number of particle sizes were considered in different cases (from 1 to 7 particle sizes), all cases having the same Sauter mean diameter as the actual PSD (375 µm), to be compared and find the minimum number of particle sizes needed to provide similar results as the case with 7 particles sizes, which is the maximum number feasible in our computational resources. The 7 cases are summarized in Table 6-2.

Table 6-2. Summary of seven simulation cases designed for the study of the effect of particle polydispersity

Case name	Number of particle sizes	Particle sizes (µm)	Mass fraction	Sauter mean diameter (µm)
Polydispersity-Case-1	1	375	1	375
Polydispersity-Case-2	2	250	1/2	375
		750	1/2	
Polydispersity-Case-3	3	250	1/3	375
		375	1/3	
		750	1/3	
Polydispersity-Case-4	4	200	1/4	375
		250	1/4	
		750	1/4	
		3000	1/4	
Polydispersity-Case-5	5	200	1/5	375
		250	1/5	
		375	1/5	
		750	1/5	
		3000	1/5	
Polydispersity-Case-6	6	200	1/6	375
		250	1/6	
		300	1/6	
		500	1/6	
		750	1/6	
		3000	1/6	
Polydispersity-Case-7	7	200	1/7	375
		250	1/7	
		300	1/7	
		375	1/7	
		500	1/7	
		750	1/7	
		3000	1/7	

Pressure drop and gas exit temperature predictions were taken as two performance parameters of the cyclone preheater. The comparative results are presented in Figure 6-5. In addition, the results of velocity and temperature profiles are also shown in Figure 6-6. The comparison shows that even with one particle size (Polydispersity-Case-1), more or less, similar predictions can be achieved (in particular for pressure drop, gas exit temperature and velocity profiles). However, four particle sizes should be included (Polydispersity-Case-4) to minimize the difference in predictions from the most expensive case (Polydispersity-Case-7), in particular considering temperature distributions. This means that four particle sizes are sufficient in this study to cover the actual PSD. Therefore, for the rest of the simulations, 4 particle sizes were used (Polydispersity-Case-4).

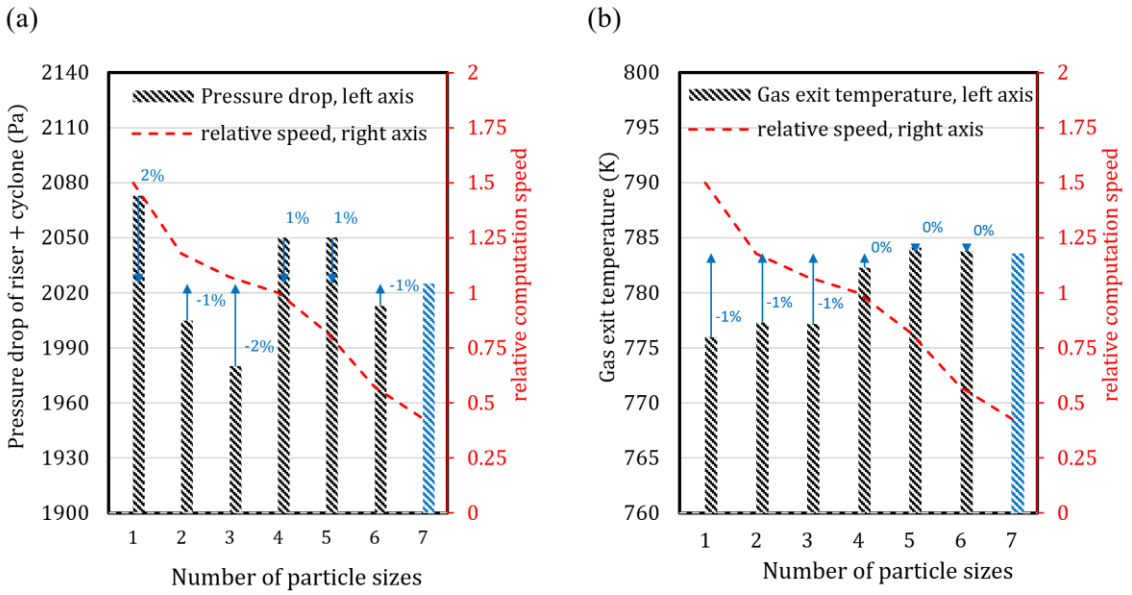

Figure 6-5. Comparison of (a) pressure drop, and (b) gas exit temperature in seven simulation cases designed for the study of the effect of particle polydispersity. The relative computation speed is also presented for each case. Presented deviations in % are based on a comparison with case 7 particle sizes (Polydispersity-Case-7).

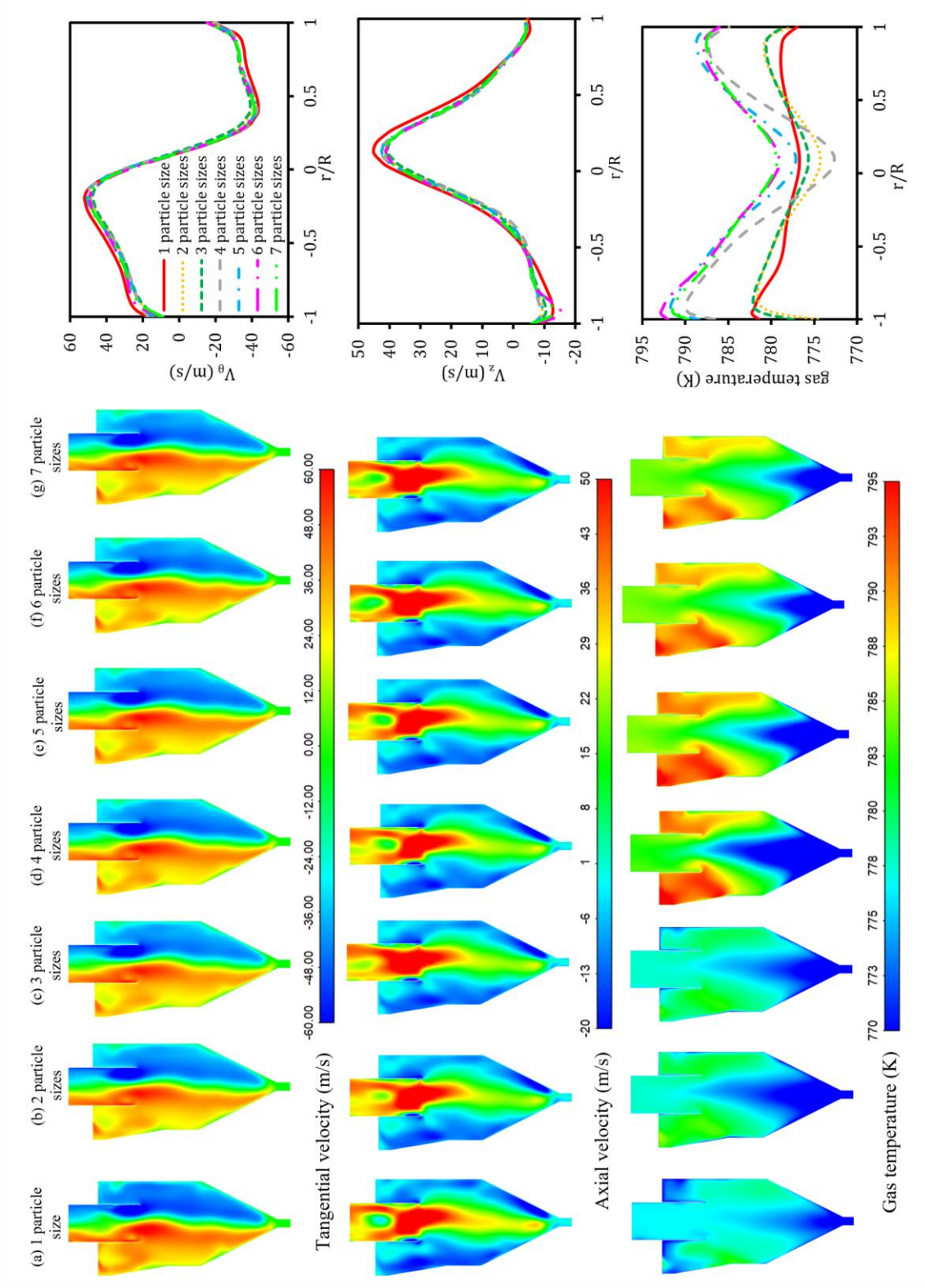

Figure 6-6. Comparison of axial and tangential velocity and gas temperature distribution in seven simulation cases designed for the study of the effect of particle polydispersity.

Table 6-3 summarizes the parameters used in the simulation. It should be mentioned that the raw material used during the experiments contains approximately 5.5 [wt.%] of moisture. In the preliminary simulations, the heating up and eventually evaporation of the moisture was included in the simulation using the wet combustion model available in Ansys Fluent 2021R1. As presented in Figure 6-7 obtained from the preliminary simulation, the water content is immediately evaporated when the particles and hot gas get in contact, such that particles entering the cyclone are totally

Table 6-3. Summary of simulation conditions

Parcel mass	5 mg, achieved from a sensitivity analysis the coarse-graining strategy was to have the same parcel mass for different particle sizes
Time step	Courant number of 300 (3 ms), achieved from a sensitivity analysis
grid	Level 3 (810 000 cells), achieved from a sensitivity analysis
Gas mixture (mass fraction)	N_2 (0.53), H_2O (0.23), CO_2 (0.13), O_2 (0.10), CO (0.01)
Gas density	Incompressible ideal gas (gas mixture with a molecular weight of 28.1 kg/kmol
Gas specific heat	A 5^{th}-order polynomial function of temperature for the gas mixture
Gas thermal conductivity	A 2^{nd}-order polynomial function of temperature for the gas mixture
Gas viscosity	A 3^{rd}-order polynomial function of temperature for the gas mixture
Particle density	2700 kg/m^3
Particle specific heat	7^{th} order polynomial function of temperature for Rock material 1 and 2
Number of particle sizes	4
Particle sizes included (mass fraction)	200 µm (1/4), 250 µm (1/4), 750 µm (1/4), 3000 µm (1/4)
Particle-particle restitution coefficient	0.7
Wall heat loss	conductive heat loss through a wall with 0.22 m thickness and thermal conductivity of 0.56 W/m.K and convective heat loss with room atmosphere with a heat transfer coefficient of 20 W/m2.K and temperature of 293 K
Particle-wall restitution coefficient (normal and tangent)	0.8

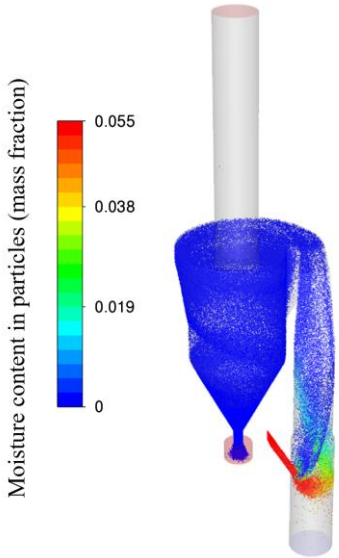

Figure 6-7. A snapshot of particles colored with moisture content obtained from preliminary simulation using wet combustion modeling

Therefore, to keep the model simple and applicable for all common cyclone preheaters operating in industries (which might not have evaporation in general), and to keep the model computationally cheap, water evaporation modeling was excluded from the calculation for the rest of the simulations. This is done by assuming that drying has already happened before particle injection. In the simulations, the energy required for this evaporation is deducted from the gas inlet energy. This deduction appears in terms of reduction in the gas temperature at the gas inlet (the temperature reported in Table 4-1 as operating conditions are reduced temperatures. Also, this 5.5 [wt.%] of moisture is deducted from the solid flow and added to the gas flow). In addition, based on the overall energy balance of the system it can be observed that 7 [wt.%] of the gas flow rate reported in Table 4-1, is false air with ambient temperature entering the system through the gaps in the system. The effect of this cold false air is also considered to modify gas inlet temperature reported in Table 4-1. It should be noted that these 5.5 [wt.%] of water content in particles and 7 [wt.%] of cold false air are uncertain and approximate assumptions.

6.5 Results and discussion

6.5.1 Mesh independency

A mesh independence study was carried out for Case-1, using five levels of mesh resolution (polyhedral mesh with prism layers). Table 4-4 provides some information about these five levels of mesh, including the average cell volume, the grid resolution, and the grid-to-parcel size ratio for each level. Since the value of $\sqrt[3]{\overline{V_{cell}}}/\overline{d_p}$ is in the order of 10^2, then it is considered a coarse-grid simulation [96].

Table 6-4. Information on levels of grids in mesh independence study. Level 3 is used for the rest of the simulations.

Grid	Number of cells (million)	$\overline{V_{cell}} = Average\ of\ cell\ volume$ (m^3)	$\sqrt[3]{\overline{V_{cell}}}/\overline{d_p}^*$ grid dimensionless resolution	$\overline{V_{cell}}/(parcel\ volume)$ grid to parcel size ratio
Level 5	0.5	5.5×10^{-5}	102	29847
Level 4	0.6	4.4×10^{-5}	94	23760
Level 3	**0.8**	$\mathbf{3.1\times10^{-5}}$	**84**	**16906**
Level 2	1.0	2.4×10^{-5}	77	12880
Level 1	1.3	1.6×10^{-5}	68	8771

* $\overline{d_p}$ is the Sauter mean diameter of particles and equals 375×10^{-6} m

A comparison of predicted pressure drop and gas exit temperature with different levels of grid resolution is presented in Figure 6-8. The results show that the predictions did not deviate substantially from the prediction of the finest mesh, even for mesh level 5. Furthermore, the comparison of flow pattern and gas temperature distributions in the five levels of mesh is presented in Figure 6-9. Again, the predictions were not noticeably different from the prediction of the finest mesh when 0.8 million cells or finer was employed (in particular regarding the gas temperature profile), which indicates that predicted results were fairly independent of mesh size when at least 810 thousand computation cells were used, therefore grids with 0.8 million computation cells (Level 3 grid in Table 4-4) is used for the rest of simulations. If coarser grids (0.5 and 0.6 million cells) are used minor changes, in particular, in temperature distributions can be observed.

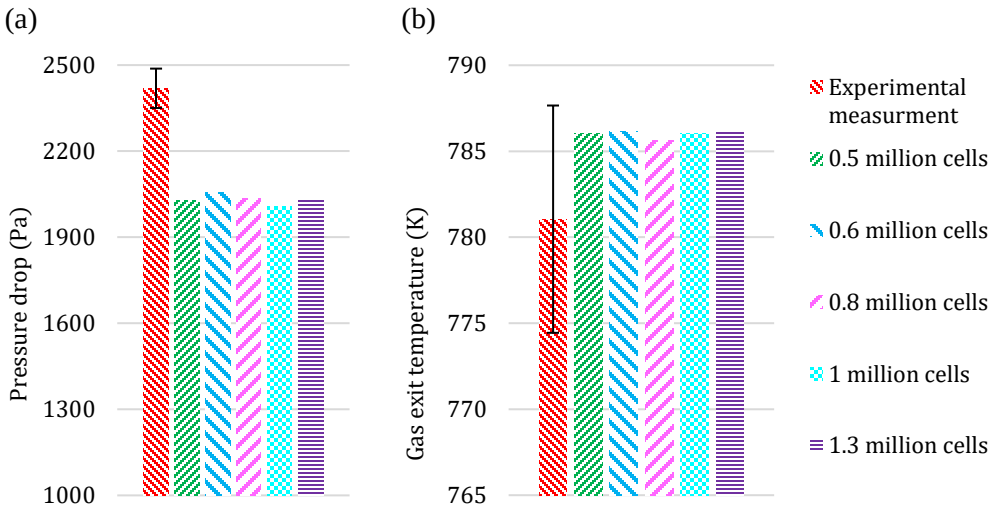

Figure 6-8. Comparison of predicated (a) pressure drop and (b) gas exit temperature obtained from five levels of mesh for case-1 operating condition

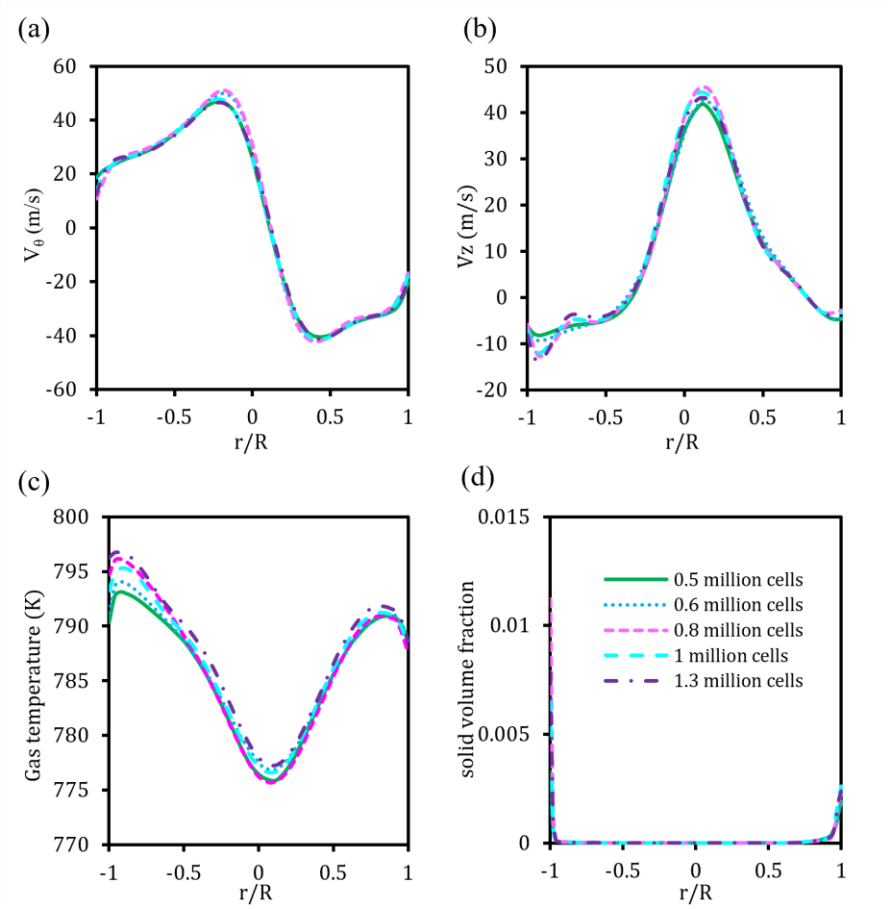

Figure 6-9. Comparison of (a) tangential velocity, (b) axial velocity, (c) gas temperature, and (d) solid volume fraction distributions in five levels of mesh for Case-1.

In addition, Table 6-5 contains convergence calculations for the three finest grid levels using the approach suggested by Roache [185,186] to analyze grid convergence and grid resolution error [184]. With α near unity as reported in Table 4-4, the solution falls within asymptotic convergence. Also, Richardson

extrapolation [7] can be used to estimate values when grid spacing disappears (f_0) with an error band (e.g., the pressure drop is estimated to be 2086 Pa with an error band of 3.338%).

Table 6-5. Grid convergence calculations using the GCI method [185,186] for the three finest grid levels. $i = 0$ is the value at zero grid space

	i	NC_i ($\# \times 10^6$)	f_i	$rg_{i,i+1}$	$eg_{i,i+1}$	$\varepsilon g_{i,i+1}$	$GCI_{i,i+1}^{fine}$ %	Rg	αg
Pressure drop (Pa)	0		2086						
	1	1.33	2032						
				1.099	-26	-0.013	3.338		
	2	1.00	2006						
				1.075	28	0.014	5.001	-0.917	0.987
	3	0.8	2034						
Gas outlet temperature (K)	0		786.2						
	1	7.5	786.2						
				1.099	-0.1	-0.0001	0.003		
	2	5.5	786.1						
				1.075	-0.4	-0.0005	0.019	0.250	0.999
	3	4.2	785.7						

6.5.2 Parcel size independency study

The coarse-graining strategy used in this study was to have the same parcel size (same parcel mass) for different particle sizes. According to preliminary simulations, the presence of too large parcels leads to variations in heat transfer calculations (e.g., gas exit temperature) and a loss of overall energy balance and therefore must be avoided. So, a study was carried out to find the largest parcel size (fastest calculation) providing overall energy balance (up to 1% energy imbalance is considered acceptable) and parcel-independent predictions. For this purpose, six parcel sizes of 1.25, 2.5, 5, 10, 20 and 100 mg, were tested. The gas exit temperature was compared in these cases as a measure of heat transfer calculations, shown in Figure 6-10. It was concluded that 5 mg or finer parcels were required. Since finer parcels will result in more expensive calculations without affecting the predictions, 5 mg parcels were used for the rest of the simulations It is worth mentioning that the pressure drop as another performance parameter of a cyclone preheater was not sensitive to the parcel size in the studied range.

In addition, a time step independence study was done; Six Courant numbers of 100, 200, 300, 400, 800, and 1600 equivalent to 1, 2, 3, 4, 8, and 16 milliseconds respectively were examined. It was demonstrated that the results were independent of time step size over the investigated range.

The findings of this study were obtained from the parcel size of 5 mg and the courant number of 300 resulting in around 3 million parcels in the domain and a time step size of 3×10^{-3} s upon achieving a steady-state solution. An Intel(R) Xeon(R) Gold 6226R with 32 processors at 2.90 GHz and with 64 GB of RAM were used with a high-speed InfiniBand network connection to perform simulations. Using the solution-independent mesh, parcel size, and time step, it took less than 2 hours to progress 1 second of simulation time. This corresponds to no more than 2.5 days to reach a steady-state solution after around 20-30 seconds of simulation time. Given available computing resources, the developed model can be easily applied and is affordable for industrial-scale cyclone modeling.

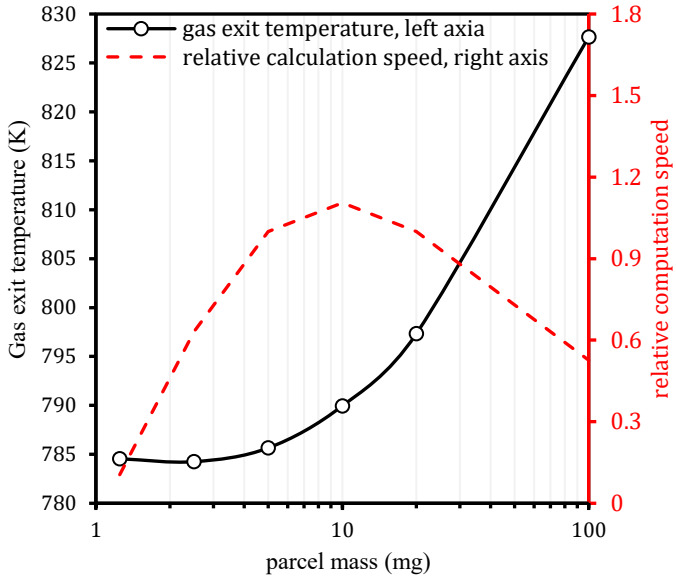

Figure 6-10. Effect of parcel size on the gas exit temperature and relative computation speed. The computation speed of the case with a 5 mg parcel is considered as the reference to report relative computation speeds.

The developed model provides stable solutions that produce reasonable predictions of particle motion, flow pattern, pressure drop, and heat transfer in fairly good agreement with experimental measurements that will be discussed in detail in the following sections. It is worth mentioning that the complexities of an actual industrial cyclone preheater such as potential internal buildups (changing the domain), oscillating operating conditions, etc. make the validation more challenging.

6.5.3 Overview of the multiphase flow

For one of the simulation cases, an overview of the simulation results in the cyclone preheater is shown in Figure 6-11, presenting average contours of gas tangential and axial velocities, gas temperature, solid volume fraction and pressure, in addition to velocity vectors. The predicted flow characteristics are consistent with flow characteristics expected in cyclones, i.e., upward flow in the inner vortex (swirling up), downward flow in the outer vortex (swirling down), and high concentration of particles near the wall (Figure 6-11 (d)). Figure 6-11 (a, f) illustrates the swirling motion expected in cyclones with a radial distribution of tangential velocity, i.e., increasing tangential velocity as moving away from the center up to a wall region where a sharp reduction is observed.

Figure 6-11 (b, f) highlights descending flow near the walls carrying particles concentrated in the near-wall region towards the dust bin and also ascending flow far from the walls, around the center as expected in cyclones. A pressure drop is observed when approaching from the wall to the center (Figure 6-11 (e)), which is a characteristic of swirling motion. Regarding the gas temperature profile in the cyclone, approaching from the wall towards the center, first, a slight increase is observed and then the temperature falls down, reaching its minimum at around the center (Figure 6-11 (c)) that is in line with expectations in the cyclone preheaters [220]. Variation of gas temperature in the cyclone main body is minor as the gas-particle heat exchange occurs mostly in the riser such that gas and particles reach the cyclone at

temperatures relatively close to the equilibrium temperature. On the other hand, a significant variation in gas temperature is observed in the riser where gas-particle heat exchange is happening.

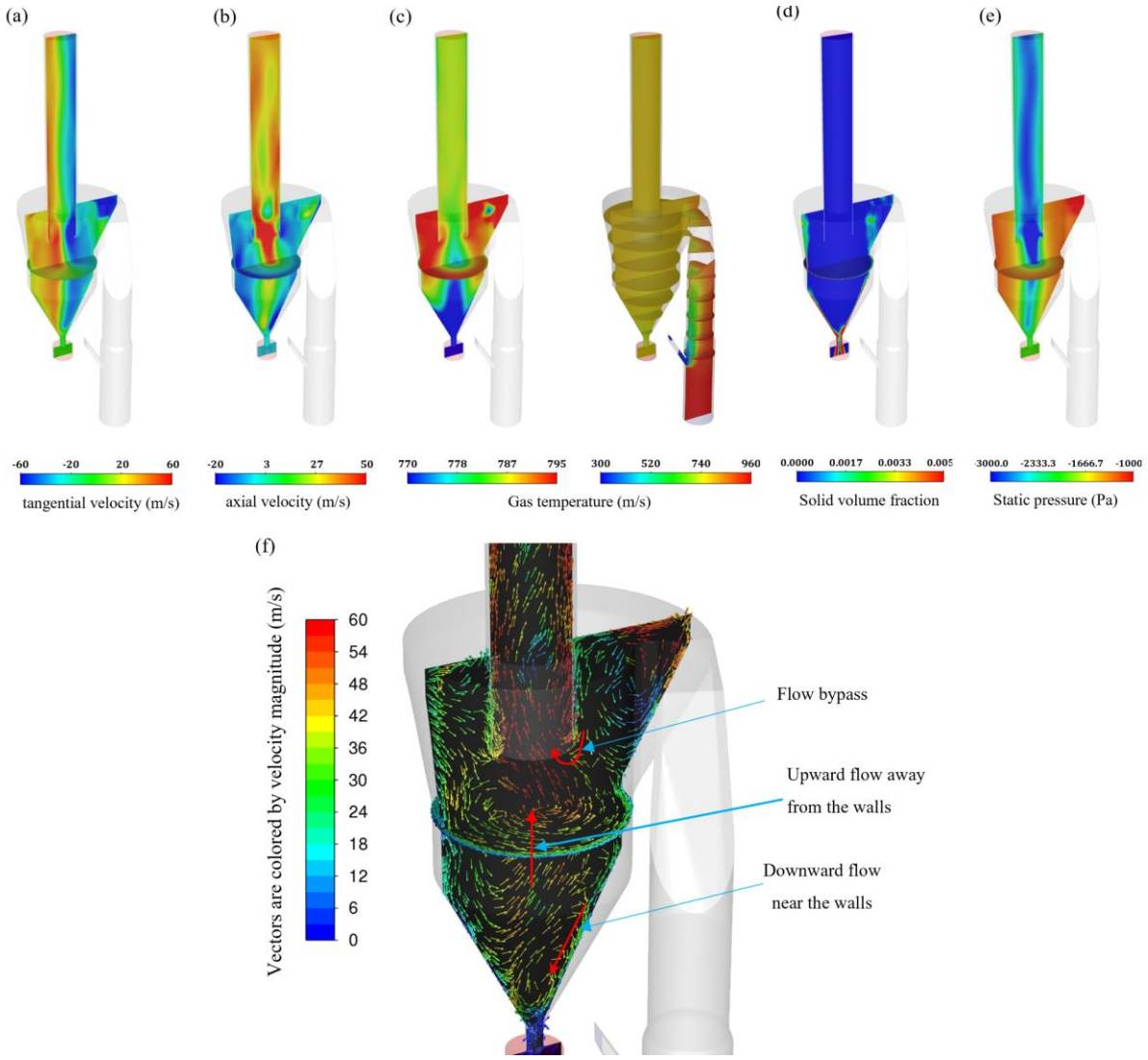

Figure 6-11. Mean (averaged over 5s after achieving steady solution) flow pattern contours in case-1 (G5.9-S3.-T960): tangential velocity (a), axial velocity (b), gas temperature (c), solid volume fraction (d), and static pressure (e), in addition to velocity vectors (f)

In the following sections, the validity of the model in terms of prediction of pressure drop, heat transfer, flow pattern and temperature profile will be presented. It is worth mentioning that the complexities of an actual industrial cyclone preheater such as potential internal buildups (changing the geometry), oscillating operating conditions, etc. make this validation more challenging.

6.5.4 Pressure drop

A comparison between the model predictions and the experimental results, for all cases, is shown in Figure 6-12. The predicted overall pressure drop is in acceptable agreement with experimental data, with the predicted values deviating from experimental measurements in the range of 16-29 %. This general underprediction of the pressure drop might be explained by the fact that the simulated geometry presented

in Figure 6-1, to some level, might be different from the actual geometry; this deviation might be caused by having an unaligned lining of refractory bricks, changes due to wall erosion, etc.

Considering all cases, the model is accurate enough to capture the trends observed in the measurements, i.e., the reduction/increase in the pressure drop when the operating conditions are changed. For example, with case-6 and case-8 having identical gas flow rates, measurements showed a slight reduction in pressure drop as the solid load increased. This reduction is due to the dampening of swirling motion when the solid load is increased [1], and simulations indicated the same (from case-6 to case-8, measurements showed a 3.5% reduction in the pressure drop and CFD simulation predicted a 3.6% reduction). Also, as the gas flow rate is increased comparing cases-5, case-6, and case-7 which have identical solid flow rates, measurements and simulations both exhibit a considerable increase in pressure drop. Gas flowing at a higher rate results in a stronger swirl and more dissipation of flow energy due to higher friction at the walls leading to a greater pressure drop [1]. Overall, experimental measurements indicated that the overall pressure drop responded more to gas flow rate rather than solid flow rate, and this was also observed in the CFD simulations.

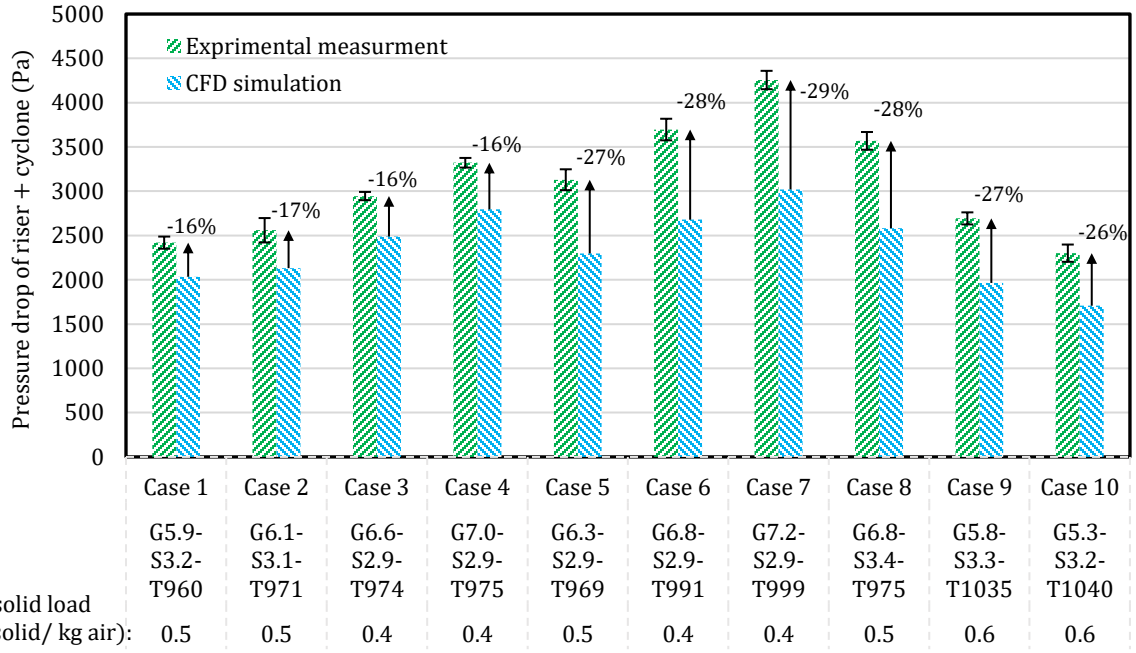

Figure 6-12. Comparison of measured and calculated overall pressure drops. The error bars show the standard deviation, and the percentages are the difference between the calculation and the measurements.

6.5.5 Heat transfer

In evaluating the model performance for heat transfer in the cyclone preheater, the gas exit temperature and heat transfer rate (calculated based on particle temperature changes, $Q = (\text{solid flow rate}).\int_{T_{p,in}}^{T_{p,out}} C_p dT$) are used as the indicator and compared with the experimental data at the applied operating conditions. The results are presented in Figure 6-13 and Figure 6-14. From Figure 6-13 and Figure 6-14, it can be seen that the model is able to simulate heat transfer quite accurately since the predicted values match well with the experimental measurements with deviations not greater than 1.1% and 9% in terms of the gas exit temperature and heat transfer rate, respectively. The observed systematic underprediction of heat transfer

rate can be explained, to some extent, by uncertainty and inaccuracy in assumptions for the amount of water content of particles (5.5 [wt.%]) and the amount of false air (7 [wt.%]).

Similar to the pressure drop predictions, the simulation of heat transfer appears to be sufficiently accurate in reflecting the trends observed in the measurements. According to simulation results, in each pair of the two cases, the temperature at the gas exit and the heat transfer rate are predicted to change in a similar manner as observed in the measurements.

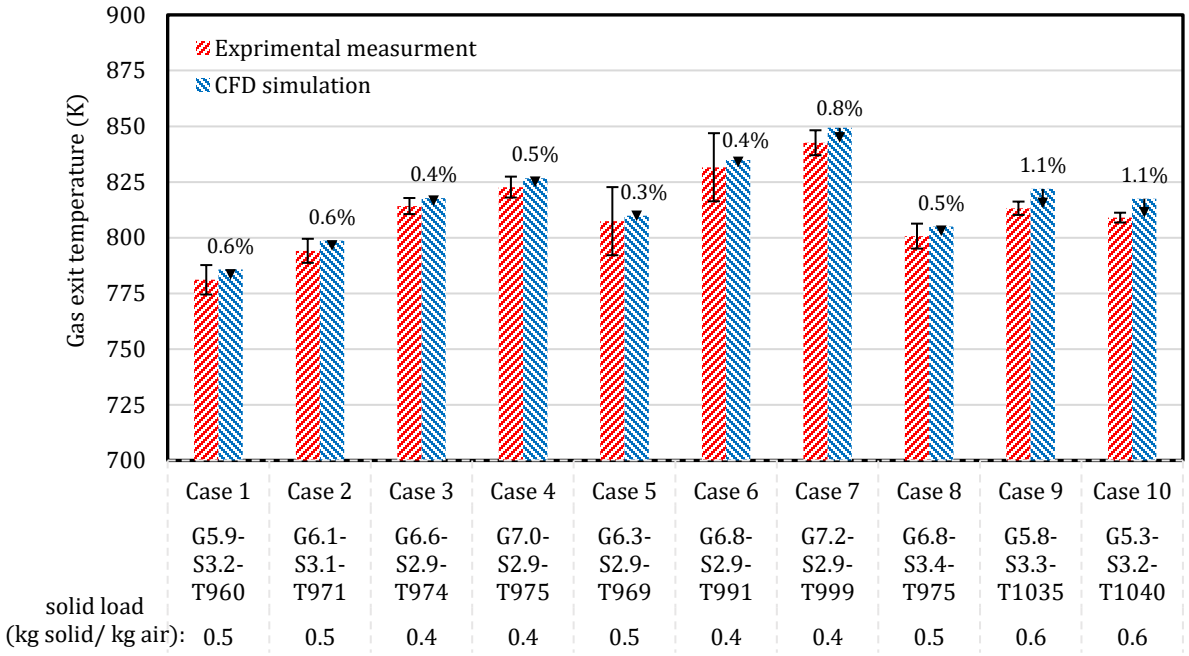

Figure 6-13. Comparison of measured and calculated gas exit temperature. The error bars indicate the standard deviation of the experimental data, and the percentages are the difference between the calculations and the measurements.

Comparing case-6 and case-8, which have identical gas flow rates, measurements showed that the heat transfer rate increased as the solid load increased, and simulations pointed in the same direction as well. Furthermore, both measurements and simulations show an increase in heat transfer rate when the rate of gas flow increases (comparing cases-5, case-6, and case-7 which have identical solid flow rates). In comparison with a general heat exchanger, both observations are intuitive (an increase in the flow rate of each medium leads to an increase in the heat transfer rate).

The heating up of particles in the cyclone preheater can be seen in snapshots of particles colored with their temperature presented for each particle size in the system separately in Figure 6-15 (a). As can be observed, gas-particle heat exchange is mostly occurring in the riser, in particular for fine particles, and gas and particles enter the cyclone with temperatures close to the equilibrium temperature. A higher heat transfer rate is observed in the riser where the gas-particle temperature difference is larger. As expected, large particles (3000 µm) are heated up more slowly because of their smaller specific surface area, and lower heat transfer coefficient (based on equation 6–2, the larger particle, the lower the heat transfer coefficient), such that they leave the cyclone with considerably lower temperature.

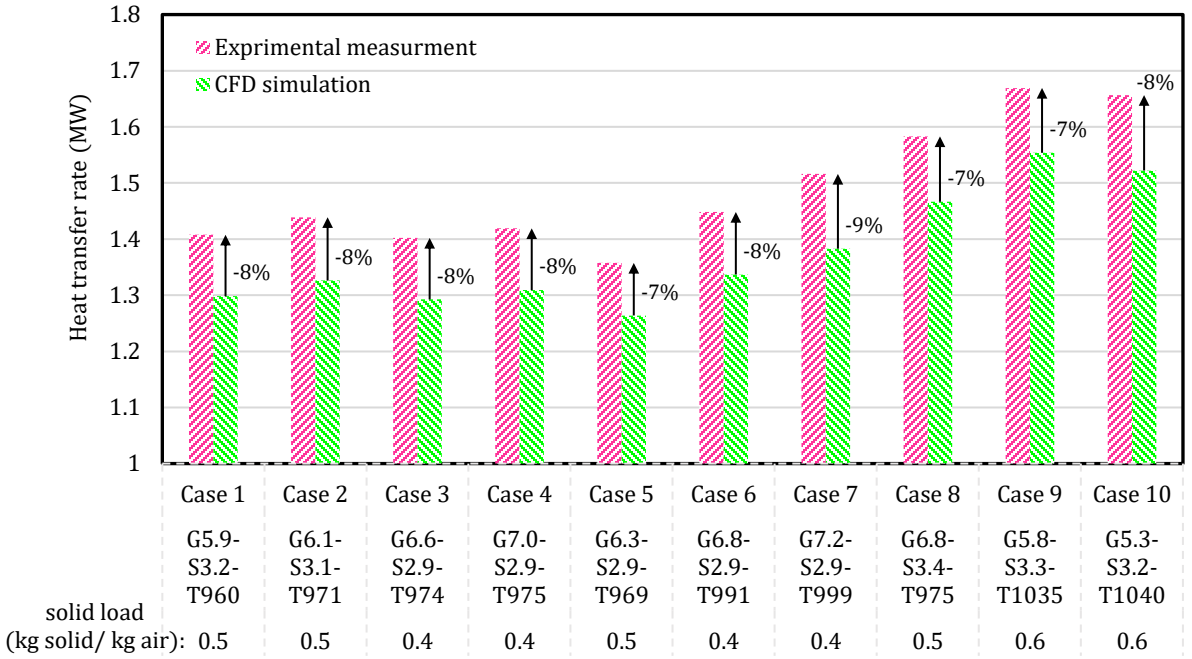

Figure 6-14. Comparison of measured and calculated heat transfer rate. The percentages are the difference between the calculations and the measurements.

Snapshots of particles colored with the Nusselt number are shown in Figure 6-15 (b) for each of the particle sizes within the system, in separate images. The larger the particle, the greater the Nusselt number as expected from equation 6–2. Particles experience the highest heat transfer coefficient where they enter the cyclone from the riser (upper part of cyclone barrel) where they experience the highest Reynolds number as a swirling motion is made in the flow. Meanwhile, in the conical part of the cyclone, the lowest heat transfer coefficient can be observed.

In general, gas-particle heat exchange consists of two stages: (1) the transfer of the heat from the bulk of the gas to the surface of the particle through the gas film adjacent to the particle (an extrinsic process) and (2) the propagation of heat by conduction inside the particle to reach iso-thermal condition within the particle (an internal process). In cases with Bi < 2, the heat exchange is controlled by the external process (a gas-film-controlled process) [216]. In the present study, to model gas-particle heat exchange, a gas-film controlled process (temperature of the particles are assumed uniform and dependent on time alone) is assumed and snapshots of particles colored with their Biot number (Bi) presented in Figure 14 (c) validate the assumption as Bi < 1 for all particles in the system.

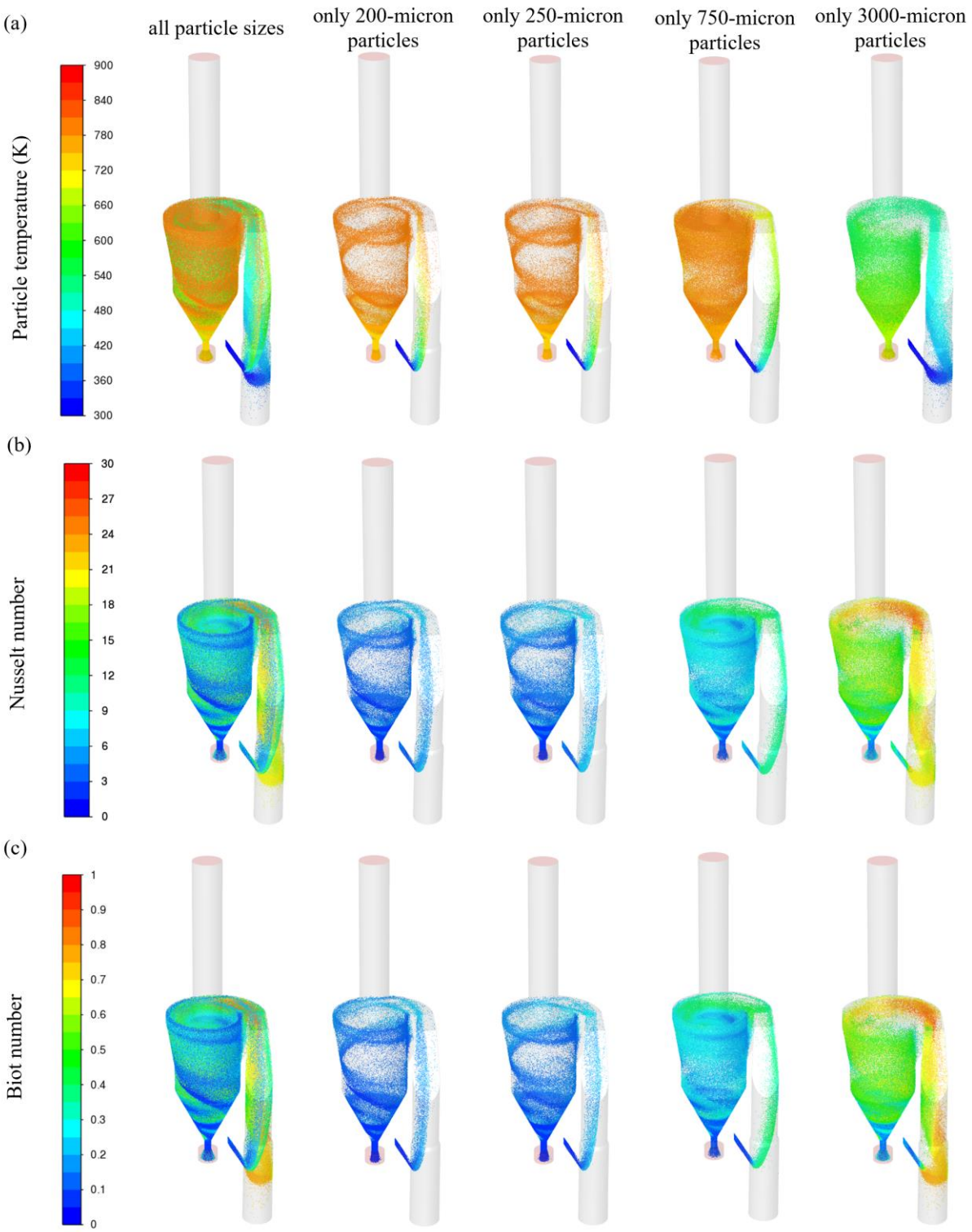

Figure 6-15. Snapshots of a converged solution of case-1 showing particles colored with their (a) temperature, (b) Nusselt number, (c) Biot number

6.5.6 Flow pattern

The axial and tangential velocity profiles obtained from LDA measurements and CFD simulations are presented in Figure 6-16(a, b) for three relatively similar operating conditions (Case-1 G5.9-S3.2-T960, Case-2 G6.1-S3.1-T971, Case-9 G5.8-S3.3-T1035). Despite there being some minor differences between the profiles obtained from LDA and CFD simulations, the agreement is satisfactory, considering the complexity of industrial-scale measurements and CFD simulations. Overall, as can be observed in the figure, the CFD model has a good ability to capture the experimentally determined profiles both in the core and in the near-wall regions. The swirl intensity, the location, and the extent of peaks in axial and tangential velocity profiles, the widths of the vortex cores (radial distance between the peaks of tangential velocity), and the locations where swirling up or swirling down vortices are captured well by the CFD model in a relatively good agreement with measurements.

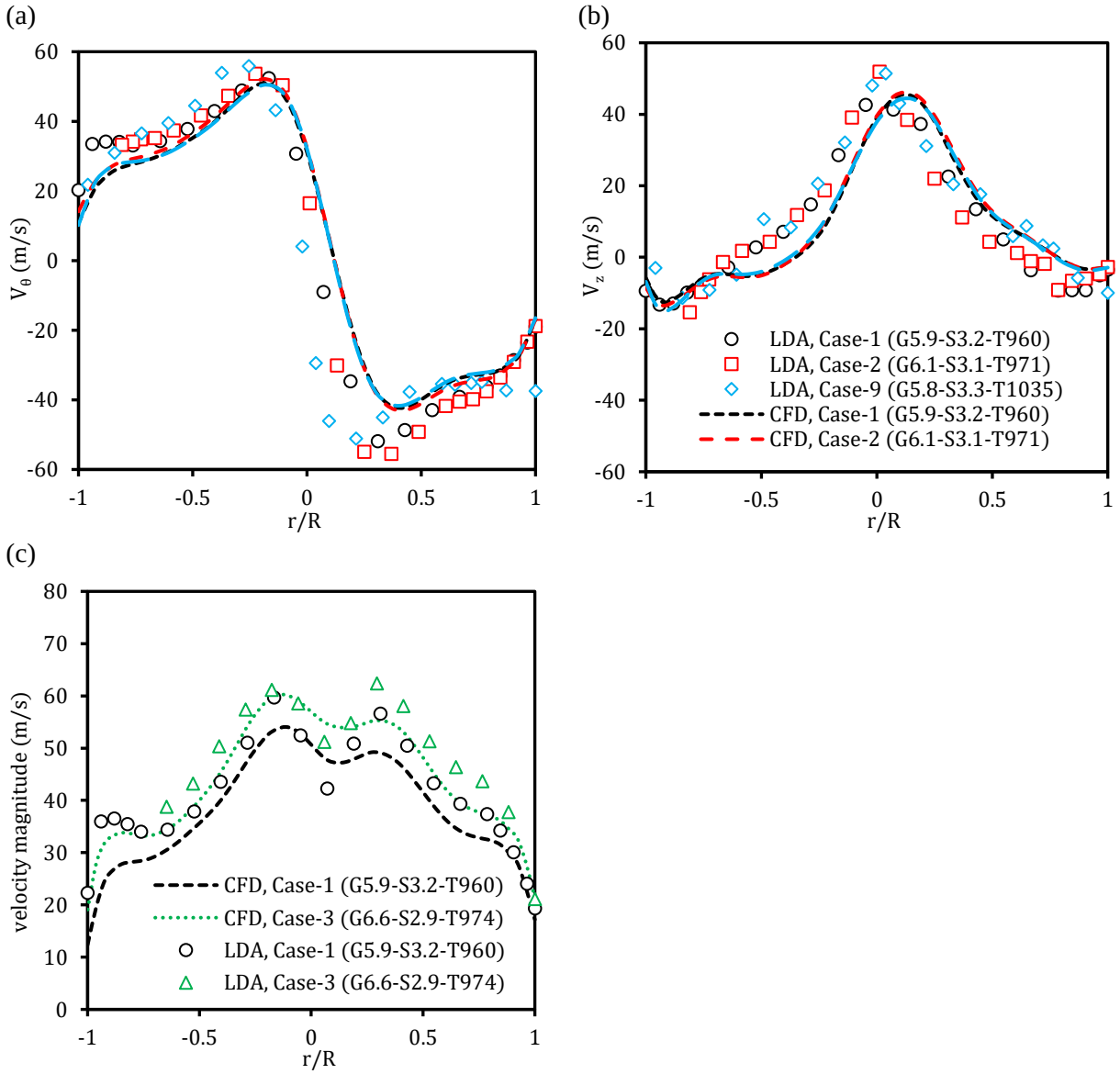

Figure 6-16. Profiles of the mean (a) tangential velocity, (b) axial velocity, and (c) velocity magnitude ($\sqrt{V_\theta{}^2 + V_z{}^2}$) obtained from LDA measurement and CFD simulation.

To see whether the model is able to capture the effect of operating conditions on the flow pattern, LDA measurements were performed under two relatively different conditions (Case-3 G6.6-S2.9-T974). The velocity magnitude ($\sqrt{V_\theta{}^2 + V_z{}^2}$) obtained from measurements and CFD simulations at these conditions is compared with those of Case-1 G5.9-S3.2-T960 in Figure 6-16 (c). As can be observed, the model is well able to capture the profile of velocity magnitude in an acceptable manner. In addition, the model is able to capture the shift in the flow pattern (increase in velocity magnitude) when the gas flow rate is increased considerably from case-1 to case-3.

6.5.7 Temperature pattern

To understand the temperature profile in a cyclone preheater, the measurements by using a thermocouple and FTIR were conducted at two operating conditions (Case-4 G7.0-S2.9-T975, Case-10 G5.3-S3.2-T1040). A comparison is shown in Figure 6-17 of the temperature profiles obtained from measurements and CFD simulations. Like in the case of velocity profiles, the agreement is quite satisfactory even though the profiles obtained from the measurements and the CFD simulations differ slightly.

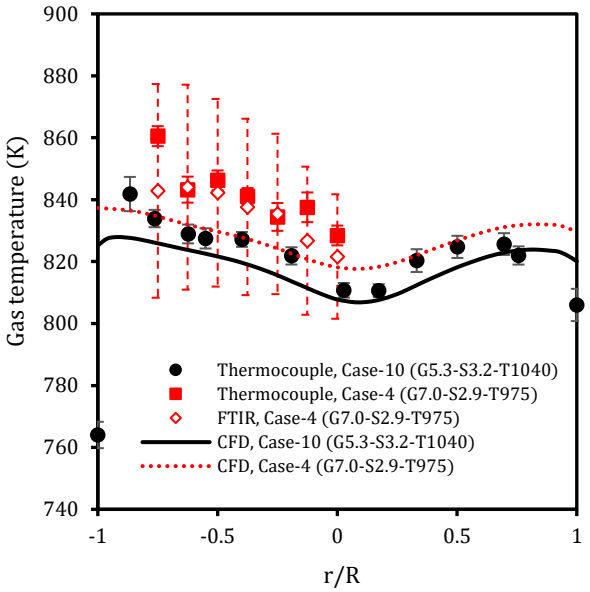

Figure 6-17. Profiles of the mean gas temperature obtained from thermocouple and FTIR measurements and CFD simulations. The error bars show the standard deviation of the measurements.

From the wall toward the center, a slight increase in the temperature is observed first, and then it declines, reaching a minimum in the center. A similar trend is observed from all measurements and CFD simulations, though the location of the maxima is not precisely agreed in the simulations and the measurements.

The observed trend (reduction in the temperature moving from the wall towards the center) also observed in similar units such as cyclone reactors [221] can be explained by how the gas flows in a cyclone. The gas flow entering a cyclone first swirls down (close to the wall) to the bottom of the cyclone and then from there swirls up in the central region up to the vortex finder and gas exit. This means that at a specific height, the gas flow in the central region has been in the cyclone and in contact with particles for a longer time compared to the gas flow close to the wall. So, the gas flow in the central region has had a longer time to

exchange heat with particles and therefore it has a relatively lower temperature. The decrease in gas temperature as approaching the wall in the region very close to the wall might be explained by the increases in particle concentration as approaching the wall (the more particle, the more heat exchange, and the lower gas temperature).

6.6 Conclusions

Industrial cyclone preheaters with high solid load have been simulated, by using a hybrid multiphase model, Dense Discrete Phase Model (DDPM), incorporating gas-particle heat exchange. For the simulation of highly turbulent swirling flow inside the cyclones, the model is coupled with a dispersed version of the k-ω sst turbulence model that is sensitive to flow rotation. The CFD model is validated by the data from an industrial cyclone preheater operating under various conditions. For the validation of the model, in addition to the pressure drop and gas and particle exit temperature as overall measurements, successful local measurements of gas velocity profiles, using the LDA, and gas temperature profiles, using thermocouple and FTIR were conducted. The measurements and validation were conducted on a full-scale industrial cyclone preheater that is a part of a factory producing insulation material.

The ability and accuracy of the developed CFD model in describing relevant phenomena present in such a device were demonstrated and tested with detailed measurements. Furthermore, the following conclusions can be stated from this study:

- An exclusive solid phase must be attributed to each particle size class present in the system in order to achieve energy balance in the system when using the DDPM model in Ansys Fluent 2021R1. Furthermore, It was concluded that the PSD in the present study can be adequately represented with four particle size classes (and consequently four solid phases) included in the model.
- The heat transfer calculations and energy balance in the system are sensitive to parcel size in a certain range. A sensitivity analysis must be performed to determine the largest parcel size and fastest calculation that will provide an overall energy balance and parcel-independent predictions. In the present case, this parcel size turned out to be a parcel with a mass of 5 mg.
- The presented model is sufficiently accurate to reflect the trends in performance parameters and flow patterns observed in the measurements when operating conditions are altered. For example, the reduction in pressure drop and the increase in total heat transfer rate when the solid load is increased in addition to the increase in the pressure drop and total heat transfer rate when the gas flow rate is increased are well predicted by the presented model.

In addition to the four-way coupling simulations (DDPM) presented in this chapter, the present case was also simulated using the two-way coupling method for comparison. This comparison is presented in Appendix C (C.2). It concludes that in the present case with relatively coarse particles, the two-way coupling method seems to be sufficient. However, to have a valid model for the whole range of particle sizes, a four-way coupling model (DDPM) should be used as two-way coupling turned out to be insufficient in the case of fine particles where agglomeration plays a role.

7 Investigation of erosion in an industrial cyclone preheater

This chapter is a reprint of the manuscript "Investigation of erosion in an industrial cyclone preheater by CFD simulations" which has been submitted for publication [222].

7.1 Abstract

In this study, a hybrid multiphase model (Dense Discrete Phase Model, DDPM) was used to investigate erosion in an industrial-scale cyclone preheater by application of Oka's erosion model. The model predictions of flow pattern and temperature profile were first validated by comparison to measurements in an industrial cyclone preheater. After that, the model prediction for erosion was tested against the results in a lab-scale cyclone reported in the literature. Furthermore, the erosion patterns and locations where erosion is severe in the industrial cyclone preheater were predicted by the model. The predicted results were qualitatively matching with the erosion observed in the cyclone during an inspection. In addition, parametric studies on operating conditions including gas and solid flow rates, particle size distribution, and gas inlet temperature were performed and the impacts on erosion as well as pressure drop and heat transfer rate, considered as key performance parameters, were evaluated. The results indicate that the gas flow rate and inlet temperature have the greatest influence on erosion in the cyclone preheater. The erosion rate is largely unaffected by solid flow rate and particle size in the studied range.

7.2 Introduction

Erosion, defined as the process of wall surface material loss due to micromechanical deformation or cracking caused by solid particle impact on a surface [126], is generally a concern in fluid-solid flows. Erosion is a serious problem in many industrial processes associated with the transport of solid particles by a fluid phase in particular pneumatic conveying systems where high velocities are necessary for transporting particulate materials. Thus, careful considerations are required regarding piping fittings (such as elbows, tees, valves and cross plugs), which are likely to introduce sudden changes in the flow direction, that can increase erosion [223].

Erosion in cyclones can be a serious problem, especially in cases where fast-moving, abrasive particles are present. Especially the larger particles with high Stokes numbers, might not follow the gas flow in the cyclone and instead impact the walls of the cyclone [1]. Most cyclones eventually undergo severe erosion requiring repair/replacement of the worn-off parts. Even in the presence of a strong refractory lining,

erosion is one of the major causes of unscheduled shutdowns, e.g., in Fluid Catalytic Cracking (FCC) [65] and stone wool production systems [6]. On top of reduced service life, cyclone wall erosion may also affect the performance of cyclones. Due to erosion, the wall surface becomes rougher which affects the pressure drop and separation efficiency of cyclones [3].

The characteristics of erosion in cyclones are described in the literature [1]. The inlet target area in the barrel which is roughly in direct view of the incoming particles, the lower part of the cone, and the upper part of the dipleg (if present), are the regions where erosion is more serious in a typical cyclone. The highest erosion rate is normally seen where the particles' angle of impact with the cylindrical wall is in a range of 15°-35°, depending on the properties of the wall material. Erosion is severe in the inlet target zone and rapidly decreases below this zone. The severity of erosion continues to decrease to a minimum value when moving further down from the inlet in the cylindrical part. However, in the conical section, erosion increases again with axial distance from the roof [1].

A tool that is able to predict erosion rates is desirable to identify areas with severe erosion and assist with minimizing the damage caused by erosion [224]. Computational fluid dynamics (CFD) is a powerful approach that can be used for this purpose, particularly since conducting erosion experiments is time-consuming and expensive, especially in industrial cases. In CFD erosion models, the Lagrangian framework is generally used for the solid phase since it allows tracking of individual particles through interactions with calculated gas velocity and pressure fields. The particle tracking provides the required input parameters for erosion models, such as particle velocity, impact angle and concentration of impacting particles. Once the impact velocity and angle of the particles hitting a surface are determined, the erosion rate and pattern can be obtained by implementing correlations for erosion. Such an approach has been extensively used in the literature to investigate erosion in elbows [127,225], valves [226], pipes [227] and cyclones [65,75,114,228].

Considering the high number of factors associated with the physical mechanism of erosion such as particle-wall collision velocity and angle, particle size, and wall and particle properties, developing an erosion model is complex. Several research groups have developed such models among which the ones by Finnie [229], McLaury [230], DNV [134], and Oka [135,136] have been extensively used for CFD erosion investigations. Among these, the Oka model appears to be the most reliable and robust [127,224], due to the fact that it is based on the measurable properties of both the eroded and erodent materials. In addition, the Oka model has been shown to offer superior performance to the DNV model in the simulation of erosion in cyclones [65,75,228,231].

A few research works are focused on CFD-based investigation of erosion in cyclones but are all limited to lab-scale cyclones operating under isothermal ambient temperature [65,75,114,228,231]. In these works, the multiphase flow is assumed to be dilute and therefore either the one-way or two-way multiphase coupling methods are used; even in Sedrez et al. [65] and Parvaz et al. [114] that focused on cyclones with relatively higher solid loads (0.2 kg solid/kg air). As far as the authors are aware, no research work in the literature focuses on CFD-based investigation of erosion in large-scale cyclones that are highly loaded and where the four-way coupling method is generally required to correctly simulate the dense multiphase flow.

The objective of this work is to simulate the erosion phenomenon in a highly loaded industrial cyclone preheater by CFD modeling using the Oka erosion model, in order to predict the erosion rate, erosion pattern, and the most likely locations for erosion. For this purpose, the erosion model was coupled with a developed hybrid multiphase model (Dense Discrete Phase Model, DDPM), which includes gas-solid heat exchange (presented in Chapter 6). The CFD model is validated against experimental data obtained in an industrial cyclone preheater, with respect to the flow pattern and temperature profile. The erosion model is validated against experimental data from a lab-scale cyclone reported in the literature [65]. In addition, the effects of key operating conditions including gas and solid flow rates, particle size distribution, and gas inlet temperature on the erosion, as well as the two important performance parameters of cyclone preheaters, the heat transfer rate and pressure drop, were investigated.

7.3 Experimental setup

For validation of the CFD model, measuring campaigns have been performed in an industrial cyclone preheater with a diameter of 1.6 m, which is a part of the Integrated Melting Furnace (IMF) system [6], operated by Rockwool A/S. A 3D view of the cyclone preheater is illustrated in Figure 7-1.

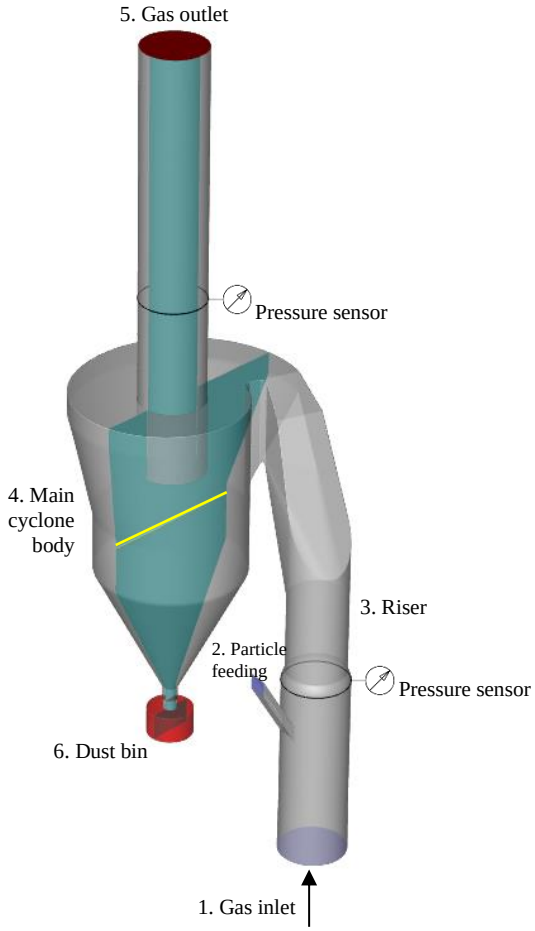

Figure 7-1. A 3D view of the geometry of the cyclone. The locations of pressure taps for measuring static pressure drop are shown. The yellow line is the line of profiles in the results and discussion section.

Laser Doppler Anemometry (LDA) and thermocouple measurements were performed to provide axial and tangential velocity and temperature profiles inside the cyclone preheater. Details of the measurements and cyclone operating conditions, e.g., the PSD (particles are in the range of 30-4000 µm with a Sauter mean diameter of 375 µm) and heat capacity of injected particles, can be found in Chapter 6. The operating conditions during the LDA measurement (Case-1), thermocouple measurement (Case-2), and a base case used for erosion investigation (Case-3) are summarized in Table 4-1. In addition to LDA and thermocouple measurements, pressure drop (measured by two pressure sensors shown in Figure 7-1), gas inlet and exit temperature, particle exit, and gas and solid flow rates were continuously monitored and logged.

Table 7-1. Summary of operating conditions. The cases are named in a way to present the main operating conditions of the case (e.g., in Case-1 G5.3-S3.5-T966, gas flow rate, solid flow rate, and gas inlet temperature are 5.3 kg/s, 3.5 kg/s, and 966 K respectively).

Parameter	**Case-1 G5.3-S3.5-T966**	**Case-2 G5.8-S3.4-T946**	**Case-3 G6.8-S2.8-T990**
Description	LDA (velocity profile)	Temperature profile	Base/reference case for the erosion study
Gas flow rate, G (kg/s)	5.3	5.8	6.8
Solid flow rate, S (kg/s)	3.5	3.4	2.8
Solid loading ratio, SL (kg solid / kg air)	0.65	0.59	0.41
Gas inlet Temperature (K)	966	946	990
Particle inlet Temperature (K)	298	298	298

7.4 Model description

7.4.1 CFD model

A hybrid multiphase model (Dense Discrete Phase Model, DDPM) coupled with a dispersed version of k-ω sst turbulence model sensitized for flow rotation, which includes gas-solid heat exchange was developed for the simulation of industrial-scale cyclone preheaters operating under high solid loadings. A detailed description of the CFD model was given in previous chapters. The same CFD model is employed in the present study to investigate the erosion phenomenon.

7.4.2 Erosion model

To investigate erosion in the cyclone preheater, the Oka erosion model [135,136] is implemented to the developed CFD model. In the Oka erosion model, erosion flux (E^R) for each computation face on the wall is defined by equation 4–1:

$$E^R = \sum_{i=1}^{N_P} \frac{E^i}{A_{face}^{(i)}} \qquad 7\text{–}1$$

where, $A_{face}^{(i)}$ is the area of the computation face on the wall surface. To obtain the global erosion rate (kg/s), E^R is integrated over the total area of the domain. In equation 4–1, the erosion rate for each wall cell face, E^i, is determined by

$$E^i = \rho_w \times E_v \times \dot{m}_p \quad 7\text{–}2$$

$$E_v = E_{90}/\rho_w \times (\frac{V_P^{(i)}}{V'})^{k_2} \times (\frac{d_P^{(i)}}{d'})^{k_3} \times f(\gamma) \quad 7\text{–}3$$

Where E_v is the volume of the eroded wall per 1 kg of collided particles. E_{90}, the reference erosion rate at 90° impact angle (the wall material mass eroded per mass of particles), which depends on the hardness of eroded (wall) material and particle material can be estimated by interpolation of data presented in Fig. 2 of [136]. $V_P^{(i)}$ and $d_P^{(i)}$ are the impact velocity and particle diameter, respectively. V' (104 m/s) and d' (326 µm) are fixed reference impact velocity and diameter used in the experiments by Oka et al. [135]. $f(\gamma)$ is a function of the impact angle (γ) defined by equation 7–4:

$$f(\gamma) = (sin\gamma)^{n_1}(1 + Hv_w(1 - sin\gamma))^{n_2} \quad 7\text{–}4$$

k_2, k_3, n_1 and n_2 in equations 7–3 and 7–4 are the parameters determined by the hardness of eroded (wall) material and particle material and can be estimated by interpolation of data presented respectively in Fig. 8, Fig. 9, Fig. 3, and Fig. 4 in the reference paper [135] of Oka model.

The constant parameters used in the erosion model by Oka [135,136] are summarized in Table 7-2. As the base case, the Vickers hardness of the particles and wall are assumed to be 9 and 18 GPa respectively (the reasoning behind this assumption is discussed in the results and discussion section where the effect of particle and wall hardness is investigated). Furthermore, a sensitivity analysis on the effect of wall and particle hardness on the erosion of the studied industrial cyclone preheater has been performed, which is discussed in the results and discussion section.

Table 7-2. Constants of the Oka erosion model (for a wall of refractory material and particles of natural rock material) used as the base case for the study of erosion in the industrial cyclone preheater.

Hv_p GPa	Hv_w GPa	$E_{90} \times 10^5$ kg/kg	k_2	k_2	n_1	n_2	V' m/s	d' µm
9	18	3.00	2.30	0.19	4.7	0.06	104	326

7.5 Results and discussion

7.5.1 Model validation

In the present study, the model validation was performed in two steps: (1) the predictions of flow pattern and temperature profile were validated against the measurements in the industrial cyclone preheater (the cyclone preheater focused on in the present study). (2) the predictions for erosion were validated against the erosion measurements in a lab-scale cyclone reported in the literature [65]. In the following sections, these validations will be discussed in detail.

7.5.1.1 CFD validation of the flow and temperature patterns

For a reliable erosion investigation, it is necessary to ensure the validity of the CFD model, in particular, regarding capturing the gas flow pattern. The gas flow pattern influences the particle motion inside the cyclone and consequently how particles hit the walls which governs the erosion rate. To validate the

predicted flow pattern, LDA measurements were conducted on the industrial-scale cyclone studied here and compared with the flow pattern obtained from CFD simulations in Figure 7-2 (a, b).

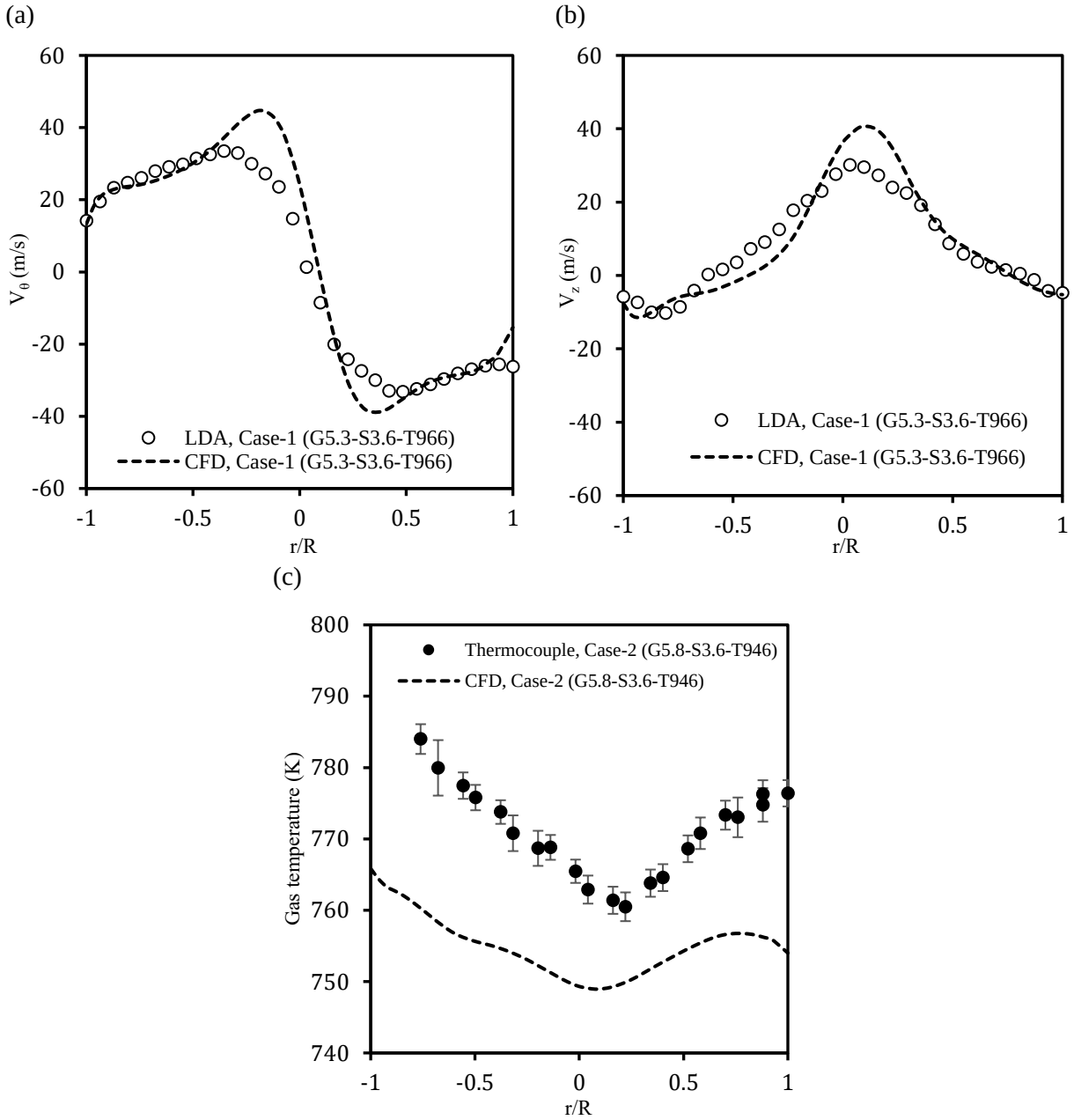

Figure 7-2. Profiles of the mean (a) tangential velocity, (b) axial velocity, and (c) gas temperature obtained from the experimental measurement and CFD simulation. The error bars show the standard deviation of the measurements.

In addition, thermocouple measurements were conducted to obtain the temperature profile inside the cyclone and compared with CFD predictions in Figure 7-2 (c). Although the temperature profile does not affect erosion directly, such a comparison validates that the heat transfer is modeled properly in the CFD simulation. It is of importance since a validated simulation of heat transfer is required for reasonable predictions of gas properties, and consequently, flow pattern which directly governs particle motion and therefore erosion rate.

The CFD model shows a high ability to capture velocity profiles both in the core and in the near-wall regions, including the intensity of swirl (regarding the velocity profiles in Figure 7-2, based on LDA measurements swirl number is approximated 0.37, while based on CFD simulation it is approximate 0.32), the location and extent of axial and tangential velocity peaks, the width of vortex cores (radial distance between tangential velocity peaks), and the locations of upward and downward vortices. Considering the difficulties of industrial-scale measurements and CFD simulations, despite some minor differences, the agreement between the LDA measurements and the CFD simulations on the velocity profiles, shown in Figure 7-2 (a, b), is generally acceptable.

To further validate the CFD model, a comparison of the gas temperature profile obtained from thermocouple measurements and CFD simulations is presented in Figure 7-2 (c); despite the minor discrepancy, an acceptable agreement is observed and the overall trend (minor reduction in the gas temperature as moving from the wall towards the center) is captured by the CFD simulation. This discrepancy might be explained by a deviation between the particle heat capacity used in CFD simulation and the actual heat capacity as the composition of natural rock materials sampled for heat capacity measurement was slightly different from the actual composition.

More comparison of CFD predictions with measurement data of flow pattern and temperature profile and further validation of the developed model under operating conditions different from what is reported here can be found in Chapter 6.

7.5.1.2 Erosion validation

No quantitative measurements of erosion in industrial cyclones is available in the literature, so the model was implemented on a relatively highly loaded lab-scale cyclone which was investigated by Sedrez et al. [65] both experimentally and numerically using the same erosion model as in the present study (Oka erosion model). They investigated the erosion rate in the entrance, conical and cylindrical parts of a lab-scale cyclone made of gypsum operating with fluid catalytic cracking (FCC) particles of 64 μm diameter. Details of the geometry and the operating condition can be found in their paper [65].

In the present study, four sets of measurements reported by Sedrez et al. [65] were used (summarized in Table 7-3); one of them was used for tuning of E_{90} in the erosion model and the other three were used for validation of the model. Constants in the erosion model including n_1, n_2, k_2, k_3, v', and d' that were obtained from the Oka model [135,136] by assuming Vickers hardness of the gypsum wall to be 0.59 GPa and Vickers hardness of FCC particles to be 10 GPa. All the constant values are listed in Table 7-4. The value of E_{90} was tuned to fit the measured global erosion rate in case Lab-scale 1 (in Table 7-3).

The pressure drop obtained from CFD simulation and experimental measurements are compared in Figure 7-3 where reasonable agreement is observed. The predicted global erosion rates for three gas flow rates are compared with measured values in Figure 7-3. The predictions are also compared to the predictions by Sedrez et al. [65] obtained from the same erosion model (Oka model). The model used by Sedrez et al. [65] and the present model are different in two major aspects: (1) the present model is a four-way coupling multiphase model while Sedrez et al. [65] used a two-way coupling model. (2) constants of the erosion model are assumed differently (they are compared in Table 7-4).

Table 7-3. Summary of studied cases on a lab-scale cyclone [65]

Case name	Gas velocity inlet (m/s)	Solid mass flow rate (g/s)	Purpose
Lab-scale 1	35	6.8	tuning of E_{90}
Lab-scale 2	25	11.8	Validation of erosion model (effect of gas flow rate on erosion)
Lab-scale 3	30	11.8	
Lab-scale 4	35	11.8	

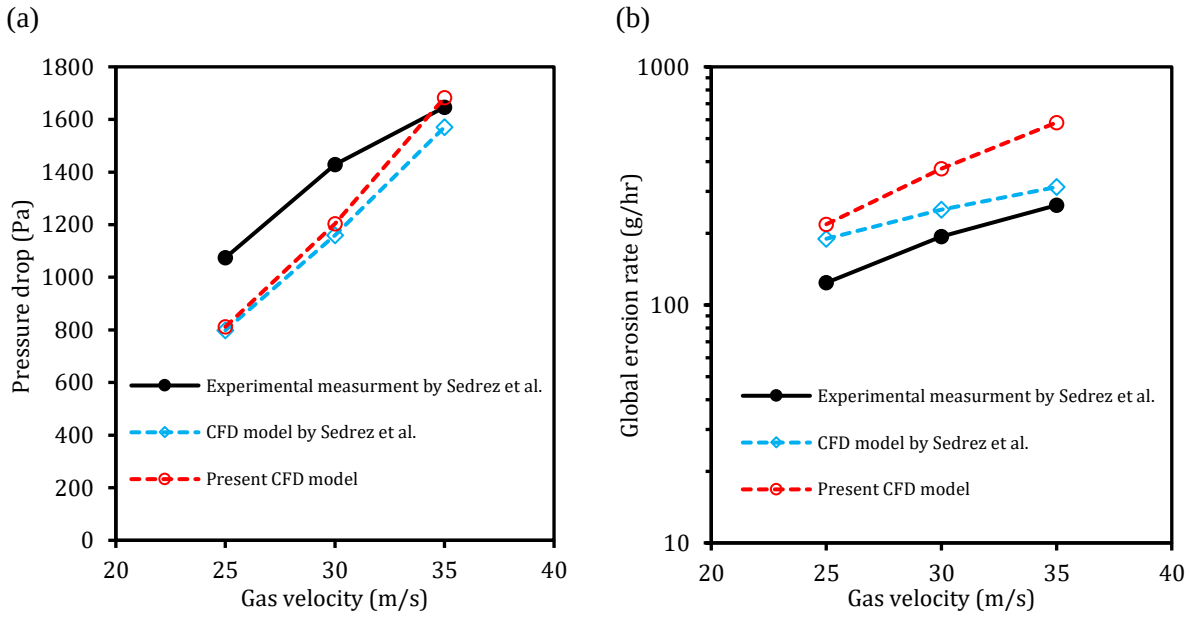

Figure 7-3. Effect of gas flow rate on (a) pressure drop and (b) global erosion rate obtained from experimental measurements and CFD simulation. The mass flow rate is 11.8 g/s for all cases.

Despite the observed discrepancy, the model can capture the trend of an increase in erosion rate due to an increase in gas flow rate. The observed systematic overprediction can be explained by the fact that in the present case the model constant (E_{90}) was calibrated for a different solid load and the model lacks modeling of the shielding effect to accurately capture the effect of solid load on the erosion.

Regarding the global erosion rate, although a relatively better agreement is observed in the simulations of Sedrez et al, the constants used in their simulations, shown in Table 7-4, seem unreasonable (in particular k_2, k_3, v', and d'). The dependence of erosion on particle velocity is assumed to be linear (k_2=1), and the erosion is assumed to be independent of particle size (k_3=0), which are not consistent with the original Oka erosion model [135,136]. Furthermore, the reference gas inlet velocity and particle diameter are clearly reported in the reference paper of the Oka erosion model [135,136] to be 104 m/s and 326 µm, respectively, while other values were used in the study of Sedrez et al. [65].

Table 7-4. Constants of the Oka erosion model (for a wall of gypsum and FCC particles) used in the lab-scale cases

	Hv_p (GPa)	Hv_w (GPa)	n_1	n_2	k_2	k_3	v' (m/s)	d' (μm)	E_{90} (kg/kg)
Present study	10	0.59	1.01	4.75	2.38	0.19	104	326	0.0133
Sedrez et al. [65]		0.59	0.67	5.2	1	0	30	64	

In erosion investigations, generally, erosion pattern, showing where erosion is more severe, is more informative and easier to predict than the quantification of erosion rates. In Sedrez et al. [65] the experimental erosion rates were reported for three sections of the cyclone (entrance, conical, and cylindrical). This allows for an evaluation of the erosion pattern by comparing the rates in each part. It can also be compared with the erosion rates in each part obtained from CFD simulation for further validation of the model. Such a comparison is presented in Figure 7-4 (a). The present CFD simulation predicts similar patterns as observed in the experiments which proves the capability of the developed CFD model in the prediction of the erosion pattern in cyclones. It also can be observed from Figure 7-4 (a) that the present CFD model better predicts the erosion pattern compared to the model by Sedrez et al. From the contours of erosion rates presented in Figure 7-4 (b), it can be observed that erosion is most severe at the entrance area, less severe at the cylindrical area, and minor at the conical part. This is observed in both the experimental results and the CFD model data.

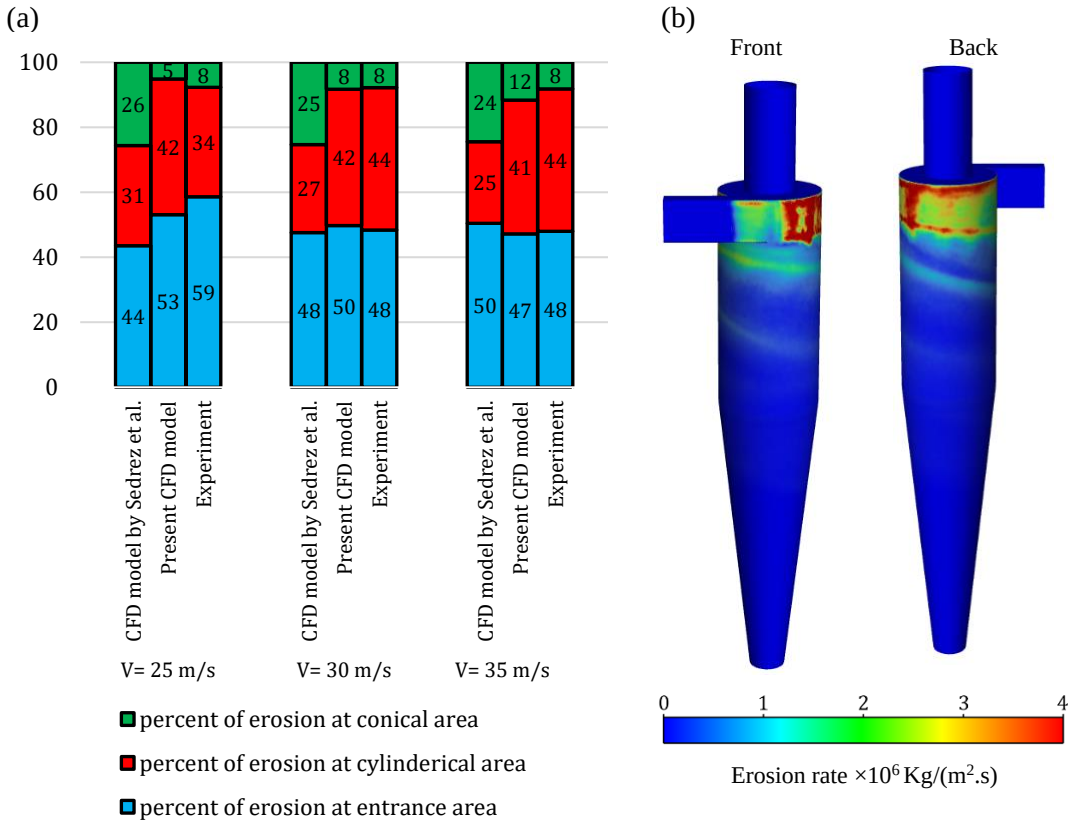

Figure 7-4. Erosion pattern in a lab-scale cyclone

7.5.2 Erosion in the industrial cyclone preheater

After the successful validation of the approach, it was used to predict the erosion rates in the industrial cyclone preheater. The model constants used for this case are listed in Table 7-2. The model is first used for the industrial cyclone preheater under a typical operating condition (Case-3 in Table 4-1) to have a better understanding of erosion in this cyclone in general. Contours of the predicted erosion rate, for this case, are presented in Figure 7-5. The most severe erosion occurs at the entrance area, inlet target area (highlighted as location 2 in the Back view in Figure 7-5), and also at the roof where particles enter the cyclone main body (highlighted as location 3 in the Back view in Figure 7-5).

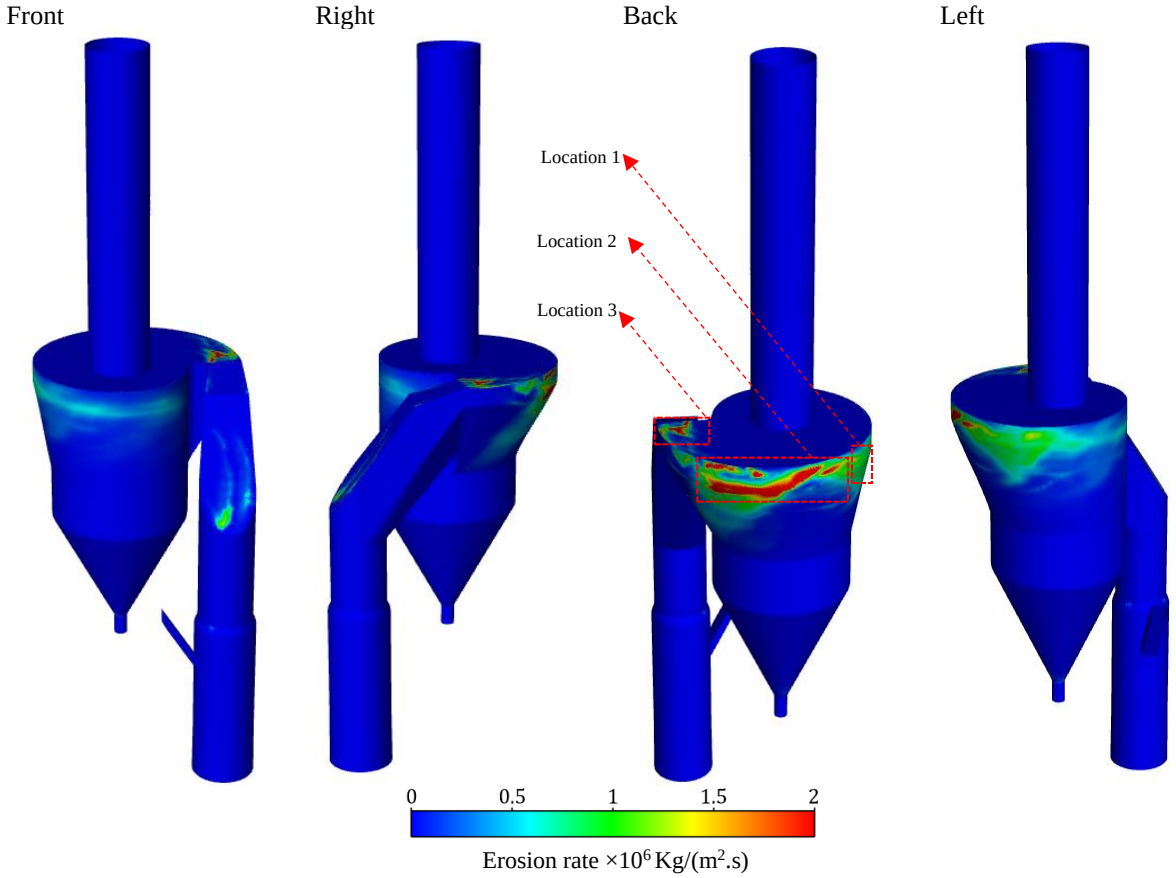

Figure 7-5. Erosion pattern on the industrial cyclone preheater operating under conditions of Case-3.

Visual inspections of the cyclone preheater interior were performed four times, each with a time span of one month to investigate the erosion pattern in the entrance part. Figure 7-6 shows the new refractory and after 3 months of operation at three locations (highlighted in the Back view of Figure 7-5). The photos clearly show that the refractory bricks are more eroded at locations 2 and 3 compared to location 1. Moreover, refractory bricks need to be replaced more frequently at locations 2 and 3 to avoid further damage to the cyclone preheater according to the factory.

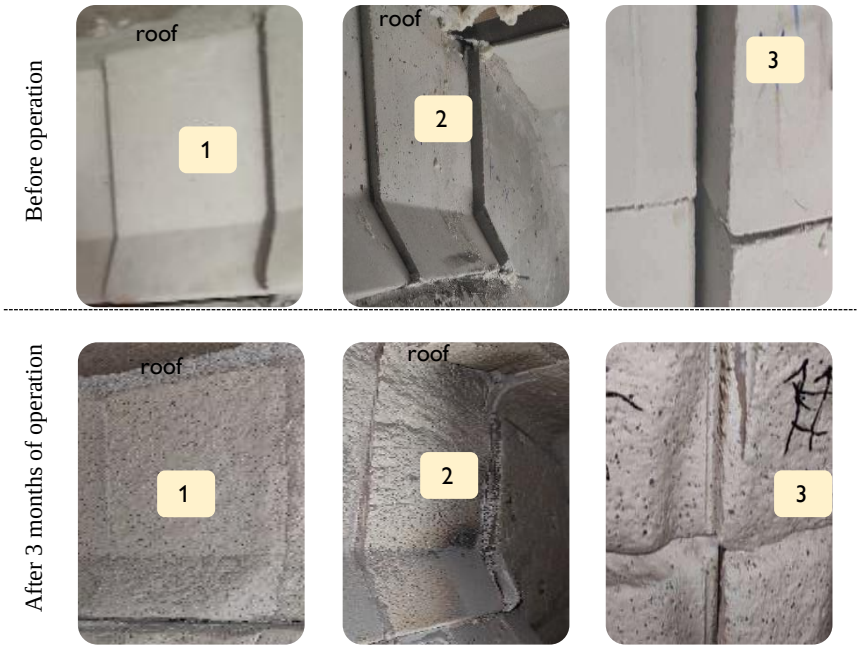

Figure 7-6. Examples of taken photos from inside of the cyclone preheater before and after three months of operation at three locations shown in Figure 7-5.

Higher rates of erosion at locations 1-3 compared to walls of the riser and the cylindrical and conical parts of the cyclone were clear from the visual inspections. Also, unlike locations 1-3 where thick erosion-resistant refractory bricks are used, other locations (the riser, cylindrical, and conical part of cyclone) are covered by castable refractory as these locations are less eroded which can also be observed in CFD simulation predictions. Visual observations at location 2 after 3 months of operations showed increased erosion when approaching the roof. To see whether the present CFD model captures this tendency, the variation of averaged predicted erosion rate with distance from the roof is calculated from CFD simulation and presented in Figure 7-7. The results indicate that the CFD model captures this tendency.

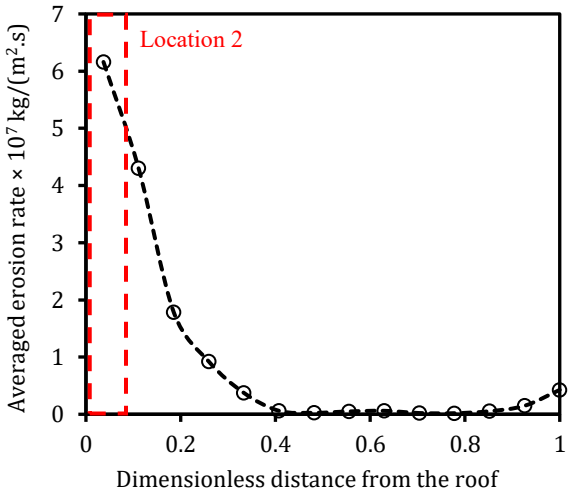

Figure 7-7. Variation of averaged erosion rate with distance from the roof

The CFD model predicted 10 g/hr of global erosion rate and predicted that the time-to-failure is 456 days of operation. The time-to-failure is defined as the shortest time of operation after which there is one spot in the cyclone where the whole thickness of refractory is eroded and the unit can no longer operate and should be shut down. This time-to-failure is calculated using the highest value of erosion rate observed in the CFD calculation using the following equation:

$$time - to - failure[day] = \frac{thickness\ [m] \times density[kg/m^3]}{highest\ erosion\ rate\ [kg/m^2 s]} \times \frac{1[day]}{86400[s]} \qquad 7\text{–}5$$

In the present study, 10 cm of refractory material thickness and a density of 2450 kg/m^3 are assumed for the calculation of time-to-failure. The failure is predicted to occur at location 2 highlighted in the Back view in Figure 7-5. In the actual plant, the failure occurs after 4-6 months, so the prediction is in the same order of magnitude, however more accurate prediction requires tuning of the constants in the erosion model based on accurate quantitative experimental measurements that are not available.

7.5.3 Parametric study

In addition to accurate predictions of important performance parameters of cyclone preheaters discussed in Chapter 6, the results from the CFD model provide reasonable erosion predictions as shown in the previous section. In this section, the effect of important operation conditions, as well as the particle and wall hardness on erosion is studied. An extensive parametric study has been performed, varying one parameter (operating condition) at a time, and assessing their effect on the global erosion rate, time-to-failure, heat transfer rate, and pressure drop.

In addition to the effect of operating conditions investigated here, the effect of some minor geometry changes on the global erosion rate, time-to-failure, heat transfer rate, and pressure drop is investigated and presented in Appendix E.

The time-to-failure results presented in this section are normalized by the time-to-failure for Case-3 (456 days). The reference case for the parametric study is Case-3 in Table 4-1 meaning that when doing a parametric study on one of the operating conditions, other operating conditions remain unchanged as in Case-3.

7.5.3.1 Effect of gas flow rate

The effect of gas flow rate on global erosion rate and time-to-failure is presented in Figure 7-8 (a). An increase in gas flow rate leads to a higher gas velocity and more intense swirling motion in the cyclone. As a result, particles will collide with the wall with greater velocity causing more erosion.

To have a better picture of what happens when the gas flow rate is increased, terms defining the erosion rate including collision frequency impact ($\dot{m}_p$), collision angle impact ($f(\gamma)$), and collision velocity impact ($(\frac{V_P^{(i)}}{V'})^{k_2}$) are monitored, averaged over time, and presented in Figure 7-9 for two gas flow rates. As can be observed, an increase in gas flow rate leads to a slightly more frequent particle-wall collision, slightly more erosive collision angle, and higher collision velocity in the cyclone main body where erosion is mostly occurring. All these contribute to an increase in the global erosion rate.

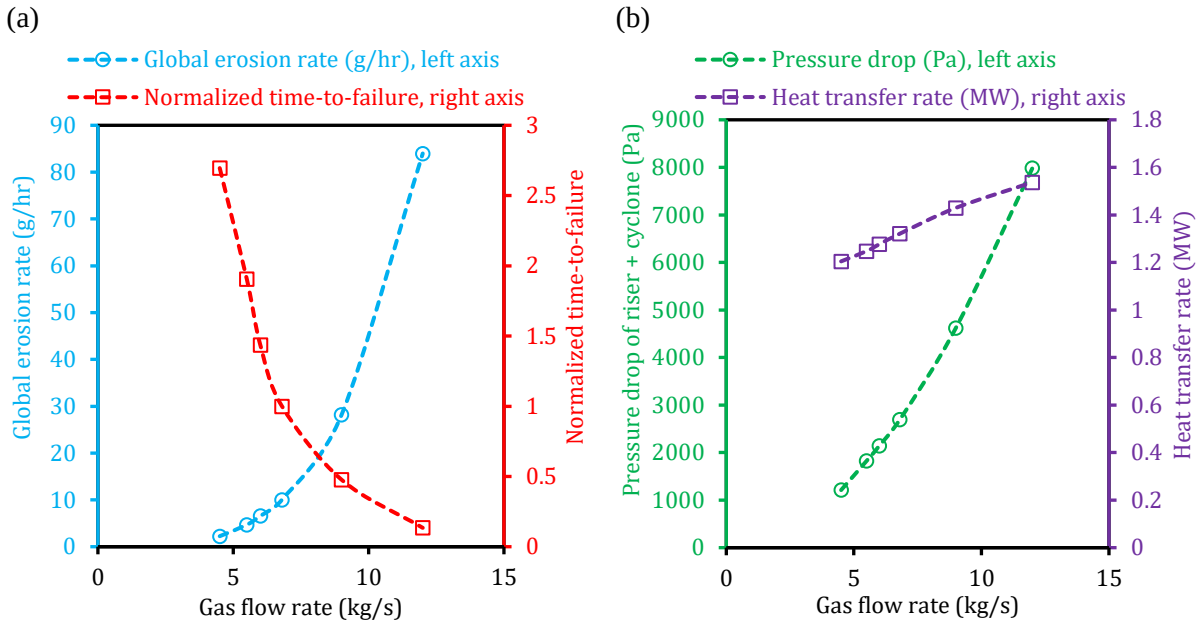

Figure 7-8. Effect of gas flow rate on (a) erosion and (b) pressure drop and heat transfer rate.

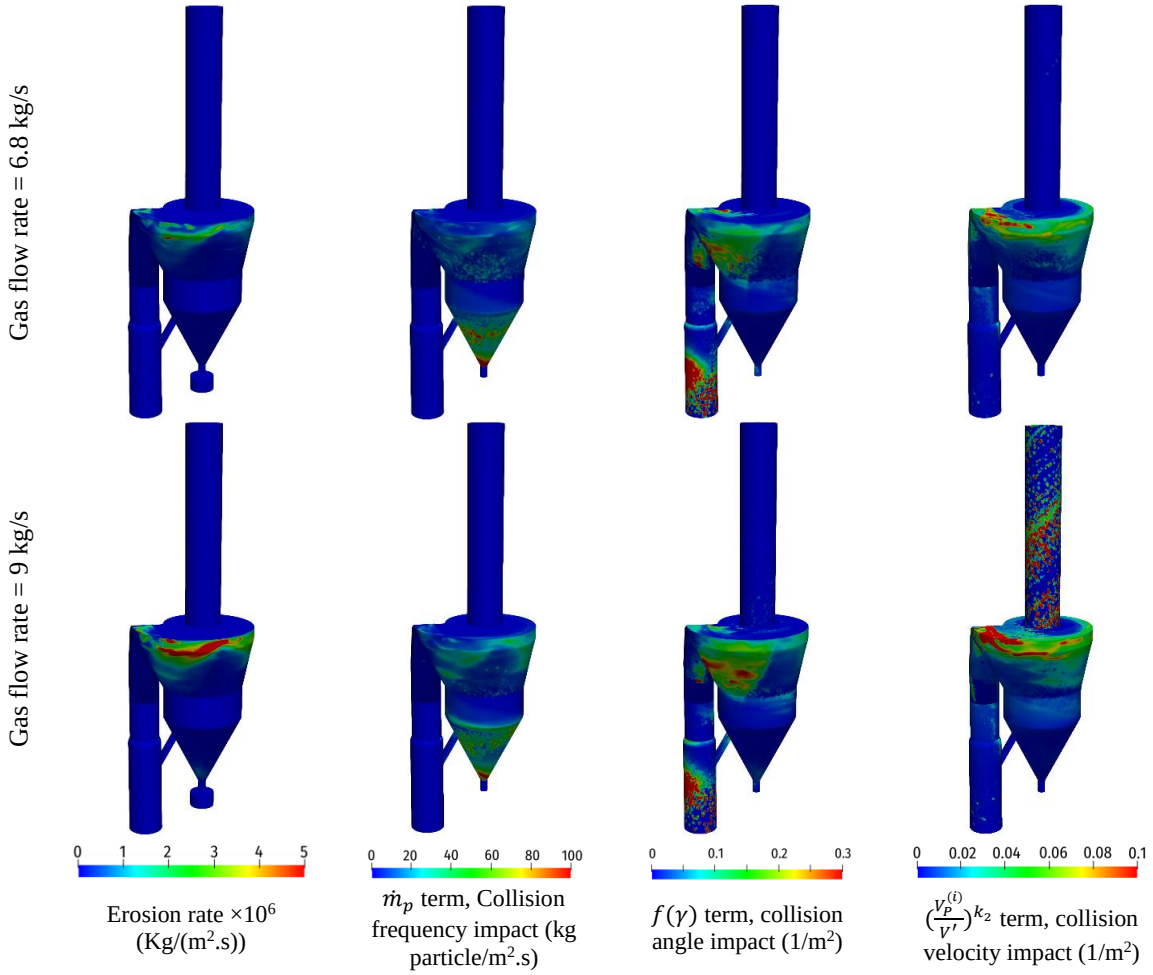

Figure 7-9. Effect of gas flow rate on collision frequency impact, collision angle impact, and collision velocity impact in erosion modeling normalized by surface area

A higher erosion rate caused by an increase in the gas flow rate will, of course, lead to a shorter time-to-failure. However, it should be noted that the predicted location of the failure is not the same for all gas flow rates. In the studied range, up to 6 kg/s, it is located around point 1 in Figure 7-10, for the gas flow rate between 6-8 kg/s, it is located around point 2 and for higher gas flow rates it is located around point 3. These changes in the location of the failure are caused by the combination of changes in the distribution of particle-wall collision frequency, angle and velocity as presented for two cases in Figure 7-9 which is basically caused by the change in the flow pattern in the cyclone.

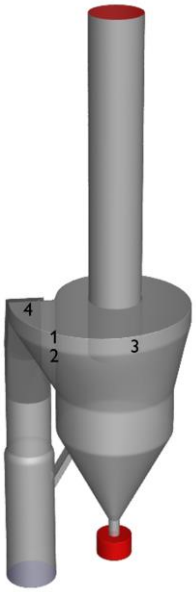

Figure 7-10. Locations where the first failure occurs (highest rate of erosion).

In addition, the effect of the gas flow rate on pressure drop and the heat transfer rate is presented in Figure 7-8 (b). As the gas flow rate is increased, a considerable increase in pressure drop is observed. The higher gas flow rate results in higher swirling velocity, and therefore higher loss of dynamic pressure in the vortex finder. In addition, a higher gas flow rate leads to more dissipation of mechanical energy due to higher friction at the walls. These both contribute to the observed higher pressure drop when the gas flow rate is increased. It should be noted that higher gas flow rates lead to higher temperatures in the system and consequently lower density which also affect the pressure drop in the system. Furthermore, as shown in Figure 7-8 (b) when the gas flow rate increases, an increase in heat transfer rate is observed which is intuitive as it is the case in any heat exchanger.

7.5.3.2 Effect of solid flow rate

Figure 7-11 shows the effect of solid flow rate on global erosion rate, time-to-failure, pressure drop, and heat transfer rate. In the studied range, counter-intuitively an increase in the solid flow rates does not lead to a significant increase in the global erosion rate. When the solid load is increased, and thereby the number of particles hitting the wall, more erosion is expected. However, no increase and even reduction of erosion rate at higher solid flow rates have been reported in cyclones [1,65] and other geometries [232,233].

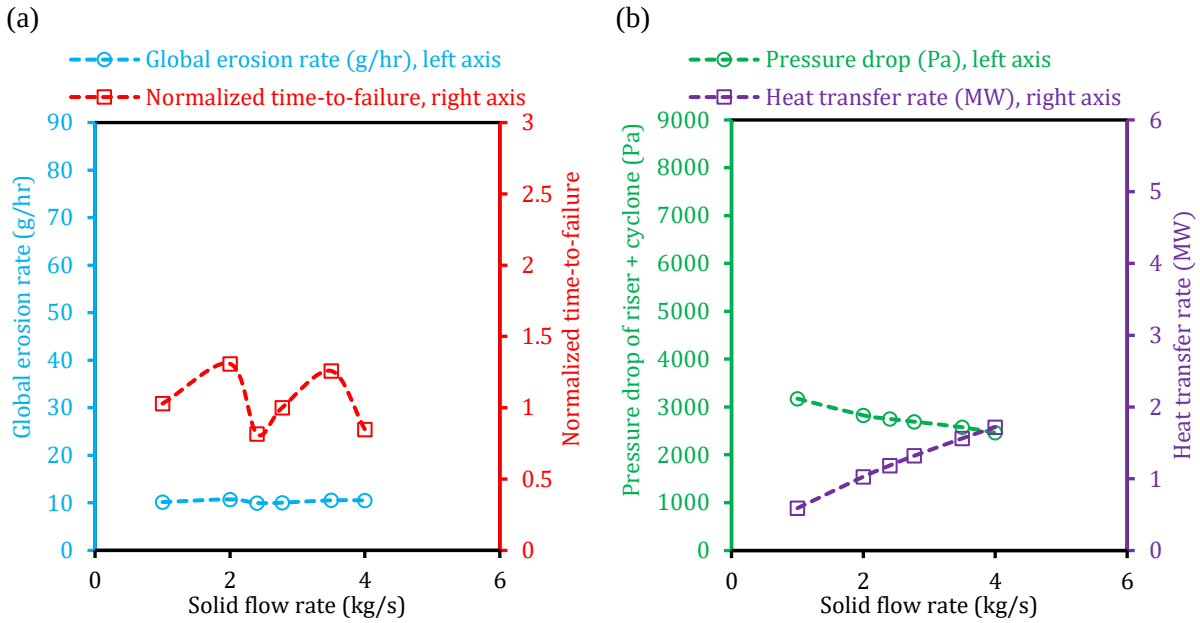

Figure 7-11. Effect of solid flow rate on (a) erosion and (b) pressure drop and heat transfer rate.

To understand the cause of this observed behaviour and to gain a better understanding of what is happening when the solid flow rate is increased, decoupled terms of collision frequency impact ($\dot{m}_p$), collision angle impact ($f(\gamma)$), and collision velocity impact ($(\frac{V_P^{(i)}}{V'})^{k_2}$) in the erosion model are presented in Figure 7-12 for two solid flow rates. As can be observed, although an increase in solid flow rate leads to more frequent particle-wall collision, it is compensated by a slightly less erosive collision angle, and considerably lower collision velocity in the cyclone main body so that the impact of solid flow rate on global erosion rate is predicted to be minor. This considerable reduction in collision velocity can be explained by the fact that higher solid flow rates lead to lower gas temperature in the cyclone, therefore higher density, lower gas velocity and less intense swirling motion which leads to a lower particle velocity and lower particle-wall collision velocity.

It is worth mentioning that, in the literature [3,4,25,26], in iso-thermal cases, the reduction in erosion when the solid flow rate is increased has been related to the so-called shielding or cushioning effect. A shield of concentrated particle regions is formed near the wall, which is believed to partially protect the wall from erosion by decreasing the energy of the particles in the near-wall region [3,4,25,26]. In DDPM multiphase model, particles are assumed point masses (no volume displacement so that two particles can possess the same location), so the model might not capture the shielding phenomenon accurately. However, in DDPM, solid stress is present in the equation of movement of particles meaning that if a cell is filled with particles, or has a high solid volume fraction, it is hard for other particles to enter that cell, so shielding effect might be partly, to some extent, captured.

To determine if this behaviour is due to the changes in the temperature, two cases with different solid flow rates (1 kg/s and 2.8 kg/s) but under iso-thermal and ambient conditions (gas and particle with the same temperature so that in both cases temperatures throughout the system are the same) were simulated. As shown in Figure 7-13, under this condition, an increase in the solid flow rate leads to a considerable increase

in the global erosion rate which confirms the suggested explanation. Comparing the case of 1 kg/s with the case of 2.8 kg/s, while the solid flow rate is increased by 180%, it was observed that particle-wall collision frequency was increased by approximately 60% suggesting that shielding effect is captured to some extent (without shielding around 180% increase in particle-wall collision frequency was expected). However, the extent of predicted shielding is not significant enough to lead to a reduction in erosion due to an increase in the solid load as reported in cyclones in the literature [1,65].

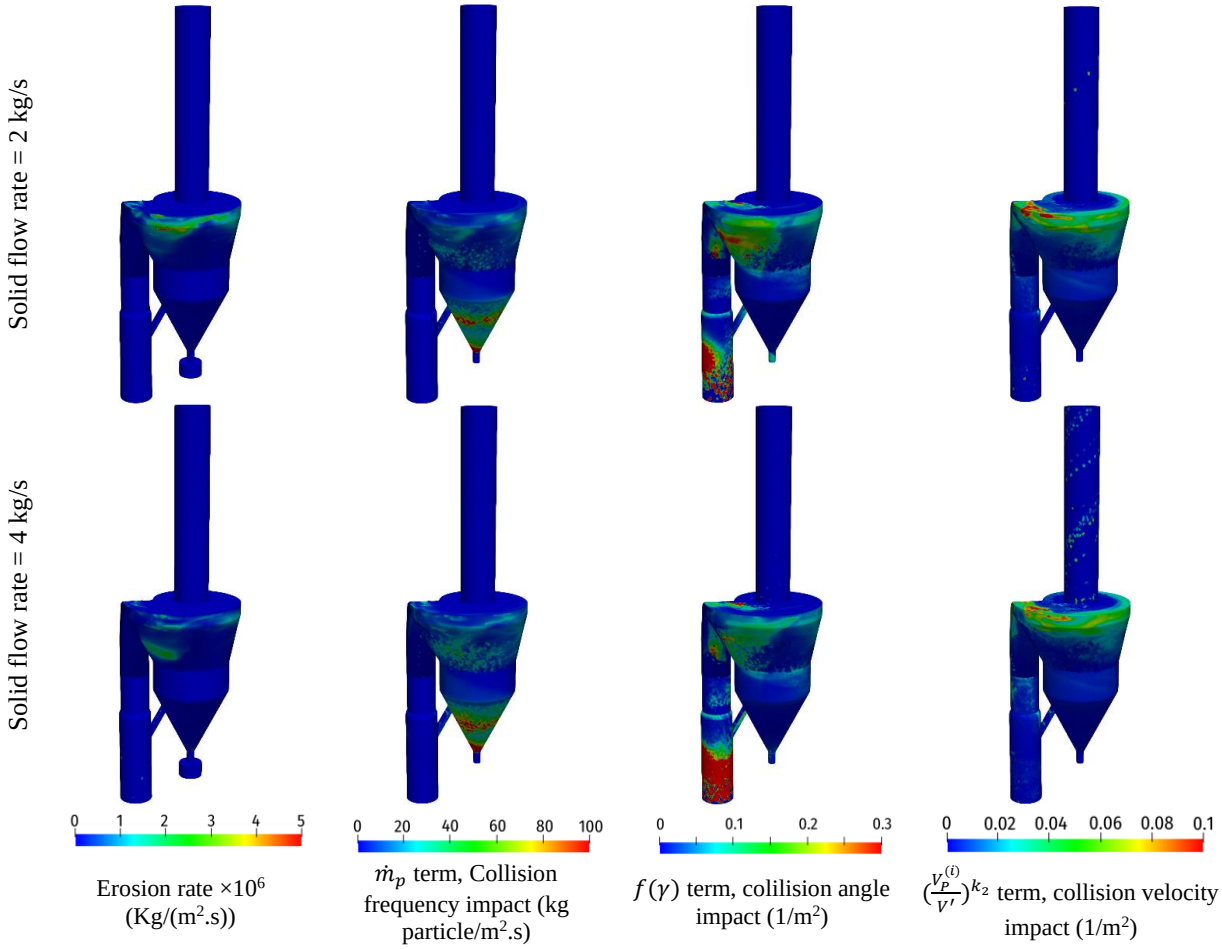

Figure 7-12. Effect of solid flow rate on collision frequency impact, collision angle impact, and collision velocity impact in erosion modeling normalized by surface area

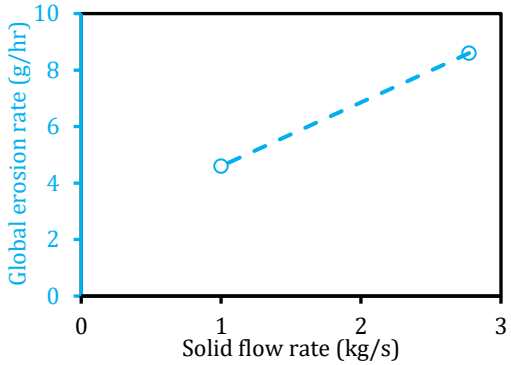

Figure 7-13. Effect of solid flow rate on global erosion rate under iso-thermal and ambient conditions: gas and particle temperature of 300 K and gas flow rate of 4.5 kg/s.

The relation between solid flow rate and time-to-failure does not seem straightforward as the effect of solid flow rate on the flow pattern and on how particles are concentrated in localized areas are complicated. The predicted location of the failure is different for different solid flow rates. In the studied range, up to 2.8 kg/s, the failure is located around point 2 in Figure 7-10 for the solid flow rate of 3.5 kg/s, it is located around point 3 and for the solid flow rate of 4 kg/s it is located around point 4.

A reduction in the pressure drop when the solid load is increased can be observed in Figure 7-11 (b). This reduction is due to the dampening of swirling motion caused by the presence of more particles and consequently lower loss of dynamic pressure in the vortex finder [1] as well as the reduction in the gas temperature due to increased solid load and consequently higher density and lower gas velocity. Like the effect of gas flow rate, when the solid flow rate increases an increase in heat transfer rate is observed.

7.5.3.3 Effect of gas inlet temperature

The effect of gas inlet temperature on the performance of the cyclone preheater was also investigated. It should be noted that in all these cases, gas mass flow rate and other operating conditions are kept fixed. The results are presented in Figure 7-14. An increase in gas inlet temperature leads to lower density and therefore higher gas velocity. This will result in stronger swirling motion in the cyclone and as a result, particles will impact the wall with higher velocity, resulting in higher erosion rates. Higher erosion rates driven by an elevation in the gas inlet temperature will naturally cause shorter time-to-failure. For the gas inlet temperatures of 800 K, 900-1400 K, and 1800 K, the predicted failure points are, respectively, located around points 4, 2, and 3 indicated in Figure 7-10.

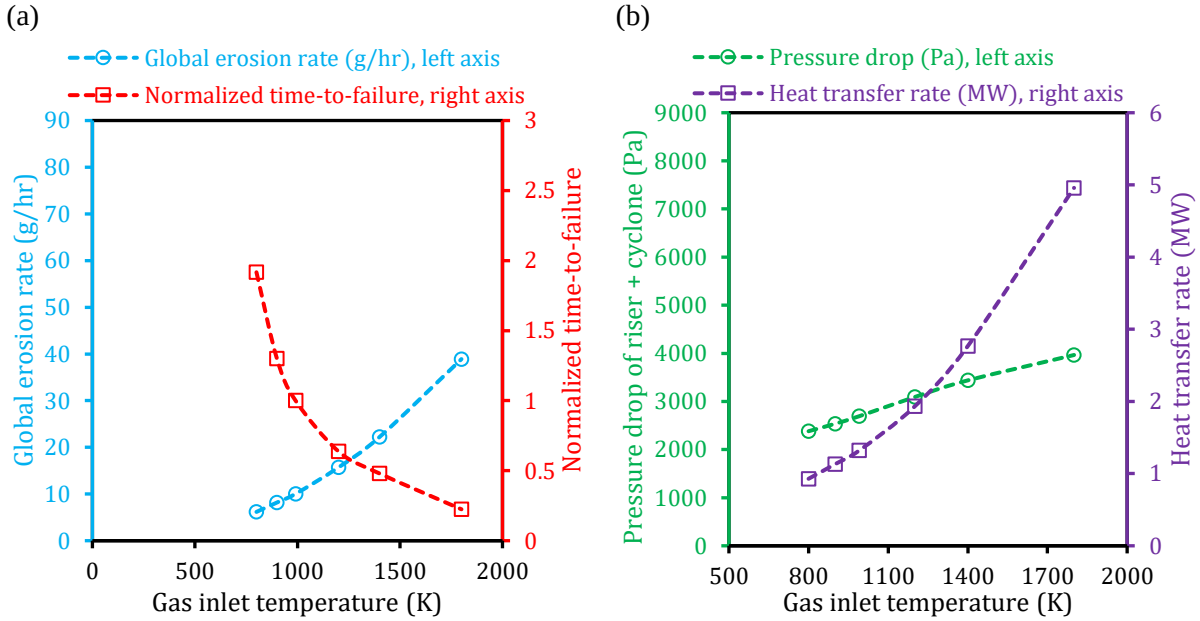

Figure 7-14. Effect of gas inlet temperature on (a) erosion and (b) pressure drop and heat transfer rate.

It should be noted that in the present study, the effect of particle temperature on its hardness has not been included. Regarding natural rock materials in the present study, it is reported to be softened considerably over 1100 K, therefore, the trend presented in Figure 7-14 (a) is only valid below 1100 K in the present case.

Decoupled terms of the erosion model are presented in Figure 7-15 for two gas inlet temperatures. As can be observed, although an increase in gas inlet temperature does not lead to a considerably different particle-wall collision frequency or collision angle, the collision velocity is increased considerably in the main cyclone body which contributes to a considerable increase in the on global erosion rate.

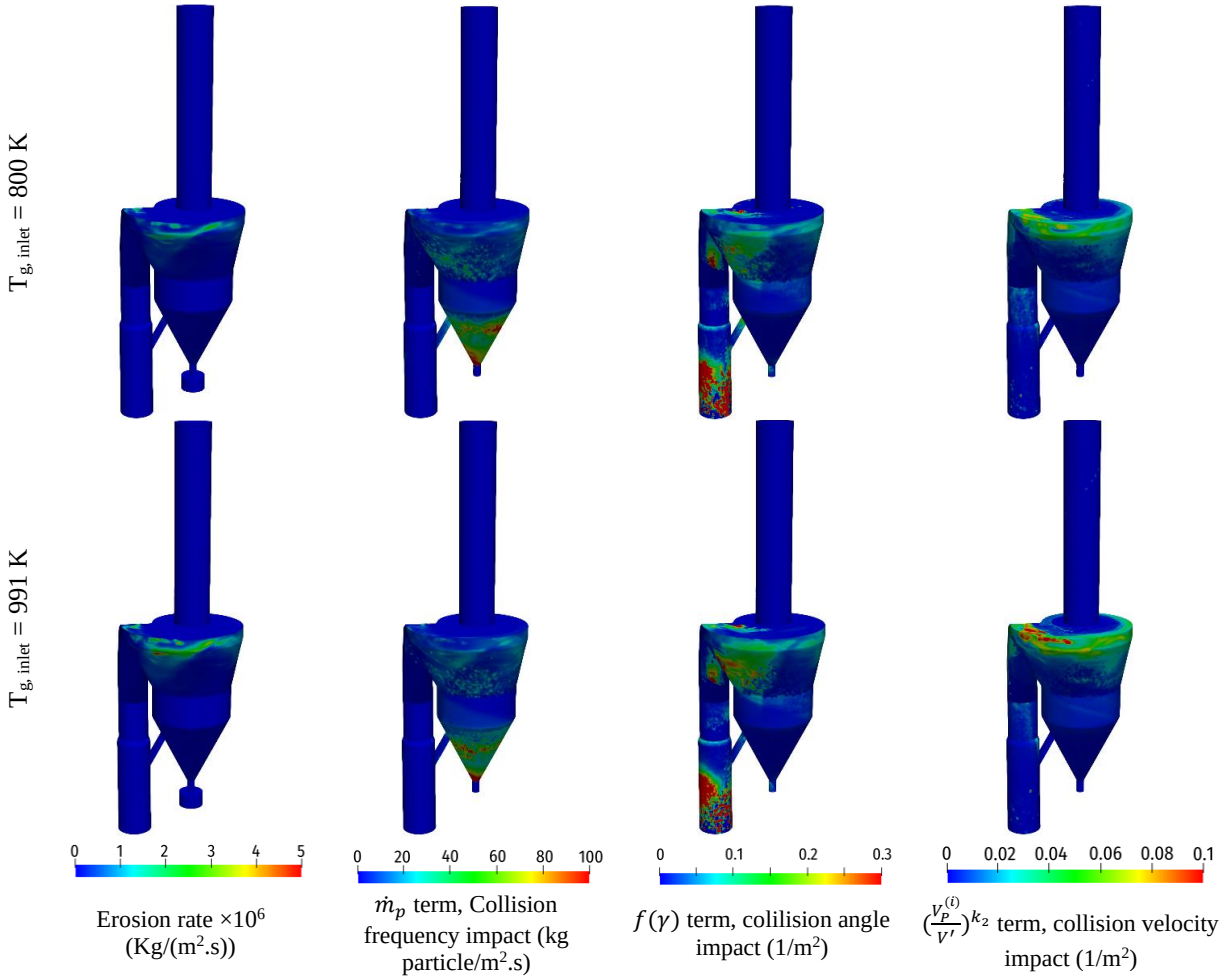

Figure 7-15. Effect of gas inlet temperature on collision frequency impact, collision angle impact, and collision velocity impact in erosion modeling normalized by surface area

According to Figure 7-14 (b), as the gas inlet temperature rises, a considerable increase in pressure drop occurs. At a higher temperature, gas velocity increases, resulting in higher friction at the walls despite a lower density, which results in a greater pressure drop. Additionally, as shown in Figure 7-14 (b), the heat transfer rate is directly and strongly dependent on the gas inlet temperature.

7.5.3.4 Effect of particle size

The influence of particle size on the performance of the cyclone preheater is presented in Figure 7-16. Five cases with different Sauter mean diameters were simulated. In all cases, four particle size classes were included, and each particle class had the same mass fraction (0.25). Particle sizes in each case are summarized in Table 7-5. As presented in Figure 7-16 (a), the effect of particle size on the global erosion

rate is minor which makes sense considering the low value of k_3 (0.19) in the Oka erosion model (equation 7–3).

Table 7-5. Summary of five simulation cases to study the effect of particle size

Case name	Particle sizes (µm)	Mass fraction
D_{32}=100 µm	53	1/4
	67	1/4
	200	1/4
	798	1/4
D_{32}=375 µm	200	1/4
	250	1/4
	750	1/4
	3000	1/4
D_{32}=500 µm	267	1/4
	333	1/4
	1000	1/4
	4001	1/4
D_{32}=600 µm	320	1/4
	400	1/4
	1200	1/4
	4799	1/4
D_{32}=1000 µm	427	1/4
	533	1/4
	1600	1/4
	6399	1/4

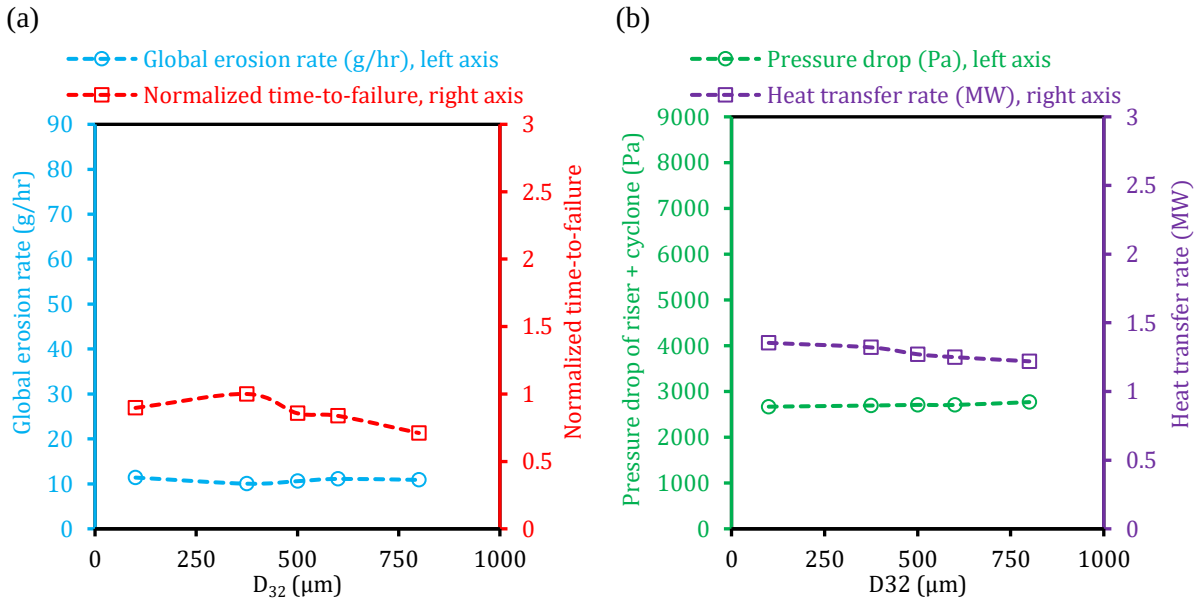

Figure 7-16. Effect of particle size on (a) erosion and (b) pressure drop and heat transfer rate.

Decoupled terms of the erosion model are presented in Figure 7-17 for two cases with considerably different D_{32} (100 and 600 µm). In general, based on the erosion model, if all other parameters are kept constant, an increase in the particle size leads to an increase in the erosion rate. As can be observed in Figure 7-17, having larger particles leads to more frequent particle-wall collisions, due to the higher inertia of particles. However, this more frequent collision of larger particles (that are more erosive than finer particles) is to

some level compensated by the fact that larger particles have considerably lower collision velocity (it takes longer for larger particles to reach gas velocity) and less erosive collision angle in the cyclone main body. This compensating effect makes the impact of the particle size on the global erosion rate to be predicted as minor.

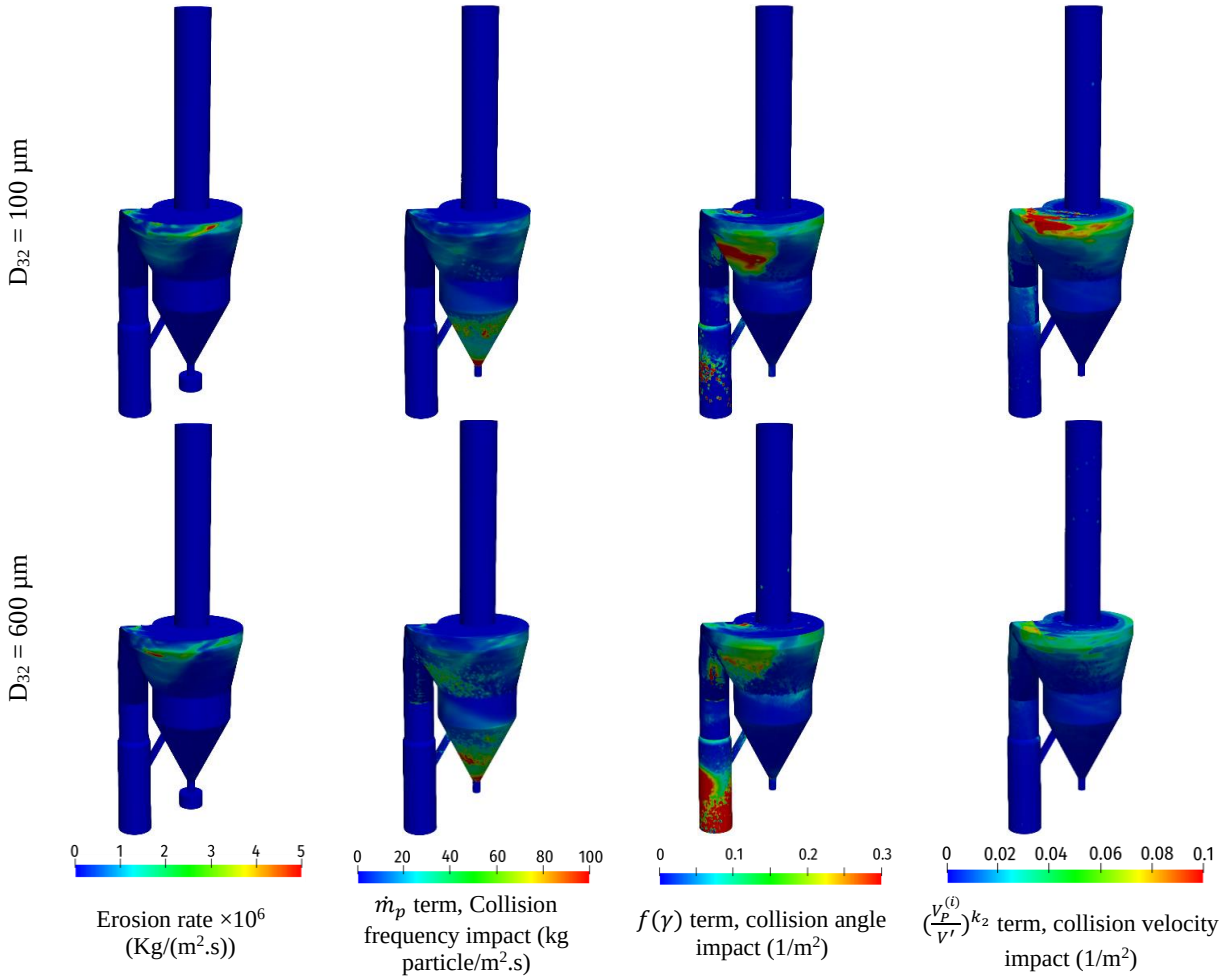

Figure 7-17. Effect of particle size on collision frequency impact, collision angle impact, and collision velocity impact in erosion modeling normalized by surface area

The failure is located around point 2 in Figure 7-10 for all studied cases except for the one with Sauter mean diameter of 100 µm which is located around point 3. As shown in Figure 7-16 (a) the impact of particle size on the heat transfer rate and pressure drop is also minor. A slight increase in pressure drop and a slight reduction in heat transfer rate is observed when larger particles are injected. As expected, large particles are heated up more slowly. Larger particles experience a lower heat transfer rate and have a smaller specific surface area. Therefore, they experience a lower local heat exchange rate which results in a lower overall heat transfer rate.

7.5.3.5 Effect of particle and wall hardness

The erosion predictions presented so far were based on the assumption of the particle Vickers hardness of 9 GPa and wall Vickers hardness of 18 GPa and using these values to obtain the constants of the Oka

erosion model by interpolations of data reported in the erosion model reference paper [135,136]. However, these Vickers hardness values are uncertain for the following reasons:

1. The particles are a mixture of several natural rock materials [30] and each might have a different hardness.
2. The Vickers hardness of each particle material was not measured either in the literature or in the present study. The Mohs hardness numbers were reported in the literature [234], and these values were converted by available rough approximation [235] to Vickers hardness. These approximations provided a range [8.8-10.8 GPa] for the Vickers hardness of particles and the value of 9 GPa was chosen in this range.
3. The Vickers hardness of refractory wall material was not measured. The Mohs hardness of similar material is reported in the literature [234]. The approximations provided a range [18-24 GPa] for the Vickers hardness of refractory wall material and the value of 18 GPa was chosen in this range.

Considering these uncertainties, two sensitivity analyses were performed to see how the global erosion rate and time-to-failure are affected by the hardness of particles and refractory material. Each set of particle and wall hardness results in different values of constants in the Oka erosion model based on the interpolations. The values obtained for the set of hardness values studied in these sensitivity analyses are summarized in Table 7-6.

Table 7-6. Summary of constants in the Oka erosion model used in the parametric study of particle and wall hardness

	Case	Hv_p GPa	Hv_s GPa	$E_{90} \times 10^5$ kg/kg	k_2	n_1	n_2
Sensitivity on particle hardness	Hv_p-2	7	**18**	2.52	2.12	6.7	0.05
	Hv_p -1	8	**18**	2.77	2.22	5.6	0.05
	Base-case	9	**18**	3.00	2.30	4.7	0.06
	Hv_p +1	10	**18**	3.22	2.39	4	0.07
	Hv_p +2	11	**18**	3.44	2.46	3.5	0.07
Sensitivity on wall hardness	Hv_w -4	**9**	14	3.48	2.30	4.3	0.08
	Hv_w -2	**9**	16	3.22	2.30	4.5	0.07
	Base-case	**9**	18	3.00	2.30	4.7	0.06
	Hv_w +2	**9**	22	2.82	2.31	4.9	0.05
	Hv_w +4	**9**	24	2.66	2.31	5.0	0.05

The results of the parametric study of particle and wall hardness are presented in Figure 7-18. As expected, the global erosion rate and time-to-failure are highly dependent on the hardness of particles and the wall. As can be observed, the dependence on particle hardness is stronger. By comparing the erosion patterns obtained using different sets of hardness values, presented in Figure 7-19, it can be seen that they all predict similar erosion patterns although the global erosion rates are different. Therefore, although accurate measurement of particle and wall hardness might help to obtain a more accurate prediction of erosion rate, approximate values can provide valuable information on the erosion pattern which is sufficient in most erosion investigations.

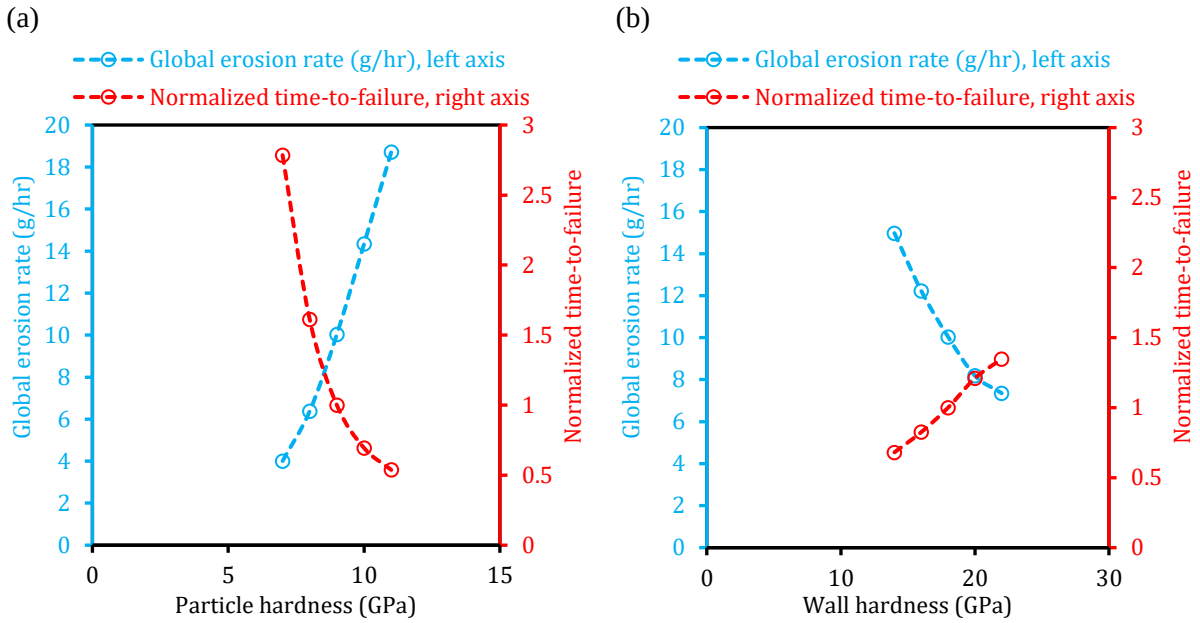

Figure 7-18. Effect of (a) particle hardness and (b) wall hardness on erosion

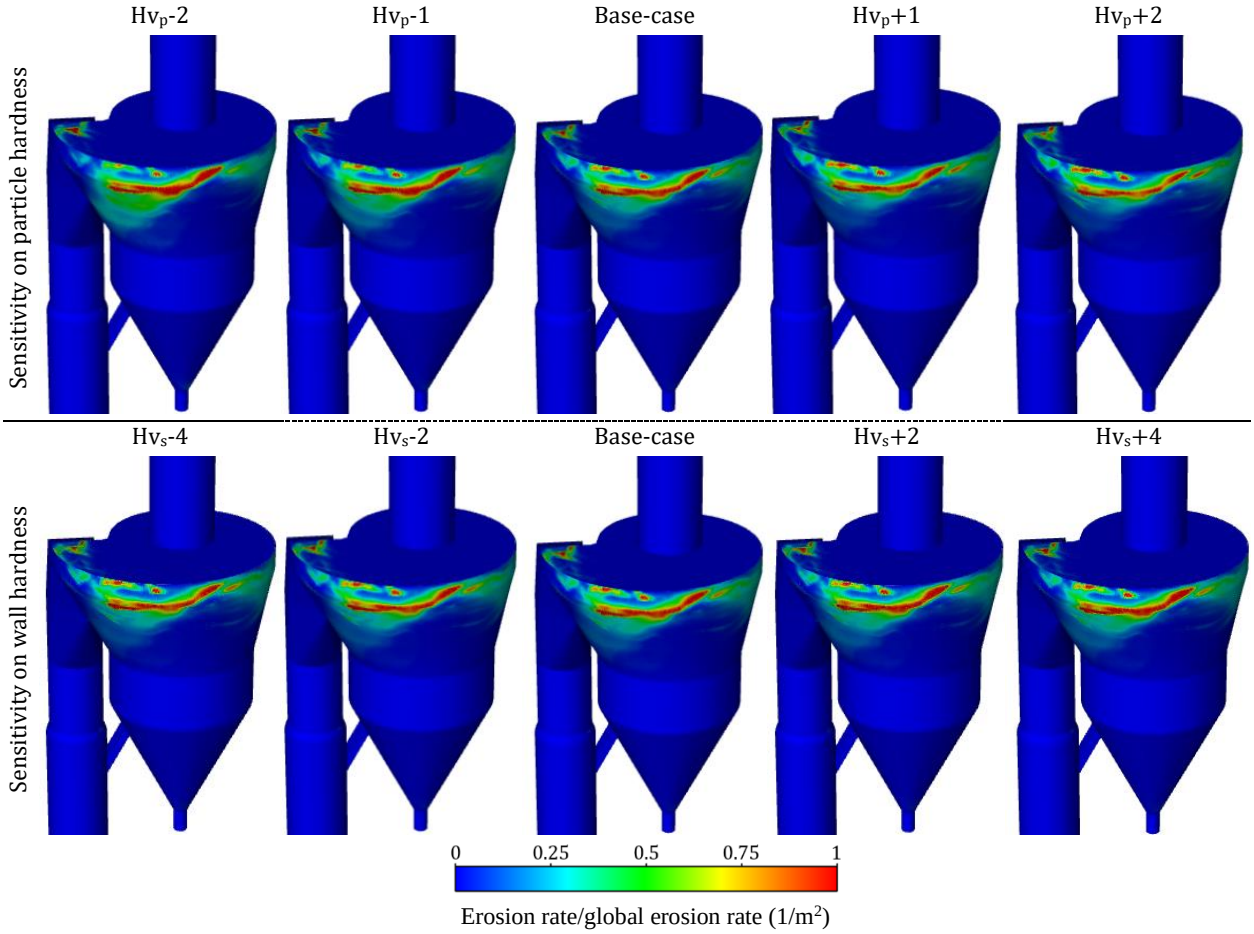

Figure 7-19. Comparison of erosion pattern obtained from tested sets of particle and wall hardness

7.6 Conclusions

Erosion investigation in a highly loaded industrial cyclone preheater was done by coupling the Oka erosion model with the hybrid Dense Discrete Phase Model, DDPM, and including gas-solid heat exchange. In addition to valid predictions of flow patterns, the developed model was able to provide reasonable predictions of erosion patterns. Locations with severe erosion obtained from the model were compared to the detected erosion during the inspection of an industrial cyclone preheater and qualitative agreement was obtained. Parametric studies on gas and solid flow rates, particle size distribution, gas inlet temperature, and particle and wall hardness were performed by which the following can be concluded:

- With the developed CFD model, the Oka erosion model [135,136] provides a reliable tool for erosion investigation in highly loaded cyclones. It is especially useful for predicting erosion patterns and areas where erosion is more severe. However, if a more accurate prediction of erosion rate is needed, accurate measurements of particle and wall material properties (hardness) in addition to the tuning of constants in the erosion model are required.
- Regarding the studied operating condition, erosion in the cyclone preheater is strongly dependent on the gas flow rate and gas inlet temperature (if the hardness of particles is not affected by the temperature). However, the effects of solid flow rate and particle size on erosion are minor. The relation of erosion with gas flow rate and inlet temperature is direct and is mainly driven by the change in the particle-wall collision velocity.
- Although an increase in solid flow rate leads to a considerably more frequent particle-wall collision (based on the present model which does not account for particle shielding), it is offset by a slightly less erosive collision angle and considerably lower collision velocity in the cyclone main body. With this compensation, the solid flow rate is predicted to have a minor effect on the global erosion rate.
- While having larger particles results in more frequent particle-wall collisions, this is somewhat offset by the fact that larger particles have lower collision velocities and less erosive collision angles in the cyclone's main body. As a result of this compensation, particle size has only a minor impact on global erosion rates.
- Although the global erosion rate is controlled by the hardness of particles and the wall, it was shown that the erosion pattern is not notably influenced by the hardness values.

8 Conclusions and future work

8.1 Conclusions

To optimize, redesign, and analyze industrial cyclone preheaters as vital components in the cement and stone wool production industries and to have a better picture of the phenomena occurring inside them a reliable CFD tool is required which is missing. Therefore, the main goal of the PhD project was to develop a comprehensive and validated CFD model for simulation of industrial cyclone preheaters, which are the essential components in several industrial processes such as cement and stone wool production.

As the first step, a comprehensive literature survey was conducted to choose an appropriate set of models including multiphase model, turbulence model, etc. It was concluded that accounting for particle-particle interaction (four-way coupling) is necessary. A relatively novel hybrid Eulerian–Lagrangian multiphase model known as the Dense Discrete Phase Model (DDPM), in Ansys Fluent, with relatively cheap computational cost and ability to handle polydispersity of particles, appears promising. Furthermore, Eddy Viscosity Models (EVMs) sensitized to rotation and curvature and Reynolds Stress Model (RSM) turbulence models seem to be good options. After selecting potential models, the project was divided into three phases which have been investigated in the following order:

8.1.1 Investigation of multiphase flow in iso-thermal highly loaded cyclones

In the first phase, the study started with the simulation of an iso-thermal, lab-scale cyclone with high loading of relatively large particles (2 mm) at ambient conditions. DDPM coupled with RSM and an EVM (k-ω sst sensitized to rotation and curvature) were implemented to evaluate the validity against available experimental measurements of pressure drop. This investigation showed that the DDPM model provides reasonable predictions of highly loaded cyclones in terms of pressure drop. The predictions are of similar accuracy as those using a more expensive multiphase model (DEM). Furthermore, it was shown that, in addition to similar predictions of pressure drop, the two tested turbulence models (RSM and k-ω sst sensitized to rotation and curvature) predict similar and reasonable flow patterns. Considering the superiority of the EVMs in terms of computational cost and stability, the k-ω sst model sensitized to rotation and curvature is used for simulation of industrial-scale cyclones where the application of RSM might not be feasible.

To continue the first phase of the project, the developed model was used to simulate an iso-thermal, highly loaded pilot-scale (1.6 m in diameter) cement cyclone, present in the FLSmidth Dania research centre. The cyclone is fed with relatively fine particles (0.5-300 μm with a mean diameter around 5 μm). Due to the instabilities of the RSM model and validated performance of the EVM model (k-ω sst sensitized to rotation and curvature) in the case of the lab-scale cyclone, DDPM coupled with the EVM model was used in this case. However, it was observed in preliminary simulations, that the model, at that state, highly underpredicted separation efficiency and overpredicted pressure drop, and therefore, the developed model needed to be modified. Compared to the case of the lab-scale cyclone modelling, this case is different in two major aspects: A large difference in the size of particles and relatively coarser grids which are inevitable in the simulation of large-scale cases. Therefore, two major modifications were investigated: (1) including a model to account for particle agglomeration regarding the fine size of particles (which are prone to the agglomeration), and (2) modifying drag calculation by using sub-grid drag models because of the relatively coarse size of grids. An agglomeration model based on a stochastic Lagrangian inter-particle collision and a sub-grid drag model were implemented into the model. It was shown that the agglomeration model significantly improves the predictions of both pressure drop and separation efficiency. On the other hand, the impact of using sub-grid drag modification was minor.

After the modifications, the model was successfully validated against the pilot-scale experimental data in terms of separation efficiency and pressure drop under different gas and solid flow rates. In addition, the model was able to capture the influence of changes in operating conditions observed in the experiments. For example, the important trend of improvement in separation efficiency when the solid load is increased was captured by the model. This study shows that in the case of fine particles involved, the inclusion of the agglomeration model for simulation of highly loaded cyclones is vital for accurate predictions of pressure drop and separation efficiency while using the sub-grid drag model only has minor improvement to the prediction of separation efficiency.

The performance of the developed model (DDPM coupled with agglomeration) is influenced by its sub-models, model parameters, and numerical parameters to various extents. The extent of influences was unknown and also there was a lack of guidance in the open literature for the proper choice of sub-models, model parameters, and numerical parameters. In addition, a list of questions needed to be answered: which EVMs are more suitable? There are several sub-models available for each term in solid stress modeling, which sub-models should be used? Are homogeneous drag models adequate or should sub-grid drag models be used? How does the extent of agglomeration affect the predictions? how do parameters such as particle-wall rebound coefficient, time step size, and coarse-graining ratio affect the predictions? To answer these questions and some others and to optimize the performance of the present CFD model, an extensive study was performed, by varying one sub-model or parameter at a time, and systematically assessing the effect on the results through comparisons with measured pressure drop and separation efficiency of the highly loaded pilot-scale cyclone.

Different options for particle-particle interaction modeling (based on the Kinetic Theory of Granular Flow, KTGF, which is employed in the DDPM), several EVM turbulence models, and several drag models (five homogeneous drag models and three heterogeneous drag models) have been evaluated. Moreover, the

particle-particle restitution coefficient (that affects particle agglomeration), and particle-wall rebound coefficient were studied. Several numerical parameters/schemes were investigated, including the discretization method, grain-to-particle size ratio, grid-to-parcel size ratio, and time step size. The investigation shows that the turbulence model and particle-particle restitution coefficient have the strongest influence on the performance of the model. Recommendations are given for a set of sub-models, model parameters, and numerical parameters providing the best prediction of the hydrodynamics of large-scale highly loaded cyclones.

8.1.2 Investigation of non-isothermal highly loaded industrial cyclone preheaters

In the second and third phases of the project, an industrial-scale (1.6 m in diameter) cyclone was simulated. This is a non-isothermal, highly loaded cyclone preheater, using relatively coarse particles, which operates at Integrate Melting Furnace (IMF) system of the ROCKWOOL A/S Doense factory producing insulation material.

In the second phase, heat transfer modeling was implemented to the CFD model developed in the first phase without the inclusion of the agglomeration model as coarse particles (50-3000 μm with a mean diameter of around 375 μm) are used. It was found that in the DDPM, to obtain an adequate energy balance in the system then two major considerations must be taken into account: (1) assigning one exclusive solid phase for each particle size class; (2) having fine enough parcel size. Regarding these two considerations, to keep the calculations as cheap as possible, two investigations were conducted: (1) investigation to find the minimum number of particle sizes required to adequately represent the actual PSD; (2) investigation to find the largest grain/parcel size providing independent results.

In this phase, the heat transfer implemented model was applied to simulate the industrial-scale cyclone preheater. The simulations were successfully validated with respect to the continuously monitored parameters such as the pressure drop and gas and particle exit temperatures, as well as the data from a measuring campaign, such as local gas velocity profiles and local gas temperature profiles under a few operating conditions. The results show that the model is sufficiently accurate to reflect the trends in performance parameters and flow patterns observed in the measurements when operating conditions are altered.

8.1.3 Investigation of erosion in an industrial cyclone preheater

In the third phase, erosion as a serious issue in some cyclones, such as the ones operating in ROCKWOOL A/S, was investigated by implementing a well-known erosion model. After testing the model against erosion measurements from a lab-scale cyclone reported in the literature, the erosion patterns in the industrial cyclone preheater were simulated. The results were qualitatively matched with inspections inside the cyclone preheater. Moreover, parametric studies on gas and solid flow rates, particle size distribution, and gas inlet temperature were carried out. Their impacts on erosion as well as pressure drop and heat transfer rate, which are considered key performance parameters, were assessed. The parametric study showed that erosion in the cyclone preheater is strongly dependent on the gas flow rate and the gas inlet temperature (if the hardness of particles is not affected by the temperature), while the effects of solid flow rate and particle size on erosion are minor.

In addition to these major investigations categorized in these three phases, a few related investigations were performed, which are summarized in appendix of the thesis.

In a nutshell, a comprehensive and validated CFD model for the simulation of highly loaded large-scale cyclones was developed using a commercial CFD solver (Ansys Fluent). The model is computationally affordable for industrial cases and provides reasonable predictions of important performance parameters of cyclone preheaters including pressure drop, separation efficiency, and heat transfer rate. In addition, the model is able to provide good predictions of the flow pattern and temperature profile, as well as reasonable erosion pattern by properly representing crucial present physical phenomena including turbulence, gas-particle interactions, particle-particle interactions, agglomeration, etc. Thus, it can be promising for the model to be used to guide engineers to troubleshoot, redesign, and optimize industrial cyclone preheaters.

In addition to these major investigations categorized in these three phases, a few related investigations were performed, which are summarized in appendix of the thesis.

8.2 Future work

Based on the study, the following activities are suggested to be conducted as future works:

1. Further validation of the developed model in an industrial-scale cyclone preheater in the cement industry

Cyclone preheaters (with diameters up to 8 m) larger than the ones investigated in the present study exist in industrial cement plants. From the industrial partners' point of view, it is important to show that the model is reliable for these larger industrial cement cyclones as well. Therefore, an industrial cement cyclone preheater (top cyclone in a 5-stage preheater tower of a cement plant) with a diameter of 6.6 m is planned to be investigated. Preliminary simulations have been done (reported in Appendix G), however further investigations and validations are required.

2. Further comparison between RSM and EVMs

In Chapter 3, these two turbulence models were compared regarding the prediction of pressure drop, but their performance in terms of predictions of separation efficiency as another important performance parameter of the cyclone was not investigated (particles present there were coarse (2 mm) which are not suitable for separation efficiency investigation). On the other hand, in the case presented in Chapter 4 where measurements of separation efficiency were available, simulation using RSM was not possible due to instabilities. Therefore, there is a need to further compare RSM and EVMs, in particular, in terms of predicting separation efficiency in either a lab-scale cyclone or a large-scale one.

3. Further validation of the developed model based on grade efficiency

So far, validation of the developed model was limited to overall separation efficiency since samples of separated and escaped particles and their PSDs were not available to validate the model based on grade efficiency (efficiency of each particle size). Therefore, grade efficiency measurements should be obtained to further validate the developed model.

4. Find a way to modify two-way coupling simulation for the case of fine particles

In Appendix C it was shown that in the case of coarse particles, the two-way coupling can work as well as DDPM, while in the case of fine particles where agglomeration plays a role, two-way coupling predictions are not acceptable. Resolving the problem of two-way coupling simulation in the case of fine particles is of importance as it is a computationally cheaper model than DDPM.

5. Improving energy coupling modeling in DDPM

In its current state, to have an adequate energy balance in the DDPM case with polydispersed particles, one exclusive solid phase must be assigned for each particle size class which makes the calculations significantly more expensive. Therefore, modifying energy coupling modeling in DDPM in a way that such a procedure can be avoided is important.

6. Measuring Vickers hardness of wall and particles

Although it was shown that the erosion pattern is not notably affected by the Vickers hardness of the wall and particles, such measurement and modifying constants in the erosion model accordingly facilitate a better prediction of the erosion rate.

7. Including radiation in heat transfer modeling

Although the temperature range of cyclone preheaters investigated in the present study (≤ 1000 K) is not in the range where radiation is important, cyclone preheaters also operate under higher temperatures where radiation might play a role. Therefore, to have a model accurate in the whole range, radiation should be included in heat transfer modeling to investigate its contribution to heat transfer.

8. Better capturing of shielding effect in erosion modeling in DDPM

Although in DDPM, the shielding effect is to some extent captured, it might be not fully resolved. Therefore, by developing a model to better account for the particle shielding effect, the effect of solid flow rate on erosion can probably be better investigated.

9. Modeling agglomeration breakage

A formed agglomerate may break due to collision with another particle or with the wall, or due to stresses imposed on the agglomerate, therefore, a model to account for agglomeration breakage might affect the predictions and should be investigated. The breakage phenomenon is quite complex, involving the properties such as the strength of particles/agglomerates, which are not available, especially for agglomerates.

10. Using DEM to find out whether particle-particle interaction forces play a role or not

In Chapter 5, it was observed that when using DDPM, excluding particle-particle interaction forces which are modeled based on KTGF would not affect the predictions notably, concluding that, at least in DDPM, particle-particle interaction forces do not play an important role. To further investigate whether particle-

particle interaction forces play a role or not, it is suggested to evaluate it using a multiphase model with higher resolution (DEM which directly resolves particle-particle interaction forces).

Appendix A

Supplementary Materials for Chapter 3

In the simulation of the lab-scale, highly-loaded cyclone using DDPM coupled with RSM and k-ω sst-cc turbulence model, several challenges were faced which were overcome by special treatments and procedures. Some of these challenges and the way how they were overcome are addressed in this appendix (A.1). In addition, velocity fluctuations obtained from two turbulence models used in Chapter 3 are presented in this appendix (A.2).

A.1 Challenges in the implementation of DDPM in a lab-scale cyclone

A.1.1 Convergence issue using RSM:

RSM is an unstable turbulence model, so coupling it with DDPM might lead to convergence issues. In preliminary cases, when using RSM, the turbulence viscosity ratio in the domain would raise leading to the divergence of the solution. A combination of the following treatments helped to solve the issue:

- Improving mesh quality: RSM is very sensitive to mesh quality; even a few low-quality cells might lead to divergence. It was observed that high turbulence viscosity ratio (which can be considered as a sign of the start of divergence) is observed where mesh quality (skewness in particular) is low. Highly skewed cells were located where the tangential inlet is connected to the cylindrical body leading to skewed cells with low angles. By making several cuts in the blocks of the ICEM meshing tool in that region, low angles of blocks were avoided leading to improvement in mesh skewness and overall quality and consequently improvement in solution stability of the RSM turbulence model.
- Starting RSM simulation with a converged solution of k-ω sst-cc: initializing cases using RSM with inlet values might lead to divergence at the beginning of the solution. However, initializing the simulation with a converged solution of k-ω sst cc not only helps to avoid such divergence but also leads to achieving a converged solution of the RSM case in a shorter flow time.

Starting simulation with the k-ε turbulence model or lower-order discretization methods or low under-relaxation factors are other ways to improve the stability of the RSM turbulence model but it did not help

significantly in the present case. In addition, specifying unrealistic turbulent boundary conditions at inlets might also lead to divergence in the RSM simulations. To avoid such unrealistic turbulent boundary conditions, it should be specified by using reasonable turbulent intensities (below 10%) and the correct hydraulic diameter of the inlet.

A.1.2 Parcel size

In preliminary simulations, there were parcels (as representative of several particles with the same properties) greater than the size of the cells which would lead to divergence because we could have cells with zero volume fraction which makes trouble for solving conservation equations. To avoid such an issue, we have to ensure all parcels are smaller than the smallest cell. To do so, the minimum volume of cells should be found, and then the parcel mass or diameter is specified so that parcels are smaller than the size of the smallest cells. In all simulations in the present study parcel volumes were smaller than half of the smallest cell volume. Although in theory parcels must be just smaller than cells size ($V_{parcell}/V_{cell}<1$), our observation shows that a value close to 1 (for example $V_{parcell}/V_{cell} = 0.9$) makes convergence problem for the solution, so it is advised to have parcels as small as possible. A large parcel leads to an unrealistic and high load of a DPM source in a cell causing the convergence issue for the solution. Smaller parcels lead to better convergence by spreading the load of a DPM source. However, it also leads to having more parcels in the domain making particle tracking slower, so a balance should be considered; although very small parcels improve convergence by spreading DPM sources in more cells, the number of parcels in the domain should be chosen carefully to be matched with available computational resources.

A.1.3 High local solid volume fraction

Having local high solid volume fractions (close to the packing limit) might lead to convergence issues. Although this did not occur in our final simulations, this issue can be overcome by increasing the transition factor in the multiphase model (the default value which worked fine in the present work is 0.75, but when high local solid volume fraction causes an issue increasing to 1 or even 1.2 might solve the problem).

A.1.4 Particles remaining in the domain

An issue that might occur is that contrary to what is expected in cyclones that particles close to the wall (at least heavier particles) should have a downward axial velocity making them be separated from the bottom, it was observed that particles (which are comparatively heavy in the present study) only swirl in the cylindrical body without any downward axial velocity, and the mass of particles inside cyclone main body increases constantly. This issue can be solved by adjusting the particle-wall restitution coefficient to reasonable values. Decreasing both normal and tangential restitution coefficients from 1 to 0.8 solved the issue.

A.1.5 Choosing a suitable time step size

Two considerations should be regarded for choosing a suitable time step size. First, it must be ensured that transient phenomena occurring inside cyclones are captured properly. In lab-scale, ordinary cyclones, it is believed that time steps below 1e-3 s can ensure such a happening [10,13,55]. Second, like most other CFD simulations time step should be chosen so that the solution would converge (enough drop in residuals) at

each time step within a reasonable number of iterations (10-20 iterations is an ideal number of iterations leading to faster flow time progress). Both considerations were taken in the present study. Using significantly larger time steps would lead to loss of convergence at each time step and then divergence and using significantly smaller time steps would lead to too slow simulation.

A.1.6 Choosing appropriate solution methods

Various combinations of different solution methods were tested and eventually, the ones mentioned were chosen. Two criteria were considered: solution accuracy and stability. The second-order discretization method was chosen for momentum, volume fraction and turbulence equations to have higher accuracy. For the pressure, the PRESTO! discretization method which is more accurate and stable in swirling flows is chosen [147]. The pressure velocity coupling method and gradient discretization method were chosen for their superiority in terms of stability.

A.1.7 Near wall treatment

When using RSM, enhanced wall treatment was chosen because this method can work quite well in a wide range of y^+ values. In meshing, the first cell height was kept constant in the whole domain, but since in cyclones, flow velocity in near-wall, in different regions (inlet, cylindrical body, conical body, etc.), is different, a wide range of y+ value is observed in the whole domain, so a treatment method that works quite well in the wide range should be chosen. The Enhanced Wall Treatment is specially designed so that one will get a good representation of the boundary layer, whether $30 < y^+ < 300$ or $y^+ \leq 1$. In the former case, the analytic wall functions are used and, in the latter, the boundary layer is fully resolved. It also should give acceptable results for $2 < y^+ < 30$, although this is not an ideal choice. So, when using enhanced wall treatment, it should only be ensured that the y^+ value is below 300 [147].

On the other hand, when using the k-ω sst-cc turbulence model, although there is not any option to choose for near-wall treatment, the strategy Ansys Fluent uses will get a good representation of the boundary layer if the y^+ value is below 300. So, when using k-ω sst-cc, it should only be ensured that the y^+ value is below 300 to have reasonable near-wall treatment.

A.1.8 Particle tracking

By default, in Ansys Fluent, the impacts of a particle on the fluid are applied only to the cells that intersect with the trajectory of that particle. However, there is an alternative approach called “Node Based Averaging” which distributes the impacts of a particle into also neighboring cells. In the present study, this alternative method is used which helps to stabilize the solution since each parcel’s effects on the flow solver are distributed more smoothly across cells. Moreover, this smoother distribution allows a reduction of grid dependency of simulations. Also, using an implicit tracking scheme for integrating the particle motion equation which is known to be unconditionally stable for all particle relaxation times improved solution stability. To ensure that none of the particle trajectories is incomplete, an excessively large number as the maximum number of time steps used to compute particle trajectories via integration of particle motion equation should be specified.

A.2 Velocity fluctuations obtained from two turbulence models

Particle motion in cyclones reflects the competition between the motion of particles to the outer wall of the cyclone due to centrifugal force (due to mean tangential velocity), and the motion of particles due to the presence of velocity fluctuations (this motion is known as turbulent dispersion) that disperses the particle throughout the entire volume. Therefore, the prediction of velocity fluctuations is important. RANS turbulence models only provide mean velocity values and RMS of velocity fluctuations, so to predict the dispersion of the particles due to the time-dependent turbulence fluctuations a model is required. In the present study, the DRW model is used. The fluid velocity in the particle tracking equation, which is the instantaneous velocity (u) includes both mean velocity ($\bar{u}$) and fluctuating velocity (u'). While mean velocity ($\bar{u}$) is directly calculated from the momentum equation, in the DRW turbulence dispersion model, the fluctuating velocity components (u') are modeled by discrete piecewise constant functions and RMS values, $\overline{u_i{}'u_i{}'}$, as follow:

$$u_i{}' = \xi\sqrt{\overline{u_i{}'u_i{}'}} \qquad 8\text{–}1$$

Therefore, in addition to the mean velocity ($\bar{u}$), reasonable predictions of RMS values of the velocity fluctuations are required for accurate prediction of particle motion. In the presented comparison of the two used turbulence models, it was observed that the k-ω sst-cc turbulence model provides quite similar distributions of mean velocities to the ones provided by RSM, but the RMS value of the velocity fluctuations obtained from both turbulence models should be compared as well as they affect particle motion based on the DRW model. Such comparison is done in Figure A-1 where profiles of RMS value of the velocity fluctuations (tangential $\sqrt{\overline{u'^2}}$, axial $\sqrt{\overline{w'^2}}$, and radial $\sqrt{\overline{v'^2}}$) at a specific height for different solid loading ratios are presented. It should be noted that in the k-ω sst-cc turbulence model RMS values of velocities are not calculated directly, however considering that this turbulence model assumes isotropy of turbulence whereby the normal stresses are equal (equation 8–2), and based on the definition of turbulence kinetic energy (equation 8–3), RMS of velocities are estimated (based on equation 8–4).

$$\overline{u'^2} = \overline{v'^2} = \overline{w'^2} \qquad 8\text{–}2$$

$$k = \frac{1}{2}\sqrt{\overline{u'^2} + \overline{v'^2} + \overline{w'^2}} \qquad 8\text{–}3$$

$$\sqrt{\overline{u'^2}} = \sqrt{\overline{v'^2}} = \sqrt{\overline{w'^2}} = \sqrt{\frac{2}{3}k} \qquad 8\text{–}4$$

A considerable discrepancy between values predicted by the two turbulence models can be observed. The k-ω sst-cc model assumes isotropic turbulence. As predicted by the more sophisticated turbulence model, RSM, this assumption seems to be erroneous; the RMS values of the velocity fluctuations predicted by RSM are not equal in each direction as observed in Figure A-1. However, in the near-wall region where, in cyclones, particles are concentrated and therefore prediction of RMS value of the velocity fluctuations is more important, the values in different directions obtained by RSM and the values obtained by k-ω sst-cc are relatively close. Whether this discrepancy is influential enough to affect particle motion and

consequently separation efficiency predictions in a cyclone, cannot be answered in this simulation case as only large particles are present which all are separated in any case.

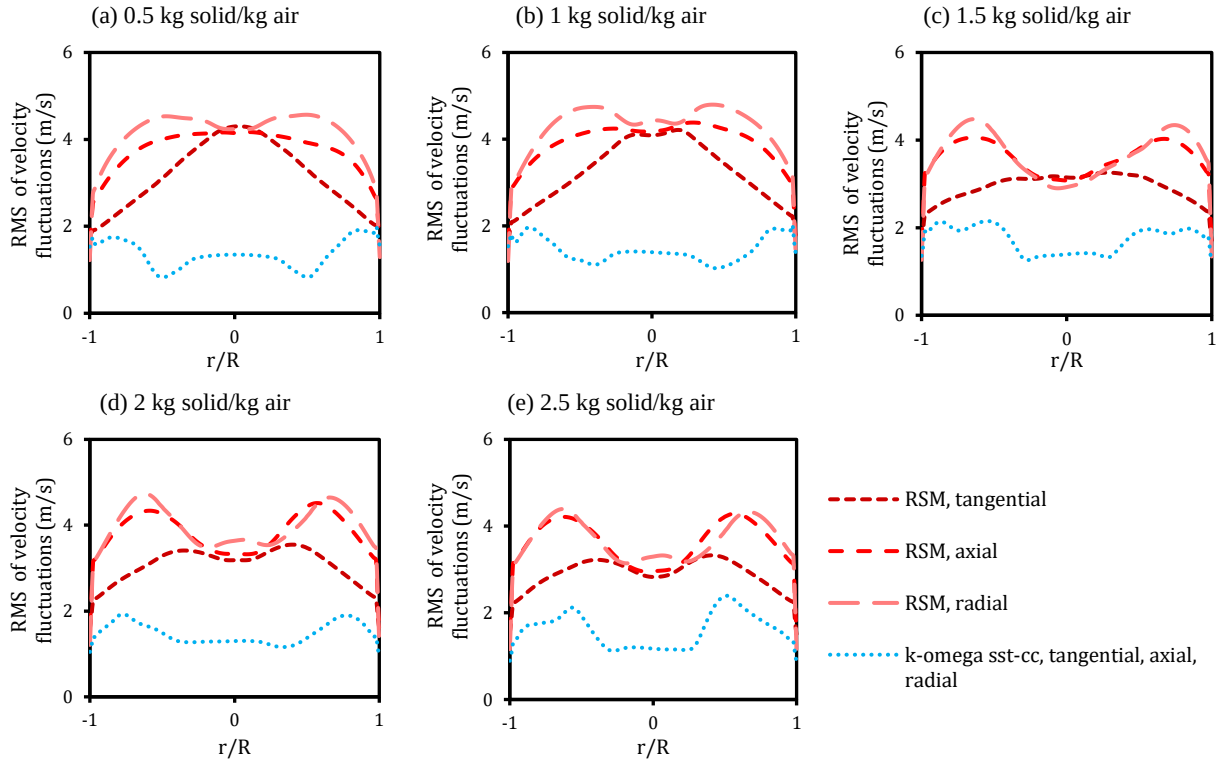

Figure A-1. Profiles of RMS value of the velocity fluctuations (tangential $\sqrt{\overline{u'^2}}$, axial $\sqrt{\overline{w'^2}}$, and radial $\sqrt{\overline{v'^2}}$) at a specific height (0.3 m away from the cyclone roof) evaluated for different solid loading ratios: (a) 0.5, (b) 1, (c) 1.5, (d) 2, and (e) 2.5 kg solid/kg air.

By increasing the solid load, the distribution of RMS values of velocity fluctuations (as representative of turbulence intensity) in the domain and also maximum values are affected. In general, a minor reduction in RMS values is observed as the load is increased (reduction in turbulence intensity), but this reduction is minor compared to the reduction in the tangential velocity caused by an increase in solid load.

Appendix B

Supplementary Materials for Chapter 4

Details of mesh generation, solver settings, solution strategy, and closure laws (for evaluation of the solid stress tensor required in DDPM) used in Chapter 4 are summarized in this appendix.

B.1 Mesh generation

Although discretizing a cyclone (or in general any other geometry) using structured mesh aligned with flow direction can minimize the numerical diffusion leading to more accurate results, in a study on the lab-scale cyclone it was shown that mesh-independent results of an unstructured mesh (polyhedral mesh with prism layer) can be almost as accurate as mesh-independent results of a structured mesh (hexahedral mesh). Considering this and the relative complexity of the pilot-scale and industrial-scale cyclone geometries, discretizing such geometries using unstructured mesh is favored. Moreover, since the ultimate goal of this project is to provide a CFD tool for industries using cyclones, an unstructured mesh that can be made more straightforwardly further encouraged us to use unstructured mesh to discretize the geometry.

Regarding the reliable performance of polyhedral mesh in the simulation of the small-scale cyclone, such a grid (polyhedral with several prism (polygonal prism) layers on the walls) was used to discretize the pilot-scale cyclone studied in the present work. An overview of the grids made is shown in Figure B-1. To perform a mesh independency study, the geometry was discretized with various numbers of cells (0.5, 1.1, 1.7, 2.9, 4.2, 5.5, and 7.5 million cells). To ensure good quality of grids, the minimum orthogonality of cells was kept above 0.15 in all cases. It should be noted that considering the limitation of the model in handling parcels larger than cells size (leading to divergence in solution), minimum cell volume should be and was checked to not be very small which in turn would force us to have very fine parcels to avoid divergence leading to more computational expensive simulations.

In all cases, 10 layers of prism layers with a first cell height of 1 mm were made on walls to ensure accurate modeling of the near-wall region which is of great importance in cyclones. y plus values on all walls were tracked during simulation to ensure they are in the acceptable range of the used wall treatment model (the turbulence model used in the present study is valid as long as the y plus values are below 300; based on the value of y plus this turbulence model automatically switches between fully resolving viscous sublayer,

using wall function, or using a smooth blending between the first two to ensure acceptable modeling of the boundary layer. However, $1 \leq y^{+} \leq 30$ should be avoided as much as possible for higher accuracy).

(a) (b)

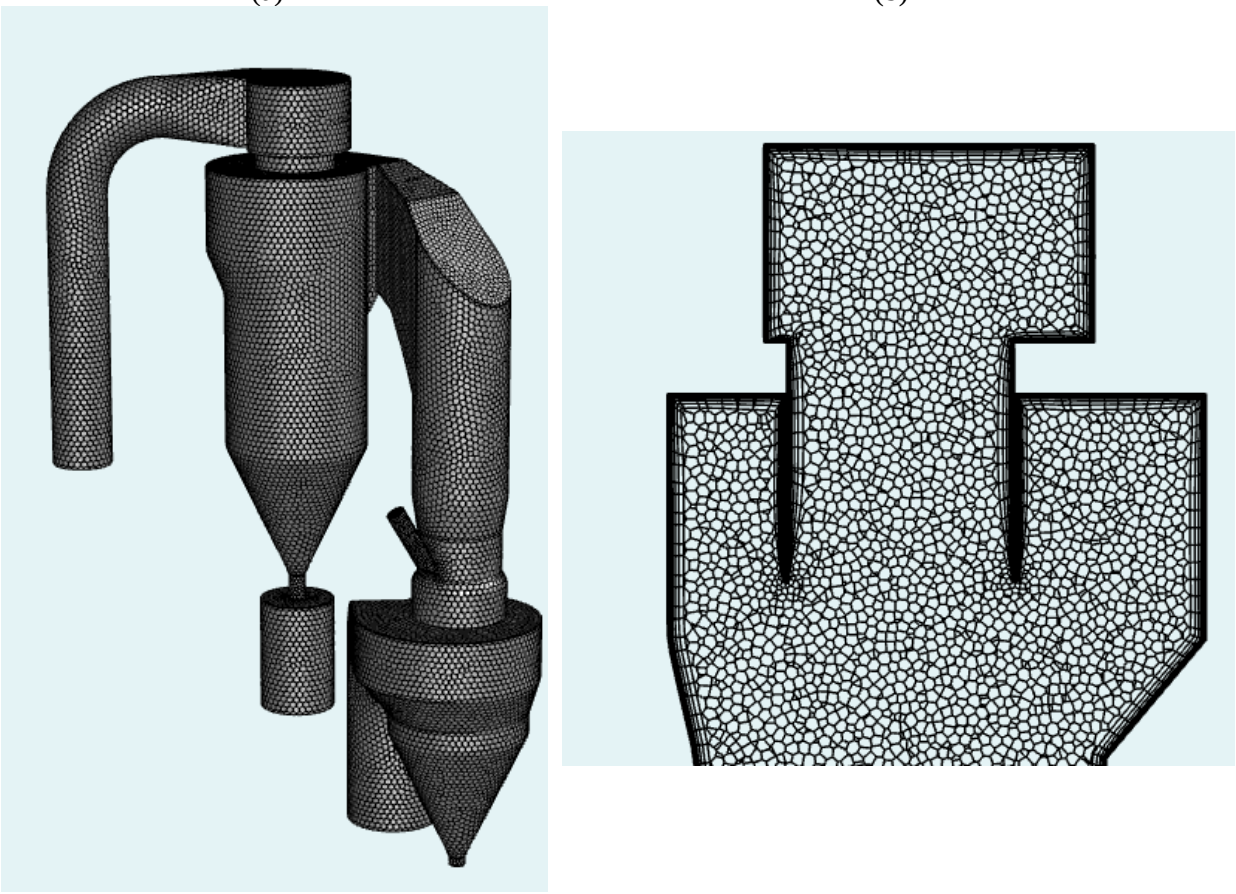

Figure B-1. (a) A 3D overview of CFD grids, and (b) a 2D overview of CFD grids in a cross-section of the geometry. The coarsest case with 0.5 million cells is shown because of the better visibility of the grids.

B.2 Solver settings and Solution strategy

In the present study, simulations were done by using the pressure-based solver in Ansys Fluent 2019R3 using the finite volume method in the Eulerian framework, while the parcels were tracked in a Lagrangian framework using an implicit tracking scheme. A phase-coupled SIMPLE algorithm was applied for pressure–velocity coupling. The gradient was discretized with the least-squares cell-based method, the momentum, turbulent kinetic energy and dissipation rate were discretized using the second-order upwind, and the volume fraction was treated with the QUIK scheme to minimize numerical diffusion and increase accuracy. The pressure was discretized using PRESTO! method for its superiority in the case of swirling motion. The convergence criteria for all equations were 1×10^{-3}. The simulations were performed in transient mode by automatically controlling the time step using the courant number (CFL) while temporal discretization was done using a first-order implicit scheme.

To facilitate the convergence, particle injections start when the single-phase (without particles) solution is converged, and then the simulation continues for at least 50 s. To ensure convergence, parameters such as

pressure drop, separation efficiency, velocities at several points, and mass of particles in the domain are tracked with flow time. The reported values in the present work are averaged values over the last 10 s of simulations.

B.3 Closure laws

To evaluate the solid stress tensor required in DDPM for modeling particle-particle interactions, the model uses several closure law equations based on the KTGF to estimate some required parameters such as bulk, collisional, kinetic and frictional viscosities. Those used in the present study are summarized in Table B-1.

Table B-1. Closure laws and parameters used for solid stress tensor dense discrete phase model based on KTGF

Modeled term or parameter	Closure model	Parameter value
Solid bulk viscosity, λ_s	Lun model	
Solid collisional viscosity, $\mu_{s,collisional}$	Gidaspow and Syamlal Model	
Solid kinetic viscosity, $\mu_{s,kinetic}$	Gidaspow model	
Solid frictional viscosity, $\mu_{s,frictional}$	Schaeffer model	
frictional pressure, $p_{frictional}$	KTGF-based	
Solid granular temperature, Θ_s	Algebraic	
Solid pressure, p_s	Lun model	
Radial distribution, $g_{0,ss}$	Lun model	
Transition factor		1
Friction packing limit, $\varepsilon_{s,max-fric}$		0.61
Packing limit, $\varepsilon_{s,max}$		0.63
particle-particle restitution coefficient, e_{ss}		0.7
The angle of internal friction, ϕ_s		30.0
Normal e_{nor} and tangential e_{tan} discrete phase particle-wall reflection coefficient		0.8
Solid-phase shear condition on walls	Specularity coefficient	1×10^{-6}

Appendix C

Comparison of two-way and four-way coupling CFD simulation

The multiphase model used in the present study, Dense Discrete Phase Model, is a four-way coupling model which in addition to gas-particle interactions, models particle-particle interactions using the KTGF model. However, in the sensitivity analysis done in Chapter 5, in particle-particle interaction force modeling, it was observed that particle-particle interaction force can be excluded without affecting the predictions considerably. This observation raised the idea that using two-way coupling might be sufficient and using four-way coupling is excessive and unnecessary in the present case. it should be noted that in addition to the inclusion or exclusion of particle-particle interaction force modeling, two-way and four-way coupling methods are also different in terms of their conservation equations where in the four-way coupling, the phase volume fraction is present in Navier–Stokes equations and in two-way coupling it is not.

To investigate this idea, for the two studied cases in the presented study (the case with finer particles presented in Chapters 4 and 5 and the case with larger particles presented in Chapters 6 and 7) two-way coupling simulations were done for specific operating conditions to be compared with four-way coupling (DDPM) simulation.

C.1 The case presented in Chapters 4 and 5 (cement cyclone)

In short, the case presented in Chapters 4 and 5, is a large-scale cyclone (Figure 4-1), operating under ambient temperature with relatively fine particles (see the PSD in Figure 4-2). As the particles are relatively fine agglomeration and its modeling plays an important role. It was shown in Chapter 4 that DDPM coupled with a stochastic agglomeration model and a sub-grid drag model can provide reasonable predictions of pressure drop and separation efficiency. It was also shown that the impact of agglomeration modeling is significant so that excluding it leads to unrealistic predictions. Here, DPM two-way coupling model is coupled with the same agglomeration and sub-grid drag models to be compared with four-way coupling (DDPM) predictions and experimental measurements for one specific operation condition (Case-2 in Table 4-1 of Chapter 4).

It is worth mentioning that considering the relatively high solid volume fraction in some locations of the domain, the solution of the DPM two-way coupling model is relatively unstable. To avoid divergence of the solution, a low value (0.01 or even lower) of under-relaxation factors for the particle source term is

required. Therefore, simulation must continue for a long enough time to ensure the particle source term is updated to its final value.

The comparison of four-way coupling (DDPM) with two-way DPM simulation, in this case, is presented in Figure C-1. In addition, the predictions are compared with experimental measurements and four-way coupling (DDPM) prediction without agglomeration modeling. As it can be observed, although 2-way coupling seems to be able to provide reasonable predictions of pressure drop, it highly underpredicts the separation efficiency.

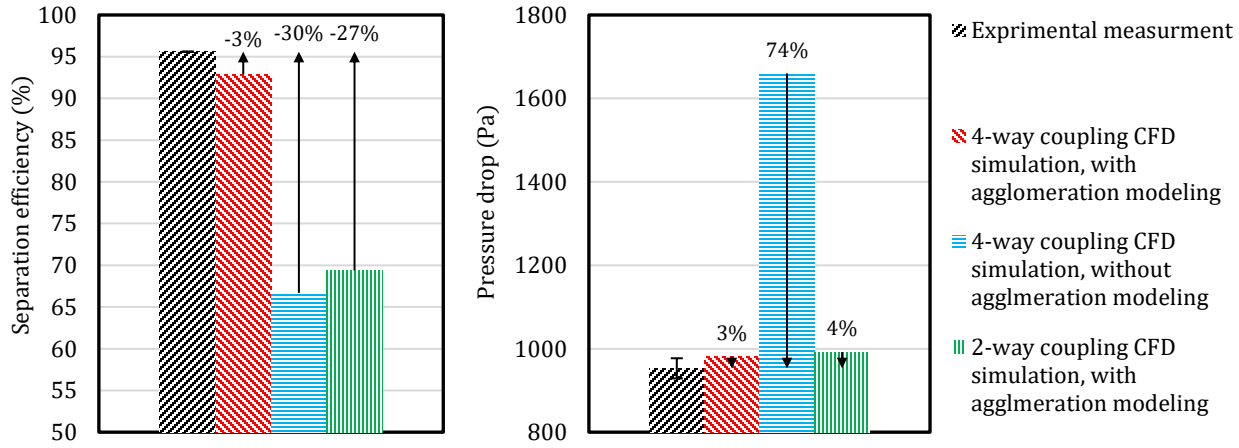

Figure C-1. Comparison among experimental measurement, four-way coupling with and without agglomeration modeling, and two-way coupling in terms of pressure drop and separation efficiency.

Since the separation efficiency prediction of two-way coupling is close to the four-way coupling (DDPM) prediction without agglomeration modeling, it was a sign that in the two-way coupling, agglomeration is not happening to a similar extent as in four-way coupling (DDPM). This can be better investigated by looking at the PSD of particles leaving the domain in the case of two-way coupling which is presented in Figure C-2 and compared with the case of four-way coupling (DDPM). it is clear that although agglomeration occurs in the case of two-way coupling (as particles leaving the domain are larger than the ones injected), the extent of agglomeration is significantly lower than in the case of four-way coupling (DDPM) and that is why separation efficiency is underpredicted.

It was shown in Figure 4-18 that at least in the case of four-way coupling (DDPM), agglomeration is mostly occurring in the injection pipe. Figure C-3 presents the comparison of the flow pattern in the injection pipe in the case of two-way coupling and the case of four-way coupling (DDPM). As it can be observed, unlike the case of four-way coupling (DDPM), in two-way coupling, the flow in the injection pipe is predicted to be chaotic. The flow pattern in the injection pipe obtained from two-way coupling looks like a not-converged (unstable) solution (even though divergence did not happen) as it seems very unrealistic to have such flow. Ansys Fluent has a strong solver that tries its best to avoid divergence, but the results should be interpreted with care in such cases where unrealistic flow is observed. Such chaotic flow is not suitable for the formation of agglomerates and that explains why minor agglomeration is observed there in the case of two-way coupling causing the discrepancy in the predictions of two-way and four-way coupling. The flow

injection pipe in the case of two-way coupling might be improved by playing with the time step or under-relaxation factor of the particle source term.

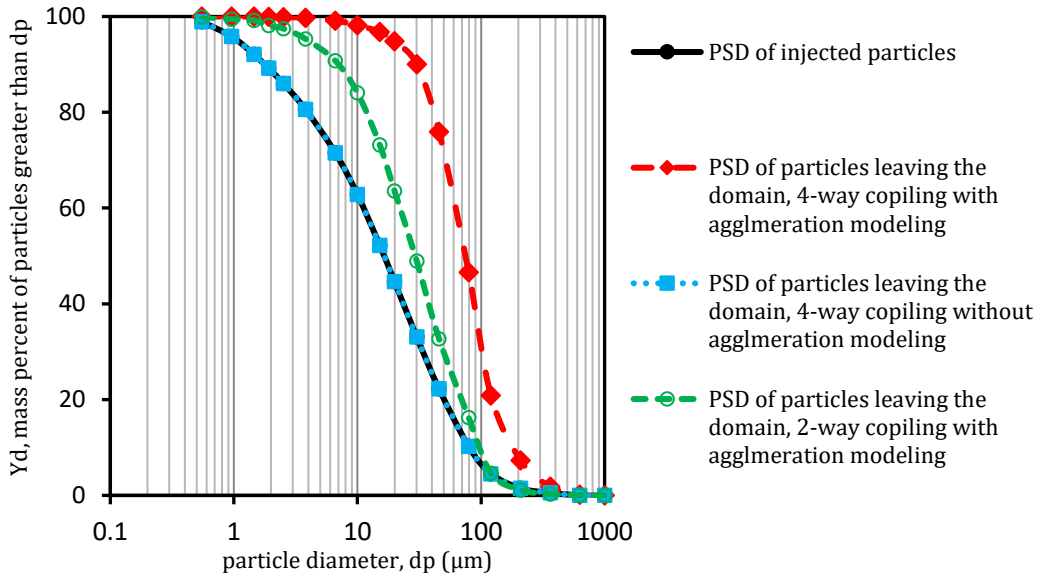

Figure C-2. Comparison among of four-way coupling with and without agglomeration modeling, and two-way coupling in terms of PSD of particles leaving the domain.

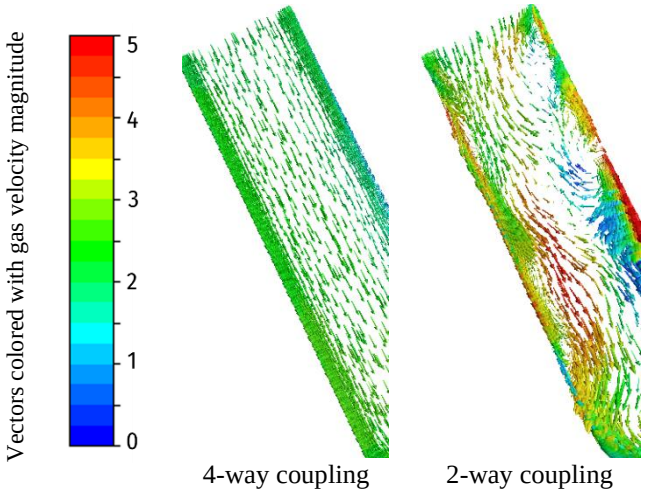

Figure C-3. Comparison between four-way coupling and two-way coupling in terms of flow pattern prediction in the injection pipe.

To further compare four-way coupling (DDPM) with two-way coupling DPM, flow patterns in the cyclone obtained from each are presented in Figure C-4. Despite discrepancies, overall, both models provide similar flow patterns. The discrepancies can be explained by the fact that the PSDs of particles present in the cyclone are different in the two models due to their different extent of agglomeration which affects the flow pattern.

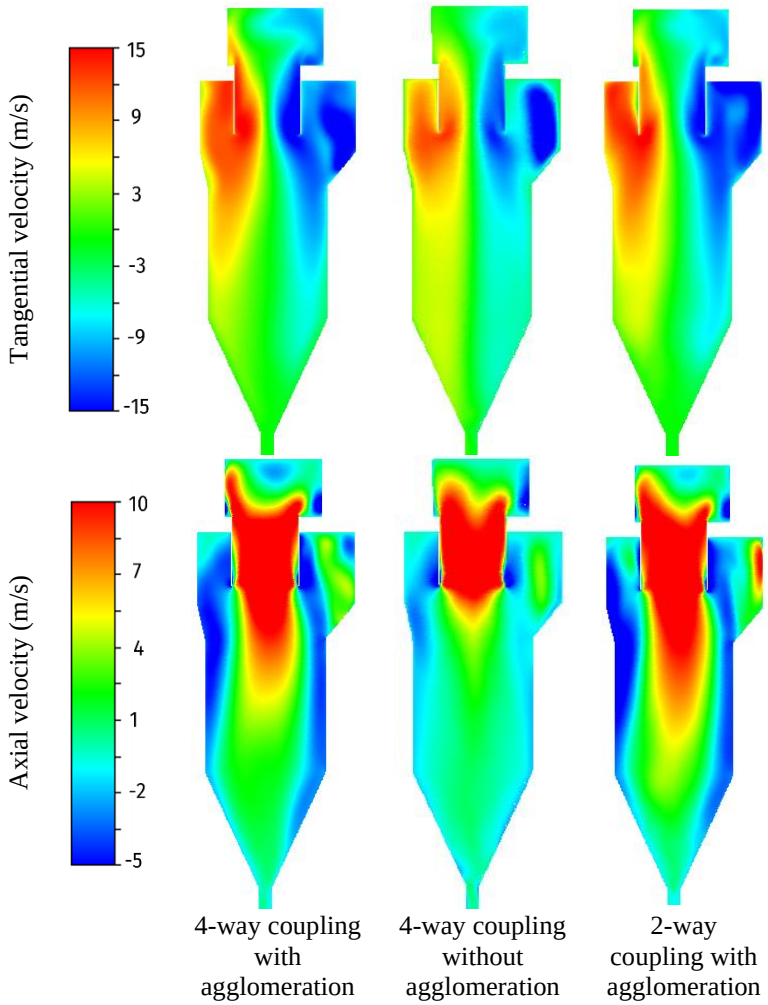

Figure C-4. Comparison among four-way coupling with and without agglomeration modeling, and two-way coupling in terms of flow pattern (time-averaged) in the cyclone main body.

Overall, regarding the significant underprediction of separation efficiency, at least in cases where agglomeration plays an important role, using four-way coupling (DDPM) over two-way coupling DPM is essential.

C.2 The case presented in Chapters 6 and 7 (stone wool cyclone)

In short, the case presented in Chapters 6 and 7, is a large-scale cyclone preheater (Figure 6-1), operating under temperatures of industrial cyclone preheaters with relatively large particles (see the PSD in Figure 6-2). The PSD is in the range where agglomeration does not play an important role and was excluded from the model. It was shown in Chapter 6 that four-way coupling (DDPM) can provide reasonable predictions of pressure drop, heat transfer rate and flow pattern in such a case. Here, DPM two-way coupling model is applied to this case to be compared with four-way coupling (DDPM) predictions and experimental measurements for one specific operation condition (Case-1 in Table 6-1).

The comparison of four-way coupling (DDPM) with two-way DPM simulation, in this case, is presented in Figure C-5. As can be observed, both models provide similar predictions of pressure drop, gas exit temperature, and heat transfer rate in reasonable agreement with experimental measurements.

Therefore, it can be concluded that in the present case where particles are relatively large so that agglomeration is not important, two-way coupling might be sufficient. It should be noted that even in such cases, the flow in locations with high solid volume fractions (such as injection pipe) might be erroneous due to not including phase volume fraction in the Navier-Stokes equations, however, regarding its minor impact in overall simulation, this error can be neglected.

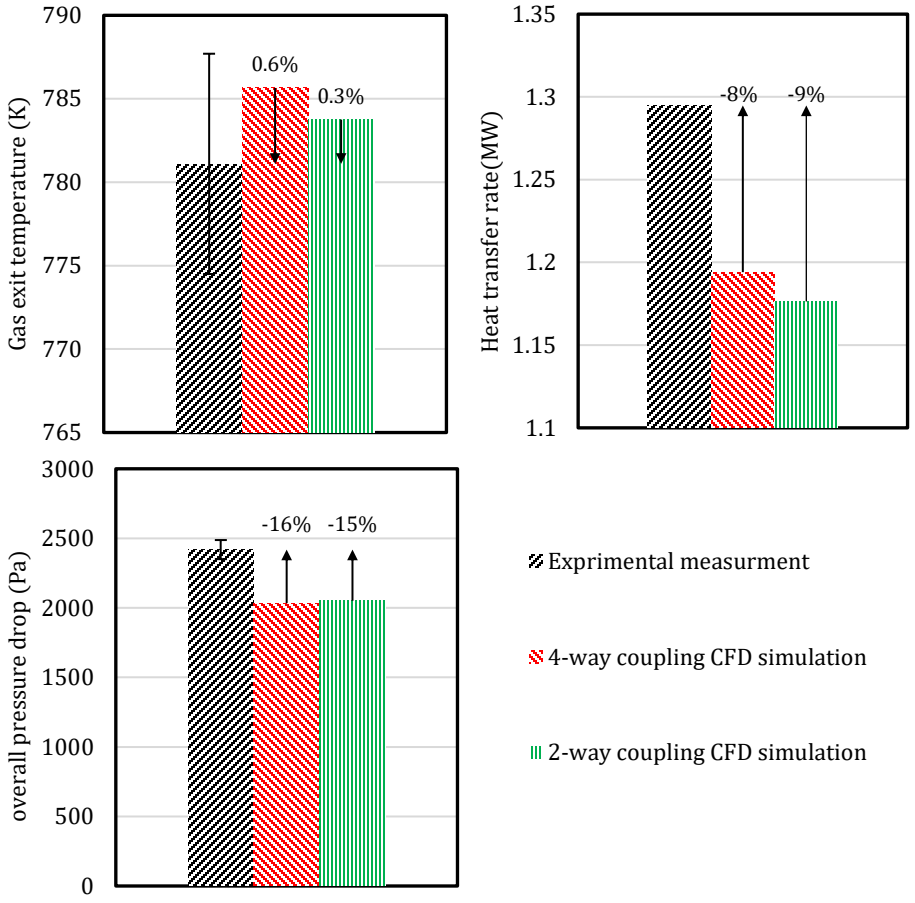

Figure C-5. Comparison among experimental measurement, four-way coupling, and two-way coupling in terms of gas exit temperature, heat transfer rate, and pressure drop.

C.3 Concluding remark

Although in cases with relatively large particles (where agglomeration is not important), two-way coupling might be sufficient, in cases with relatively fine particles (where agglomeration is important) using a four-way coupling model such as DDPM is necessary. Therefore, to have a valid model for the whole range of particle sizes, it is better to use a four-way coupling model (DDPM). Furthermore, a four-way coupling model ensures a reasonable flow pattern in locations with high local solid volume fractions such as injection pipes which might be of importance in some cases.

Appendix D

Comparison of gas-particle energy coupling approaches in DDPM

It was shown in Chapter 6 that in the way the energy conservation equation and gas-particle heat exchange is implemented in the DDPM multiphase model in Ansys Fluent, in cases with poly-dispersed particles, to have energy balance in the system, one exclusive solid phase is required to be assigned for each particle size class present in the system. For example, if four particle sizes are present in the system, four solid/dispersed phases are needed each to be assigned to one of the size classes to have an overall closed energy balance in the system. However, in the DDPM simulation of cyclone preheaters in the cement industry where relatively fine particles are present, even such a procedure could not obtain the energy balance in the system.

Up to version 2022R1, Ansys Fluent had only one option to model the gas-particle heat exchange which was to model it through an Eulerian approach (details of which can be found in the Ansys Fluent theory guide [147]). Since this approach would cause the mentioned energy imbalance in cases with fine particles, in Ansys Fluent 2022R2, a new feature was introduced to resolve the issue. In this new feature[§], gas-particle energy coupling is done via source term as in two-way coupling DPM modeling.

In the present appendix, these two approaches are compared in the two studied cases in the presented study (the case with finer particles presented in Chapters 4 and 5 and the case with larger particles presented in Chapters 6 and 7) for specific operating conditions.

D.1 The case presented in Chapters 4 and 5 (cement cyclone)

The case presented in Chapters 4 and 5 is operating under ambient temperature with relatively fine particles (see the PSD in Figure 4-2). To investigate heat transfer modeling a hypothetical case with all operating conditions as Case-2 in Table 4-1 except for the gas and particle inlet temperatures to be 700 and 300 K respectively is assumed. The case was once simulated using gas-particle energy coupling modeling via the

[§] This is a Beta feature in Ansys Fluent 2022R2 and can be activated via Text User Interface (TUI) with the following command:
/define/models/dpm/interaction/ddpm-energy-coupling-via-source-term? Yes
This feature was added to resolve the issue energy imbalance issue after it was proven to Ansys by the authors.

Eulerian approach and once via source term. It should be noted that in both cases six particle size classes (based on the PSD in Figure 4-2) each assigned to one exclusive solid phase were included in the simulation.

The comparison between energy coupling via the Eulerian approach and energy coupling via source term in terms of the energy balance of the whole system is presented in Figure D-1. As mentioned and can be observed in Figure D-1, energy coupling via the Eulerian approach ends up with a significant energy imbalance which makes the predictions nonsense. On the other hand, energy coupling via the source term provides an acceptable energy balance when the solution converges meaning that the new feature of Ansys Fluent introduced in the 2022R2 version actually resolves the issue observed in older versions.

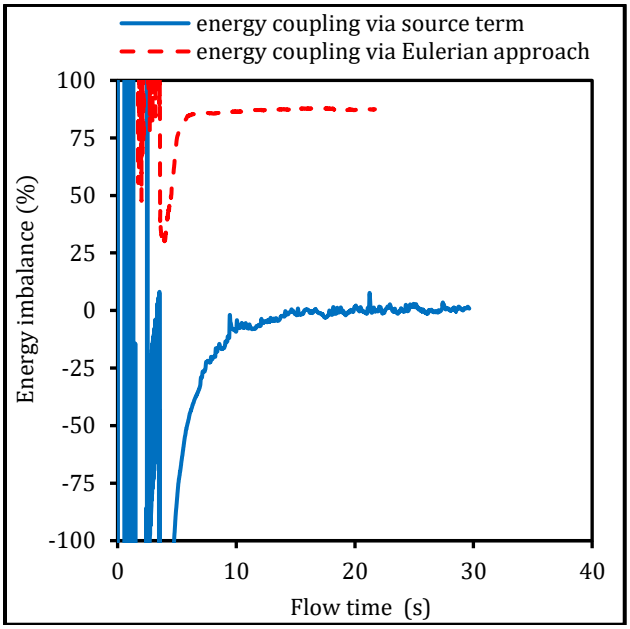

Figure D-1. Comparison of the energy balance of the whole system between energy coupling via the Eulerian approach and energy coupling via source term in the case of a cyclone preheater operating relatively fine particles.

Therefore, for the simulation of gas-particle heat exchange in the case of fine particles (based on our experience, roughly finer than 100 µm), it is necessary to model gas-particle energy coupling via source term to achieve an acceptable energy balance in the system.

D.2 The case presented in Chapters 6 and 7 (stone wool cyclone)

The case presented in Chapters 6 and 7 is a cyclone preheater with relatively large particles (see the PSD in Figure 6-2) so that even with energy coupling via the Eulerian approach an acceptable energy balance can be achieved. However, the predictions obtained from the two approaches appeared to be slightly different. To compare the two approaches Case-1 in Table 6-1 which was already simulated using gas-particle energy coupling modeling via the Eulerian approach (the results were presented in Chapter 6) was also simulated by energy coupling via source term. It should be noted that in both cases 4 particle size classes (based on the discussion in Chapter 6) each assigned to one exclusive solid phase were included in the simulation.

The comparison between energy coupling via the Eulerian approach and energy coupling via source term in terms of predicted gas exit temperature, heat transfer rate, and pressure drop is presented in Figure D-2. The predictions are also compared with experimental measurements. As can be observed, although the predictions of both approaches are similar, in particular in terms of heat transfer rate, energy coupling via source term provides better predictions. Therefore, although in this case with large particles, energy coupling via source term is not as crucial as the case with fine particles (finer than 100 µm), such an approach slightly improves heat-transfer-related predictions and is the superior approach.

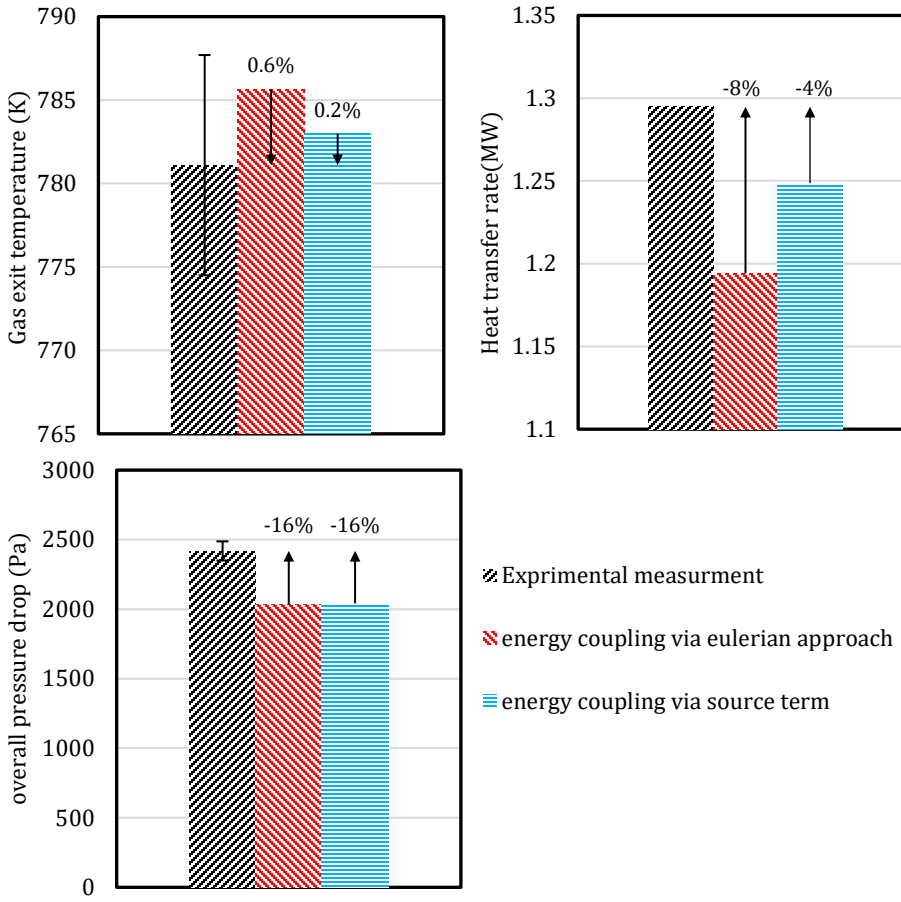

Figure D-2. Comparison among experimental measurement, CFD simulation with energy coupling via the Eulerian approach and CFD simulation with energy coupling via source term in terms of gas exit temperature, heat transfer rate, and pressure drop.

D.3 Concluding remark

Energy coupling via source term instead of the Eulerian approach is necessary in the case of fine particles (finer than 100 µm) to achieve a close energy balance and slightly improves the predictions in the case of large particles. Therefore, to have a valid model for the whole range of particle sizes, energy coupling via source term should be used when doing heat transfer simulation using DDPM.

Appendix E

Non-isothermal simulation of a cyclone preheater (with a diameter of 1.6 m) in the cement industry (with fine particles)

In Chapters 6 and 7, a cyclone preheater with relatively large particles (see the PSD in Figure 6-2) was simulated under non-isothermal condition by including heat transfer modeling. However, for the case with relatively fine particles (the case in Chapters 4 and 5) which is the case of cyclones in the cement industry, heat transfer modeling was excluded from the simulation (as the measurements were done under ambient temperature). It was shown in Appendix D that in the case of fine particles, a specific consideration should be considered to include heat transfer modeling. By taking this consideration (gas-particle energy coupling via source term) into account, in the present appendix, a hypothetical cyclone preheater case (under non-isothermal condition) with geometry and PSD presented in Chapter 4 is simulated to show the ability of the developed CFD model in the simulation of cyclone preheaters in cement industry. Moreover, the other objective is to find the minimum number of particle size classes required to properly cover the actual PSD in the simulation of a highly loaded cyclone preheater in the cement industry.

E.1 Case description

The operating and boundary conditions of this hypothetical case are presented in Table E-1. The geometry and PSD presented in Chapter 4 is investigated here. The model presented in Chapter 6 (DDPM multiphase model coupled with k-ω sst turbulence model in addition to heat transfer modeling) was implemented for the present case. In addition, as the particles in the present case are fine and prone to agglomeration, the agglomeration model presented in Chapter 4 was implemented as well. Other details of the CFD model are summarized in Table E-1.

Table E-1. Operating and boundary conditions and simulation settings

Parameter	value
Air flow rate (kg/s)	8.2
Gas inlet temperature (K)	700
Particle injection flow rate (kg/s)	4.7
Particle injection temperature (K)	300
Solid loading ratio (kg solid / kg air)	0.57
Particle density (kg /m^3)	3100
Particle specific heat capacity (J/kg.K)	1680
Gas density (kg/m^3)	Incompressible ideal gas
Gas molecular weight (kg/kmol)	29
Gas viscosity (kg/m.s)	1.8317e-05
Gas thermal conductivity (W/m.K)	0.024
Gas-specific heat capacity (J/kg.K)	1006
Parcel mass	40 mg
Time step	Courant number of 200 (5 ms)
Grid	300 000 polyhedral grids with prism layers
Number of particle sizes	4, 5, 6, 7, and 8
Particle-particle restitution coefficient	0.7
Particle-wall restitution coefficient (normal and tangent)	0.8

E.2 The effect of polydispersity of particles

As discussed in Chapter 6 to achieve energy balance in the system, one exclusive solid phase is needed for each particle class included in the model in DDPM. On the other hand, a greater number of solid phases results in heavier and more expensive numerical calculations. Therefore, it is important to find the minimum number of particle sizes required to adequately represent the actual PSD in the studied case. For this purpose, a study was designed where a various number of particle sizes were considered in different cases (from 4 to 8 particle sizes), based on the actual PSD of particles, to be compared and find the minimum number of particle sizes needed to provide similar results as the case with 8 particles sizes, which is the maximum number feasible in our computational resources. The 5 different PSDs (with 4, 5, 6, 7, and 8 number of particle size classes) are presented in Figure E-1.

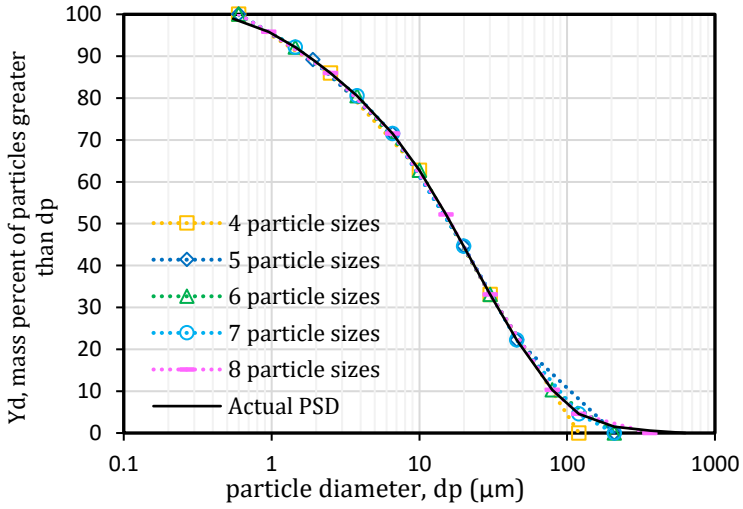

Figure E-1. The 5 different PSDs (with 4, 5, 6, 7, and 8 number of particle size classes) tested in the present study

Pressure drop, gas exit temperature, and separation efficiency predictions were taken as three performance parameters of the cyclone preheater. The comparative results are presented in Figure E-2. In addition, the results of velocity, temperature, and solid volume fraction distribution are also shown in Figure E-3, Figure E-4 and Figure E-5 respectively. The comparison shows that even with four particle sizes, more or less, similar predictions can be achieved (in particular for pressure drop, gas exit temperature and presented distributions). However, six particle sizes should be included to minimize the difference in predictions from the most expensive case (8 particle size classes), in particular considering the separation efficiency predictions. This means that six particle sizes are sufficient in this study to cover the actual PSD. In addition, PSDs of particles leaving the domain obtained from different injected PSDs as representative of the extent of agglomeration are presented in Figure E-6. In the case of 6, 7, and 8 particle sizes, the PSD of particles leaving the domain are similar showing that a similar extent of agglomeration has occurred in these cases. This further confirms that 6 particle size classes are sufficient to cover the PSD.

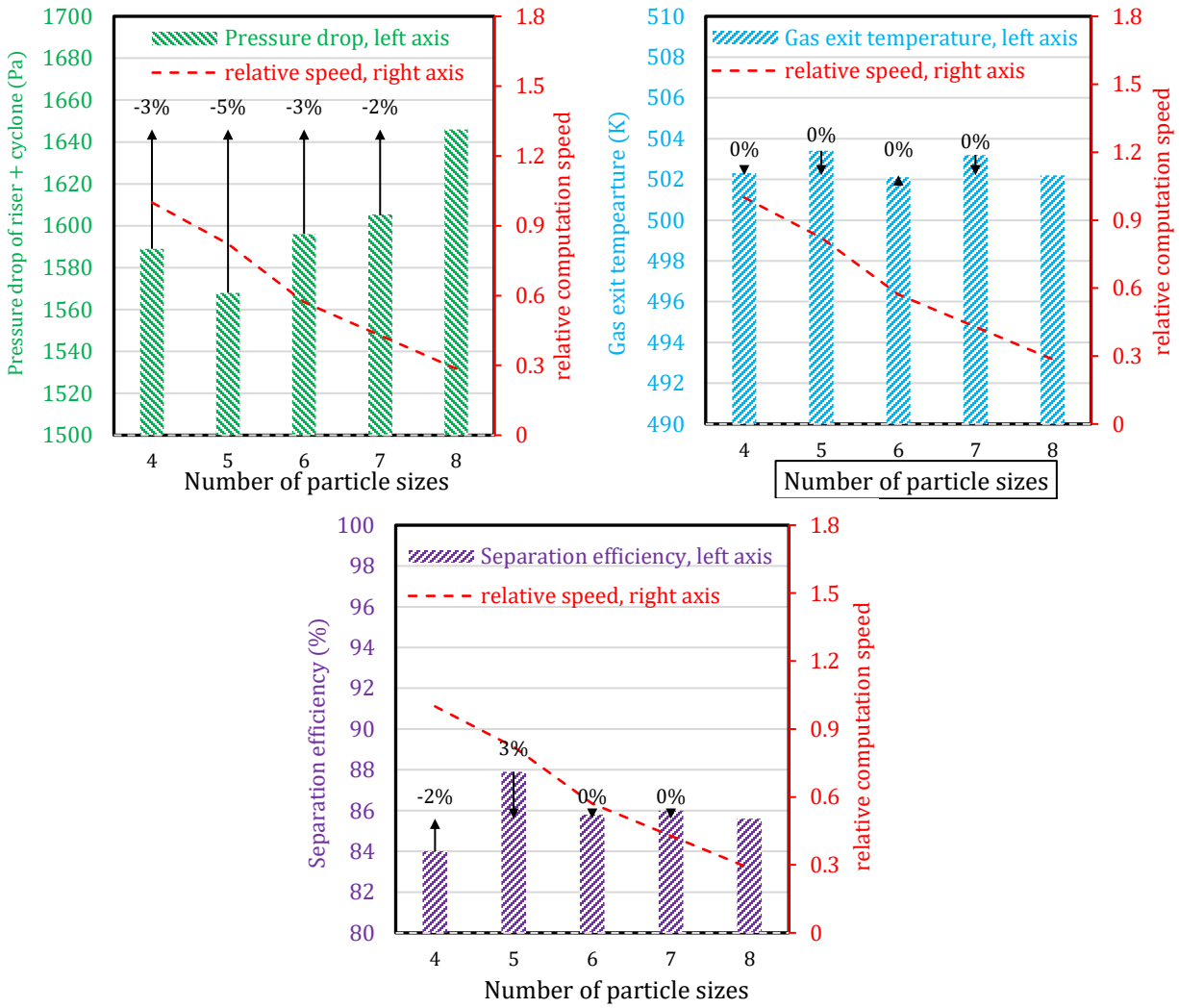

Figure E-2. Comparison of pressure drop, gas exit temperature and separation efficiency in five simulation cases designed for the study of the effect of particle polydispersity. The relative computation speed is also presented for each case. Presented deviations in % are based on a comparison with the case with 8 particle size classes.

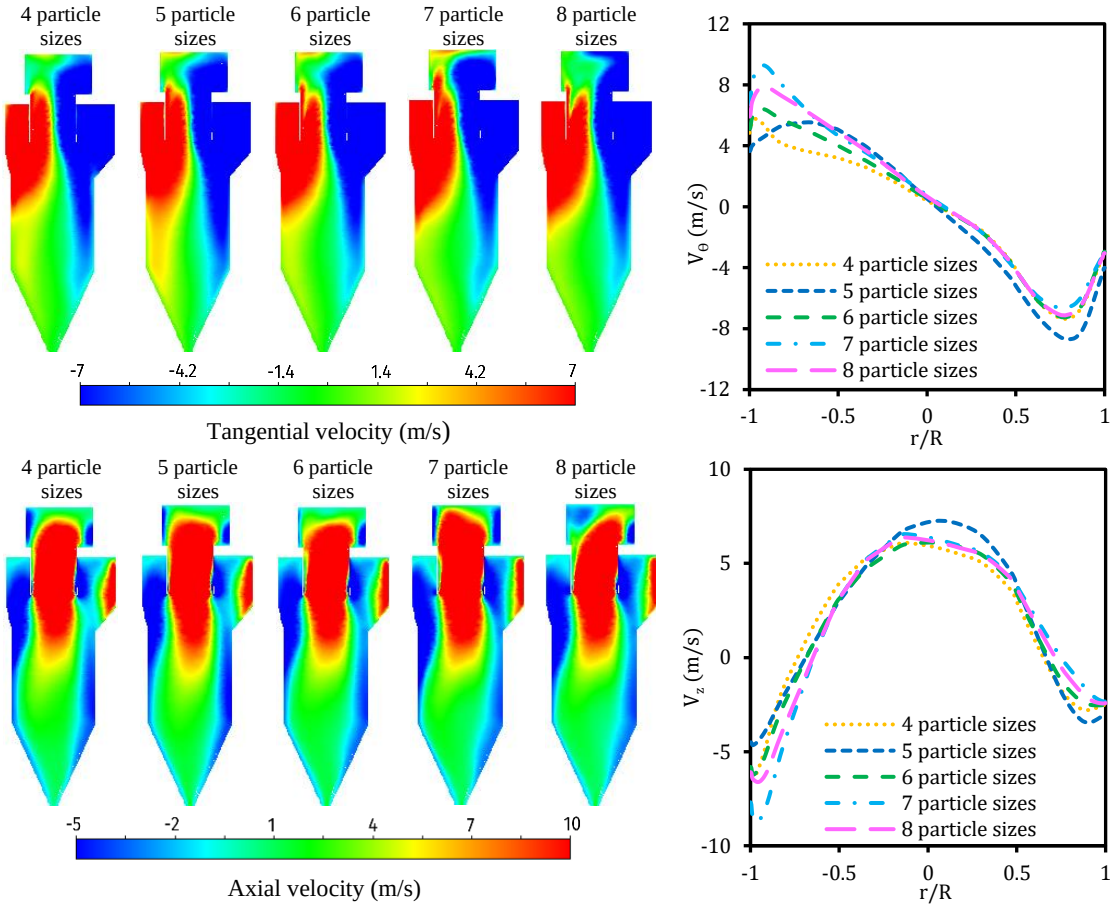

Figure E-3. Comparison of axial and tangential distribution in five simulation cases designed for the study of the effect of particle polydispersity.

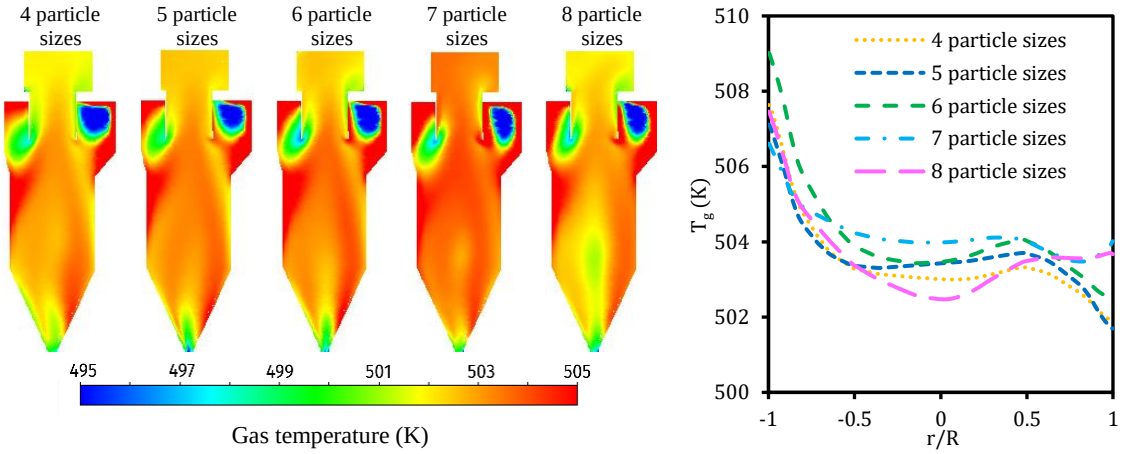

Figure E-4. Comparison of gas temperature distribution in five simulation cases designed for the study of the effect of particle polydispersity.

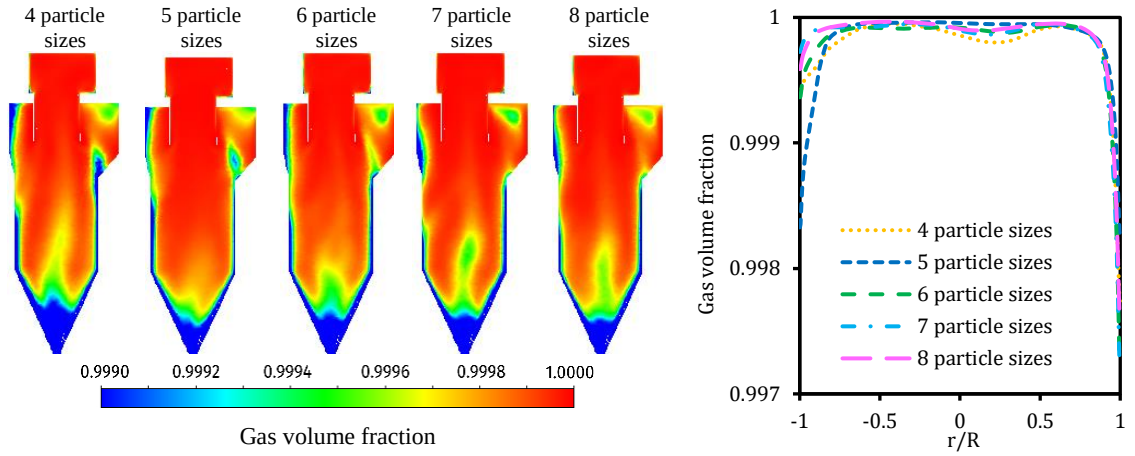

Figure E-5. Comparison of gas volume fraction distribution in five simulation cases designed for the study of the effect of particle polydispersity.

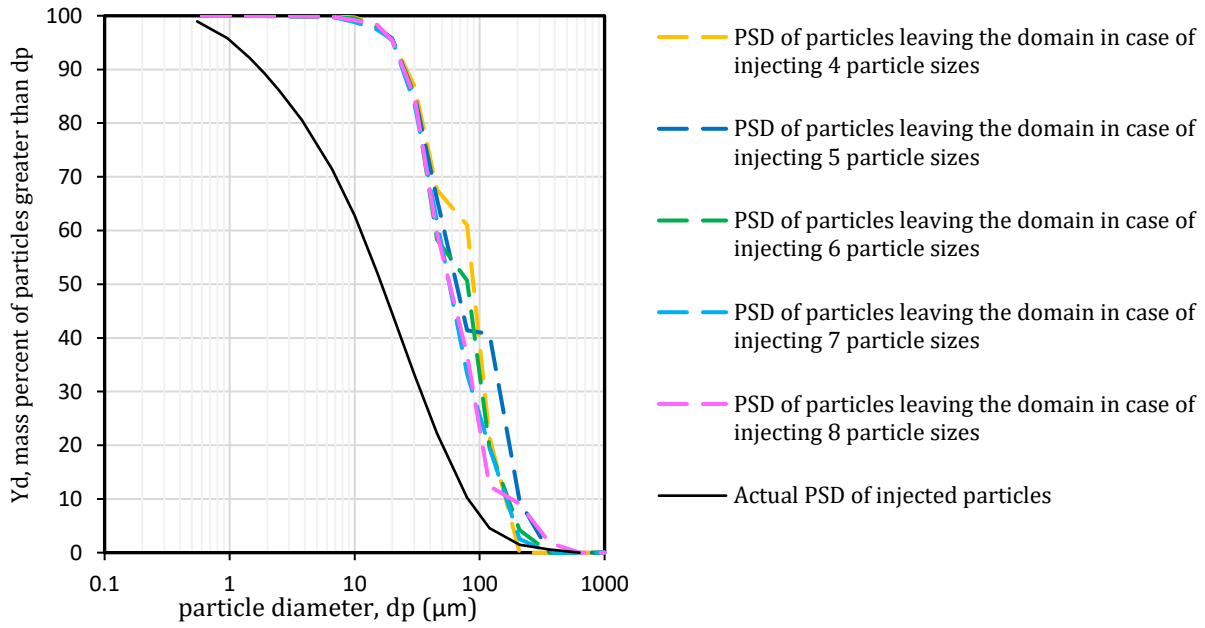

Figure E-6. Comparison of PSD of particles leaving the domain in five simulation cases designed for the study of the effect of particle polydispersity.

E.3 Concluding remark

It was concluded in Chapter 6 that for relatively large PSD in the Rockwool system, at least four particle sizes are required to properly cover the actual PSD to simulate the cyclone preheater. However, in the present appendix, it was shown that in the case of relatively fine particles in the cement industry where particle agglomeration is important six particle sizes are required. For six particle sizes to be included in DDPM, six exclusive solid phases each assigned to one of the particle sizes are needed to achieve the energy balance. Moreover, gas-particle energy coupling must be done via the source term as discussed in Appendix D. The present investigation showed the developed CFD model is able to provide a verified non-isothermal simulation of cyclone preheaters operating with fine particles as in the cement industry with some specific considerations which were mentioned in the present appendix.

Appendix F

Effect of minor geometry changes on the performance of an industrial cyclone preheater

The overall objective of the present PhD project was to develop a validated CFD tool for the simulation of highly loaded industrial cyclone preheaters as a function of geometry, operating conditions, particle properties, etc. to be later used by the engineers in related industries to troubleshoot, redesign, or optimize industrial cyclone preheaters. Such a validated CFD tool was developed and presented in this thesis. In this appendix, an example of the application of this CFD tool to improve the performance of a cyclone preheater will be presented.

As discussed in Chapter 7, wall erosion is a serious issue in particular in the case of cyclone preheaters operating in stone wool productions. Engineers at Rockwool are looking for ways to reduce erosion and consequently reduce maintenance expenses in the case of their cyclones. In particular, they were wondering whether some minor changes in the geometry could cause a notable change in the erosion rate.

Engineers at Rockwool suggested seven minor changes in the geometry (presented in Figure 7-1) to be tested. In the present study, these changes were applied to the geometry, then all these seven new geometries were discretized, and the developed model presented in Chapters 6 and 7 was implemented to simulate these geometries. The simulations were done under the operating conditions of Case-3 in Table 7-1.

The geometry presented in Chapter 7 was considered as the base case to be compared with these 7 new geometries. All investigated geometries are presented in Figure F-1 and briefly described as follows:

Geometry 1: The geometry presented in Figure 7-1, the base case
Geometry 2: The connection from the riser to the cyclone's main body is made curvier
Geometry 3: Two injection ports instead of one in the base case
Geometry 4: The injection port is wider than the base case
Geometry 5: The angle of the injection port is changed to 45˚(the angle in the base case is 30˚)
Geometry 6: The injection port is moved down
Geometry 7: The injection port is moved up
Geometry 8: The area of the inlet of the cyclone’s main body is made smaller by 30%

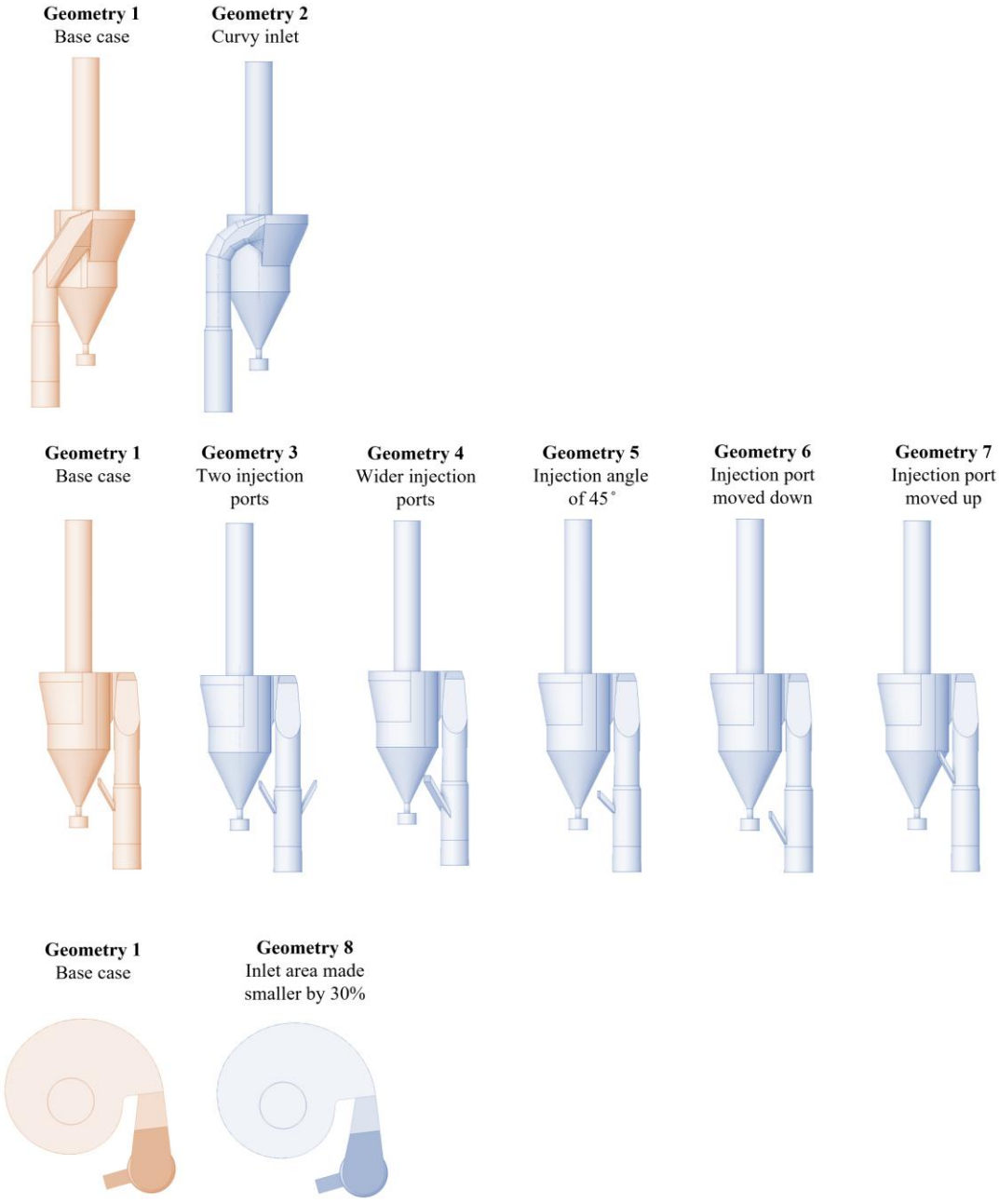

Figure F-1. Differences in investigated geometries.

The CFD simulations in addition to erosion investigations were performed for these 7 new geometries to be compared with the base case. In addition to erosion rate, pressure drop and heat transfer rate as two other important performance parameters of cyclone preheaters are calculated to be compared as well.

The comparison is presented in Figure F-2. As can be observed, none of the changes affects the heat transfer rate (gas and solid exit temperatures) notably. Although making the injection port wider or changing the angle of injections do not affect the erosion rate significantly, apparently making the connection curvier or using two injection ports notably reduce the erosion rate. Making the connection curvier also notably

reduces the pressure drop. Apparently, the altitude of the injection port also affects the erosion rate; the higher altitude of the injection port, the lower the erosion rate (the extent is shown in Figure F-2). By making the inlet area smaller, gas and particles experience higher velocity at the inlet which leads to a higher erosion rate and also higher pressure drop.

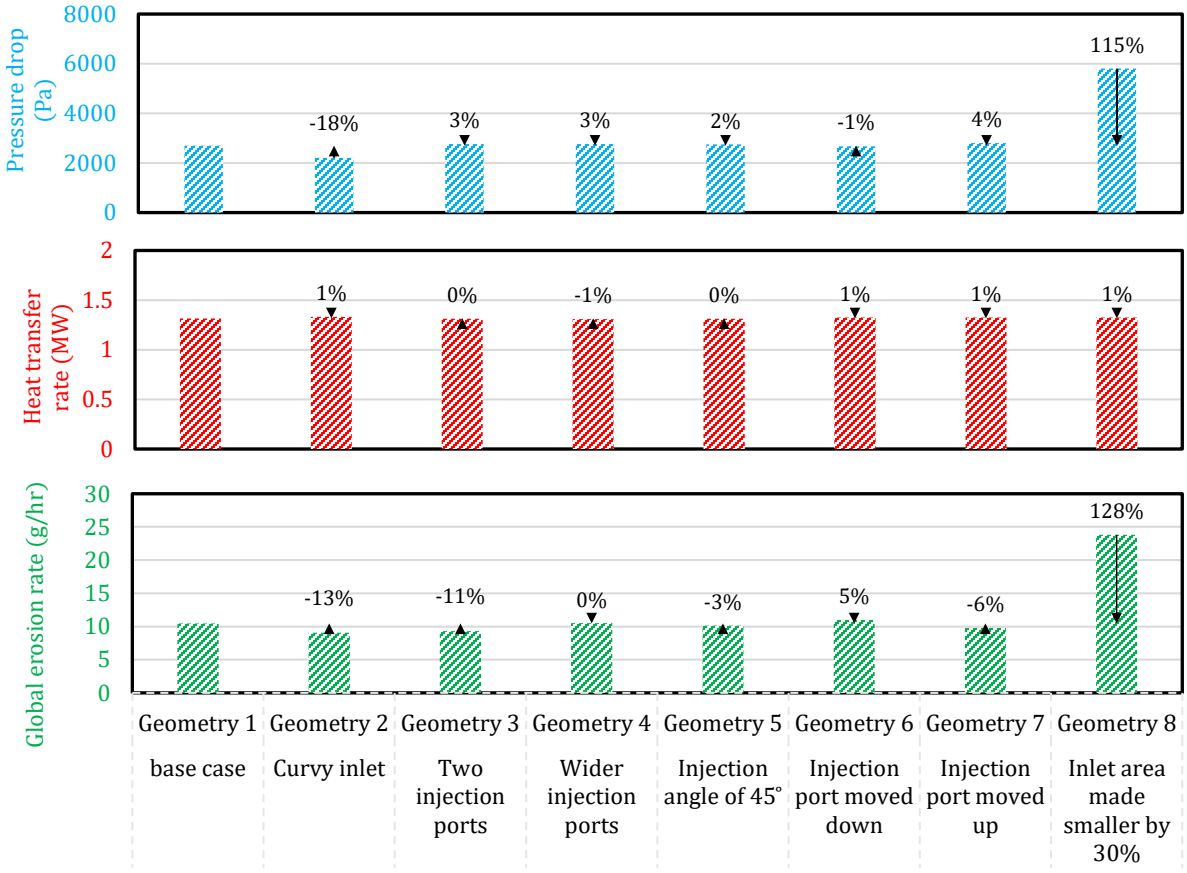

Figure F-2. Comparison of pressure drop, heat transfer rate and global erosion rate between different investigate geometries

Overall, by making the connection curvier, having two injection ports, moving the injection port upward, and making the inlet area larger, the overall erosion rate can be reduced notably without affecting the heat transfer rate considerably.

In addition, to these investigations of minor changes in the geometry, there was a question of whether the particle injection velocity would affect the overall erosion rate and other performance parameters of the cyclone preheater. To answer this question, three injection velocities (1, 2.5, 4 m/s) were tested in the base case. The effect of the injection velocity on the erosion rate, pressure drop and heat transfer rate is presented in Figure F-3 showing that the impact is minor. A minor increase in the erosion rate with an increase in the injection velocity can be observed.

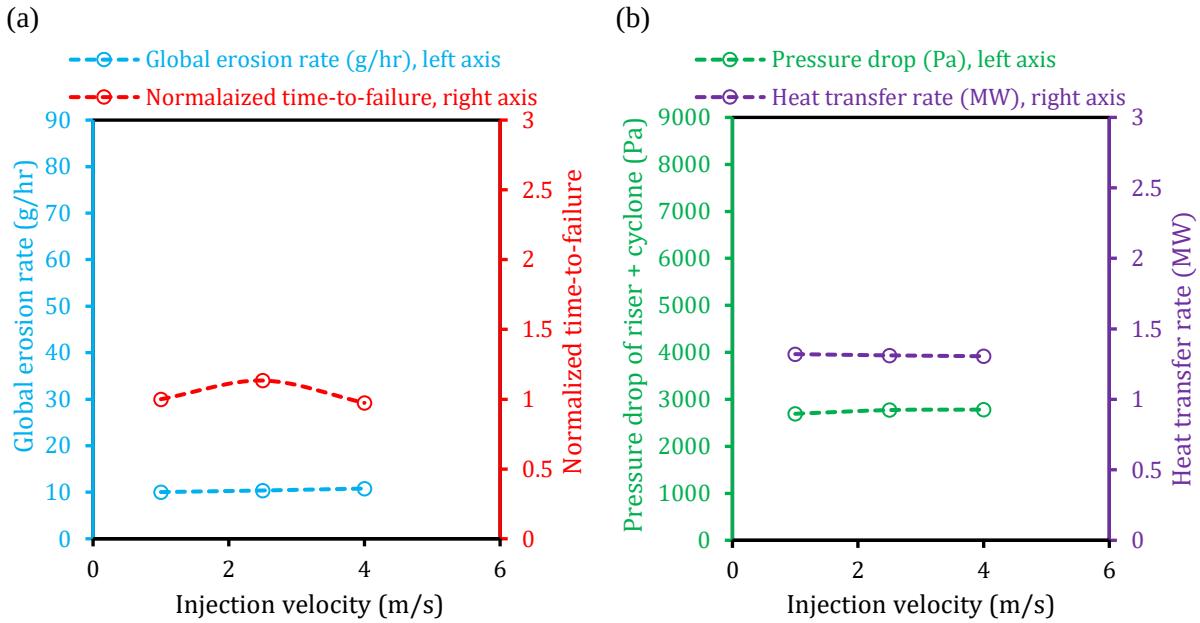

Figure F-3. Effect of particle injection velocity on (a) erosion and (b) pressure drop and heat transfer rate

F.1 Concluding remark

In Chapters 5 and 7, it was shown the developed model can be used to investigate how operating conditions would affect the performance of a cyclone preheater. In the present appendix, by an example, it was shown that the developed CFD tool can also be used to see how changes in the geometry of the cyclone preheater would affect its performance.

By investigating a couple of minor changes, it can be concluded that the erosion in the cyclone preheater can be reduced by making the connection curvier, having two injection ports instead of one, moving the injection port upward, and making the inlet area larger. These changes would not worsen the pressure drop and heat transfer rate notably as two other performance parameters of cyclone preheaters.

Appendix G

Simplified, isothermal CFD Simulation of an industrial-scale cyclone preheater (with a diameter of 6.6 m) in the cement industry (with fine particles)

In the present study, a pilot-scale cement cyclone preheater with a diameter of 1.6 m has been investigated and presented in Chapters 4 and 5. However, larger cyclone preheaters (with diameters up to 8 m) usually exist in industrial cement plants, which have not been simulated in the present work so far. Therefore, to evaluate and show the ability of the developed model in simulation of larger-scale cement cyclones, an industrial cement cyclone preheater (top cyclone in a 5-stage preheater tower of a cement plant) with a diameter of 6.6 m was simulated. Details of the simulation and some of the results are summarized in the present appendix.

G.1 Case description

As presented in Figure G-1, a typical cement production process consists of several cyclone preheaters in a cascade configuration. The focus of the present study is the top cyclone (cyclone 1) in this configuration. In addition, cyclone 2 is included in the simulation as the swirling motion that exists at its outlet might affect the gas-solid flow in the top cyclone.

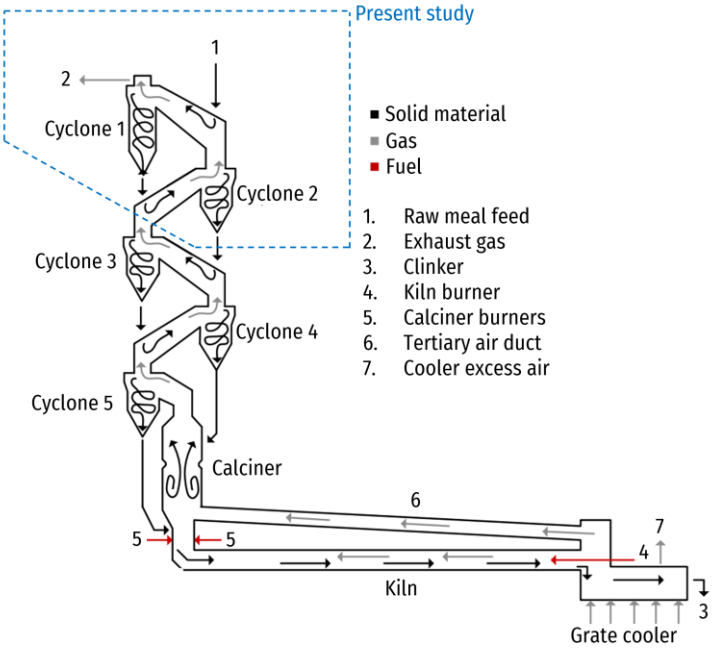

Figure G-1. Typical process flowsheet of cement production [5]

A 3D overview of these two cyclones simulated in the present study is shown in Figure G-2. Hot gas with particle carry-over coming from cyclone 3, first enters the riser of cyclone 2. In the riser of cyclone 2, particles separated from cyclone 1 are reinjected to the flow. Then the gas carries all particles to cyclone 2 where larger particles are separated into its dust bin and finer ones will be carried with gas to the riser of cyclone 1. In the riser of cyclone 1, the cold raw solid material (kiln feed) is fed into the gas flow. Then the gas carries all particles to cyclone 1 where larger ones will be separated into its dust bin and reinjected to the riser of cyclone 2 and finer ones will escape with gas to the gas outlet.

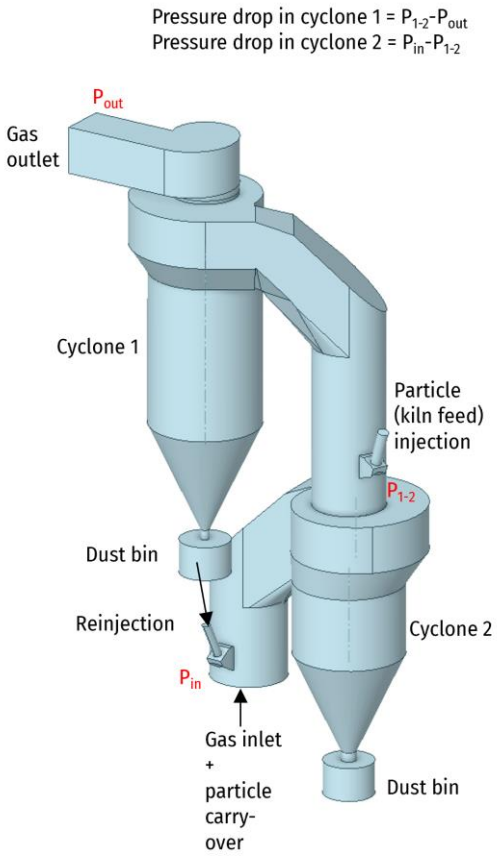

Figure G-2. 3D overview of the geometry. Dust bins added here are for the purpose of CFD simulation and do not exist in the actual plant.

G.2 Assumptions, simulation conditions, and boundary and operating conditions

Considering the large and complex system of the present case, to keep the model simple and computationally cheap, a couple of simplifications and assumptions were made which are summarized as follows and also in Table G-1:

- Considering that gas-particle heat exchange is almost complete in the riser, it is expected that the temperature changes are minor in the cyclone main body. Therefore, since the focus of the present study is the top cyclone, the isothermal condition was assumed in the current simulation. This assumption arises the challenge that the flow pattern, in particular, in the riser of cyclone riser 1

which controls the amount of fall-through of particles and amount of fine carry-overs might notably deviate from reality as in reality in the riser, the temperature changes notably.

- For the same reason, the gas temperature in the top cyclone is assumed to be equal to the gas temperature at the gas outlet. Therefore, the properties of gas in the isothermal simulation were assumed based on the gas temperature at the gas outlet.
- Gas and solid flow rates and also the amount of particle carry-over from cyclone 3 (all summarized in Table G-1) were assumed based on estimations of an in-house process tool.

A summary of assumed boundary and operation conditions is presented in Table G-1.

The domain was discretized using 1.2 million polyhedral cells (with 10 prism layers on the walls). The model presented in Chapter 4 (DDPM multiphase model coupled with k-ω sst turbulence model with curvature correction, agglomeration model, and revised Sarkar drag model) was implemented for the present case and one simulation case was run successfully. Preliminary simulation results are presented here.

Table G-1. Summary of assumed operation conditions

Parameter	Value	Assumption
Gas flow rate at the gas inlet	79.5 kg/s	Assumed to be equal to the estimated top-cyclone gas outlet flow rate
Particle (kiln feed) injection flow rate	50.3 kg/s	Engineering estimation
PSD of kiln feed	10 particle sizes	Measured kiln feed PSD presented in Figure G-5
Flow rate of particle carry-over coming with inlet gas	10.3 kg/s	Estimated solid flow rate escaped from cyclone 3
PSD of particle carry-over coming with inlet gas	10 particle sizes	Not measured, assumed to be the same as PSD of particles escaped from cyclone 1 presented in Figure G-5
Particle density	2700 kg/m^3	
Gas density	0.563 kg/m^3	Assumed based on the gas temperature at the gas outlet
Gas viscosity	2.98e-5 kg/m.s	Assumed based on the gas temperature at the gas outlet, mass averaged based on estimated gas composition
Operating temperature	630 K	Isothermal, properties at estimated gas outlet temperature
Gas composition		A Mixture of mostly N_2 (0.5), CO_2 (0.4), and H_2O (0.1)

G.3 Results and discussion

The simulation continued until tracked parameters reached their final converged value. In Figure G-3, variations of important particle masses and also pressure drop in two cyclones are tracked with time showing that a final converged solution is obtained. Then, the solution was averaged for 10 s to obtain mean values to report.

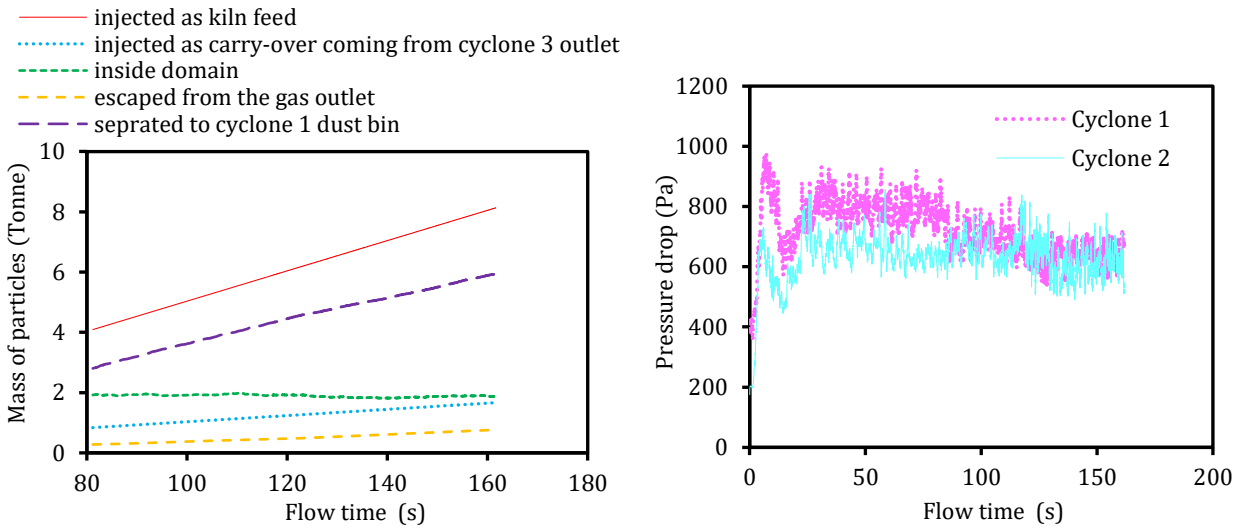

Figure G-3. Some of the important parameters tracked with time to ensure solution convergence

The flow pattern and solid volume fraction distribution obtained from this simulation are presented in Figure G-4. Although there are no available measurements to compare with, the obtained flow pattern is matched with the expectation from cyclones. A swirling down vortex close to the wall of the cyclone and a swirling up vortex in the core region. Solid volume fraction distribution shows that particles are mostly concentrated close to the wall as expected. The predicted separation efficiency and pressure drop obtained from the present CFD simulation are presented in Table G-2 and are compared with the process tool estimations. The comparison shows that both values from CFD are underpredicted compared to the process tool estimation.

Table G-2. CFD predictions of pressure drop and separation efficiency compared with process tool estimations. Separation efficiency is calculated based on particles that escaped from cyclone 1 and particles injected into the riser of cyclone 1.

	Separation efficiency (%)	Pressure drop (Pa)
Process tool estimation	91.7	1267
Present CFD simulation	85.7	638

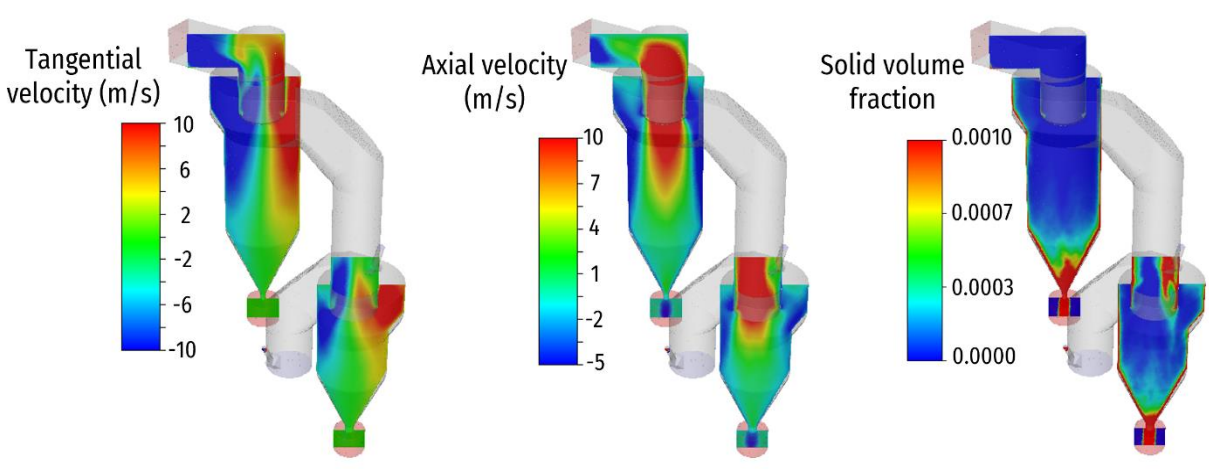

Figure G-4. Flow pattern and volume fraction distribution.

In the present case, samples of particles escaping to the gas outlet and also particles separated in cyclone 1 were taken to be analyzed. The PSDs of these samples are presented in Figure G-5 where they are compared against PSDs obtained from the CFD simulation. Although regarding both PSD of escaped and separated particles, CFD simulation predicted overall larger particles compared to the measured PSD, the overall shape of PSD and range of particle sizes are similar. The comparison shows that CFD predictions do not match measurements perfectly. The CFD simulation predicts the D_{50} of escaped particles to be around 4 µm while it is measured to be around 2 µm. On the other hand, The CFD simulation predicts the D_{50} of separated particles to be around 10 µm while it is measured to be around 5 µm. It seems that the overall size of particles going to cyclone 1, in reality, is finer than the size in the CFD simulation. It is because both PSD of escaped and separated predicted by the CFD model are larger than measured ones.

As can be observed, the measured PSD of both separated and escaped particles are finer than the measured PSD of kiln feed which shows some extent of carry-over of fine particles from cyclone 2 to cyclone 1. However, in the CFD simulation, not only the amount of these fines is predicted to be minor, a considerable amount of particles injected as kiln feed falls to cyclone 2. This considerable amount of fall-through can explain the difference between CFD and the process tool predictions of predicted pressure drop and separation efficiency (the process tool estimates a balance of around 10 kg/s of particles coming from cyclone 2 to cyclone 1 which is not observed in CFD simulation)

The deviation in the amount of fall through and fine carry-over coming to cyclone 1 might be explained by iso-thermal assumption; in reality, the gas temperature in cyclone 2 and its riser is higher than the assumed gas temperature. Having a higher gas velocity as a result of higher gas temperature in cyclone 2 can lead to less fall-through of solid material and increased dust carryover to cyclone 1. It might also be to some extent due to having an unrealistic injection of particles in CFD simulation (it is reported that the amount of fall-through is to some extent a function of the material pipe and the spreader plate which is not investigated carefully in the present study).

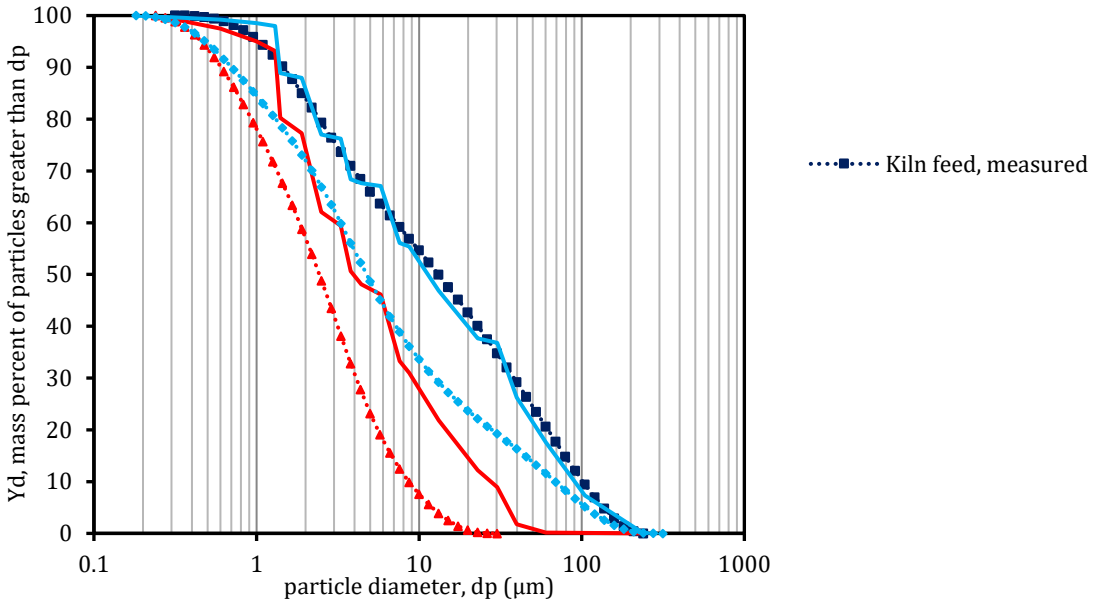

Figure G-5. Comparison of measured and predicted PSDs of separated and escapes particles.

G.4 Concluding remark

As the first step of simulating an industrial-scale cement cyclone, by considering several assumptions, an iso-thermal CFD simulation was done successfully. The model provides a converged solution in a computationally efficient manner (with 1M cells, with 32 computational nodes 1 s of the flow time progress is achieved in 1 hour). CFD simulation provides reasonable pressure drop, separation efficiency, and flow pattern predictions which are roughly matched with expectations. The CFD simulation predictions were compared with measurements of PSD of separated and escaped particles. Despite the discrepancy, overall, the predictions are acceptable.

G.5 Future work

The following is suggested to be done as future works in this case to improve the predictions:

- Better including fine particles coming from lower stage to cyclone 1 (based on estimation from process tool)
- conducting a non-isothermal simulation
- Mesh independence is required to be conducted

References

[1] A. Hoffmann, L. Stein, Gas Cyclones and Swirl Tubes, Springer Berlin Heidelberg, 2007. https://doi.org/10.1007/978-3-540-74696-6.

[2] M. Wasilewski, Analysis of the effects of temperature and the share of solid and gas phases on the process of separation in a cyclone suspension preheater, Sep. Purif. Technol. 168 (2016) 114–123. https://doi.org/10.1016/j.seppur.2016.05.033.

[3] M. Nakhaei, B. Lu, Y. Tian, W. Wang, K. Dam-Johansen, H. Wu, CFD modeling of gas-solid cyclone separators at ambient and elevated temperatures, Processes. 8 (2020) 228. https://doi.org/10.3390/pr8020228.

[4] H. Mikulčić, M. Vujanović, M.S. Ashhab, N. Duić, Large eddy simulation of a two-phase reacting swirl flow inside a cement cyclone, Energy. 75 (2014) 89–96. https://doi.org/10.1016/j.energy.2014.04.064.

[5] C. Maarup, K. Dam-Johansen, K. Clement, K. Hjuler, Gas-Solid Heat Exchanger for Cement Industry, Ph.D. Thesis, Technical University of Denmark, 2013. https://orbit.dtu.dk/en/publications/gas-solid-heat-exchanger-for-cement-production.

[6] V. Schultz-Falk, Waste recycling in an integrated melting furnace for stone wool production, Ph.D. Thesis, Technical University of Denmark, 2020. https://orbit.dtu.dk/files/239705051/PhD_Thesis_Vickie_Schultz_Falk.pdf.

[7] K. Jønck, CFD Modelling of Melting Cyclones for Stone Wool Production, Ph.D. Thesis, Technical University of Denmark, 2021. https://orbit.dtu.dk/en/publications/cfd-modelling-of-melting-cyclones-for-stone-wool-production.

[8] C. Cortés, A. Gil, C. Cortes, A. Gil, C. Cortés, A. Gil, Modeling the gas and particle flow inside cyclone separators, Prog. Energy Combust. Sci. 33 (2007) 409–452. https://doi.org/10.1016/j.pecs.2007.02.001.

[9] K.W. Chu, B. Wang, D.L. Xu, Y.X. Chen, A.B. Yu, CFD–DEM simulation of the gas–solid flow in a cyclone separator, Chem. Eng. Sci. 66 (2011) 834–847. https://doi.org/10.1016/j.ces.2010.11.026.

[10] I.S. Hwang, H.J. Jeong, J. Hwang, Numerical simulation of a dense flow cyclone using the kinetic theory of granular flow in a dense discrete phase model, Powder Technol. 356 (2019) 129–138. https://doi.org/10.1016/j.powtec.2019.08.008.

[11] S. Schneiderbauer, M.F. Haider, F. Hauzenberger, S. Pirker, A Lagrangian-Eulerian hybrid model for the simulation of industrial-scale gas-solid cyclones, Powder Technol. 304 (2016) 229–240. https://doi.org/10.1016/j.powtec.2016.07.064.

[12] J. Gimbun, CFD Simulation of Aerocyclone Hydrodynamics and Performance at Extreme Temperature, Eng. Appl. Comput. Fluid Mech. 2 (2008) 22–29. https://doi.org/10.1080/19942060.2008.11015208.

[13] G. Gronald, J.J. Derksen, Simulating turbulent swirling flow in a gas cyclone: A comparison of various modeling approaches, Powder Technol. 205 (2011) 160–171. https://doi.org/10.1016/j.powtec.2010.09.007.

[14] A. Avci, I. Karagoz, Effects of flow and geometrical parameters on the collection efficiency in cyclone separators, J. Aerosol Sci. 34 (2003) 937–955. https://doi.org/10.1016/S0021-8502(03)00054-5.

[15] W.M. H K Versteeg, An introduction to computational fluid dynamics : the finite volume method, M (2015) 500.

[16] J. Ferziger, M. Perić, R. Street, Computational methods for fluid dynamics, Berlin: springer, 2002. https://link.springer.com/content/pdf/10.1007/978-3-319-99693-6.pdf.

[17] F. Boysan, W.. Ayers, J. Swithenbank, A fundamental mathematical modelling approach to cyclone design, Trans Inst Chem Eng. 60 (1982) 222–230.

[18] F. Boysan, B.C.R. Ewan, J. Swithenbank, W.H. Ayers, Experimental and theoretical studies of cyclone separator aerodynamics, in: Inst. Chem. Eng. Symp. Ser., 1983: pp. 305–319. https://doi.org/10.1016/b978-0-08-028785-0.50025-3.

[19] M.D. Slack, R.O. Prasad, A. Bakker, F. Boysan, Advances in Cyclone Modelling Using Unstructured Grids, Chem. Eng. Res. Des. 78 (2000) 1098–1104. https://doi.org/10.1205/026387600528373.

[20] B. Wang, D.L. Xu, K.W. Chu, A.B. Yu, Numerical study of gas-solid flow in a cyclone separator, Appl. Math. Model. 30 (2006) 1326–1342. https://doi.org/10.1016/j.apm.2006.03.011.

[21] T.G. Chuah, J. Gimbun, T.S.Y.Y. Choong, A CFD study of the effect of cone dimensions on sampling aerocyclones performance and hydrodynamics, 162 (2006) 126–132. https://doi.org/10.1016/j.powtec.2005.12.010.

[22] K. Elsayed, C. Lacor, The effect of cyclone inlet dimensions on the flow pattern and performance, Appl. Math. Model. 35 (2011) 1952–1968. https://doi.org/10.1016/j.apm.2010.11.007.

[23] L.S. Brar, R.P. Sharma, K. Elsayed, The effect of the cyclone length on the performance of Stairmand high-efficiency cyclone, Powder Technol. 286 (2015) 668–677. https://doi.org/10.1016/j.powtec.2015.09.003.

[24] H. Yoshida, Three-dimensional simulation of air cyclone and particle separation by a revised-type cyclone, Colloids Surfaces A Physicochem. Eng. Asp. 109 (1996) 1–12. https://doi.org/10.1016/0927-7757(95)03469-2.

[25] M.S. Shin, H.S. Kim, D.S. Jang, J. Do Chung, M. Bohnet, A numerical and experimental study on a high efficiency cyclone dust separator for high temperature and pressurized environments, Appl. Therm. Eng. 25 (2005) 1821–1835. https://doi.org/10.1016/j.applthermaleng.2004.11.002.

[26] F. Mariani, F. Risi, C. Poggiani, Numerical study of the separation efficiency and heat exchange

performance in a complex gas-solid separator, Int. J. Comput. Methods Exp. Meas. 4 (2016) 142–152. https://doi.org/10.2495/CMEM-V4-N2-142-152.

[27] F. Mariani, F. Risi, C.N. Grimaldi, Separation efficiency and heat exchange optimization in a cyclone, Sep. Purif. Technol. 179 (2017) 393–402. https://doi.org/10.1016/j.seppur.2017.02.024.

[28] R.D. Luciano, B.L. Silva, L.M. Rosa, H.F. Meier, Multi-objective optimization of cyclone separators in series based on computational fluid dynamics, Powder Technol. 325 (2018) 452–466. https://doi.org/10.1016/j.powtec.2017.11.043.

[29] A.J. Hoekstra, J.J. Derksen, H.E.A. Van Den Akker, An experimental and numerical study of turbulent swirling flow in gas cyclones, Chem. Eng. Sci. 54 (1999) 2055–2065. https://doi.org/10.1016/S0009-2509(98)00373-X.

[30] A.J. Hoekstra, Gas Flow Field and Collection Efficiency of Cyclone Separators, Ph.D. Thesis, Delft University of Technology, 2000.

[31] I. Karagoz, F. Kaya, CFD investigation of the flow and heat transfer characteristics in a tangential inlet cyclone, Int. Commun. Heat Mass Transf. 34 (2007) 1119–1126. https://doi.org/10.1016/j.icheatmasstransfer.2007.05.017.

[32] H.I. Erol, O. Turgut, R. Unal, Experimental and numerical study of Stairmand cyclone separators: a comparison of the results of small-scale and large-scale cyclones, Heat Mass Transf. 55 (2019) 2341–2354. https://doi.org/10.1007/s00231-019-02589-y.

[33] Y. Jo, C. Tien, M.B. Ray, Development of a post cyclone to improve the efficiency of reverse flow cyclones, Powder Technol. 113 (2000) 97–108. https://doi.org/10.1016/S0032-5910(00)00206-0.

[34] C. Fredriksson, Exploratory Experimental and Theoretical Studies of Cyclone Gasification of Wood Powder, Ph.D. Thesis, Luleå tekniska universitet, 1999.

[35] J. Gimbun, T.G. Chuah, A. Fakhru'l-Razi, T.S.Y. Choong, The influence of temperature and inlet velocity on cyclone pressure drop: A CFD study, Chem. Eng. Process. Process Intensif. 44 (2005) 7–12. https://doi.org/10.1016/j.cep.2004.03.005.

[36] W.D. Griffiths, F. Boysan, Computational fluid dynamics (CFD) and empirical modelling of the performance of a number of cyclone samplers, J. Aerosol Sci. 27 (1996) 281–304. https://doi.org/10.1016/0021-8502(95)00549-8.

[37] M. Azadi, M. Azadi, A. Mohebbi, A CFD study of the effect of cyclone size on its performance parameters, J. Hazard. Mater. 182 (2010) 835–841. https://doi.org/10.1016/j.jhazmat.2010.06.115.

[38] R. Hreiz, C. Gentric, N. Midoux, Numerical investigation of swirling flow in cylindrical cyclones, Chem. Eng. Res. Des. 89 (2011) 2521–2539. https://doi.org/10.1016/j.cherd.2011.05.001.

[39] T. Mothilal, K. Pitchandi, Influence of inlet velocity of air and solid particle feed rate on holdup mass and heat transfer characteristics in cyclone heat exchanger, J. Mech. Sci. Technol. 29 (2015) 4509–4518. https://doi.org/10.1007/s12206-015-0950-z.

[40] J.W. Lee, H.J. Yang, D.Y. Lee, Effect of the cylinder shape of a long-coned cyclone on the stable flow-field establishment, Powder Technol. 165 (2006) 30–38. https://doi.org/10.1016/j.powtec.2006.03.011.

[41] L. Ma, D.B. Ingham, X. Wen, Numerical modelling of the fluid and particle penetration through small sampling cyclones, J. Aerosol Sci. 31 (2000) 1097–1119. https://doi.org/10.1016/S0021-8502(00)00016-1.

[42] Y.H. Alahmadi, A.F. Nowakowski, Modified shear stress transport model with curvature correction for the prediction of swirling flow in a cyclone separator, Chem. Eng. Sci. 147 (2016) 150–165. https://doi.org/10.1016/j.ces.2016.03.023.

[43] K. Jang, G.G. Lee, K.Y. Huh, Evaluation of the turbulence models for gas flow and particle transport in URANS and LES of a cyclone separator, Comput. Fluids. 172 (2018) 274–283. https://doi.org/10.1016/j.compfluid.2018.04.032.

[44] P.R. Spalart, M. Shur, On the Sensitization of Turbulence Models to Rotation and Curvature, Aerosp. Sci. Technol. 1 (1997) 297–302. https://doi.org/10.1016/S1270-9638(97)90051-1.

[45] D. Knight, P. Saffman, Turbulence model predictions for flows with significant mean streamline curvature, in: American Institute of Aeronautics and Astronautics (AIAA), 1978. https://doi.org/10.2514/6.1978-258.

[46] A. Hellsten, Some improvements in Menter'S k - ω SST turbulence model, in: 29th AIAA Fluid Dyn. Conf., American Institute of Aeronautics and Astronautics Inc., 1998: pp. 1–11. https://doi.org/10.2514/6.1998-2554.

[47] P.E. Smirnov, F.R. Menter, Sensitization of the SST turbulence model to rotation and curvature by applying the Spalart-Shur correction term, J. Turbomach. 131 (2009) 1–8. https://doi.org/10.1115/1.3070573.

[48] Q. Zhang, Y. Yang, A new simpler rotation/curvature correction method for Spalart-Allmaras turbulence model, Chinese J. Aeronaut. 26 (2013) 326–333. https://doi.org/10.1016/j.cja.2013.02.009.

[49] T.P. Dhakal, D.K. Walters, W. Strasser, Numerical study of gas-cyclone airflow: An investigation of turbulence modelling approaches, Int. J. Comut. Fluid Dyn. 28 (2014) 1–15. https://doi.org/10.1080/10618562.2013.878800.

[50] T.P. Dhakal, D.K. Walters, A Three-equation variant of the SST k-w model sensitized to rotation and curvature effects, J. Fluids Eng. Trans. ASME. 133 (2011). https://doi.org/10.1115/1.4004940.

[51] S. Wang, H. Li, R. Wang, X. Wang, R. Tian, Q. Sun, Effect of the inlet angle on the performance of a cyclone separator using CFD-DEM, Adv. Powder Technol. 30 (2019) 227–239. https://doi.org/10.1016/j.apt.2018.10.027.

[52] F.J. de Souza, R. de Vasconcelos Salvo, D.A. de Moro Martins, Large Eddy Simulation of the gas–particle flow in cyclone separators, Sep. Purif. Technol. 94 (2012) 61–70. https://doi.org/10.1016/j.seppur.2012.04.006.

[53] S.K. Shukla, P. Shukla, P. Ghosh, Evaluation of numerical schemes using different simulation methods for the continuous phase modeling of cyclone separators, Adv. Powder Technol. 22 (2011) 209–219. https://doi.org/10.1016/j.apt.2010.11.009.

[54] J. Jiao, Z. Liu, Y. Zheng, Evaluations and Modifications on Reynolds Stress Model in Cyclone Simulations, Chem. Eng. Technol. 30 (2007) 15–20. https://doi.org/10.1002/ceat.200600311.

[55] P. Kozołub, A. Klimanek, R.A. Białecki, W.P. Adamczyk, Numerical simulation of a dense solid particle flow inside a cyclone separator using the hybrid Euler–Lagrange approach, Particuology. 31 (2017) 170–180. https://doi.org/10.1016/j.partic.2016.09.003.

[56] A.N. Huang, N. Maeda, S. Sunada, T. Fukasawa, H. Yoshida, H.P. Kuo, K. Fukui, Effect of cold air stream injection on cyclone performance at high temperature, Sep. Purif. Technol. 183 (2017) 293–303. https://doi.org/10.1016/j.seppur.2017.04.012.

[57] E. Kashani, A. Mohebbi, M.G. Heidari, CFD simulation of the preheater cyclone of a cement plant and the optimization of its performance using a combination of the design of experiment and multi-gene genetic programming, Powder Technol. 327 (2018) 430–441. https://doi.org/10.1016/j.powtec.2017.12.091.

[58] E.D. Cristea, P. Conti, Hybrid eulerian multiphase-dense discrete phase model approach for numerical simulation of dense particle-laden turbulent flows within vertical multi-stage cyclone heat exchanger, Am. Soc. Mech. Eng. Fluids Eng. Div. FEDSM. 2 (2018) 1–15. https://doi.org/10.1115/FEDSM2018-83058.

[59] E.-D. Cristea, P. Conti, CFD Simulation of Large Dust Collection Cyclones Positioned Vertically in Staggered Downward Cascade Arrangement, in: Proc. ASME 2013 Fluids Eng. Div. Summer Meet., American Society of Mechanical Engineers, 2013: pp. 1–10. https://doi.org/10.1115/FEDSM2013-16245.

[60] D. Winfield, M. Cross, N. Croft, D. Paddison, I. Craig, Performance comparison of a single and triple tangential inlet gas separation cyclone: A CFD Study, Powder Technol. 235 (2013) 520–531. https://doi.org/10.1016/j.powtec.2012.10.026.

[61] M. Wasilewski, S. Anweiler, M. Masiukiewicz, Characterization of multiphase gas–solid flow and accuracy of turbulence models for lower stage cyclones used in suspension preheaters, Chinese J. Chem. Eng. 27 (2019) 1618–1629. https://doi.org/10.1016/j.cjche.2018.11.019.

[62] F. Ficici, V. Ari, Optimization of the Preheater Cyclone Separators Used in the Cement Industry, Int. J. Green Energy. 10 (2013) 12–27. https://doi.org/10.1080/15435075.2011.647365.

[63] G. Wan, G. Sun, X. Xue, M. Shi, Solids concentration simulation of different size particles in a cyclone separator, Powder Technol. 183 (2008) 94–104. https://doi.org/10.1016/j.powtec.2007.11.019.

[64] A.N. Huang, K. Ito, T. Fukasawa, K. Fukui, H.P. Kuo, Effects of particle mass loading on the hydrodynamics and separation efficiency of a cyclone separator, J. Taiwan Inst. Chem. Eng. 90 (2018) 61–67. https://doi.org/10.1016/j.jtice.2017.12.016.

[65] T.A. Sedrez, R.K. Decker, M.K. da Silva, D. Noriler, H.F. Meier, Experiments and CFD-based erosion modeling for gas-solids flow in cyclones, Powder Technol. 311 (2017) 120–131. https://doi.org/10.1016/j.powtec.2016.12.059.

[66] J. Wei, H. Zhang, Y. Wang, Z. Wen, B. Yao, J. Dong, The gas-solid flow characteristics of cyclones, Powder Technol. 308 (2017) 178–192. https://doi.org/10.1016/j.powtec.2016.11.044.

[67] S. Pirker, D. Kahrimanovic, A combined method for simulating gas-particle flows in highly laden cyclones, in: 5th Int. Conf. CFD Process Ind., Melbourne, 2006: p. 6. https://flair.monash.edu.au/intranet/proceedings/cfd2006/PDFs/096Pir.pdf.

[68] L.Y. Hu, L.X. Zhou, J. Zhang, M.X. Shi, Studies on strongly swirling flows in the full space of a volute cyclone separator, AIChE J. 51 (2005) 740–749. https://doi.org/10.1002/aic.10354.

[69] J.J. Derksen, H.E.A. van den Akker, S. Sundaresan, Two-way coupled large-eddy simulations of the gas-solid flow in cyclone separators, AIChE J. 54 (2008) 872–885. https://doi.org/10.1002/aic.11418.

[70] K. Elsayed, C. Lacor, CFD modeling and multi-objective optimization of cyclone geometry using desirability function, Artificial neural networks and genetic algorithms, Appl. Math. Model. 37 (2013) 5680–5704. https://doi.org/10.1016/j.apm.2012.11.010.

[71] K. Elsayed, C. Lacor, The effect of cyclone vortex finder dimensions on the flow pattern and performance using LES, Comput. Fluids. 71 (2013) 224–239. https://doi.org/10.1016/j.compfluid.2012.09.027.

[72] J.J. Derksen, Separation performance predictions of a stairmand high-efficiency cyclone, AIChE J. 49 (2003) 1359–1371. https://doi.org/10.1002/aic.690490603.

[73] J.J. Derksen, S. Sundaresan, H.E.A. van den Akker, Simulation of mass-loading effects in gas-solid cyclone separators, Powder Technol. 163 (2006) 59–68. https://doi.org/10.1016/j.powtec.2006.01.006.

[74] O.L. Sgrott, M. Sommerfeld, Influence of inter-particle collisions and agglomeration on cyclone performance and collection efficiency, Can. J. Chem. Eng. 97 (2019) 511–522. https://doi.org/10.1002/cjce.23371.

[75] H. Tofighian, E. Amani, M. Saffar-Avval, A large eddy simulation study of cyclones: The effect of sub-models on efficiency and erosion prediction, Powder Technol. (2019). https://doi.org/10.1016/j.powtec.2019.10.091.

[76] W.P. Martignoni, S. Bernardo, C.L. Quintani, Evaluation of cyclone geometry and its influence on performance parameters by computational fluid dynamics (CFD), Brazilian J. Chem. Eng. 24 (2007) 83–94. https://doi.org/10.1590/S0104-66322007000100008.

[77] S. Elghobashi, On predicting particle-laden turbulent flows, Appl. Sci. Res. 52 (1994) 309–329. https://doi.org/10.1007/BF00936835.

[78] X. Chen, J. Wang, A comparison of two-fluid model, dense discrete particle model and CFD-DEM method for modeling impinging gas-solid flows, Powder Technol. 254 (2014) 94–102. https://doi.org/10.1016/J.POWTEC.2013.12.056.

[79] C.T. Crowe, J.D. Schwarzkopf, M. Sommerfeld, Y. Tsuji, Multiphase Flows with Droplets and Particles, CRC Press, 2011. https://doi.org/10.1201/b11103.

[80] D. Schellander, S. Schneiderbauer, S. Pirker, Numerical study of dilute and dense poly-dispersed gas-solid two-phase flows using an Eulerian and Lagrangian hybrid model, Chem. Eng. Sci. 95 (2013) 107–118. https://doi.org/10.1016/j.ces.2013.03.037.

[81] H. Safikhani, A. Hajiloo, M.A. Ranjbar, Modeling and multi-objective optimization of cyclone separators using CFD and genetic algorithms, Comput. Chem. Eng. 35 (2011) 1064–1071. https://doi.org/10.1016/j.compchemeng.2010.07.017.

[82] Y. Su, A. Zheng, B. Zhao, Numerical simulation of effect of inlet configuration on square cyclone separator performance, Powder Technol. 210 (2011) 293–303. https://doi.org/10.1016/j.powtec.2011.03.034.

[83] R. Xiang, S.H. Park, K.W. Lee, Effects of cone dimension on cyclone performance, J. Aerosol Sci. 32 (2001) 549–561. https://doi.org/10.1016/S0021-8502(00)00094-X.

[84] S. Bernardo, M. Mori, A.P. Peres, R.P. Dionísio, 3-D computational fluid dynamics for gas and gas-particle flows in a cyclone with different inlet section angles, Powder Technol. 162 (2006) 190–200. https://doi.org/10.1016/j.powtec.2005.11.007.

[85] S. Yuu, T. Jotaki, Y. Tomita, K. Yoshida, The reduction of pressure drop due to dust loading in a conventional cyclone, Chem. Eng. Sci. 33 (1978) 1573–1580. https://doi.org/10.1016/0009-2509(78)85132-X.

[86] P.A. Patterson, R.J. Munz, Gas and Particle Flow Patterns in Cyclones at Room and Elevated Temperatures, Can. J. Chem. Eng. 74 (1996) 213–221. https://doi.org/10.1002/cjce.5450740206.

[87] Y. Zhu, K.W. Lee, Experimental study on small cyclones operating at high flowrates, J. Aerosol Sci. 30 (1999) 1303–1315. https://doi.org/10.1016/S0021-8502(99)00024-5.

[88] L.S. Brar, R.P. Sharma, R. Dwivedi, Effect of vortex finder diameter on flow field and collection efficiency of cyclone separators, Part. Sci. Technol. 33 (2015) 34–40. https://doi.org/10.1080/02726351.2014.933144.

[89] B. Zhao, Development of a new method for evaluating cyclone efficiency, Chem. Eng. Process. Process Intensif. 44 (2005) 447–451. https://doi.org/10.1016/j.cep.2004.06.007.

[90] S. Obermair, J. Woisetschläger, G. Staudinger, Investigation of the flow pattern in different dust outlet geometries of a gas cyclone by laser Doppler anemometry, Powder Technol. 138 (2003) 239–251. https://doi.org/10.1016/j.powtec.2003.09.009.

[91] F. Zhou, G. Sun, Y. Zhang, H. Ci, Q. Wei, Experimental and CFD study on the effects of surface roughness on cyclone performance, Sep. Purif. Technol. 193 (2018) 175–183. https://doi.org/10.1016/j.seppur.2017.11.017.

[92] J. Ding, D. Gidaspow, A bubbling fluidization model using kinetic theory of granular flow, AIChE J. 36 (1990) 523–538. https://doi.org/10.1002/aic.690360404.

[93] D. Gidaspow, Multiphase Flow and Fluidization, Elsevier, 1994. https://doi.org/10.1016/C2009-0-21244-X.

[94] H.F.H. Meier, M. Mori, Gas-solid flow in cyclones: The Eulerian-Eulerian approach, Comput. Chem. Eng. 22 (1998) 8–11. https://doi.org/10.1016/s0098-1354(98)00114-8.

[95] H. Enwald, E. Peirano, A.-E. Almstedt, Eulerian two-phase flow theory applied to fluidization, Int. J. Multiph. Flow. 22 (1996) 21–66. https://doi.org/10.1016/S0301-9322(96)90004-X.

[96] A.T. Andrews IV, P.N. Loezos, S. Sundaresan, Coarse-grid simulation of gas-particle flows in vertical risers, Ind. Eng. Chem. Res. 44 (2005) 6022–6037. https://doi.org/10.1021/ie0492193.

[97] A.A. Vegini, H.F. Meier, J.J. Less, M. Mori, Computational fluid dynamics (CFD) Analysis of cyclone separators connected in series, Ind. Eng. Chem. Res. 47 (2008) 192–200. https://doi.org/10.1021/ie061501h.

[98] B. Zhao, H. Shen, Y. Kang, Development of a symmetrical spiral inlet to improve cyclone separator performance, Powder Technol. 145 (2004) 47–50. https://doi.org/10.1016/j.powtec.2004.06.001.

[99] P.A. Cundall, O.D.L. Strack, A discrete numerical model for granular assemblies, Geotechnique. 29 (1979) 47–65. https://doi.org/10.1680/geot.1979.29.1.47.

[100] S.B. Kuang, K. Li, R.P. Zou, R.H. Pan, A.B. Yu, Application of periodic boundary conditions to CFD-DEM simulation of gas–solid flow in pneumatic conveying, Chem. Eng. Sci. 93 (2013) 214–228. https://doi.org/10.1016/j.ces.2013.01.055.

[101] J.-W. Zhou, Y. Liu, C. Du, S. Liu, Effect of the particle shape and swirling intensity on the breakage of lump coal particle in pneumatic conveying, Powder Technol. 317 (2017) 438–448. https://doi.org/10.1016/j.powtec.2017.05.034.

[102] R. Sun, H. Xiao, Diffusion-based coarse graining in hybrid continuum-discrete solvers: Applications in CFD-DEM, Int. J. Multiph. Flow. 72 (2015) 233–247. https://doi.org/10.1016/j.ijmultiphaseflow.2015.02.014.

[103] F. Fulchini, M. Ghadiri, A. Borissova, B. Amblard, S. Bertholin, A. Cloupet, M. Yazdanpanah, Development of a methodology for predicting particle attrition in a cyclone by CFD-DEM, Powder Technol. 357 (2019) 21–32. https://doi.org/10.1016/j.powtec.2019.08.101.

[104] H. Zhou, Z. Hu, Q. Zhang, Q. Wang, X. Lv, Numerical study on gas-solid flow characteristics of ultra-light particles in a cyclone separator, Powder Technol. 344 (2019) 784–796. https://doi.org/10.1016/j.powtec.2018.12.054.

[105] H.P. Zhu, Z.Y. Zhou, R.Y. Yang, A.B. Yu, Discrete particle simulation of particulate systems: A review of major applications and findings, Chem. Eng. Sci. 63 (2008) 5728–5770. https://doi.org/10.1016/j.ces.2008.08.006.

[106] S. Pirker, D. Kahrimanovic, C. Kloss, B. Popoff, M. Braun, Simulating coarse particle conveying by a set of Eulerian, Lagrangian and hybrid particle models, Powder Technol. 204 (2010) 203–213. https://doi.org/10.1016/j.powtec.2010.07.033.

[107] E. Muschelknautz, Die Berechnung von Zyklonabscheidern für Gase, Chemie Ing. Tech. 44 (1972) 63–71. https://doi.org/10.1002/cite.330440112.

[108] S. Pirker, D. Kahrimanovic, G. Aichinger, Modeling mass loading effects in industrial cyclones by a combined Eulerian-Lagrangian approach, Acta Mech. 204 (2009) 203–216. https://doi.org/10.1007/s00707-008-0086-7.

[109] E. Cristea, P. Conti, Coupled 3-D CFD-DDPM Numerical Simulation of Turbulent Swirling Gas-Particle Flow Within Cyclone Suspension Preheater of Cement Kilns, in: ASME 2016 Fluids Eng. Div. Summer Meet., American Society of Mechanical Engineers, 2016: pp. 1–12. https://doi.org/10.1115/FEDSM2016-7596.

[110] K. Elsayed Khairy, C. Lacor, Optimization of the cyclone separator geometry for minimum pressure drop using mathematical models and CFD simulations, Chem. Eng. Sci. 65 (2010) 6048–6058. https://doi.org/10.1016/j.ces.2010.08.042.

[111] H. Safikhani, M.A. Akhavan-Behabadi, M. Shams, M.H. Rahimyan, Numerical simulation of flow field in three types of standard cyclone separators, Adv. Powder Technol. 21 (2010) 435–442. https://doi.org/10.1016/j.apt.2010.01.002.

[112] L.S. Brar, K. Elsayed, Analysis and optimization of multi-inlet gas cyclones using large eddy simulation and artificial neural network, Powder Technol. 311 (2017) 465–483. https://doi.org/10.1016/j.powtec.2017.02.004.

[113] M. Wasilewski, L.S. Brar, Optimization of the geometry of cyclone separators used in clinker burning process: A case study, Powder Technol. 313 (2017) 293–302. https://doi.org/10.1016/j.powtec.2017.03.025.

[114] F. Parvaz, S.H. Hosseini, K. Elsayed, G. Ahmadi, Numerical investigation of effects of inner cone on flow field, performance and erosion rate of cyclone separators, Sep. Purif. Technol. 201 (2018) 223–237. https://doi.org/10.1016/j.seppur.2018.03.001.

[115] T. Mothilal, K. Pitchandi, Effect of vortex finder dimension on holdup mass and heat transfer rate in cyclone heat exchanger-CFD approach Effect of vortex finder dimension on holdup mass and heat transfer rate in cyclone heat exchanger-CFD approach, Int. J. Comput. Aided Eng. Technol. 10 (2018) 27–28. https://doi.org/10.1504/IJCAET.2018.088829.

[116] A. Kępa, The efficiency improvement of a large-diameter cyclone - The CFD calculations, Sep. Purif. Technol. 118 (2013) 105–111. https://doi.org/10.1016/j.seppur.2013.06.040.

[117] L. Shi, D.J. Bayless, G. Kremer, B. Stuart, CFD Simulation of the Influence of Temperature and Pressure on the Flow Pattern in Cyclones, Ind. Eng. Chem. Res. 45 (2006) 7667–7672. https://doi.org/10.1021/IE051167+.

[118] M. Bohnet, Influence of the gas temperature on the separation efficiency of aerocyclones, Chem. Eng. Process. Process Intensif. 34 (1995) 151–156. https://doi.org/10.1016/0255-2701(94)04001-X.

[119] P.A. Patterson, R.J. Munz, Cyclone collection efficiencies at very high temperatures, Can. J. Chem. Eng. 67 (1989) 321–328. https://doi.org/10.1002/cjce.5450670219.

[120] D. Geldart, Types of gas fluidization, Powder Technol. 7 (1973) 285–292. https://doi.org/10.1016/0032-5910(73)80037-3.

[121] C.W. Haig, A. Hursthouse, S. McIlwain, D. Sykes, The effect of particle agglomeration and attrition on the separation efficiency of a Stairmand cyclone, Powder Technol. 258 (2014) 110–124. https://doi.org/10.1016/j.powtec.2014.03.008.

[122] M. Sommerfeld, Validation of a stochastic Lagrangian modelling approach for inter-particle collisions in homogeneous isotropic turbulenceg, Int. J. Multiph. Flow. 27 (2001) 1829–1858. https://doi.org/10.1016/S0301-9322(01)00035-0.

[123] J. Paiva, R. Salcedo, P. Araujo, Impact of particle agglomeration in cyclones, Chem. Eng. J. 162 (2010) 861–876. https://doi.org/10.1016/j.cej.2010.06.025.

[124] C.A. Ho, M. Sommerfeld, Numerical Study on the Effect of Agglomeration for the Particle Separation in a Gas Cyclone, in: Proc. ASME/JSME Jt. Fluids Eng. Conf. (2003), Fluids Eng. Div. Summer Meet., ASMEDC, 2003: pp. 1315–1317. https://doi.org/10.1115/FEDSM2003-45671.

[125] C.J. Meyer, D.A. Deglon, Particle collision modeling – A review, Miner. Eng. 24 (2011) 719–730. https://doi.org/10.1016/J.MINENG.2011.03.015.

[126] J.G.A. Bitter, A study of erosion phenomena part I, Wear. 6 (1963) 5–21. https://doi.org/10.1016/0043-1648(63)90003-6.

[127] G.C. Pereira, F.J. de Souza, D.A. de Moro Martins, Numerical prediction of the erosion due to particles in elbows, Powder Technol. 261 (2014) 105–117. https://doi.org/10.1016/j.powtec.2014.04.033.

[128] M. Jafari, Z. Mansoori, M. Saffar Avval, G. Ahmadi, A. Ebadi, Modeling and numerical investigation of erosion rate for turbulent two-phase gas–solid flow in horizontal pipes, Powder Technol. 267 (2014) 362–370. https://doi.org/10.1016/j.powtec.2014.08.004.

[129] C. Huang, P. Minev, J. Luo, K. Nandakumar, A phenomenological model for erosion of material in a horizontal slurry pipeline flow, Wear. 269 (2010) 190–196. https://doi.org/10.1016/j.wear.2010.03.002.

[130] G.R. Wang, F. Chu, S. y Tao, L. Jiang, H. Zhu, Optimization design for throttle valve of managed pressure drilling based on CFD erosion simulation and response surface methodology, Wear. 338–339 (2015) 114–121. https://doi.org/10.1016/j.wear.2015.06.001.

[131] K.W. Chu, S.B. Kuang, A.B. Yu, A. Vince, G.D. Barnett, P.J. Barnett, Prediction of wear and its effect on the multiphase flow and separation performance of dense medium cyclone, Miner. Eng. 56 (2014) 91–101. https://doi.org/10.1016/j.mineng.2013.10.029.

[132] H. Arabnejad, S. Sajeev, A. Guimmarra, R. Vieira, S.A. Shirazi, Experimental study and modeling of sand erosion in the gas-liquid cylindrical cyclone GLCC separators, Proc. - SPE Annu. Tech.

Conf. Exhib. 2016-Janua (2016). https://doi.org/10.2118/181736-ms.

[133] W.I. Mazyan, A. Ahmadi, J. Brinkerhoff, H. Ahmed, M. Hoorfar, Enhancement of cyclone solid particle separation performance based on geometrical modification: Numerical analysis, Sep. Purif. Technol. 191 (2018) 276–285. https://doi.org/10.1016/j.seppur.2017.09.040.

[134] D.N. Veritas, Recommended practice RP O501 erosive wear in piping systems, 2005.

[135] Y.I. Oka, K. Okamura, T. Yoshida, Practical estimation of erosion damage caused by solid particle impact: Part 1: Effects of impact parameters on a predictive equation, Wear. 259 (2005) 95–101. https://doi.org/10.1016/J.WEAR.2005.01.039.

[136] Y.I. Oka, T. Yoshida, Practical estimation of erosion damage caused by solid particle impact: Part 2: Mechanical properties of materials directly associated with erosion damage, Wear. 259 (2005) 102–109. https://doi.org/10.1016/J.WEAR.2005.01.040.

[137] Z. Ji, Z. Xiong, X. Wu, H. Chen, H. Wu, Experimental investigations on a cyclone separator performance at an extremely low particle concentration, Powder Technol. 191 (2009) 254–259. https://doi.org/10.1016/j.powtec.2008.10.015.

[138] X. Gao, T. Li, A. Sarkar, L. Lu, W.A. Rogers, Development and validation of an enhanced filtered drag model for simulating gas-solid fluidization of Geldart A particles in all flow regimes, Chem. Eng. Sci. 184 (2018) 33–51. https://doi.org/10.1016/j.ces.2018.03.038.

[139] T. McKeen, T. Pugsley, Simulation and experimental validation of a freely bubbling bed of FCC catalyst, Powder Technol. 129 (2003) 139–152. https://doi.org/10.1016/S0032-5910(02)00294-2.

[140] W. Wang, J. Li, Simulation of gas–solid two-phase flow by a multi-scale CFD approach—of the EMMS model to the sub-grid level, Chem. Eng. Sci. 62 (2007) 208–231. https://doi.org/10.1016/j.ces.2006.08.017.

[141] Y. Igci, S. Pannala, S. Benyahia, S. Sundaresan, Validation studies on filtered model equations for gas-particle flows in risers, Ind. Eng. Chem. Res. 51 (2012) 2094–2103. https://doi.org/10.1021/ie2007278.

[142] S. Schneiderbauer, S. Pirker, Filtered and heterogeneity-based subgrid modifications for gas-solid drag and solid stresses in bubbling fluidized beds, AIChE J. 60 (2014) 839–854. https://doi.org/10.1002/aic.14321.

[143] S. Radl, S. Sundaresan, A drag model for filtered Euler-Lagrange simulations of clustered gas-particle suspensions, Chem. Eng. Sci. 117 (2014) 416–425. https://doi.org/10.1016/j.ces.2014.07.011.

[144] A. Ozel, J. Kolehmainen, S. Radl, S. Sundaresan, Fluid and particle coarsening of drag force for discrete-parcel approach, Chem. Eng. Sci. 155 (2016) 258–267. https://doi.org/10.1016/j.ces.2016.08.014.

[145] L.T. Zhu, Y.X. Liu, J.X. Tang, Z.H. Luo, A material-property-dependent sub-grid drag model for coarse-grained simulation of 3D large-scale CFB risers, Chem. Eng. Sci. 204 (2019) 228–245. https://doi.org/10.1016/j.ces.2019.04.026.

[146] F. Zafiryadis, A.D. Jensen, Y. Laxminarayan, W. Lin, E.A. Hove, M.B. Larsen, H. Wu, Predicting cold gas-solid flow in a pilot-scale dual-circulating fluidized bed: Validation of computational particle fluid dynamics model, Powder Technol. 381 (2021) 25–43. https://doi.org/10.1016/j.powtec.2020.11.070.

[147] A. Fluent, ANSYS Fluent Theory Guide, Canonsburg, PA, 2019. http://www.ansys.com.

[148] C.Y. Wen, Y.H. Yu, Mechanics of fluidization, in: Chem. Eng. Progress, Symp. Ser., 1996: pp. 100–111.

[149] M.M. Gibson, B.E. Launder, Ground effects on pressure fluctuations in the atmospheric boundary layer, J. Fluid Mech. 86 (1978) 491–511. https://doi.org/10.1017/S0022112078001251.

[150] S. Fu, B. Launder, M. Leschziner, Modelling strongly swirling recirculating jet flow with Reynolds-stress transport closures, in: 6th Symp. Turbul. Shear Flows, Toulouse, 1987: pp. 17_6_1-17_6_6.

[151] B.E. Launder, Second-moment closure and its use in modelling turbulent industrial flows, Int. J. Numer. Methods Fluids. 9 (1989) 963–985. https://doi.org/10.1002/fld.1650090806.

[152] B.J. Daly, F.H. Harlow, Transport Equations in Turbulence, Cit. Phys. Fluids. 13 (1970) 2634. https://doi.org/10.1063/1.1692845.

[153] S. Sarkar, B. Lakshmanan, Application of a Reynolds stress turbulence model to the compressible shear layer, AIAA J. 29 (1991) 743–749. https://doi.org/10.2514/3.10649.

[154] M. Syamlal, W. Rogers, T.J. O`Brien, MFIX documentation theory guide, Oak Ridge, TN, 1993. https://doi.org/10.2172/10145548.

[155] C.K.K. Lun, S.B. Savage, D.J. Jeffrey, N. Chepurniy, Kinetic theories for granular flow: inelastic particles in Couette flow and slightly inelastic particles in a general flowfield, J. Fluid Mech. 140 (1984) 223–256. https://doi.org/10.1017/S0022112084000586.

[156] F.L. Fassani, L. Goldstein, A study of the effect of high inlet solids loading on a cyclone separator pressure drop and collection efficiency, Powder Technol. 107 (2000) 60–65. https://doi.org/10.1016/S0032-5910(99)00091-1.

[157] A.C. Hoffmannc, A. van Santen, R.W.K. Allen, R. Clift, Effects of geometry and solid loading on the performance of gas cyclones, Powder Technol. 70 (1992) 83–91. https://doi.org/10.1016/0032-5910(92)85058-4.

[158] M. Mirzaei, P.A. Jensen, M. Nakhaei, H. Wu, S. Zakrzewski, H. Zhou, W. Lin, A hybrid multiphase model accounting for particle agglomeration for coarse-grid simulation of dense solid flow inside large-scale cyclones, Powder Technol. 399 (2022) 117186. https://doi.org/10.1016/J.POWTEC.2022.117186.

[159] R. Dewil, J. Baeyens, B. Caerts, CFB cyclones at high temperature: Operational results and design assessment, Particuology. 6 (2008) 149–156. https://doi.org/10.1016/j.partic.2008.01.002.

[160] I.S. Hwang, H.J. Jeong, J. Hwang, Effects of vortex finder length on flow field and collection efficiency of cyclone in an industrial-scale circulating fluidized bed boiler: Numerical study, Int. J. Energy Res. (2020) er.5430. https://doi.org/10.1002/er.5430.

[161] C. Anh Ho, M. Sommerfeld, Modelling of micro-particle agglomeration in turbulent flows, Chem. Eng. Sci. 57 (2002) 3073–3084. https://doi.org/10.1016/S0009-2509(02)00172-0.

[162] M. Sommerfeld, S. Stübing, A novel Lagrangian agglomerate structure model, Powder Technol. 319 (2017) 34–52. https://doi.org/10.1016/j.powtec.2017.06.016.

[163] H. Mothes, F. Loffler, ZUM EINFLUSS DER PARTIKELAGGLOMERATION AUF DIE ABSCHEIDUNG IM GASZYKLON, Staub, Reinhaltung Der Luft. 44 (1984) 9–14.

[164] J. Reppenhagen, A. Schetzschen, J. Werther, Find the optimum cyclone size with respect to the fines

in pneumatic conveying systems, Powder Technol. 112 (2000) 251–255. https://doi.org/10.1016/S0032-5910(00)00299-0.

[165] O. Molerus, M. Glückler, Development of a cyclone separator with new design, Powder Technol. 86 (1996) 37–40. https://doi.org/10.1016/0032-5910(95)03035-2.

[166] A. Gil, C. Cortés, L.M. Romeo, J. Velilla, Gas-particle flow inside cyclone diplegs with pneumatic extraction, Powder Technol. 128 (2002) 78–91. https://doi.org/10.1016/S0032-5910(02)00215-2.

[167] A. Majumder, H. Shah, P. Shukla, J.P. Barnwal, Effect of operating variables on shape of "fish-hook" curves in cyclones, Miner. Eng. 20 (2007) 204–206. https://doi.org/10.1016/j.mineng.2006.10.002.

[168] R.L. Salcedo, Collection efficiencies and particle size distributions from sampling cyclones — comparison of recent theories with experimental data, Can. J. Chem. Eng. 71 (1993) 20–27. https://doi.org/10.1002/cjce.5450710104.

[169] B. Popoff, B. Markus, A Lagrangian approach to dense particulate flows, in: Proc. ICMF 2007, 6th Int. Conf. Multiph. Flow, Leipzig, 2007.

[170] S.C.R. Dennis, S.N. Singh, D.B. Ingham, The steady flow due to a rotating sphere at low and moderate Reynolds numbers, J. Fluid Mech. 101 (1980) 257–279. https://doi.org/10.1017/S0022112080001656.

[171] B. Oesterlé, T.B. Dinh, Experiments on the lift of a spinning sphere in a range of intermediate Reynolds numbers, Exp. Fluids. 25 (1998) 16–22. https://doi.org/10.1007/s003480050203.

[172] Y. Tsuji, Y. Morikawa, T. Tanaka, N. Nakatsukasa, M. Nakatani, Numerical simulation of gas-solid two-phase flow in a two-dimensional horizontal channel, Int. J. Multiph. Flow. 13 (1987) 671–684. https://doi.org/10.1016/0301-9322(87)90044-9.

[173] M. Sommerfeld, Modeling of Particle-Wall Collisions in Confined Gas-Particle Flows, Artic. Int. J. Multiph. Flow. (1992). https://doi.org/10.1016/0301-9322(92)90067-Q.

[174] M. Sommerfeld, S. Lain, Parameters influencing dilute-phase pneumatic conveying through pipe systems: A computational study by the Euler/Lagrange approach, Can. J. Chem. Eng. 93 (2015) 1–17. https://doi.org/10.1002/cjce.22105.

[175] J. Xie, W. Zhong, A. Yu, MP-PIC modeling of CFB risers with homogeneous and heterogeneous drag models, Adv. Powder Technol. 29 (2018) 2859–2871. https://doi.org/10.1016/j.apt.2018.08.007.

[176] L.T. Zhu, Y.N. Yang, D.T. Pan, Z.H. Luo, Capability assessment of coarse-grid simulation of gas-particle riser flow using sub-grid drag closures, Chem. Eng. Sci. 213 (2020) 115410. https://doi.org/10.1016/j.ces.2019.115410.

[177] J. Yu, X. Gao, L. Lu, Y. Xu, C. Li, T. Li, W.A. Rogers, Validation of a filtered drag model for solid residence time distribution (RTD) prediction in a pilot-scale FCC riser, Powder Technol. 378 (2021) 339–347. https://doi.org/10.1016/j.powtec.2020.10.007.

[178] H. Lei, L.T. Zhu, Z.H. Luo, Study of filtered interphase heat transfer using highly resolved CFD–DEM simulations, AIChE J. 67 (2021). https://doi.org/10.1002/AIC.17121.

[179] X. Gao, T. Li, W.A. Rogers, Assessment of mesoscale solid stress in coarse-grid TFM simulation of Geldart A particles in all fluidization regimes, AIChE J. 64 (2018) 3565–3581. https://doi.org/10.1002/AIC.16341.

[180] L.T. Zhu, J.X. Tang, Z.H. Luo, Machine learning to assist filtered two-fluid model development for dense gas–particle flows, AIChE J. 66 (2020). https://doi.org/10.1002/AIC.16973.

[181] J.H. Cloete, S. Cloete, S. Radl, S. Amini, On the choice of closure complexity in anisotropic drag closures for filtered Two Fluid Models, Chem. Eng. Sci. 207 (2019) 379–396. https://doi.org/10.1016/j.ces.2019.06.006.

[182] L.T. Zhu, B. Ouyang, H. Lei, Z.H. Luo, Conventional and data-driven modeling of filtered drag, heat transfer, and reaction rate in gas–particle flows, AIChE J. 67 (2021). https://doi.org/10.1002/AIC.17299.

[183] O'Rourke P.J, Collective Drop Effects on Vaporizing Liquid Sprays, Ph.D. Thesis, Princeton University, 1981.

[184] L. Zhu, Y. Liu, L. ZH, An effective three-marker drag model via sub-grid modeling for turbulent fluidization, Chem. Eng. Sci. 192 (2018) 759–773. https://doi.org/https://doi.org/10.1016/j.ces.2018.08.026.

[185] P. Roache, Perspective: a method for uniform reporting of grid refinement studies, J. Fluids Eng. 116 (1994) 405–413. https://doi.org/https://doi.org/10.1115/1.2910291.

[186] P.J. Roache, Quantification of uncertainty in computational fluid dynamics, Annu. Rev. Fluid Mech. 29 (1997) 123–160. https://doi.org/10.1146/ANNUREV.FLUID.29.1.123.

[187] W.P. Adamczyk, G. Węcel, M. Klajny, P. Kozołub, A. Klimanek, R.A. Białecki, Modeling of particle transport and combustion phenomena in a large-scale circulating fluidized bed boiler using a hybrid Euler-Lagrange approach, Particuology. 16 (2014) 29–40. https://doi.org/10.1016/j.partic.2013.10.007.

[188] H.F. Meier, M. Mori, Anisotropic behavior of the Reynolds stress in gas and gas-solid flows in cyclones, Powder Technol. 101 (1999) 108–119. https://doi.org/10.1016/S0032-5910(98)00162-4.

[189] A. Gil, L.M. Romeo, C. Cortés, Effect of the Solid Loading on a PFBC Cyclone with Pneumatic Extraction of Solids, Chem. Eng. Technol. 25 (2002) 407–415. https://doi.org/10.1002/1521-4125(200204)25:4<407::AID-CEAT407>3.0.CO;2-4.

[190] M. Mirzaei, P.A. Jensen, M. Nakhaei, H. Wu, S. Zakrzewski, H. Zhou, W. Lin, CFD-DDPM coupled with an agglomeration model for simulation of highly loaded large-scale cyclones: Sensitivity analysis of sub-models and model parameters, Powder Technol. (2022) 118036. https://doi.org/10.1016/J.POWTEC.2022.118036.

[191] M. Morin, L. Raynal, S.B.R. Karri, R. Cocco, Effect of solid loading and inlet aspect ratio on cyclone efficiency and pressure drop: Experimental study and CFD simulations, Powder Technol. 377 (2021) 174–185. https://doi.org/10.1016/j.powtec.2020.08.052.

[192] V. Singh, S. Srivastava, R. Chaval, V. Vitankar, B. Basu, M.C. Agrawal, Simulation of gas-solid flow and design modifications of cement plant cyclones, in: Fifth Int. Conf. CFD Process Ind., 2006: pp. 1–8.

[193] T. Tsuji, K. Yabumoto, T. Tanaka, Spontaneous structures in three-dimensional bubbling gas-fluidized bed by parallel DEM–CFD coupling simulation, Powder Technol. 184 (2008) 132–140. https://doi.org/10.1016/J.POWTEC.2007.11.042.

[194] P. Ostermeier, S. DeYoung, A. Vandersickel, S. Gleis, H. Spliethoff, Comprehensive investigation and comparison of TFM, DenseDPM and CFD-DEM for dense fluidized beds, Chem. Eng. Sci. 196 (2019) 291–309. https://doi.org/10.1016/j.ces.2018.11.007.

[195] M. Adnan, N. Zhang, F. Sun, W. Wang, Numerical Simulation of a Semi-Industrial Scale CFB Riser using Coarse-Grained DDPM-EMMS Modelling, (2017). https://doi.org/10.1002/cjce.23071.

[196] D. Misiulia, A.G. Andersson, T.S. Lundström, Computational Investigation of an Industrial Cyclone Separator with Helical-Roof Inlet, Chem. Eng. Technol. 38 (2015) 1425–1434. https://doi.org/10.1002/ceat.201500181.

[197] J. Houben, Experimental Investigations and cfd Simulations on Particle Depositions in Gas Cyclone Separators , Ph.D. Thesis, University of Leoben, 2011.

[198] M. Alletto, M. Breuer, Large-eddy simulation of the particle-laden turbulent flow in a cyclone separator, in: High Perform. Comput. Sci. Eng. '13 Trans. High Perform. Comput. Center, Stuttgart 2013, Springer International Publishing, 2013: pp. 377–392. https://doi.org/10.1007/978-3-319-02165-2_26.

[199] H. Shalaby, K. Wozniak, G. Wozniak, Numerical Calculation of Particle-Laden Cyclone Separator Flow Using Les, Eng. Appl. Comput. Fluid Mech. 2 (2008) 382–392. https://doi.org/10.1080/19942060.2008.11015238.

[200] D.G. Schaeffer, Instability in the evolution equations describing incompressible granular flow, J. Differ. Equ. 66 (1987) 19–50. https://doi.org/10.1016/0022-0396(87)90038-6.

[201] G. Ahmadi, D. Ma, A thermodynamical formulation for dispersed multiphase turbulent flows—1, Int. J. Multiph. Flow. 16 (1990) 323–340. https://doi.org/10.1016/0301-9322(90)90062-N.

[202] D. Gidaspow, R. Bezburuah, J. Ding, Hydrodynamics of circulating fluidized beds: kinetic theory approach, in: 7th Fluid. Conf., Illinois Institute of Technology, Department of Chemical Engineering, Chicago, Illinois, 1992: pp. 75–82.

[203] S. Tenneti, R. Garg, S. Subramaniam, Drag law for monodisperse gas–solid systems using particle-resolved direct numerical simulation of flow past fixed assemblies of spheres, Int. J. Multiph. Flow. 37 (2011) 1072–1092. https://doi.org/https://doi.org/10.1016/j.ijmultiphaseflow.2011.05.010.

[204] R. Beetstra, M.A. van der Hoef, J.A.M. Kuipers, Drag force of intermediate Reynolds number flow past mono- and bidisperse arrays of spheres, AIChE J. 53 (2007) 489–501. https://doi.org/10.1002/aic.11065.

[205] R. Di Felice, The voidage function for fluid-particle interaction systems, Int. J. Multiph. Flow. 20 (1994) 153–159. https://doi.org/10.1016/0301-9322(94)90011-6.

[206] A. Li, G. Ahmadi, Dispersion and Deposition of Spherical Particles from Point Sources in a Turbulent Channel Flow, Aerosol Sci. Technol. 16 (1992) 209–226. https://doi.org/10.1080/02786829208959550.

[207] M. Adnan, J. Sun, N. Ahmad, J.J. Wei, Validation and sensitivity analysis of an Eulerian-Eulerian two-fluid model (TFM) for 3D simulations of a tapered fluidized bed, Powder Technol. 396 (2022) 490–518. https://doi.org/10.1016/J.POWTEC.2021.08.057.

[208] F. Marchelli, C. Moliner, B. Bosio, E. Arato, A CFD-DEM sensitivity analysis: The case of a pseudo-2D spouted bed, Powder Technol. 353 (2019) 409–425. https://doi.org/10.1016/J.POWTEC.2019.05.035.

[209] C. Moliner, F. Marchelli, L. Ong, A. Martinez-Felipe, D. Van der A, E. Arato, Sensitivity analysis and validation of a Two Fluid Method (TFM) model for a spouted bed, Chem. Eng. Sci. 207 (2019) 39–53. https://doi.org/10.1016/J.CES.2019.06.008.

[210] F. Parvaz, S.H. Hosseini, K. Elsayed, G. Ahmadi, Influence of the dipleg shape on the performance of gas cyclones, Sep. Purif. Technol. 233 (2020) 116000. https://doi.org/10.1016/j.seppur.2019.116000.

[211] M. Trefz, E. Muschelknautz, Extended cyclone theory for gas flows with high solids concentrations, Chem. Eng. Technol. 16 (1993) 153–160. https://doi.org/10.1002/CEAT.270160303.

[212] J. Chen, M. Shi, A universal model to calculate cyclone pressure drop, Powder Technol. 171 (2007) 184–191. https://doi.org/10.1016/j.powtec.2006.09.014.

[213] M. Mirzaei, S. Clausen, H. Wu, M. Nakhaei, H. Zhou, K. Jønck, P.A. Jensen, W. Lin, CFD simulation and experimental validation of multiphase flow in industrial cyclone preheaters [unpublished journal paper], 2023.

[214] M. Siadaty, S. Kheradmand, F. Ghadiri, Study of inlet temperature effect on single and double inlets cyclone performance, Adv. Powder Technol. 28 (2017) 1459–1473. https://doi.org/10.1016/J.APT.2017.03.015.

[215] A.V.S.S.K.S. Gupta, P.K. Nag, Prediction of heat transfer coefficient in the cyclone separator of a CFB, Int. J. Energy Res. 24 (2000) 1065–1079. https://doi.org/https://doi.org/10.1002/1099-114X(20001010)24:12<1065::AID-ER644>3.0.CO;2-%23.

[216] A. Jain, B. Mohanty, B. Pitchumani, K.S. Rajan, Studies on gas-solid heat transfer in cyclone heat exchanger, in: J. Heat Transfer, 2006: pp. 761–768. https://doi.org/10.1115/1.2217748.

[217] S. Clausen, A. Fateev, S.L. Hvid, Combustion zone investigation in fuel flexible suspension fired boilers , Experimental, Risø, 2011. http://orbit.dtu.dk/files/23335570/Combustion zone investigation in fuel flexible suspension fired boilers, Experimental.pdf.

[218] J. Bak, S. Clausen, FTIR emission spectroscopy methods and procedures for real time quantitative gas analysis in industrial environments, Meas. Sci. Technol. 13 (2002) 150–156. https://doi.org/10.1088/0957-0233/13/2/302.

[219] S. Clausen, Local measurement of gas temperature with an infrared fibre-optic probe, Meas. Sci. Technol. 7 (1996) 888–896. https://doi.org/10.1088/0957-0233/7/6/005.

[220] A.P. Baskakov, V.N. Dolgov, Y.M. Goldobin, Aerodynamics and heat transfer in cyclones with particle-laden gas flow, Exp. Therm. Fluid Sci. 3 (1990) 597–602. https://doi.org/10.1016/0894-1777(90)90076-J.

[221] C.S. Svith, W. Lin, K. Dam-Johansen, H. Wu, An experimental and modelling study of the Selective Non-Catalytic Reduction (SNCR) of NOx and NH3 in a cyclone reactor, Chem. Eng. Res. Des. 183 (2022) 331–344. https://doi.org/10.1016/j.cherd.2022.05.014.

[222] M. Mirzaei, S. Clausen, H. Wu, M. Nakhaei, H. Zhou, K. Jønck, P.A. Jensen, W. Lin, Investigation of erosion in an industrial cyclone preheater by CFD simulations [unpublished journal paper], (2023).

[223] D. Mills, Preface, in: Pneum. Conveying Des. Guid., Elsevier, 2004: pp. xi–xii. https://doi.org/10.1016/B978-075065471-5/50000-9.

[224] C.A.R. Duarte, F.J. de Souza, V.F. dos Santos, Numerical investigation of mass loading effects on elbow erosion, Powder Technol. 283 (2015) 593–606. https://doi.org/10.1016/J.POWTEC.2015.06.021.

[225] X. Chen, B.S. McLaury, S.A. Shirazi, Application and experimental validation of a computational

fluid dynamics (CFD)-based erosion prediction model in elbows and plugged tees, Comput. Fluids. 33 (2004) 1251–1272. https://doi.org/10.1016/J.COMPFLUID.2004.02.003.

[226] Z. Lin, X. Sun, T. Yu, Y. Zhang, Y. Li, Z. Zhu, Gas–solid two-phase flow and erosion calculation of gate valve based on the CFD-DEM model, Powder Technol. 366 (2020) 395–407. https://doi.org/10.1016/J.POWTEC.2020.02.050.

[227] M. Parsi, K. Najmi, F. Najafifard, S. Hassani, B.S. McLaury, S.A. Shirazi, A comprehensive review of solid particle erosion modeling for oil and gas wells and pipelines applications, J. Nat. Gas Sci. Eng. 21 (2014) 850–873. https://doi.org/10.1016/j.jngse.2014.10.001.

[228] J. Foroozesh, F. Parvaz, S.H. Hosseini, G. Ahmadi, K. Elsayed, N.U. Babaoğlu, Computational fluid dynamics study of the impact of surface roughness on cyclone performance and erosion, Powder Technol. 389 (2021) 339–354. https://doi.org/10.1016/J.POWTEC.2021.05.041.

[229] I. Finnie, Erosion of surfaces by solid particles, Wear. 3 (1960) 87–103. https://doi.org/10.1016/0043-1648(60)90055-7.

[230] B.S. McLaury, S.A. Shirazi, J.R. Shadley, E.F. Rybicki, Modeling erosion in chokes, Am. Soc. Mech. Eng. Fluids Eng. Div. FED. 236 (1996) 773–781.

[231] E. Dehdarinejad, M. Bayareh, Impact of non-uniform surface roughness on the erosion rate and performance of a cyclone separator, Chem. Eng. Sci. 249 (2022) 117351. https://doi.org/10.1016/J.CES.2021.117351.

[232] R. Macchini, M.S.A. Bradley, T. Deng, Influence of particle size, density, particle concentration on bend erosive wear in pneumatic conveyors, Wear. 303 (2013) 21–29. https://doi.org/10.1016/J.WEAR.2013.02.014.

[233] M. Mahdavi, S. Karimi, … S.S.-F., undefined 2016, Parametric study of erosion under high concentrated slurry: experimental and numerical analyses, Asmedigitalcollection.Asme.Org. (2016). https://doi.org/10.1115/FEDSM2016-7718.

[234] E.M. Winkler, Stone: Properties Durability in Man's Environment, Springer Vienna, Vienna, 1973. https://doi.org/10.1007/978-3-7091-4120-5.

[235] J. Ralph, "Welcome to mindat.org," Hudson Inst. Mineral. (2017). mindat.org.